MAXIMUM CHAT UTILIZATION IN ASPHALT PAVING AT THE TAR CREEK SUPERFUND SITE – TEST ROAD

Prepared by:

Nazimuddin Wasiuddin
Musharraf Zaman
Robert W. Nairn
Sinniah K. Navaratnarajah
Rajul V. Teredesai
School of Civil Engineering and Environmental Science
The University of Oklahoma, Norman, OK, 73019

Submitted to:

Angela Brunsman
Tar Creek Coordinator, Land Protection Division
Oklahoma Department of Environmental Quality
Oklahoma City, OK, 73101-1677

Submitted: April 2008
Revised: January 2009

MAXIMUM CHAT UTILIZATION IN ASPHALT PAVING AT THE TAR CREEK SUPERFUND SITE – TEST ROAD

Final Report

Submitted to:

Angela Brunsman
Tar Creek Coordinator
Land Protection Division
Oklahoma Department of Environmental Quality
Oklahoma City, Oklahoma 73101-1677

Prepared by:

Nazimuddin Wasiuddin
Musharraf Zaman
Robert W. Nairn
Gerald Miller
Sinniah K. Navaratnarajah
Rajul V. Teredesai

Submitted by:

The Office of Research Administration
731 Elm Avenue, Rm. 134
University of Oklahoma
Norman, Oklahoma 73019

Submitted: April 2008
Revised: January 2009

DISCLAIMER

The contents of this report reflect the views of the authors who are responsible for the facts and the accuracy of the information presented herein. The contents do not necessarily reflect the official views of the Oklahoma Department of Environmental Quality (ODEQ). This report does not constitute a standard, specification, or regulations.

ACKNOWLEDGEMENT

We would like to express our sincere appreciation to the Oklahoma Department of Environmental Quality (ODEQ) for providing funds for this project through the Oklahoma Plan for Tar Creek (OPTC) initiative. Specifically, we would like to thank Angela Brunsman, Mary Jane Calvey, Kelly Dixon, Dennis Datin, David Cates, Scott Thompson and Heather Mallory, all from ODEQ, for their valuable assistance during the course of this study. We express special thanks and appreciation to Danny Gierhart and Eric Roberts from the ODOT Materials Division for their technical assistance in this project. We are also thankful to Paul Green, Tim Bray and Mark Wilson from ODOT Division 8 for their assistance with profilograph testing and distress survey. We gratefully acknowledge the assistance of Glover Construction, Muskogee, Oklahoma for construction of the Test Road and associated tasks including milling and repaving. We are thankful to the Tri-State Asphalt staff for their role in the construction of the Test Road. We would like to thank Burgess Engineering and Testing, Inc. from Moore, Oklahoma for conducting the falling weight deflectometer and ground penetrating radar tests. We are especially thankful to County Commissioner John Clarke for his interest and valuable assistance. We are also grateful to Robert Knox, Joakim Laguros, Keith Strevett, Naji Khoury, Selvamohan Selvaratnam, Charbel Khoury, and others whose assistance and support were crucial in the completion of this project We express our appreciation to the OU Purchasing staff for their assistance with the bidding.

Finally, we are especially thankful to Dr. Thomas Landers, Dean, OU College of Engineering, for his important role in the Oklahoma Plan for Tar Creek.

TABLE OF CONTENTS

ACKNOWLEDGEMENT.....iii
LIST OF TABLES.....viii
LIST OF FIGURES.....x
ABSTRACT.....xv

CHAPTER 1 INTRODUCTION..... 1
1.1 Background..... 1
1.2 Scope and Objectives..... 3
1.3 Structure and Reporting..... 3

CHAPTER 2 PRE-BIDDING STUDY AND BIDDING PROCESS..... 7
2.1 General..... 7
2.2 Pre-Bidding Study.....7
2.2.1 Site Selection..... 7
2.2.2 Soil Sampling and Laboratory Testing..... 8
2.2.3 Field Testing..... 9
2.2.4 Stabilization of Chat with Cement Kiln Dust (CKD) and Class C Fly Ash (CFA)..... 11
2.2.5 Chat Asphalt Surface and Base Mix Design..... 13
2.3 Bidding Process.....15
2.3.1 Preparation of the Bid Package..... 15
2.3.2 Bidding Process.....16

CHAPTER 3 CONSTRUCTION REPORT.....25
3.1 General..... 25
3.2 Construction of the Test Road..... 25
3.2.1 Test Road Sections..... 25
3.2.2 Construction..... 26
3.2.3 Treatment of the Existing Subgrade.....27
3.2.4 Hauling and Spreading of Chat, CFA and CKD..... 28
3.2.5 Mixing and Compaction.....29
3.2.6 Curing.....30
3.2.7 Problems Encountered During the Curing Period and Before Paving..... 31
3.2.8 Paving.....31

CHAPTER 4 LABORATORY TESTING OF STABILIZED-CHAT BASE..... 50
4.1 General..... 50
4.2 Properties of Pile Run Chat..... 50
4.2.1 Gradation..... 50
4.2.2 L.A. Abrasion..... 51
4.2.3 Specific Gravity.....51
4.3 Properties of Class C Fly Ash (CFA).....52
4.4 Properties of Cement Kiln Dust (CKD)..... 52

4.5 Moisture-Density Relationship....53
4.6 Test Matrix.... 54
4.7 Specimen Preparation....55
4.8 Seismic Modulus Test.... 55
4.9 Unconfined Compressive Strength (UCS) Test.... 59
4.10 Modulus of Elasticity (E_{UCS})....60
4.11 Indirect Tensile Strength Test.... 62

CHAPTER 5 LABORATORY TESTING OF CHAT-ASPHALT.... 80
5.1 General.... 80
5.2 Design of HMA Surface and Base.... 80
5.2.1 Gradation of Chat and Non-Chat Aggregates.... 80
5.2.2 Selection of Mix Type and Asphalt Binders.... 81
5.2.3 Preparation of Trial Blends.... 82
5.2.4 Testing of Aggregate Properties....83
5.2.5 Selection of Final Blend....85
5.2.6 Determination of OAC....86
5.3 Collection of Materials....87
5.4 Cyclic Indirect Tension Resilient Modulus Test....87
5.4.1 Sample Preparation for M_R Testing....88
5.4.2 M_R Test Procedure....89
5.4.3 Accuracy of Deflection Value in M_R Calculation....90
5.4.4 Variation of Cyclic Indirect Tension Resilient Modulus.... 91
5.4.5 Variation of M_R with Stress Ratio.... 91
5.4.6 M_R Values at Selected Stress Ratio....94
5.4.7 Effect of Binder Content on Resilient Modulus....95
5.4.8 Effect of Air Voids on Resilient Modulus....96
5.4.9 Effect of Aggregate Sizes on Resilient Modulus.... 97
5.4.10 Variation of M_R with Temperature.... 98
5.4.11 A Model to Predict Resilient Modulus.... 99
5.5 APA Rut Test....101
5.5.1 Effect of Binder Content on Rut Depth.... 103
5.5.2 Effect of Air Voids on Rut Depth....104
5.5.3 Effect of Percentage Fines on Rut Depth.... 105
5.5.4 General Model to Predict Rutting Potential.... 105
5.5.5 Correlation between M_R and APA Rut....106
5.6 Fatigue Test....108
5.7 Permeability Test.... 111

CHAPTER 6 FIELD TESTING OF STABILIZED-CHAT BASE.... 158
6.1 General....158
6.2 Spectral Analysis of Surface Waves (SASW).... 158
6.3 Falling Weight Deflectometer (FWD)....160
6.4 Ground Penetrating Radar (GPR)....162
6.5 Dynamic Cone Penetration Test on Stabilized-Chat Base....163

CHAPTER 7 FIELD TESTING OF CHAT-ASPHALT BASE AND SURFACE..... 175
7.1 General.....175
7.2 Falling Weight Deflectometer Test.....175
7.3 Relative Comparison between M_R and E_{FWD}.....177
7.4 Spectral Analysis of Surface Waves (SASW)..... 178
7.5 Ground Penetrating Radar (GPR)..... 179

CHAPTER 8 MILLING, REPAVING AND DISTRESS SURVEYING..... 192
8.1 General.....192
8.2 Milling and Repaving..... 192
8.2.1 Pavement Inspection (March 2006).....192
8.2.2 Milling..... 192
8.2.3 Repaving..... 193
8.2.4 Asphalt Content of Millings..... 194
8.2.5 Rut Test on Repaving Mix (OHD L 43)..... 194
8.2.6 Moisture Susceptibility Test on Repaving Mix (AASHTO T 283).....195
8.3 Pavement Inspection (January 2007) 195
8.4 Pavement Distress Survey (June and July, 2007)..... 195
8.4.1 Evaluation of Smoothness.....196
8.4.2 Pavement Distress Survey.....197
8.4.3 Conclusive Remarks on Distress Survey..... 201

CHAPTER 9 CONCLUSIONS AND RECOMMENDATIONS.....224
9.1 Summary.....224
9.2 Conclusions.....225
9.3 Recommendations.....231

REFERENCES.....232

APPENDIX A: SAMPLE CALCULATION OF WATER APPLICATION RATE FOR SECTION TS-2..... 242

APPENDIX B-1: MIX DESIGN SHEET FOR TAR CREEK BASE MIX.....244

APPENDIX B-2: MIX DESIGN SHEET FOR TAR CREEK SURFACE MIX..... 245

APPENDIX B-3: MIX DESIGN SHEET FOR DAVIS BASE MIX..... 246

APPENDIX B-4: MIX DESIGN SHEET FOR OKC BASE MIX..... 247

APPENDIX C: COMPACTION LEVEL MEASUREMENTS ON CHAT-ASPHALT COURSE.....249

APPENDIX D: MATLAB PROGRAM FOR PROCESSING SASW DATA.....251

APPENDIX E: PLOTS OF TRANSFER FUNCTION..... 253
APPENDIX F: APA RUT RESULTS.....276

APPENDIX G: TAR CREEK ASPHALT ROAD RUT SURVEY..... 280

List of Tables

Table 2.1 Boring Log Obtained from Pre-Construction Testing..... 18
Table 2.2 Summary of DCP Results Along the Test Road Sections..... 18
Table 2.3 UCS Test Results for CFA Stabilized Raw Chat Samples..... 19
Table 2.4 UCS Test Results for CKD Stabilized Raw Chat Samples..... 19
Table 2.5 Volumetric Properties of Different Mixes..... 19
Table 2.6 Results of Performance Tests..... 20

Table 3.1 Summary of Density Measurements Using Nuclear Density Gauge..... 34
Table 3.2 Summary of Chat Usage in Different Sections.....34
Table 3.3 Summary of Density Measurements on Stabilized-Chat Base..... 35

Table 4.1 Chemical Properties of CFA, CKD, Alite and Belite (Lafarge, 2005; Kamon and Nontananandh, 991)..... 64
Table 4.2 Summary of OMCs and MDDs..... 64
Table 4.3 Specimen Test Matrix for Laboratory Study..... 64
Table 4.4 Statistical Analysis of NDT Results (E*) for CFA-Stabilized Specimens..... 65
Table 4.5 Statistical Analysis of NDT Results (E*) for CKD-Stabilized Specimens.....65
Table 4.6 Summary of NDT Test Results (E*).....65
Table 4.7 Summary of UCS Test Results (E*)..... 66
Table 4.8 Statistical Analysis for the Results of UCS Test..... 66
Table 4.9 Summary of Elastic Modulus (E) Results from UCS Tests.....67
Table 4.10 Statistical Analysis of Elastic Modulus (E) for CFA-Stabilized Specimens Before Removing The Outliers.....67
Table 4.11 Statistical Analysis of Elastic Modulus (E) for CFA-Stabilized Specimens After Removing The Outliers..... 67
Table 4.12 Summary of Indirect Tensile Strength Test Results..... 68

Table 5.1 Gradations of Chat from Different Sources.....115
Table 5.2 Proportions of Aggregates.....115
Table 5.3 Gradations of Trial Blends..... 115
Table 5.4 Bulk Specific Gravity of Trial Blends.....116
Table 5.5 Consensus Aggregate Properties of Trial Blends.....116
Table 5.6 Source Aggregate Properties..... 116
Table 5.7 G_{mb} and G_{mm} Values of the Trial Blends.....116
Table 5.8 Volumetric Properties of the Trial Blends..... 117
Table 5.9 Estimated Volumetric Properties of the Trial Blends at the Estimated OAC.... 117
Table 5.10 Specific Gravity and Theoretical Maximum Density of Different Mixes.....117
Table 5.11(a) Volumetric Properties at Different Asphalt Binder Contents..... 117
Table 5.11(b) Volumetric Properties at Different Asphalt Binder Contents..... 118
Table 5.12 Volumetric Properties at OAC..... 118
Table 5.13 Summary of Mix Properties for the Collected Loose HMA Mixes..... 118
Table 5.14 Number of Loading Cycle Used in Each Stress Sequence.....119

Table 5.15 Measured M_R for Test Road Base Mix Laboratory Specimens..... 120
Table 5.16 Measured M_R for Test Road Surface Mix Laboratory Specimens..... 121
Table 5.17 Measured M_R for Test Road Cores.....122
Table 5.18 Linear Model Parameters for Test Road Specimens (M_R = A + BR)..... 123
Table 5.19 Semi-Log Model Parameters for Test Road Specimens ($M_R = A B^R$)..... 124
Table 5.20 Log-Log Model Parameers for Test Road Specimens ($M_R = A R^B$).....125
Table 5.21 Average M_R for the Stress Ratios 0.20, 0.35 and 0.50.....126
Table 5.22 Materials and Mix Properties..... 127
Table 5.23 Percentage Difference in M_R Values of Field Cores
with Respect to Laboratory Speciemens..... 127
Table 5.24 Measured and Predicted Model Parameters..... 128
Table 5.24 Measured and Predicted Model Parameters (Cont'd)..... 129
Table 5.25 Sensitivity Check for M_R Model by Changing Each Variable by 20%..... 129
Table 5.26 Matrix of APA Rut Results..... 130
Table 5.27 Predicted Rut Depth from Material and Mix Properties..... 131
Table 5.28 Predicted M_R and APA Rut Depth at 2000 and 8000 Loading Cycles..... 132
Table 5.29 Models for Predicted M_R and APA Rut Depth
at 2000 and 8000 Loading Cycles..... 132
Table 5.30 APA Fatigue Results..... 133
Table 5.31 Measured and Predicted Fatigue Cycles..... 133
Table 5.32 Permeability Test Results.....134
Table 5.33 Comparison of Measured and Predicted Permeability Values.....134

Table 6.1 Summary of Modulus from SASW Test (E_{SASW}) and FWD Test (E_{FWD})..... 165
Table 6.2 Summary of GPR Results.....165

Table 7.1 FWD Back-Calculated Moduli for Chat-Asphalt Base and Surface Course.....181
Table 7.1A Comparison of Moduli from FWD Tests..... 182
Table 7.2 FWD Back-Calculated Moduli for Davis Site..... 183
Table 7.3 FWD Back-Calculated Moduli for OKC Site..... 183
Table 7.4 Comparison of Modulus from FWD Test and
M_R by Semi-Log Model (Davis Site).....184
Table 7.5 Comparison of Modulus from FWD Test and
M_R by Semi-Log Model (Test Road)..... 184
Table 7.6 Comparison of Modulus from FWD Test and
M_R by Semi-Log Model (OKC Site)..... 184
Table 7.7 Moduli and HMA Thicknesses from SASW Test for the Test Road Site.....185
Table 7.8 Comparison of FWD Test and SASW Moduli for the Test Road Site.....185

Table 8.1 Asphalt Content by Ignition Method.....203
Table 8.2 Rut Depths for Repaving Mix..... 203
Table 8.3 Moisture Susceptibility Test Results.....203
Table 8.4 Results of Profilograph Testing.....204
Table 8.5 ODOT Special Provision 430-2QA Smoothness Pay Factors.....204
Table 8.6 Distress Summary.....205

List of Figures

Figure 2.1 Location of Test Road in Cardin, Ottawa County, Oklahoma.....21
Figure 2.2 Test Road Site Before Construction, Looking West.....21
Figure 2.3 Locations of Boreholes and DCP Tests at Test Site..... 22
Figure 2.4 Summary of Dynamic Cone Penetration (DCP) Test Results..... 23
Figure 2.5 Summary of CBR Results Based on DCP Tests..... 24

Figure 3.1 Plan View of Four Test Sections..... 36
Figure 3.2 Sketch of Typical Section No.3 (TS-3)..... 36
Figure 3.3 Sketch of Typical Section No.1 (TS-1)..... 37
Figure 3.4 Sketch of Typical Section No.4 (TS-4)..... 37
Figure 3.5 Sketch of Typical Section No.2 (TS-2)..... 37
Figure 3.6 Flow Chart of Construction Process..... 38
Figure 3.7 Compaction of Existing Subgrade..... 39
Figure 3.8 Measuring Density Using a Nuclear Density Gauge.....39
Figure 3.9 Moisture-Density Relationship for Subgrade Soil in Section TS-2..... 40
Figure 3.10 Layout of Locations for Density Measurement During Subgrade Compaction.. 40
Figure 3.11 Chat Unloading at Test Road Site..... 41
Figure 3.12 A Motor Grader Spreading Chat..... 41
Figure 3.13 Measurement of Loose Lift Thickness..... 42
Figure 3.14 Windrows Constructed Along the Road Edges..... 42
Figure 3.15 Unloading CKD from Truck..... 43
Figure 3.16 Water Tanker and Pulver Mixer Working at the Site..... 43
Figure 3.17 Vibratory Roller Compacting Stabilized-Chat..... 44
Figure 3.18 Scarification of Subgrade Soil in Section TS-3..... 44
Figure 3.19 Emulsion Coated Stabilized-Chat Base..... 45
Figure 3.20 Flooding in Section TS-3..... 45
Figure 3.21 Reconstruction of Section TS-3.....46
Figure 3.22 Mechanical Broom..... 46
Figure 3.23 Paving Operation in Progress..... 47
Figure 3.24 Locations of Localized Base Failures in Section TS-2..... 47
Figure 3.25 Localized Failure Zone with Overlaying Chat-Asphalt Base Course Removed. 48
Figure 3.26 Corrected Failure Zone..... 48
Figure 3.27 Test Road After Paving with Chat-Asphalt surface Course..... 49

Figure 4.1 Sooner Chat Pile, Looking South..... 69
Figure 4.2 Gradation of Pile Run Chat..... 69
Figure 4.3 Moisture-Density Curve for Pile Run Chat..... 70
Figure 4.4 Moisture-Density Curve for Chat + 10% CFA..... 70
Figure 4.5 Moisture-Density Curve for Chat + 10% CKD..... 71
Figure 4.6 Molds and Rammer Used for Specimen Preparation..... 71
Figure 4.7 Seismic Test.....72
Figure 4.8 Typical Results of a Laboratory Seismic Test.....72

Figure 4.9 Output of NDT for Specimen "CKD-2"..... 73
Figure 4.10 Concept of Box Plot (Reproduced from McDonald 1999)..... 73
Figure 4.11 Box Plot for CFA-Stabilized Chat Specimen "CFA-1".....74
Figure 4.12 Box Plot for CFA-Stabilized Chat Specimen "CFA-2".....74
Figure 4.13 Box Plot for CKD-Stabilized Chat Specimen "CKD-1"..... 75
Figure 4.14 Box Plot for CKD-Stabilized Chat Specimen "CKD-2"..... 75
Figure 4.15 Specimen in MTS Frame for UCS Test.....76
Figure 4.16 Determination of Elastic Modulus from UCS Test Stress-Strain Curve..... 76
Figure 4.17 CFA-Stabilized Chat Specimen at Failure Showing Cracks During UCS Test...77
Figure 4.18 Typical Stress-Strain Curve for CFA-Stabilized Chat with Unloading-Reloading Sequence..... 77
Figure 4.19 Stress-Strain Curve for CKD-Stabilized Chat with Loading and Unloading..... 78
Figure 4.20 Set-up for Indirect Tensile Strength Test.....78
Figure 4.21 Failed Specimens After Indirect Tensile Strength Test..... 79
Figure 4.22 Summary of UCS and ITS Results for CFA-Stabilized and CKD-Stabilized Specimens.....79

Figure 5.1 Gradation of Trial Blends for Surface Mix..... 135
Figure 5.2 Gradation of Trial Blends for Base Mix.....135
Figure 5.3 Collection of Loose Chat-Asphalt Mix from the Test Road Site..... 136
Figure 5.4 A Diametrically Loaded Cylindrical Specimen for Cyclic Indirect Tension Testing.....136
Figure 5.5 Coring for Laboratory Testing of Test Road.....137
Figure 5.6 Cyclic Indirect Tension Resilient Modulus Test Specimen..... 137
Figure 5.7 Heavy Duty Asphalt Saw..... 138
Figure 5.8 Heavy Duty Coring Machine..... 139
Figure 5.9 Computer Controlled MTS Digital Data Acquisition System.....139
Figure 5.10 LVDTs Attached to the Cyclic Indirect Tension Resilient Modulus Test Specimen.....140
Figure 5.11 Temperature Chamber and Loading Setup Connected with the MTS Frame.... 140
Figure 5.12 Variation of M_R with Stress Ratio for Laboratory specimen at T = 41 ºF..... 141
Figure 5.13 Variation of M_R with Stress Ratio for Laboratory specimen at T = 77 ºF..... 141
Figure 5.14 Variation of M_R with Stress Ratio for Laboratory specimen at T = 104 ºF..... 142
Figure 5.15 Variation of M_R with Stress Ratio for Field Cores at T = 41 ºF.....142
Figure 5.16 Variation of M_R with Stress Ratio for Field Cores at T = 77 ºF.....142
Figure 5.17 Variation of M_R with Stress Ratio for Field Cores at T = 104 ºF.....143
Figure 5.18 Variation of M_R with Binder Content (Laboratory Specimens).....143
Figure 5.19 Variation of M_R with Binder Content (Field Cores)..... 144
Figure 5.20 Variation of M_R with Air Voids (Laboratory Specimens)..... 144
Figure 5.21 Variation of M_R with Air Voids (Field Cores)..... 145
Figure 5.22 Variation of M_R with Percentage Passing No. 200 Sieve (Laboratory Specimens)..... 145
Figure 5.23 Variation of M_R with Percentage Passing No. 200 Sieve (Field Cores).....146
Figure 5.24 Variation of M_R with Temperature for Laboratory specimens at R = 0.20.....146
Figure 5.25 Variation of M_R with Temperature for Laboratory specimens at R = 0.35.....147

Figure 5.26 Variation of M_R with Temperature for Laboratory specimens at R = 0.50..... 147
Figure 5.27 Variation of M_R with Temperature at R = 0.35 (Laboratory Specimens)..... 148
Figure 5.28 Variation of M_R with Temperature at R = 0.35 (Field Cores)..... 148
Figure 5.29 Average Decrease of M_R when Temperature increases from 41 ºF to 104 ºF... 149
Figure 5.30 Calculated and Predicted Model Parameter A for Power Model..... 149
Figure 5.31 Calculated and Predicted Model Parameter B for Power Model..... 150
Figure 5.32 Calculated and Predicted M_R from Power Model ($M_R = A\ B^R$)..... 150
Figure 5.33 APA Fatigue Sample Molds Secured in the Sample Tray..... 151
Figure 5.34 APA Rut Sample Mold and Molds Secured in the Sample Tray..... 151
Figure 5.35 Calculated and Predicted Rut Depths..... 152
Figure 5.36 Variation of Rut Depth at 2000 cycles with M_R at R = 0.20 and T = 77 ºF..... 152
Figure 5.37 Variation of Rut Depth at 2000 cycles with M_R at R = 0.35 and T = 77 ºF..... 153
Figure 5.38 Variation of Rut Depth at 2000 cycles with M_R at R = 0.50 and T = 77 ºF..... 153
Figure 5.39 Variation of Rut Depth at 8000 cycles with M_R at R = 0.20 and T = 77 ºF..... 153
Figure 5.40 Variation of Rut Depth at 8000 cycles with M_R at R = 0.35 and T = 77 ºF..... 154
Figure 5.41 Variation of Rut Depth at 8000 cycles with M_R at R = 0.50 and T = 77 ºF..... 154
Figure 5.42 Comparison Between Calculated and Predicted Fatigue Cycles..... 155
Figure 5.43 Karol-Warner's Falling Head Permeameter..... 156
Figure 5.44 Comparison Between Calculated and Predicted Permeability Values..... 157

Figure 6.1 Plan of the Test Road Showing the Locations of SASW Tests..... 166
Figure 6.2 SASW Test in Progress at Test Road..... 166
Figure 6.3 Plan View of The SASW Test Set Up..... 167
Figure 6.4 FWD Testing Equipment..... 167
Figure 6.5 Typical Force Output from FWD (Bandara and Briggs, 2004)..... 168
Figure 6.6 Typical Location of Loading Plate and Deflection Sensors for FWD Testing (Bandara and Briggs, 2004)..... 168
Figure 6.7 Summary of Modulus Values Obtained from Different Tests..... 169
Figure 6.8 GPR Testing at the Test Road Site..... 169
Figure 6.9 Principle of GPR (after USDOT, 2005b)..... 170
Figure 6.10 GPR Results for South Lane..... 171
Figure 6.11 GPR Results for North Lane..... 172
Figure 6.12 Locations for Post-Construction Coring and DCP Test..... 173
Figure 6.13 Summary of Post-Construction DCP Results..... 174

Figure 7.1 FWD Back-Calculated Modulus for Tar Creek Site..... 186
Figure 7.2 FWD Back-Calculated Modulus for Davis Site..... 186
Figure 7.3 FWD Back-Calculated Modulus for OKC Site..... 187
Figure 7.4 Comparison of Laboratory M_R at R = 0.20, E_{FWD} at 9 kip Load for Davis Site 187
Figure 7.5 GPR Thickness Profile for South Lane, Test Road Site..... 188
Figure 7.6 GPR Thickness Profile for North Lane, Tar Creek Site..... 189
Figure 7.7 Layer Profiles (Westbound Lane) from GPR Test (October 2007)..... 190
Figure 7.8 Layer Profiles (Eastbound Lane) from GPR Test (October 2007)..... 191

Figure 8.1 Longitudinal Cracks (South Lane) 206
Figure 8.2 A Close-Up View of a Longitudinal Crack (South Lane) 206

Figure 8.3 Growing Longitudinal Crack (South Lane)..... 207
Figure 8.4 Close-Up Shot of a Growing Longitudinal Crack (South Lane)..... 207
Figure 8.5 Settlement on the Sides..... 208
Figure 8.6 Milling Started from the East End of the Test Road..... 208
Figure 8.7 The ROTO-MILL Pavement Profiler..... 209
Figure 8.8 Milling Teeth of the ROTO-MILL Pavement Profiler..... 209
Figure 8.9 The Teeth of the ROTO-MILL are in Action..... 210
Figure 8.10 ROTO-MILL Throws Out Millings into a Truck..... 210
Figure 8.11 Completion of the First Run of the ROTO-MILL..... 211
Figure 8.12 Second Run of the ROTO-MILL..... 211
Figure 8.13 Completion of the Third Run of the ROTO-MILL..... 212
Figure 8.14 Fourth Run of the ROTO-MILL..... 212
Figure 8.15 Collection of Millings After First Run..... 213
Figure 8.16 Collection of Millings After Fourth Run..... 213
Figure 8.17 The Mechanical Broom Used for Cleaning After Milling..... 214
Figure 8.18 Cleaning with a Mechanical Broom..... 214
Figure 8.19 Asphalt Paver Manufactured by Barber Greene..... 215
Figure 8.20 Paver is Accepting Asphalt Mix from a Truck..... 215
Figure 8.21 Paving the East Bound Lane..... 216
Figure 8.22 Paving the West Bound Lane..... 216
Figure 8.23 Collected Loose Asphalt Mix from the Second Truck..... 217
Figure 8.24 The Ingersoll-Rand Roller..... 217
Figure 8.25 Compaction of the East Bound Lane..... 218
Figure 8.26 Measurement of the Level of Compaction Using A PQI Gauge..... 218
Figure 8.27 Finished Road after Milling, Repaving and Compaction..... 219
Figure 8.28 Crack-Free Section of TS-3..... 219
Figure 8.29 Edge Deterioration in TS-3..... 220
Figure 8.30 Small Longitudinal Crack in TS-1..... 220
Figure 8.31 Transverse Crack in TS-2..... 221
Figure 8.32 Ames Profilograph..... 221
Figure 8.33 Sample Profilograph Printout..... 222
Figure 8.34 Marked Station Number at Previous Station..... 222
Figure 8.35 Rut Measuring Devices..... 223
Figure 8.36 Snow and Ice Removal Scraped Areas..... 223

Figure B.1 Gradation Curve for All Four HMA Mixes..... 248

Figure E.1 Transfer Function for Specimen CFA-1 (Hit-1)..... 253
Figure E.2 Transfer Function for Specimen CFA-1 (Hit-2)..... 253
Figure E.3 Transfer Function for Specimen CFA-1 (Hit-3)..... 254
Figure E.4 Transfer Function for Specimen CFA-1 (Hit-4)..... 254
Figure E.5 Transfer Function for Specimen CFA-1 (Hit-5)..... 255
Figure E.6 Transfer Function for Specimen CFA-1 (Hit-6)..... 255
Figure E.7 Transfer Function for Specimen CFA-1 (Hit-7)..... 256
Figure E.8 Transfer Function for Specimen CFA-1 (Hit-8)..... 256
Figure E.9 Transfer Function for Specimen CFA-1 (Hit-9)..... 257

Figure E.10 Transfer Function for Specimen CFA-1 (Hit-10).....257
Figure E.11 Transfer Function for Specimen CFA-1 (Hit-11).....258
Figure E.12 Transfer Function for Specimen CFA-1 (Hit-12).....258
Figure E.13 Transfer Function for Specimen CFA-2 (Hit-1).....259
Figure E.14 Transfer Function for Specimen CFA-2 (Hit-2).....259
Figure E.15 Transfer Function for Specimen CFA-2 (Hit-3).....260
Figure E.16 Transfer Function for Specimen CFA-2 (Hit-4).....260
Figure E.17 Transfer Function for Specimen CFA-2 (Hit-5).....261
Figure E.18 Transfer Function for Specimen CFA-2 (Hit-6).....261
Figure E.19 Transfer Function for Specimen CFA-2 (Hit-7).....262
Figure E.20 Transfer Function for Specimen CFA-2 (Hit-8).....262
Figure E.21 Transfer Function for Specimen CFA-2 (Hit-9).....263
Figure E.22 Transfer Function for Specimen CFA-2 (Hit-10).....263
Figure E.23 Transfer Function for Specimen CFA-2 (Hit-11).....264
Figure E.24 Transfer Function for Specimen CFA-2 (Hit-12).....264
Figure E.25 Transfer Function for Specimen CKD-1 (Hit-1).....265
Figure E.26 Transfer Function for Specimen CKD-1 (Hit-2).....265
Figure E.27 Transfer Function for Specimen CKD-1 (Hit-3).....266
Figure E.28 Transfer Function for Specimen CKD-1 (Hit-4).....266
Figure E.29 Transfer Function for Specimen CKD-1 (Hit-5).....267
Figure E.30 Transfer Function for Specimen CKD-1 (Hit-6).....267
Figure E.31 Transfer Function for Specimen CKD-1 (Hit-7).....268
Figure E.32 Transfer Function for Specimen CKD-1 (Hit-8).....268
Figure E.33 Transfer Function for Specimen CKD-1 (Hit-9).....269
Figure E.34 Transfer Function for Specimen CKD-1 (Hit-10).....269
Figure E.35 Transfer Function for Specimen CKD-1 (Hit-11).....270
Figure E.36 Transfer Function for Specimen CKD-1 (Hit-12).....270
Figure E.37 Transfer Function for Specimen CKD-2 (Hit-1).....271
Figure E.38 Transfer Function for Specimen CKD-2 (Hit-2).....271
Figure E.39 Transfer Function for Specimen CKD-2 (Hit-3).....272
Figure E.40 Transfer Function for Specimen CKD-2 (Hit-4).....272
Figure E.41 Transfer Function for Specimen CKD-2 (Hit-5).....273
Figure E.42 Transfer Function for Specimen CKD-2 (Hit-6).....273
Figure E.43 Transfer Function for Specimen CKD-2 (Hit-7).....274
Figure E.44 Transfer Function for Specimen CKD-2 (Hit-8).....274
Figure E.45 Transfer Function for Specimen CKD-2 (Hit-9).....275
Figure E.46 Transfer Function for Specimen CKD-2 (Hit-10).....275

Figure F.1 APA Rut with Number of Cycles for Tar Creek Surface Mix.....276
Figure F.2 APA Rut with Number of Cycles for Tar Creek Base Mix.....276
Figure F.3 APA Rut with Number of Cycles for Tar Creek Cores.....277
Figure F.4 APA Rut with Number of Cycles for Davis Base Mix.....277
Figure F.5 APA Rut with Number of Cycles for Davis Cores.....278
Figure F.6 APA Rut with Number of Cycles for OKC Base Mix.....278
Figure F.7 APA Rut with Number of Cycles for OKC Cores.....279

ABSTRACT

Chat refers to mine tailings from the abandoned mines in the Tri-State Mining District of Oklahoma, Kansas and Missouri. In year 2000, Oklahoma Governor Frank Keating formed a task force, The Tar Creek Superfund Task Force (TCSTF), to examine the impacts of the Tar Creek Superfund site. The task force made recommendations on several studies including assessing the use of raw chat or pile run chat in pavement applications. The departments of transportation in Oklahoma, Kansas and Missouri have been using small amounts of pile run chat (about 20%) as an aggregate material in hot mix asphalt (HMA). The research team conducted a two-year systematic laboratory study to develop mix designs using pile run chat in HMA for both base course and surface course applications. It was reported that as much as 80% and 50% chat can be used safely in a chat-asphalt surface course and a base course, respectively. Also, an exploratory study, conducted by the research team showed that blending 55% chat with 35% limestone and then mixing either 10% class C fly ash (CFA) or 10% cement kiln dust (CKD) could yield a base course, called stabilized chat base in this report, that would be strong enough to support a design ESAL of 0.3 million or less. This field demonstration project was undertaken to evaluate the performance of chat-asphalt and stabilized-chat base. This project was part of several activities, collectively called Oklahoma Plan for Tar Creek (OPTC), that was undertaken to address some of the environmental concerns in the region.

A 3100 ft. long Test Road was constructed near Cardin, Oklahoma. The Test Road was divided into four different sections (TS-1, TS-2, TS-3 and TS-4, see section 3.2.1 for details) depending on the stabilizing agent used and the thickness of the chat-asphalt surface and base courses. The stabilized-chat bases consist of pile run chat from the Sooner Pile and was mixed

with either 10% CFA or 10% CKD, while the chat-asphalt surface and base courses have 80% and 50% pile run chat, respectively, from the Tri-State Asphalt plant.

The moisture-density relationships were established for CFA and CDK-stabilized bases and commonly used performance tests, namely moduli (elastic and seismic), unconfined compressive strength (UCS) and indirect tensile strength (ITS), were conducted. The laboratory test data indicate that the unconfined compressive strength (UCS) of chat stabilized with 10% CFA was approximately 163 psi, while the UCS of chat stabilized with 10% CKD was significantly lower, approximately 73 psi. The elastic modulus determined from the unloading-reloading curve under uniaxial loading in UCS testing was approximately 59 ksi for CFA-stabilized chat and 25 ksi for CKD-stabilized chat. Comparatively, the average seismic moduli of CFA-stabilized chat and CKD-stabilized chat were approximately 868 ksi and 197 ksi, respectively. The indirect tensile strength (ITS) of CFA-stabilized chat was approximately 19 psi, while that of CKD-stabilized chat was only 8 psi. Overall, it was observed that strength of pile run chat improved substantially due to cementitious stabilization.

Selected field tests, namely ground penetrating radar (GPR), falling weight deflectometer (FWD), and spectral analysis of surface waves (SASW), were performed to back-calculate the pavement design parameters in a non-destructive manner. GPR test data were used to determine as-built thicknesses of different layers in the pavement structure. The GPR test results revealed that, on average, the thickness of the stabilized-chat base in the Test Road is within 0.2-in. to 0.7-in. of the design thickness. The HMA layer thicknesses obtained from the GPR data are fairly consistent and close to the respective design thicknesses. The FWD results showed that the elastic modulus of CFA-stabilized chat is about 2.4 times the modulus of the CKD-stabilized chat.

Unlike stabilized bases, one type of modulus test, namely the cyclic indirect tension resilient modulus (M_R), was performed for chat-asphalt surface and base courses. The M_R tests were performed with varying stress ratios ranging from 0.15 to 0.70 and three test temperatures, namely 5°C, 25°C and 40°C (i.e., 41°F, 77°F and 104°F). Other important performance characteristic tests of chat-asphalt namely, APA rut, APA fatigue and permeability, were also performed in the laboratory. The average resilient modulus value at a stress ratio 0.20 and a test temperature of 25°C (77°F) was 5,992 MPa (869 ksi) for the Test Road base course and 2,565 MPa (372 ksi) for the surface course. Specific mix properties, namely air voids, binder content, specific gravity of aggregates and sizes of aggregates were identified as the influential factors in the test results. The APA rut test results showed that the Test Road mixes are susceptible to rutting. The APA fatigue results indicate that the Test Road has a greater fatigue resistance. The average permeability value for the Test Road surface mix was found to be 10.8×10^{-6} cm/s (4.3×10^{-6} in/s). The corresponding permeability of the base mix was 2.4×10^{-6} cm/s (0.9×10^{-6} in/s).

Two types of moduli, from FWD and SASW tests, were determined for the stabilized bases as well as for the chat-asphalt surface and base courses. Overall, the results show that E_{SASW} is approximately four times higher at Section TS-4 and six times higher at Section TS-2 than the corresponding E_{FWD} values. Milling and repaving operations were performed and pertinent laboratory tests were performed on millings and repaving mix. A distress survey was also performed which included drainage inspection, rut measurement and crack mapping. The road was found to be in fairly good condition after more than two and a half years in service. However, the drainage during the heavy rainfall was found to be a major concern. Overall, this study demonstrated that both the stabilized-chat bases and chat-asphalt surface and base courses

can be used effectively in road construction in the Tar Creek region and elsewhere. The environmental findings pertaining to this study will be reported in a separate report.

CHAPTER 1 INTRODUCTION

1.1 Background

The Tri-State Mining District in northeast Oklahoma, southeast Kansas and southwest Missouri was the site of substantial zinc and lead ore extraction since the mid 19th century. This activity in Oklahoma resulted in a total of 165 million tons of chat (i.e., chert fragments) of which approximately 75 million tons is currently stockpiled in large quantities on the surface of the Tar Creek Superfund Site (Hughes, 2002; Wasiuddin et al., 2005). The stockpiled chat contains elevated levels of lead, zinc and cadmium, raising potentially serious human health and ecological concerns. County chat roads (unpaved) create dust and serious health hazards. A study by the Indian Health Services (IHS) showed that 21% of the children living in the mining area had elevated blood lead levels (USEPA, 1999; Wahnee et al., 2000).

In 2000, Oklahoma Governor Frank Keating formed the Tar Creek Superfund Task Force (TCSTF) to examine the impact of the Tar Creek Superfund site. The Chat Usage Subcommittee was asked to "find ways to alleviate the health and environmental hazards caused by the presence of the chat" (Ref??). The task force made recommendations on several studies including assessing the use of pile run chat[1] in pavement applications. The departments of transportation in Oklahoma, Kansas and Missouri have been using pile run chat as an aggregate material in hot mix asphalt (HMA). In a study by Hamid (2004) it was reported that the Oklahoma Department of Transportation (ODOT) uses a relatively small percentage (up to 20%) of washed chat in HMA for surface and base course applications. However, no combined environmental and engineering study has been undertaken, so far, in any of the three states using chat for road construction.

[1] In this report, the words "pile run chat" and "raw chat" are used interchangeably.

Wasiuddin et al. (2005) conducted a two-year laboratory study to develop mix designs using pile run chat (from the Kenoyer North Pile) as one of the primary ingredients in HMA, called "chat-asphalt" in this report. It was reported that as much as 80% and 50% chat can be used safely in a surface course and a base course, respectively. Both chat-asphalt mixes met the ODOT requirements for air voids and other volumetric properties as well as moisture susceptibility, APA rut, and permeability (see Chapter 2 for details). It was also reported that pile run chat is an excellent source of aggregate in HMA.

Another laboratory study by Hughes (2002) evaluated the performance of chat, mixed with subgrade soil and stabilized with class C fly ash (CFA), for roadway applications. Teredesai et al. (2005) conducted an exploratory study to evaluate the effect of two stabilizing agents on the engineering properties of pile run chat from the Kenoyer North pile. The effect of different amounts of CFA and cement kiln dust (CKD), namely, 5%, 10%, and 15%, was evaluated. Results showed that blending 55% pile run chat with 35% limestone and then mixing either 10% CFA or 10% CKD could yield a base course strong enough to support a design ESAL of 0.3 million or less (ODOT, 1999). This study was limited to one engineering property, unconfined compressive strength (UCS), and it did not address any field implementation.

Since field situations are very different from laboratory situations in terms of scale, loading environment and other factors, a field demonstration project was undertaken in this study. The objective of this study was to evaluate the performance of a Test Road with stabilized chat as a base, and chat-asphalt as a base course and a surface course. Details of the site evaluation, design, construction and evaluation of the Test Road are included in this report. Using pile run chat as a paving material (i.e., stabilized-chat and chat-asphalt) is expected to accelerate the use of chat and address dust problems in the Tar Creek Superfund Site.

1.2 Scope and Objectives

As noted in the preceding section, the major objective of this field demonstration project was to evaluate the performance of chat-asphalt and stabilized-chat in paving. Only the engineering aspect of the Test Road is discussed in this report. The environmental aspects performed under separate funding, will be covered in a separate report.

An unpaved chat road segment was selected in coordination with the Oklahoma Department of Environmental Quality (ODEQ). Mix designs from Wasiuddin et al. (2005) were included in the bid package to maximize the use of pile run chat in chat-asphalt. The exploratory study by Teredesai et al. (2004) provided the design-related information in the bid package for CKD and CFA stabilized-chat. A Test Road was constructed with four different sections, having varying combinations of chat-asphalt surface, chat-asphalt base, CKD stabilized-chat and CFA stabilized-chat. Pertinent laboratory and field tests were conducted at various stages of this project. After about a year and a half in service, a segment of the Test Road was milled and repaved using chat-asphalt, and tests were conducted on both millings and repaving materials. Also, a distress survey of the Test Road, including drainage, rut depth measurement and crack mapping was performed following about two and half years in service. Finally, FWD and GPR tests were conducted to further assess the Test Road performance in terms of changes in in-situ moduli of stabilized-chat bases and chat-asphalt base and surface courses.

1.3 Project Structure and Reporting

To document the events and the test results from the present study, this report is divided into nine chapters. Chapter 1 describes why this field demonstration project was initiated. It states the objectives and the scope of the project. It also provides the overall layout of this report.

After the objectives and the scope of the project were set, a bidding package was prepared to select a paving contractor for the Test Road. The pre-bidding study required site selection, site characterization, soil sampling, laboratory testing and HMA mix design. Chapter 2 states the reasons for the site selection. It also includes soil sampling and site characterization data from commonly used geotechnical tests. Soil classification tests were performed in the laboratory and Dynamic Cone Penetration (DCP) tests were performed at four selected locations in the field. To maximize the use of chat in the surface mix, the mix design with 80% raw chat from the Kenoyer North Pile was included in the bidding package from the study by Wasiuddin et al. (2005). For the same reason, chat-asphalt base mix with 50% raw chat was selected for inclusion in the bidding package. As mentioned earlier, the exploratory study by Teredesai et al. (2004) provides the technical information for CFA and CKD stabilized bases. Chapter 2 also discusses the bidding items, bidding process and the selection of the contractor.

After the contractor was selected the road work started on October 4, 2004. Chapter 3 presents a comprehensive construction report. At first, it describes the four road sections constructed. Then it discusses the treatment of the existing subgrade, followed by the hauling of materials, mixing, compaction and curing of stabilized bases. Finally, the paving of chat-asphalt bases and surfaces is discussed. The Test Road was constructed using chat from the Sooner Pile for stabilized bases and from Tri-State Asphalt for chat-asphalt surface and base courses.

Chapter 4 describes the laboratory tests of the CFA and CKD stabilized bases. It includes discussion of moisture-density relationships that are essential for establishing optimum moisture content for stabilized bases. In the laboratory tests, chat from the Sooner Pile was used instead of the Kenoyer North Pile (used previously in the exploratory study by Teredesai et al., 2005.) Two types of modulus tests, namely seismic modulus and elastic modulus, were performed in the

laboratory for stabilized bases. The samples used in these tests were also used for the UCS tests. Finally, indirect tensile strength (ITS) tests were performed on a new set of samples. Chapter 4 contains the results of all these laboratory tests on stabilized bases.

Chapter 5 describes the laboratory tests on the chat-asphalt surface and base courses, which include the mix designs with chat from Tri-State Asphalt instead of the Kenoyer North Pile. Unlike stabilized bases, one type of modulus test, cyclic indirect tension resilient modulus test, was performed on the chat-asphalt. The resilient moduli obtained for these mixes were compared with those from two other sites, Davis and Oklahoma City. This chapter also discusses the variation of resilient modulus with stress ratio and temperature. The effects of air voids, binder content and aggregate size were also discussed. APA rut test is a performance test used frequently by ODOT. This chapter compares the rut depth from this site to the two other sites mentioned above. The effect of air voids, binder content, percent fines and the relation between resilient modulus and rut depth are also discussed in this chapter. Finally, the results of the fatigue tests and the permeability tests are presented.

Three non-destructive tests, namely spectral analysis of surface waves (SASW), falling weight deflectometer (FWD) and ground penetrating radar (GPR) were performed in the field to analyze the performance of the stabilized bases. SASW and FWD tests measure the moduli of different layers in the pavement while GPR measures their thicknesses. Chapter 6 discusses these tests. This chapter also includes the results of the dynamic cone penetration (DCP) tests performed on the stabilized bases.

The two types of moduli determined for the stabilized bases were also determined for chat-asphalt surface and base courses. The pavement layer thicknesses were determined using

GPR. Chapter 7 presents the field test results. It also compares the modulus values obtained from SASW and FWD.

The milling and repaving operations performed on a part of the Test Road are described in Chapter 8. The tests on millings and the repaving mix, namely, asphalt content, APA rut and moisture sensitivity, are described in this chapter. Also, this chapter includes a distress survey, including rutting, cracking and smoothness, of the Test Road after more than two and a half years in service. Finally, in Chapter 9 the conclusions and the recommendations of this study are presented.

CHAPTER 2 PRE-BIDDING STUDY AND BIDDING PROCESS

2.1 General

This chapter discusses the pre-bidding study that included site selection for the Test Road, site characterization (laboratory and field testing) and chat-asphalt mix design. This chapter also discusses the bidding process and selection of the contractor.

2.2 Pre-Bidding Study

2.2.1 Site Selection

At the beginning it was decided that an unpaved chat road located west of Commerce or Cardin, Oklahoma (most likely in Township 28 North Range 22 East or Township 29 North Range 22 East) would be selected for the Test Road project. A preliminary site visit was conducted by the research team, in cooperation with personnel from the Oklahoma Department of Environmental Quality (ODEQ), to observe such factors as existing roadway elevation, width, orientation (North-South or East-West), drainage, right of way and proximity to other chat roads. Based on this site visit, several potential county road sites were identified (e.g., county road S530 between county roads E20 and E50, west of Commerce, and E30 between S530 and S550, west of Cardin) for the proposed project. A discussion was then held with the ODEQ personnel concerning the relative merits and demerits of each site. Finally, county road E30, near Cardin, Oklahoma, as illustrated in Figure 2.1, was selected for paving. The site starts from the intersection of county roads S530 and E30. A photographic view of the road site before construction is shown in Figure 2.2. The area surrounding the road is relatively flat, covered with large fields of soy bean and pasture. A close visual observation of the area revealed lack of a well defined drainage system. For example, the drainage ditches between these roads and the neighboring fields are shallow and subjected to frequent damage due to the harvesting machines.

As discussed subsequently, lack of adequate drainage became a major problem during construction and performance assessment of the Test Road.

The location of the Test Road was selected based on the following considerations:

1. The Test Road will suppress dust in existing chat road and thereby suppress health hazards due to dust. As one can see from Figure 2.2, the original road was unpaved road, covered with chat and other locally available aggregates.
2. Another reason for the proposed road site is that a number of roads in the vicinity are also unpaved chat roads and are potential sources of dust and air pollution. In future these unpaved chat roads can also be paved.
3. Hauling cost of chat to the construction site was also an important factor.
4. From an environmental point of view, the orientation of the road was selected based on the wind direction effects.
5. Finally, the discussions with the local county commissioner also played a key role in the site selection, where the usefulness of this demonstration project was considered important.

2.2.2 Soil Sampling and Laboratory Testing

Limited geotechnical investigations were conducted on the existing subgrade layer of the selected site. As part of this investigation, boreholes were drilled using a hand auger at four selected locations, as shown in Figure 2.3. Subgrade soils from these boreholes were collected and classified based on visual observations described in the ASTM D 2488-93 method. A summary of the soil type is presented in Table 2.1. The subgrade soil was found to be brown clayey silt with some moisture within the top 8-in. For depths between 8-in. and 24-in., the soil

was classified primarily as fat clay with reddish brown mottles. Also, traces of chat could be seen in the soil to a depth of 8-in.

2.2.3 Field Testing

Dynamic Cone Penetration (DCP) tests were performed at four selected locations in accordance with the test procedure described in SHT (1992). These locations, called DCP-1, DCP-2, DCP-3, and DCP-4, are illustrated in Figure 2.3. At least one DCP test was performed in each of the four test sections, namely TS-1, TS-2, TS-3 and TS-4. A description of each test section is given in Section 3.2.1. The DCP tests were performed down to a depth of 0.9-m (35.4-in.). The DCP results were assumed to be representative of the entire sections. The DCP results are summarized in terms of incremental cone index (ICI), which represents the depth of penetration per blow of the DCP hammer (SHT, 1992). A lower ICI value indicates a stronger or stiffer material, while a higher DCP value indicates a weaker subgrade. Complete DCP profiles for all locations are shown in Figure 2.4. From these plots several interesting observations are made.

1. The ICI values for DCP-1 exhibit an increase with depth up to 0.3-m (11.8-in.) and then decrease in the remaining depth, 0.9-m (35.4-in.). It is an indication that the strength of the subgrade soil decreases with depth, up to 0.3-m (11.8-in.), beyond which an increase in the strength is observed. Specifically, the maximum ICI value at 0.3-m is 68 mm/blow (2.56-in./blow). From 0.3-m (11.8-in.) to 0.9-m (35.4-in.), the ICI values vary between 68 mm/blow (2.56-in./blow) and 30 mm/blow (1.18-in./blow), with the minimum ICI (10 mm/blow or 0.39-in./blow) occurring at approximately 0.83-m (32.7-in.).
2. For DCP-2, the ICI values are relatively low (10 mm/blow or 0.39-in./blow to 20 mm/blow or 0.79-in./blow) and did not exhibit any significant changes down to a depth

of 0.35-m (13.7-in.). For depths between 0.35-m (13.7-in.) and 0.9-m (35.4-in.), the ICI values are higher (40 mm/blow or 1.57-in./blow to 50 mm/blow or 1.97-in./blow). However, the changes in these values are not significant. It is an indication that the soil stratum at this location can be divided into two layers. The lower layer is about three times weaker than the upper layer. A weaker layer can be underlain by a stronger layer depending upon depositional characteristics, human interventions and other factors (Bowles, 1996).

3. The ICI values of DCP-3 show that the subgrade layer at this location can be divided into three different layers based on their average ICI values. The first layer has a thickness of 0.15-m, with an average ICI value of 50 mm/blow. The second layer (0.15-m or 5.9-in. to 0.3-m or 11.8-in.) is significantly stronger with an average ICI value of 10 mm/blow or 0.39-in./blow. The third layer (average ICI = 30 mm/blow or 1.18-in./blow) from a depth of 0.3-m (11.8-in.) to a depth of 0.9-m (35.4-in.) is stronger than the top layer but weaker than the middle layer.
4. As in DCP-3, the variation in the ICI values with depth for DCP-4 reveals three different layers with different strengths. The first layer (top layer) has an average ICI value of 10 mm/blow (0.39-in./blow) and a thickness of 0.2-m (7.87-in.). Comparatively, the second layer having a thickness of 0.5-m (19.7-in.) exhibits a higher average ICI value of approximately 25 mm/blow (0.98-in./blow). As for the third or bottom layer, it has an average ICI value of approximately 15 mm/blow (0.59-in./blow), which is higher than the corresponding value for the first layer but lower than the second layer.

The aforementioned ICI values were used to evaluate the California Bearing Ratio (CBR) values at each location. The following relation, as used by the Oklahoma Department of Transportation (ODOT), was used to convert ICI to CBR (Hensley and Rose, 2005):

$$\text{Log (CBR)} = 2.81 - 1.321 \log (\text{ICI}) \tag{2.1}$$

where, ICI is represented in millimeters per blow (mm/blow).

The CBR values at each location are plotted as a function of depth in Figure 2.5. From this figure, the CBR values vary with depth, as expected. For example, DCP-1 has an average CBR value of approximately 20 up to 0.2-m (7.9-in.), beyond which a much lower value of approximately 5 is observed. For DCP-2, the top layer (up to 0.35-m) has an average CBR value of 50 and the bottom layer exhibits a lower value of less than 5. Given these variabilities, it was decided to average the CBR values at each location for simplicity, and use these average values to represent the overall behavior of each test section. The CBR values from DCP-1, DCP-2, DCP-3, and DCP-4, were used to represent the behavior of subgrade soils at each test Section: TS-1, TS-2, TS-3, and TS-4 (see Section 3.2.1 for details). Table 2.2 presents a summary of DCP and CBR values for each section along the Test Road. From Table 2.2, it can be observed that section TS-2 has a weak subgrade with a CBR value of 10 in accordance with the guidelines by Hensley and Rose (2005). Also, subgrades in sections TS-1 and TS-2 are considered good for pavement construction based on their CBR values of 39 and 25, respectively. Section TS-4 has a normal subgrade with an average CBR value of 18.

2.2.4 Stabilization of Chat with Cement Kiln Dust (CKD) and Class C Fly Ash (CFA)

In order to prepare a bid for the Test Road project, an exploratory laboratory study was performed by Teredesai et al. (2005) to stabilize raw chat with CKD and CFA. Following the work of Wasiuddin et al. (2005) that used as much as 80% pile run chat in a chat-asphalt surface

mix and as much as 50% chat in a base mix in an environmentally sound manner, Teredesai et al. (2005) also used chat from the Kenoyer North Pile in their study. That study was, however, exploratory in nature and was performed only for bidding purposes. It was limited to one engineering property (UCS) and it did not address any field implementation issues.

The effect of different amounts of CFA and CKD, namely, 5%, 10%, and 15%, was evaluated in that exploratory study. The compressive strength of stabilized specimens exhibited an increase with the increase in the percentages of CFA and CKD. Two samples for each percentage of additive, were molded to replicate the results. The results of the UCS tests on CFA-stabilized specimens are summarized in Table 2.3. The average UCS value for the raw chat stabilized with 15% CFA and cured for 28 days is 758 psi. The corresponding UCS for 14-day cured specimens is 296 psi. Raw chat stabilized with 10% CFA yielded an unconfined compressive strength value of 140 psi after 14 days of curing and 516 psi after 28 days of curing, which is more than two times the 14 day strength, indicating that CFA is a rather slow reacting agent. The process of strength gain in the case of CFA stabilization is slow in the first 14 days but accelerates afterward.

Since raw chat samples without any stabilizing agents could not be tested because of lack of cohesion and specimen integrity, no UCS results are available for raw chat. A significant gain in UCS is achieved by adding 10% CFA. By increasing the percentage of CFA from 10 to 15, the UCS increased from 516 psi to 758 psi. The UCS results for chat stabilized with 5% CFA and cured for 28 days were incorrect due to some possible experimental errors. All of the UCS tests were performed at a strain rate of 1 in. per minute. Recent studies have shown that if the strain rate if reduced to 1 % of the sample height, as recommended by ASTM, then the 28-day UCS value for stabilized chat drops to 150 psi for CFA stabilization and 60 psi for CKD stabilization.

The results of the UCS tests on CKD stabilized raw chat samples are summarized in Table 2.4. With 10% CKD in the mix, a UCS value of 69 psi is achieved after 14 days of curing. The UCS value increased to 128 psi when the curing time was increased to 28 days. It can be seen from Table 2.4 that the change in water content in matrix having 10% CKD did not have any effect on UCS values after 14 days of curing. But, after 28 days of curing specimens compacted at 5.5% water content showed a higher UCS value of 127 psi than specimens compacted at 9% water content that yielded a UCS value of 96 psi. The 15% CKD stabilized-chat, however, showed a considerable increase in the UCS value with increasing in the water content from 5.5% to 9%. The strength increase for 14-day cured samples was from 35 psi to 170 psi. The average UCS value of 28-day cured specimens with 15% CKD and 9% water content was found to be 283 psi.

Since pile run chat gradation did not meet the ODOT requirements for a Type A aggregate base, locally available limestone from Vinita Quarry was blended with chat to meet the gradation requirements. Results showed that blending 55% chat with 35% limestone and then mixing either 10% CFA or 10% CKD could yield a base course that would be strong enough to support a design ESAL of 0.3 million or less and meet the ODOT specifications (ODOT, 1999).

2.2.5 Chat-Asphalt Surface and Base Mix Design

Both designs met the ODOT requirements for air voids and other volumetric properties, as shown in Table 2.5. It can be seen that the optimum binder content of the surface mix is 7%, while the optimum binder content of the base mix is 5.4%. The increased binder content of the surface mix is due to the increased amount of fine materials in the surface mix than in the base mix.

Moisture susceptibility tests were performed on samples with air voids between 6% and 8% according to AASHTO T 283 (Table 2.6). The tensile strength ratio (TSR) of the base mix is 0.82, which is 2% higher than the minimum allowed of 80%. In this mix, a PG 64-22 asphalt binder was used, which is not a polymer modified binder. It is possibly due to this asphalt binder that this mix marginally met the moisture susceptibility criteria. The TSR of the surface mix is 92%, which is much higher than the minimum of 80% required by ODOT. This mix used the PG 70-28 binder, which is a polymer-modified binder, and it generally performs well against moisture-induced damage.

APA rut tests were performed at 147.2º F (64º C) according to the OHD L-43 method, as followed by the ODOT. Table 2.6 illustrates the rut depths for base mixes. The average rut depth for the base mix was measured as 4.1 mm (0.16 in), which is below the maximum allowed rut depth of 5.0 mm (0.2 in), as set by ODOT for a base mix. For the surface mix, the average rut depth was found to be 1.8 mm (0.07 in), which is below the limit. Use of a better binder in the surface mix (PG 70-28) could be the possible reasons for such excellent performance.

To better understand the void structure, permeability tests were performed following the OHD L-44 method, although this test method does not necessarily confirm the saturation level of a sample. Permeability tests were performed on samples with air voids between 6% and 8%. The percent air voids was measured following the AASHTO T 166 method. Table 2.6 shows the permeability test results. The average permeability values are much lower than the maximum of 125E-05 cm/sec (49.21E-05 in/sec) allowed by ODOT.

Based on the above major findings, Wasiuddin et al. (2005) concluded that pile run chat is an excellent source of aggregate in chat-asphalt. Moreover, environmental tests were performed on the chat-asphalt and it was concluded that chat-asphalt can be used safely as

roadway materials (Wasiuddin et al., 2005). Based on the recommendations from the Wasiuddin et al. (2005) study, 80% and 50% chat were selected to be used in the surface and base course, respectively, of the Test Road.

2.3 Bidding Process

2.3.1 Preparation of the Bid Package

After the pre-bidding study, a bid package was prepared. The proposed length of the road was 5,300 feet. The designed Equivalent Single Axle Load (ESAL) was +0.3 million. The bid also contained milling and repaving of 100 feet of the proposed Test Road. The different items of the bid package are discussed as follows.

Requisition Form - A one-page requisition form contains the summary of the overall specifications of the project. It also lists the detailed items and specifications that were attached to the bid package. It includes the total price of the project and contact information.

List of Potential Bidders – The bid was open to all vendors. However, a list of 10 potential bidders was submitted with the bid package.

Road Plan – A road map was attached with the bid package. A description of the typical sections was provided.

Pay Items – A list of the pay items, including the milling and repaving operations, was provided in the package.

General Project Notes – General project notes containing information on payment, traffic control, surfacing and materials were also provided.

Chat-asphalt Mix Design Sheet – The surface and base mix designs with 80% and 50% pile run chat, respectively, as performed by Wasiuddin et al. (2005) were included in the bid package.

ODOT Specifications – The following ODOT specifications were attached.

1. 326-1(a-j)99	Subgrade Stabilization
2. 390	Chat/Fly Ash Stabilized Base (Special Provisions)
3. 411-3QA	QC/ZA for Plant Mix Asphalt Concrete Pavement
4. 411-4(a)99	Plant Mix Asphalt Concrete Pavement
5. 702-1(a-b)99	Cement Kiln Dust
6. 708-1(a)99	Plant Mix Bituminous Bases and Surfaces-Materials
7. 708-3(a-g)99	Plant Mix Bituminous Bases and Surfaces-Superpave
8. 708-4(a)99	Plant Mix Bituminous Bases and Surfaces-Shoulders
9. 708-5(a-b)99	Job-Mix Formulation of Asphalt Concrerte

2.3.2 Bidding Process

The bid package was submitted to the University of Oklahoma Purchasing Department on July 1, 2004. On July 30, 2004, the Purchasing Department reported that two bids were received; one from Glover Construction Co., Inc. and the other from APAC-Oklahoma, Inc. The lowest bid was offered by the Glover Construction Inc. A four member Selection Committee headed by Dr. Gerald Miller, University of Oklahoma, evaluated the bids. The other members of the Selection Committee were Dr. Thomas Landers, Dr. Musharraf Zaman and Dr. Joakim Laguros, all from University of Oklahoma. Also, to assist the bidding process, Dr. Robert Nairn attended some meetings and met with personnel in the purchasing office. It was found that even the lowest (although the quoted price by the above two contractors were very close) bid exceeded (about 66% higher) the expected cost of the project. The committee reevaluated their specifications in the bid package and made the following changes to significantly reduce the cost.

1. The initial proposed length of the Test Road was about one mile (5300 feet). In the revised bid, the length was reduced to 0.6 mile (3,150 feet).
2. The source of the chat was changed from the Kenoyer North Pile to the Sooner Pile and the Tri-State Asphalt, respectively, for stabilized-chat base and chat-asphalt. The hauling cost played a key role in making these changes.
3. The binder grading of chat-asphalt surface course was changed from PG 70-28 to PG 64-22. Also, the likelihood of colder weather during construction was responsible for this change.

Finally, the committee selected Glover Construction, Inc. as the contractor for the Test Road construction, including the aforementioned changes/revisions to the bid.

Table 2.1 Boring Log Obtained from Pre-Construction Testing

Depth (in)	Bore Hole Number			
	B1	B2	B3	B4
0	Brown and silty clay (CL) damp	Brown clayey silt (CL-ML)	Silty fine to coarse sand (moist),chat (SM)	Brown grey clayey silt, damp (CL-ML)
1				
2				
3				
4				
5			Grey brown moist silty clay (CL)	
6				
7				
8			Grey clayey silt (CL-ML)	
9	Reddish brown mottles (CH) moist and plastic	Reddish brown clay (CH)		Red- brown mottled clay (CH) damp
10				
11				
12				
13	Brown mottles (CH) moist and plastic			
14				
15				
16			Grey clayey silt (more clayey)(CL-ML)	
17	Brown mottles (CH) moist and plastic	Moist fat clay (CH)		
18				
19				
20				
21				
22				
23				
24				
Chainage (from west end)	150 ft	1,150 ft	2,150 ft	3,150 ft

Table 2.2 Summary of DCP Results Along the Test Road Sections

Depth (in.)	DCP	ICI (mm/blow)	CBR (%)	Avg. CBR (%)	Section
0 to 11.8	DCP-1	10 to 65	20	10	TS-3
11.8 to 35.4	DCP-1	30 to 65	5		TS-3
0 to 13.7	DCP-2	10 to 15	50	39	TS-1
13.7 to 35.4	DCP-2	40 to 60	4		TS-1
0 to 13.7	DCP-3	10 to 12	24	18	TS-4
13.7 to 35.4	DCP-3	40 to 50	6		TS-4
0 to 7.9	DCP-4	5 to15	50	25	TS-2
7.9 to 27.5	DCP-4	25 to 35	10		TS-2
27.5 to 35.4	DCP-4	20 to 25	20		TS-2

Table 2.3 UCS Test Results for CFA Stabilized Raw Chat (Kenoyer North Pile) Samples (Water Content 5.5%)

% Chat	% CFA	Curing Period (days)	Failure Stress (psi)
95	5	14	91.5
		28	38.5
90	10	14	140.2
		28	516
85	15	14	296
		28	758.2

Table 2.4 UCS Test Results for CKD Stabilized Raw Chat (Kenoyer North Pile) Samples

% Chat	% CKD	Curing period (days)	Water Content	
			5.5%	9%
			Failure Stress (psi)	Failure Stress (psi)
95	5	14	40.3	-
		28	47.6	-
90	10	14	69.4	67.6
		28	127.5	96.1
85	15	14	34.8	170.6
		28	-	283.7

Table 2.5 Volumetric Properties of Different Mixes

	Base Mix with 50% Raw Chat	Surface Mix with 80% Raw Chat
Effective Specific Gravity of Aggregate	2.595	2.596
Theoretical Maximum Density	2.397	2.339
Optimum Binder Content (%)	5.4	7
Voids in Mineral Aggregates (%)	13.2	16.6
Req. Voids in Mineral Aggregates (%)	Min. 13	Min. 15
Voids Filled with Asphalt (%)	69.8	76
Req. Voids Filled with Asphalt (%)	65-76	65-76
Asphalt Absorption (%)	1.35	1.42
Dust Proportion (%)	1.4	1.05

Table 2.6 Results of Performance Tests

	Moisture Susceptibility Test		Rut Test at 64ºC		Permeability Test	
Mix	**Tensile Stress Ratio**	**Min. Allowed**	**Avg. Rut Depth (mm[1])**	**Max. Allowed (mm)**	**Average Permeability (E-05 cm/sec[1])**	**Max. Allowed (E-05 cm/sec)**
Base Mix	0.82	0.8	4.1	5	10	125
Surface Mix	0.92	0.8	1.8	4	2.94	125

[1]1 inch = 25.4 mm = 2.54 cm

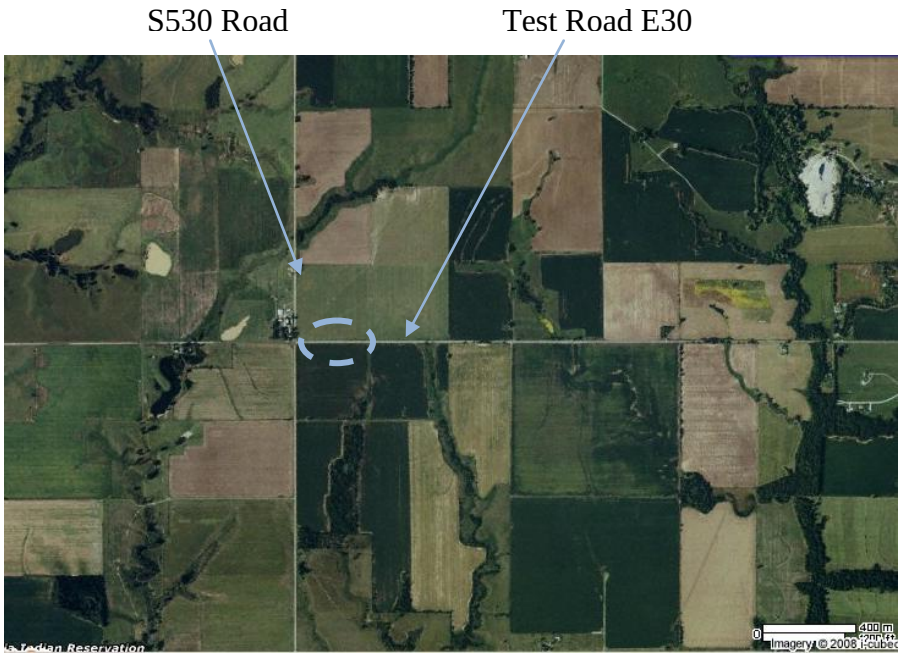

Figure 2.1 Location of Test Road in Cardin, Ottawa County, Oklahoma

Figure 2.2 Test Road Site Before Construction, Looking West

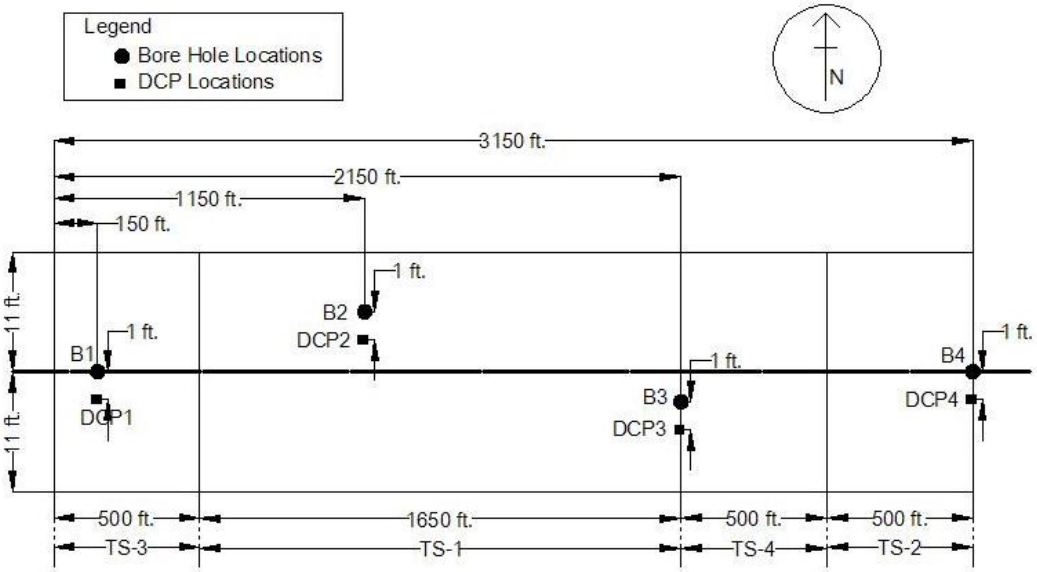

Figure 2.3 Locations of Boreholes and DCP Tests at Test Site

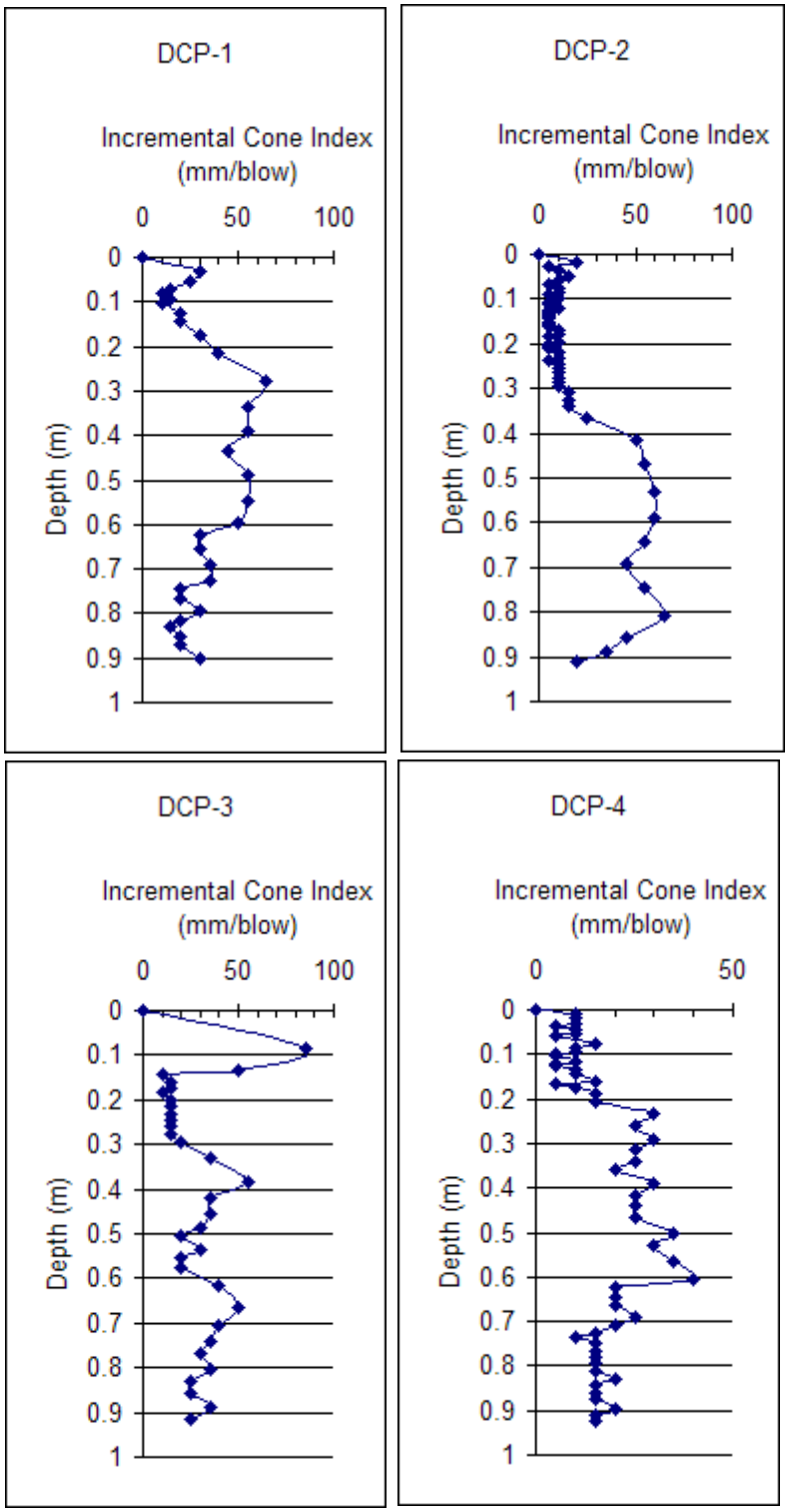

Figure 2.4 Summary of Dynamic Cone Penetration (DCP) Test Results

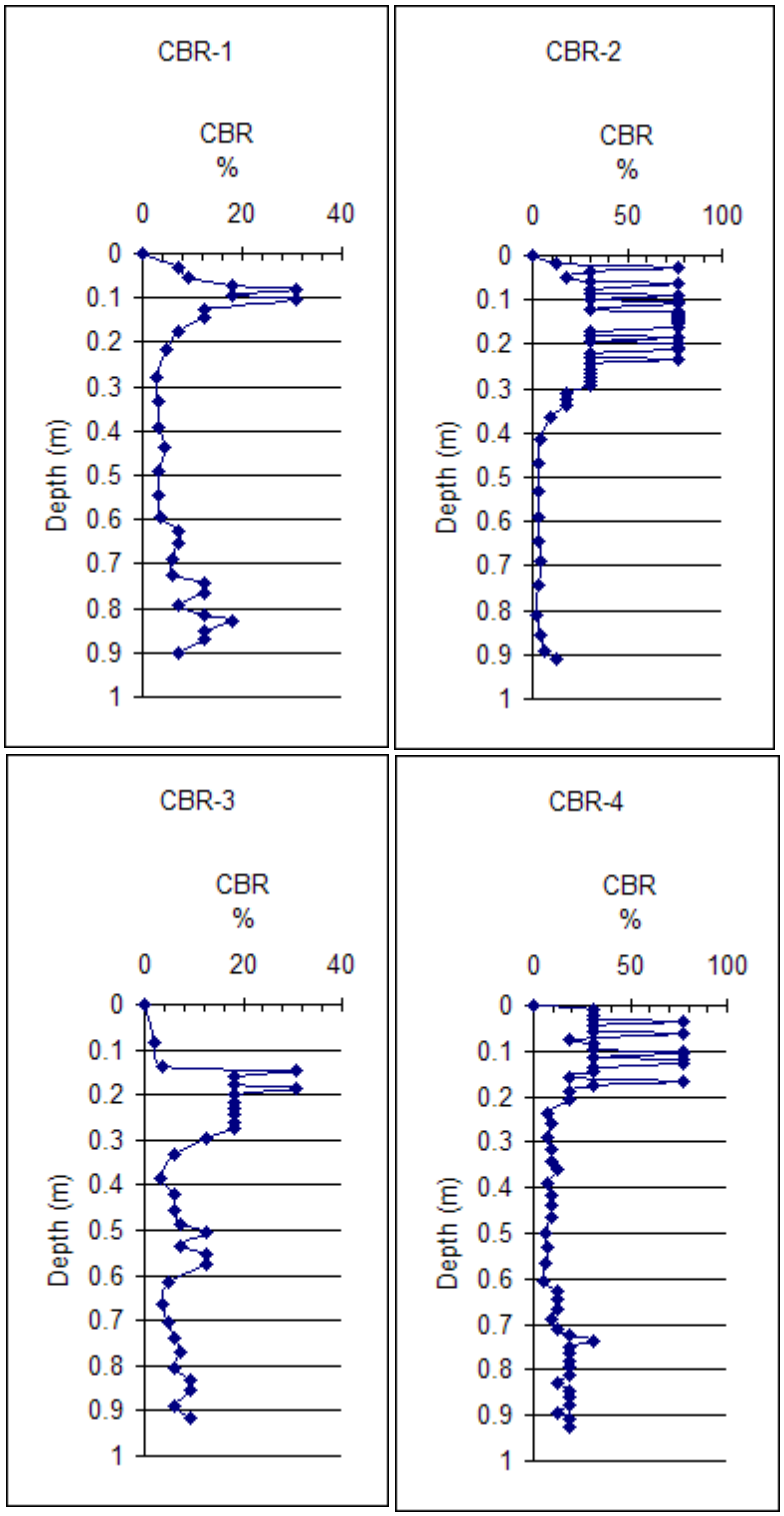

Figure 2.5 Summary of CBR Results Based on DCP Tests

CHAPTER 3 CONSTRUCTION REPORT

3.1 General

This chapter is devoted to presenting the construction phases of the Test Road. An introduction of the different sections of the Test Road is also presented.

3.2 Construction of the Test Road

As mentioned in Chapter 2, a Test Road was constructed on County Road E30 in Ottawa County, Oklahoma to evaluate the performance of CFA-stabilized chat, CKD-stabilized chat, and chat-asphalt surface and base courses. Also, an important objective of this study was to demonstrate the use of pile run chat in an environmentally appropriate manner. This report covers only the engineering aspects of the field demonstration. Environmental testing and monitoring were conducted under separate funding and findings will be presented in a separate report.

3.2.1 Test Road Sections

To evaluate the effect of chat as a stabilized aggregate base, the Test Road was divided into four sections, as shown in Figure 3.1. The first section starting from the intersection of county roads S530 and E30, designated as TS-3, has a length of approximately 500-ft. A typical profile of this section is shown in Figure 3.2. TS-3 consists of four layers. (1) The top layer is 1.5-in. thick; it consists of type "S5" chat-asphalt containing 80% pile run chat. (2) The layer below is a 2.5-in. thick chat-asphalt of type "S3." This mix contains 50% pile run chat (Tri-State Asphalt) blended with locally available limestone. (3) The third layer has a thickness of 6-in. It consists of subgrade soil stabilized with 10% CFA. (4) The bottom layer is the existing subgrade soil. It is basically fat clay (having liquid limit at 63 and plasticity index of 34) with some reddish brown mottles, as described in Section 2.2.2.

The second section starting from the east end of TS-3 is designated as TS-1. It has an approximate length of 1,650-ft. This section is paved with the same chat-asphalt surface and base courses as in TS-3. The chat-asphalt surface course has a thickness of 1.5-in., while the chat-asphalt base course has a thickness of 2.5-in. These layers are overlaid on top of a stabilized-chat layer. The stabilized-chat layer has a thickness of 6-in. and it consists of pile run chat (Sooner Pile) stabilized with 10% CFA. The three layers are underlain by the existing composite chat/soil subgrade, as shown in Figure 3.3.

The third section, designated as TS-4, starts from the east end of TS-1 and extends 500-ft. to the east, as shown in Figure 3.1. This section consists of a top layer of 1.5-in. thick chat-asphalt surface course with 80% pile run chat (Tri-State Aspalt) (Figure 3.4). The layer below is a 2.5-in. thick chat-asphalt base course of type "S3". The third layer consists of CKD-stabilized chat having a thickness of 6-in. This layer is underlain by the existing chat/soil subgrade layer.

The fourth section, designated as TS-2, has a length of 500-ft. A typical profile of this section is shown in Figure 3.5. This section is essentially same as TS-1 except the thickness of the chat-asphalt base layer is 5-in. instead of 2.5-in. and the thickness of stabilized chat base is 3.5-in. instead of 6-in.

3.2.2 Construction

The sequence of construction of the Test Road is shown in the flow chart in Figure 3.6. Broadly, the construction of the Test Road was divided into three phases. The first phase consisted of grading, leveling, and compacting the existing subgrade. The second phase consisted of constructing the stabilized base, and the last phase involved paving the road with chat-asphalt base and surface courses. These phases are discussed in the following sections.

3.2.3 Treatment of the Existing Subgrade

The existing subgrade was graded, leveled, and compacted so that a reasonable conformity with the typical sections, grades, and density was achieved, as specified by ODOT (1999). The work started on October 4, 2004 and was completed in two days. The subgrade was graded uniformly using a motor grader. The motor grader, manufactured by John Deere (model number 770 CH having 155-185 HP), had a weight of about 32,780-lb. It had a turning radius of 22-ft. and a blade size of 14-ft. by 2-ft. Since the site was relatively uniform, no additional fill materials were needed from external sources. Following the grading operation, the surface was compacted with the help of an Ingersoll Rand vibratory roller (model number SD-100/115), as shown in Figure 3.7. On average, two to three passes with strong vibrations and one pass without any vibration were needed to achieve the desired level of compaction. A nuclear density gauge, shown in Figure 3.8, was used to measure the *in-situ* density of the compacted subgrade. The field density (determined by the nuclear gauge) was compared with the laboratory moisture-density results. The moisture-density curve of the subgrade soil (from area around borehole B-4 and depth between 2-in. and 9-in.) is shown in Figure 3.9. From Figure 3.9, the maximum dry density (MDD) of chat/soil subgrade is approximately 126 pcf at the optimum moisture content (OMC) of 6.4%. For simplicity, the nuclear density gauge was calibrated with respect to this MDD. From a visual inspection of the soil profile as well as DCP data, it is recognized that both the MDD and OMC would be different in different test sections. If the field density was not between 95% and 100% of the MDD, additional passes were made. Figure 3.10 shows the layout of the 11 locations selected for density measurements. A comparison between the field and laboratory densities is presented in Table 3.1. From Table 3.1, the densities in the field ranged between 96% and 102% of the MDD obtained from the Proctor tests. As noted above, since the

moisture-density relationship was established from soil from only one location due to time constraints, it may not be applicable for subgrade soils throughout the Test Road. Therefore, some variations in the maximum field compaction levels were observed. Also, the moisture contents in the subgrade soil (from the nuclear density gauge), at these locations (having compaction level more than 100%) were different (5.8%, 4.4%, and 6.2%) than the OMC obtained from the laboratory (6.4%). Overall, the compaction level achieved was considered acceptable in accordance with the ODOT specifications (ODOT, 1999).

3.2.4 Hauling and Spreading of Chat, CFA and CKD

Pile run chat was hauled from the Sooner Pile, located about 6 miles from the Test Road site, on October 7, 2004. Figure 3.11 shows a photographic view of a truck unloading the chat at the test site. Two trucks were used for hauling chat at a rate of one trip per 45 minutes, each carrying about 20 tons per trip. The chat was spread with a motor grader (Figure 3.12) on the compacted subgrade. The un-compacted thickness of the pile run chat, called loose lift thickness, was kept larger than the desired thickness after compaction. The loose lift was maintained at 5-in. in section TS-4 where the compacted thickness of the stabilized-chat was targeted to be 3.5-in (Figure 3.13). The loose lift thickness was maintained at 7-in. in sections TS-1 and TS-2, where the compacted thickness of the stabilized-chat was targeted to be 6-in. Loose lift thicknesses were monitored manually as shown in Figure 3.13. Windrows, having a height of about 12-in., were constructed with extra chat laid along the edges of the road using the motor grader blades. Windrows were used to help protect CFA and CKD from wind after being spread on the loose chat (see Figure 3.14). No chat was laid in section TS-3, since TS-1 did not contain any stabilized-chat base. Table 3.2 shows the consumption of chat in each test section for the construction of the stabilized base. Altogether, about 1,933 tons of chat were utilized for the base

course construction. CFA and CKD were hauled from Lafarge Corp., Tulsa in trucks, unloaded (see Figure 3.15) and spread with the help of a motor grader.

3.2.5 Mixing and Compaction

The mixing operation followed the spreading of chat and CFA/CKD on October 8, 2004. The mixing and compaction continued through October 13, 2004. A water tanker and a pulver mixer were used for *in-situ* mixing of chat with CFA and CKD. The water supply from the truck was adjusted to 2.996[2] gallons per square yard in TS-2 to 5.63 gallons per square yard in TS-4 and, to 4.28 gallons per square yard in TS-1 (as per the OMC for the respective sections). It is important to note that the work related to TS-3 started after the completion of the other three sections. This approach facilitated the construction sequence, since TS-3 does not contain a stabilized-chat base.

A pulver mixer, also called a stabilizer (model number RS325), manufactured by CMI (Terex), having a power of 330 HP with M11 Turbocharged engine, was used for mixing. The width of the mixer was 6.2-ft. Hence, the mixer had to be used in four parallel passes (along the length of the road) in order to cover the entire width of the pavement. As shown in Figure 3.16, the pulver mixer followed the water tanker, mixing the chat with CFA/CKD. The teeth of the pulver mixer were lowered down to the depth of the loose lift of the chat to ensure through mixing.

A 14-ton vibratory roller manufactured by Ingersoll Rand (SD-100/115) was used to compact the stabilized-chat. Figure 3.17 shows the roller compacting the stabilized-chat mix. A pattern of four passes with heavy vibratory mode and two passes with static mode (no vibration) was followed to reach the desired density. Heavy vibratory mode helps in compaction of the chat-CFA/CKD mix at or near maximum dry density. Static mode helps in smoothing the surface

[2] See Appendix A for details

of the compacted base. A nuclear density gauge was used to check the quality of compaction. The results of the density tests are shown in Table 3.3. From Table 3.3 it can be observed that compaction achieved in sections TS-2, TS-4 and TS-1 was in the range of 88% to 95% with an average compaction of approximately 94%.

After completion of compaction of the stabilized-chat bases for TS-1, TS-2, and TS-4, heavy rainfall occurred for two days forcing the work to be shut down. On the third day, the research team examined the Test Road and found out that the moisture contents at different locations in TS-3 ranged between 11% and 14%. These values are approximately 4.5% and 7.5% higher than the optimum moisture content (OMC) of the subgrade soil in this section. Also, these moisture contents were 2.5% and 6.5% higher than the OMC value of the subgrade soil with 10% CFA. No attempts were made to let the section dry out to a lower moisture content due to time and weather constraints. The work was resumed by scarifying the wet subgrade to a depth of 6-in. using a ripper (see Figure 3.18). After that, CFA was spread on top of the scarified layer and mixed thoroughly using the pulver mixer. The vibratory roller, described earlier, was used to compact the CFA-stabilized chat-soil. The achieved density was approximately 88% of the maximum dry density, determined from the Proctor test. The presence of high moisture content in the mixture prior to compaction was responsible for such a low field density.

3.2.6 Curing

After compaction, the compacted stabilized-chat base was coated with an SS-5 emulsion (a slow-setting emulsion) to protect it from moisture infiltration and to assure a suitable environment for the chemical reaction to take place. The emulsion was spread on the road with the help of a tanker equipped with a sprayer attached to the rear of the truck to achieve a uniform spraying. The rate of application of emulsion was about 0.05 gallons per square yard. Figure 3.19

shows the compacted stabilized-chat base covered with the emulsion for curing. After coating, the road was closed to traffic for 14 days to allow the stabilized layer to cure. However, some farm vehicles used the compacted base prematurely resulting in localized base failures (see Section 3.2.7).

3.2.7 Problems Encountered During the Curing Period and Before Paving

During the curing period (14 days), a heavy rainfall occurred in Ottawa County, causing flooding in the Test Road area. Actually, TS-3 was entirely soaked with water as shown in Figure 3.20, because of its low elevation compared to other sections. Due to the lack of a well defined drainage network in this area, water was trapped at this specific section, and caused a significant increase in the moisture content. It is also important to note that the stabilized base was subjected to traffic, specifically, fire trucks. Excessive moisture contents in TS-3 and traffic loads caused a major deformation (rut) in TS-3. Consequently, the research team[3] decided to place a limestone aggregate base on the top of the existing layer (Figure 3.21). The limestone utilized had a maximum aggregate size of 1.5-in. and a percent passing No. 200 sieve of approximately 4%. The average thickness of this unbound aggregate base layer is 6-in.

3.2.8 Paving

Placing the Chat-Asphalt Base Course - The paving-related work started on November 11, 2004. Day temperatures during this period varied between 47°F to 54°F. Prior to laying any chat-asphalt layer, the cured stabilized-chat base was first cleaned with the help of a mechanical broom, as shown in Figure 3.22. The chat-asphalt base course (S3-type mix) was laid first on the east bound lane and then on the west bound lane. The design sheet for the S3 mix is attached in

[3] Research Team consisted of Mr. Bill Adams (Owner of Tri-State Asphalt Company), Mr. Tim Murphy (Project Manager, Glover Construction), Mr. John Clarke (County, Commissioner, Ottawa County), Dr. Tom Landers (University of Oklahoma), Dr. Musharraf Zaman (University of Oklahoma), Dr. Joakim Laguros (University of Oklahoma), and Mr. Danny Gierhart (Bituminous Engineer, Oklahoma Department of Transportation).

APPENDIX B. Paving was performed with a paver manufactured by Caterpillar (model number AP-1050B) having a hopper capacity of 21-cu ft. An Extend-A-Mat B Screed (Model 10-20B) was used to achieve a paving width of 10-ft. A total of 1,079 tons of S3 mix was consumed for all the sections. After laying the mix, a vibratory roller (see Figure 3.23) was used for compaction. A pattern of two passes with heavy vibratory mode and one pass with static mode (no vibration) was followed by the vibratory roller to achieve the desired density. A light-duty roller manufactured by Bomag (Model number: BW 100 AD-3), also called a finish roller, was used to smooth the asphalt surface and remove the marks of the vibratory roller. A nuclear density gauge was used to check the level of compaction (see APPENDIX C for details). A total of 147 measurements were taken throughout the Test Road. Statistical analyses were performed to find the mean and standard deviation. It was found that the field densities of the compacted chat-asphalt base course were in the range of 126 pcf (85% compaction) and 147 pcf (99% compaction) with an average density of 132 pcf (91% compaction). The target density for the chat-asphalt base course was approximately 141 pcf (94% compaction).

Problems Encountered Prior to Placing the Chat-Asphalt Surface Course – Another problem was encountered by the research team after construction of the chat-asphalt base course. On November 15, 2004, the research team visually inspected the Test Road. Localized chat-asphalt base course failure was observed at three locations in TS-2, as shown in Figure 3.24. The research team suspects that failure resulted due to the farm vehicles that used the Test Road prematurely. Figure 3.25 shows a photographic view of the failure zone with the overlaying chat-asphalt base removed. The area was compacted and repaved as shown in Figure 3.26, prior to placing the chat-asphalt surface course.

Placing the Chat-Asphalt Surface Course – A tack coat was applied on the chat-asphalt base course before the construction of surface course. The tack coat ensures proper bonding between the two adjoining asphalt layers. An "S5" type chat-asphalt mix was used for the construction of the surface course. The design sheet for the S5 mix is included in APPENDIX B. As noted earlier in Section 2.3.2, the original binder content was changed from a PG 70-28 to a PG 64-22, as advised by the research team, for the following reasons: (1) presence of polymer in PG 70-28 would result in rapid setting of the mix in cold weather, making it difficult, if not impossible, to achieve proper compaction; and (2) using a PG 64-22 binder would be more economical.

The chat-asphalt surface course was laid on the west bound lane first starting from the east end of the project (from section TS-2). A total of 654 tons of S5 mix was consumed. A nuclear density gauge was used for checking the densities at regular intervals during construction of the chat-asphalt surface course. The densities of the compacted chat-asphalt surface course were found to be in the range of 117 pcf (80% compaction) and 146 pcf (99% compaction) with an average density of 132 pcf (90% compaction). The compaction data obtained during the construction of chat-asphalt surface course are attached in APPENDIX C. The target density for chat-asphalt surface course was 138 pcf (94% compaction). Variations of densities achieved in the field from the target density may have resulted due to limited resources utilized (such as quality of compacter). Figure 3.27 shows a photographic view of the completed Test Road.

Table 3.1 Summary of Density Measurements Using Nuclear Density Gauge

Point	**Typical Section**	**Dry Density From Field** (pcf)	**Moisture From Field** (%)	**MDD From Lab.** (pcf)	**OMC From Lab.** (%)	**Relative Comapaction** (%)
1	TS-3	126.2	4.2	126	6.4	100
2	TS-3	124.7	7.5	126	6.4	99
3	TS-1	126.7	6.2	126	6.4	101
4	TS-1	126.2	7.8	126	6.4	100
5	TS-1	126.5	3.6	126	6.4	100
6	TS-1	127.4	5.8	126	6.4	101
7	TS-1	121.4	8.7	126	6.4	96
8	TS-1	128.1	4.4	126	6.4	102
9	TS-4	123.5	9.7	126	6.4	98
10	TS-2	125.8	7.8	126	6.4	100
11	TS-2	120.9	8.9	126	6.4	96
Average		125.2	6.8	126	6.4	99

Table 3.2 Summary of Chat (Sooner Pile) Usage, in Different Sections

Typical Section No.	**Length (ft.)**	**Thickness (inches)**	**Properties**	**Tons of chat**
TS-1	1,650	6	Chat + 10% CFA	1,237
TS-2	500	3.5	Chat + 10% CFA	266
TS-3	500	6	Subgrade + 10% CFA	0
TS-4	500	6	Chat + 10% CKD	303
			Total	**1806 Tons**

Table 3.3 Summary of Density Measurements on Stabilized-Chat Base

				Depth of Testing						Laboratory Results		
				2"		4"		6"				
Section	D (ft.)	L (ft.)	Pt. No.	MDD (pcf)	w (%)	MDD (pcf)	w (%)	MDD (pcf)	w (%)	MDD (pcf)	OMC (%)	R (%)
TS-2	100	9	1	130	8.1	133	8.1	-	-	138	6.1	95
	250	17	2	125	8.8	128	8.8	-	-	138	6.1	92
	400	9	3	127	9.8	128	9.8	-	-	138	6.1	92
TS-4	600	9	4	-	-	126	8	125	8.2	136	7.1	93
	750	17	5	-	-	120	12	119	12.2	136	7.1	88
	900	9	6	-	-	128	9.1	126	11.2	136	7.1	94
TS-1	1,300	9	7	-	-	123	8.1	122	8.8	138	6.1	89
	1,600	17	8	-	-	129	5.1	126	5.2	138	6.1	92
	1,900	9	9	-	-	131	5.3	129	5.5	138	6.1	94
	2,200	17	10	-	-	122	5	120	5.1	138	6.1	88
	2,500	9	11	-	-	129	5.7	130	5.2	138	6.1	94
TS-3	2,750	9	12	-	-	117	8.5	115	8.6	126	8.6	92
	2,850	9	13	-	-	116	13	112	13.4	126	8.6	91
	2,850	13	14	-	-	120	9.7	120	8.5	126	8.6	95
	2,850	17	15	-	-	123	7.9	128	7.2	126	8.6	98
	1,950	9	16	-	-	112	15.9	112	12.6	126	8.6	89
	1,950	13	17	-	-	108	16.1	111	10.7	126	8.6	87
	3,050	9	18	-	-	112	14.5	110	14.3	126	8.6	88
	3,050	13	19	-	-	112	14.2	111	12.3	126	8.6	89
	3,050	17	20	-	-	125	8.8	121	9	126	8.6	98

R (%) : Relative Compaction

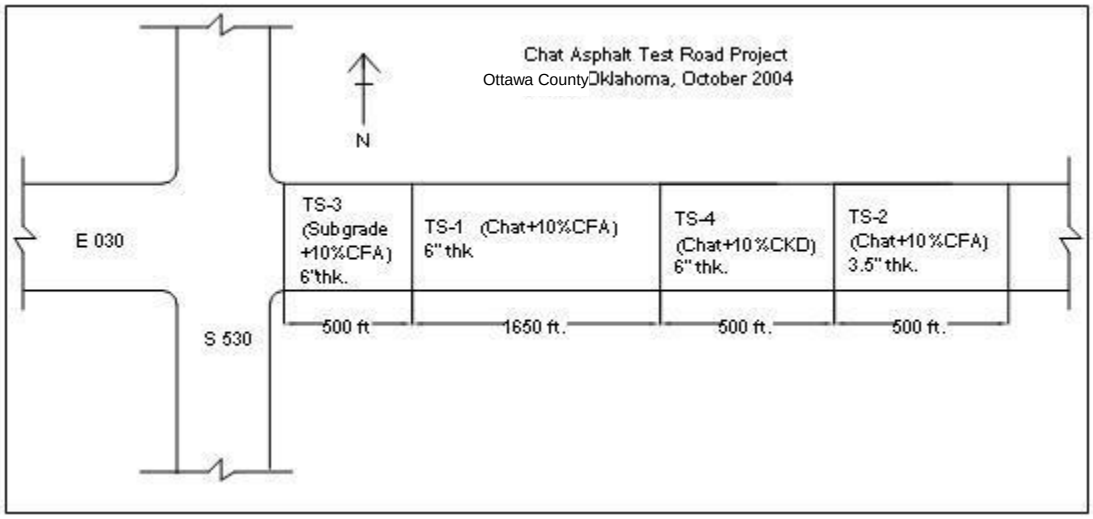

Figure 3.1 Plan View of Four Test Sections

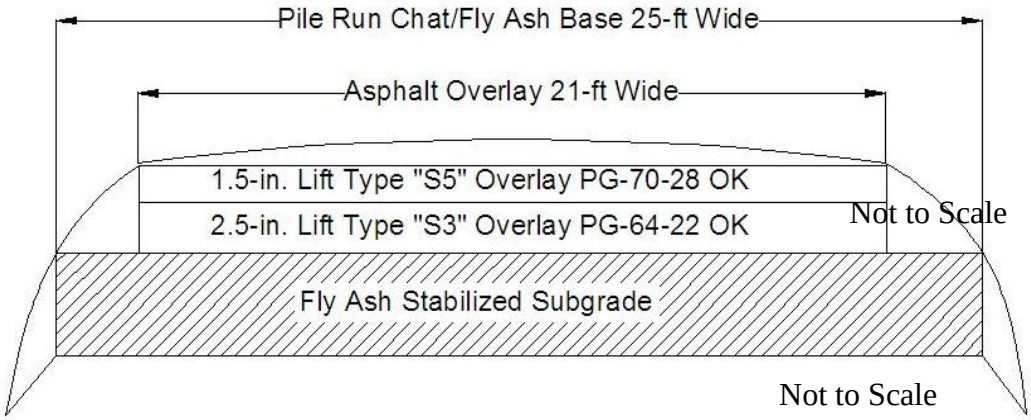

Figure 3.2 Sketch of Typical Section No. 3 (TS-3)

Not to Scale

Figure 3.3 Sketch of Typical Section No. 1 (TS-1)

Not to Scale

Figure 3.4 Sketch of Typical Section No. 4 (TS-4)

Not to Scale

Figure 3.5 Sketch of Typical Section No. 2 (TS-2)

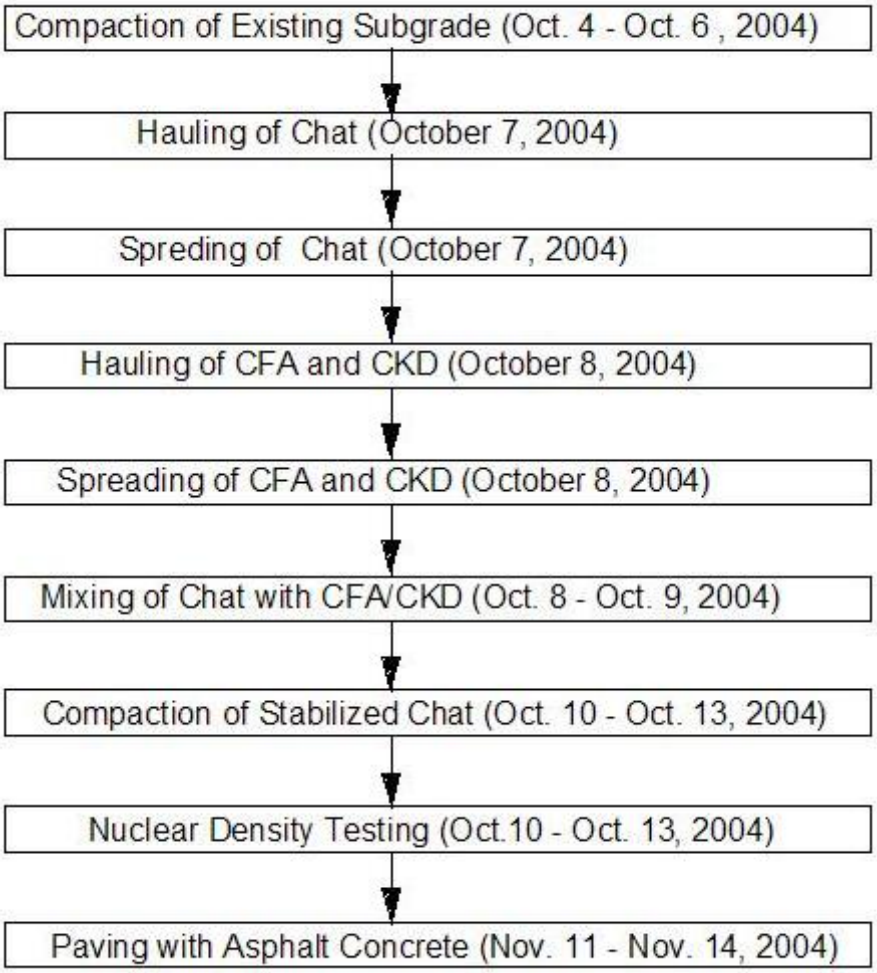

Figure 3.6 Flow Chart of Construction Process

Figure 3.7 Compaction of Existing Subgrade

Figure 3.8 Measuring Density Using a Nuclear Density Gauge

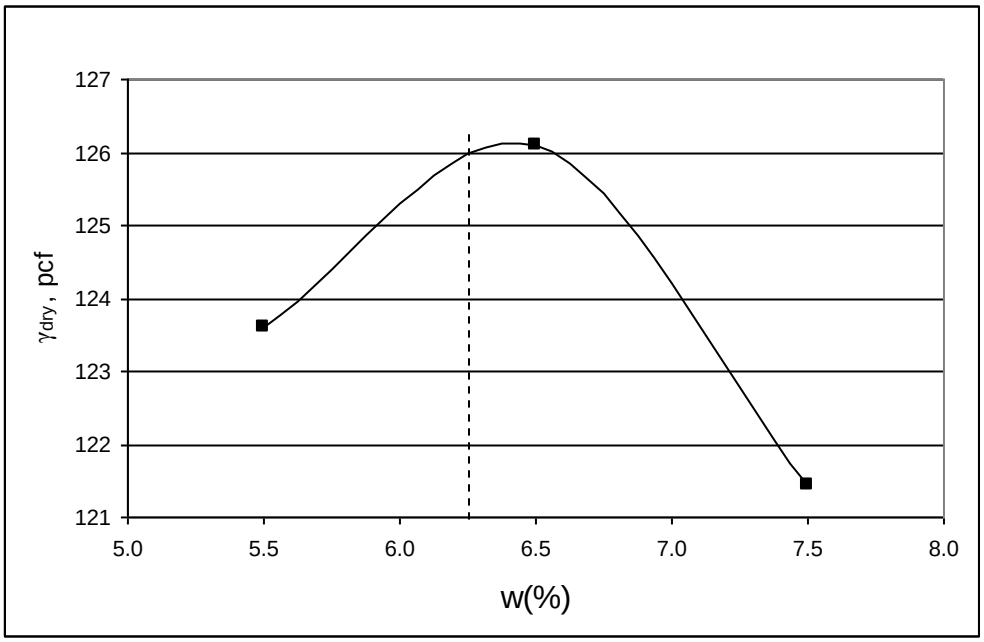

Figure 3.9 Moisture-Density Relationship for Subgrade Soil in Section TS-2

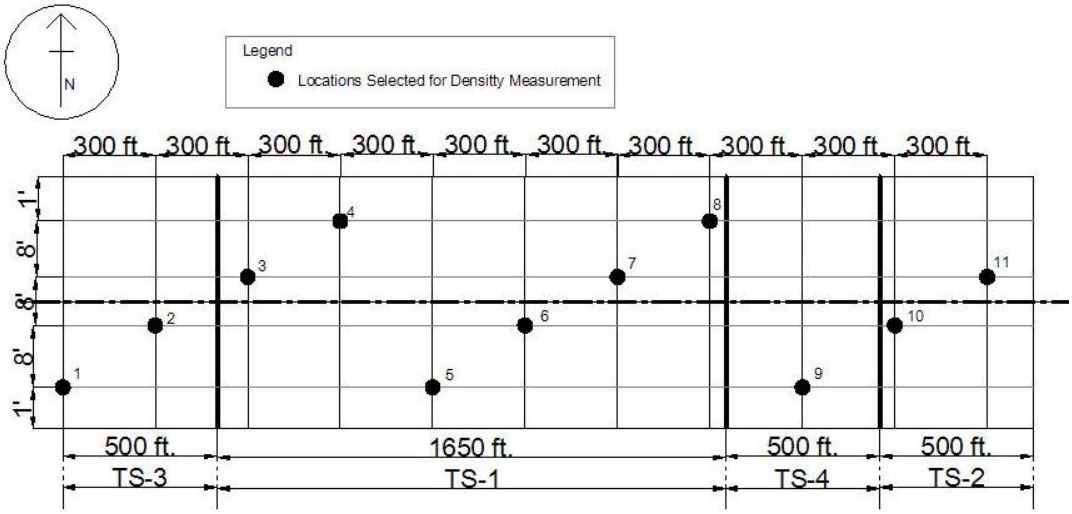

Figure 3.10 Layout of Locations for Density Measurement During Subgrade Compaction

Figure 3.11 Chat (Sooner Pile) Unloading at Test Road Site

Figure 3.12 A Motor Grader Spreading Chat (Sooner Pile)

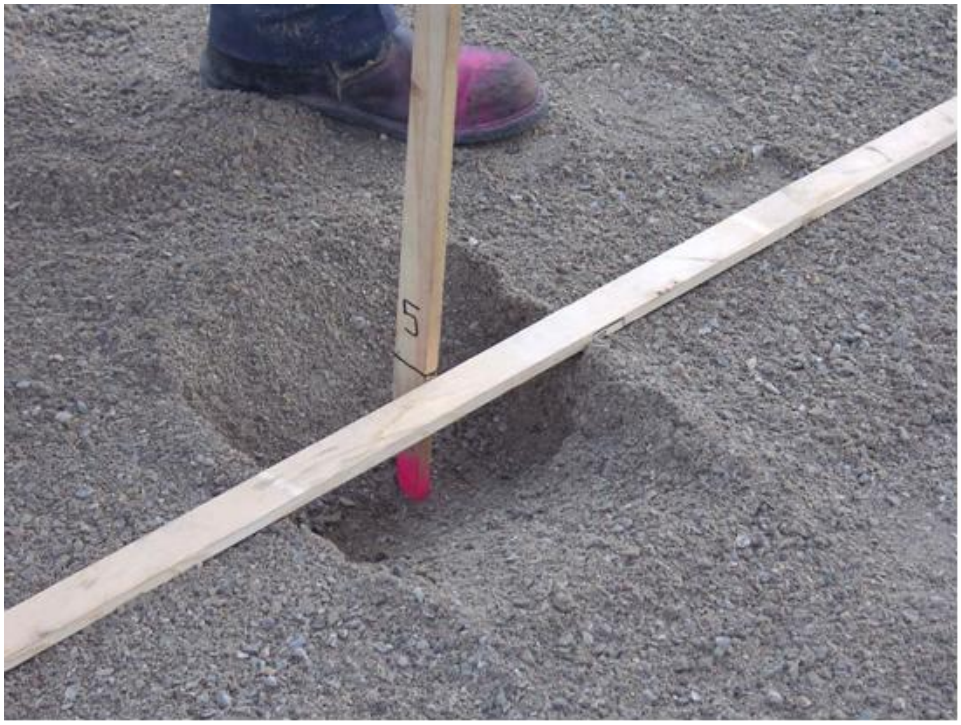

Figure 3.13 Measurement of Loose Lift Thickness

Figure 3.14 Windrows Constructed Along the Road Edges

Figure 3.15 Unloading CKD from Truck

Figure 3.16 Water Tanker and Pulver Mixer Working at the Site

Figure 3.17 Vibratory Roller Compacting Stabilized-Chat (Sooner Pile)

Figure 3.18 Scarification of Subgrade Soil in Section TS-3

Figure 3.19 Emulsion Coated Stabilized-Chat Base

Figure 3.20 Flooding in Section TS-3

Figure 3.21 Reconstruction of Section TS-3

Figure 3.22 Mechanical Broom

Figure 3.23 Paving Operation in Progress

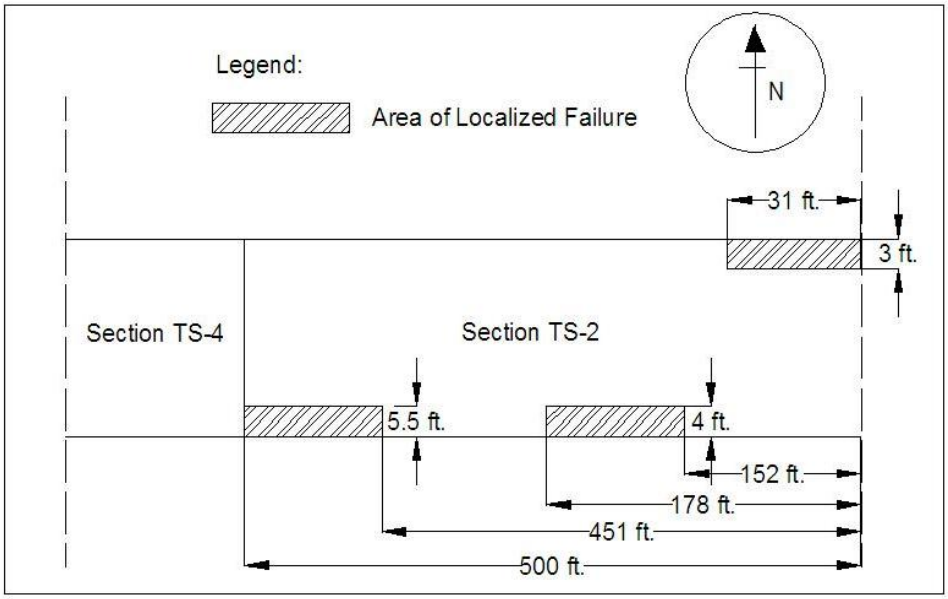

Figure 3.24 Locations of Localized Base Failures in Section TS-2

Figure 3.25 Localized Failure Zone with Overlaying Chat-Asphalt Base Course Removed

Figure 3.26 Corrected Failure Zone

Figure 3.27 Test Road After Paving with Chat-Asphalt Surface Course

CHAPTER 4 LABORATORY TESTING OF STABILIZED-CHAT BASE

4.1 General

Bench scale laboratory tests were performed in this project to examine the suitability of stabilized chat as a roadway base. Unwashed chat from the Sooner Pile was stabilized with class C fly ash (CFA) and cement kiln dust (CKD), and specimens of stabilized chat were prepared for laboratory testing. The laboratory tests performed in this study include moisture-density, seismic modulus, unconfined compressive strength, and indirect tensile strength. Results of this experimental program are presented in this chapter.

4.2 Properties of Pile Run Chat

The chat used in this study was collected from the Sooner Pile, located in Ottawa County, Oklahoma. A photographic view of the Sooner chat pile is shown in Figure 4.1. Bulk chat samples were collected and conventional laboratory tests, namely, gradation, Log Angeles (L.A.) abrasion, and specific gravity were performed in accordance with the ASTM test procedures.

4.2.1 Gradation

The gradation curve of the pile run chat was determined in accordance with the ASTM C 136 test method. Figure 4.2 shows the average gradation curve (based on five replicates) compared to the upper and lower limits of Type A aggregate base specified by the Oklahoma Department of Transportation (ODOT, 1999). From Figure 4.2, the maximum aggregate size (MAS) of the pile run chat is 9.5-mm (3/8-in.), while the lower limit of MAS in Type A aggregate base is 19.1-mm (3/4-in.). The percent passing US Standard No. 200 sieve is approximately 4.7% (determined in accordance with ASTM C-117 test method), which is on the lower end of the gradation curves for a type A aggregate base. Comparatively, the percent passing US Standard No. 200 sieve for the Kenoyer North Pile was approximately 3.5%

(Wasiuddin et al., 2005 and Teredesai et al., 2005). It is an indication that the latter has less fines than the Sooner Pile. Also, from Figure 4.2, it is evident that the average gradation curve for pile run chat does not fall within the gradation band marked by the upper and the lower limits of a Type A aggregate base. For grain size more than 0.8 mm (US Standard No. 20 sieve), the gradation curve for pile run chat lies outside the gradation limits for a Type A aggregate base. It is an indication that pile run chat does not satisfy the ODOT gradation requirements, and thus would generally not be used alone as an aggregate base. Since one of the objectives of this study was to demonstrate the use of stabilized-pile run chat as a roadway base, no other aggregates were blended with chat although the pile run chat did not meet the specifications (ODOT, 1999).

4.2.2 L.A. Abrasion

Los Angeles (L.A.) abrasion tests were performed on three replicates in accordance with the ASTM C 131 test method. The average L.A. abrasion value was found to be approximately 21 with a standard deviation of 0.43. These L.A. values indicate that pile run chat is a very hard material and meets the ODOT specifications (L.A. abrasion value smaller than 40) for an aggregate base. Comparatively, Teredesai et al. (2005) reported an average L.A. abrasion value of approximately 18 for chat from the Kenoyer North pile.

4.2.3 Specific Gravity

The specific gravity of both coarse (larger than US Standard No. 4 sieve) and fine particles (smaller than US Standard No. 40 sieve) were evaluated in accordance with the ASTM C 127 and ASTM C 128 test methods, respectively. It was found that the specific gravity of the coarse particles was about 2.51. Comparatively, the fine aggregate had a specific gravity of approximately 2.68.

4.3 Properties of Class C Fly Ash (CFA)

Class C fly ash (CFA) used in this study was provided by Lafarge Corporation, Tulsa, Oklahoma. For consistency in results, CFA from the same source was used in both field and laboratory studies. The CFA used had a combined silica, alumina, and ferric oxide (SAF) content of approximately 64%. The average calcium oxide (CaO) content was approximately 24%. Additional physical and chemical properties are presented in Table 4.1. The loss on ignition (LOI) value for CFA was approximately 0.16%.

4.4 Properties of Cement Kiln Dust (CKD)

Cement kiln dust (CKD) for this study was also provided by Lafarge Corporation of Tulsa, Oklahoma. It is known that the physical and chemical properties of CKD vary from plant to plant, depending on the feed materials, type of kiln operation, dust collection facility, and the fuel used. As in the case of CFA, the same CKD source was used in both field and laboratory studies to ascertain consistency. CKD had a CaO content of approximately 48% and a SAF content of approximately 20%. The self-cementing characteristic (hydraulic reactivity) is expressed in terms of hydration modulus, which is defined as the ratio of CaO and SAF (Kamon and Nontananandh, 1991). The hydration modulus is determined with respect to Alite and Belite cement compounds. Their chemical compositions and the calculated hydraulic moduli are given in Table 4.1. For material quality control (acceptance/rejection) purposes, Kamon and Nontananandh (1991) suggested that a cement stabilizer should have a hydration modulus between 2.67 and 1.76, respectively for Alite and Belite. From Table 4.1, the hydration modulus of CKD is 2.47 which satisfies this requirement. Having self-cementing characteristics, CKD is expected to react with soils or aggregates in a manner similar to Portland cement (Miller et al., 1999). Also, the Oklahoma ODOT recommends a hydration ratio between 2.0 and 2.6 for CKD when used as a stabilizing agent for soils. Since no separate limits are available for aggregates,

these limits are used here for chat. The alkali content (K_2O + Na_2O) in CKD was about 1.48% whereas, the total amount of reactive oxides was found to be 22.3%. Note that for better reactivity the total amount of reactive oxides in CKD should be more than 18%, which is the case here.

It can be noted from Table 4.1 that CFA and CKD differ significantly in terms of their chemical composition. These differences in chemical composition are expected to influence the engineering properties of the stabilized specimens and the performance of stabilized bases in the field. The LOI for CKD was 26.03% compared to only 0.16% for CFA. It is an indication that CKD-stabilized specimens would have lower strength than CFA-stabilized specimens (Lafarge, 2005; Kamon and Nontananandh, 1991).

4.5 Moisture-Density Relationship

Moisture-density relationships for pile run chat (Sooner Pile) and stabilized-chat were established in accordance with the ASTM D 1557 test method. A summary of the optimum moisture content (OMC) and the maximum dry density (MDD) is presented in Table 4.2 (Teredesai, 2005). It is evident that stabilized-chat (either with CFA or CKD) has higher OMC and MDD than unstabilized-chat. As recommended by Khoury (2001), the amount of water added to the mixture before compaction was recorded and the actual moisture content (w_b) of a specimen was calculated. After mixing and compaction, the specimen was extruded and placed in an oven at 110°C (230°F) to determine its actual moisture content (w_a). The dry densities were calculated using this water content (w_a). Correction to the water content for oversize particles (i.e., above US sieve No. 4) was applied in accordance with the ASTM D 4718 test method. The moisture-density curves for pile run chat, chat stabilized with CFA and chat stabilized with CKD, are shown in Figures 4.3, 4.4 and 4.5, respectively. The OMC for pile run chat was

approximately 6.0%. The average OMCs for chat mixed with CFA and CKD were found to be 6.6% and 7.7%, respectively. Also, it can be observed that the difference between w_a and w_b are 0.1%, 0.5% and 0.65% for pile run chat, chat stabilized with 10% CFA and chat stabilized with 10% CKD, respectively. A larger difference between w_a and w_b for stabilized-chat is mostly due to loss of moisture during mixing and chemical reactions during compaction and drying (Khoury, 2001). The OMC based on w_b was used to mold specimens for unconfined compressive strength (UCS) tests and indirect tensile strength tests. The maximum dry density (MDD) of pile run chat increased from about 127.7 pcf to 138.4 pcf (8%) due to mixing with CFA. The corresponding increase in MDD for CKD-stabilized chat was from 127.7 pcf to 136.7 pcf (7%). The OMC of chat mixed with CFA was only slightly higher (about 1%) than that of the pile run chat. Khoury (2001) reported a one percent unit increase in OMC due to the addition of 10% CFA to limestone aggregate. Also, Baghdadi et al. (1995) reported that the OMC of dune sand increased by 2% due to the addition of 10% CKD.

4.6 Test Matrix

The test matrix used for the laboratory testing program is shown in Table 4.3. Specimens of two different sizes (4-in. in diameter x 8-in. in height and 6-in. in diameter x 4.58-in. in height) were molded.

The 4-in. x 8-in. specimens were divided into two groups: (1) specimens in Group 1 were tested for the seismic modulus (E*) using a non-destructive technique (NDT), and then tested for their UCS; and (2) specimens in Group 2 were used to evaluate the elastic modulus using the unloading-reloading curve (stress-strain) and the UCS values. Specimens of size 6-in. x 4.58-in. were tested only for the indirect tensile strength.

4.7 Specimen Preparation

Cylindrical specimens (4-in. x 8-in.) were prepared using a split mold, as shown in Figure 4.6. Pile run chat was dried in an oven at 110°C (230°F) for approximately 24 hours to ensure that it was dry. The amount of CFA or CKD to be added was determined from the dry weight of the aggregate. The amount of water needed was calculated using the OMC determined from the moisture-density relationships. Mixing of chat and CFA or CKD was done in accordance with the method reported by Khoury (2001). In the first step, dry chat was uniformly mixed with CFA or CKD. In the second step, 1/3 of the total amount of water was added and mixed thoroughly. In the third step, an equal amount of water was added and mixed until a uniform mix was obtained. In the last step, the remaining water was added and mixed thoroughly to obtain a uniform mixture. After mixing, each specimen was compacted in 5 layers, each with 60 blows of a 5.5-lb rammer to reach approximately 98% MDD. Specimens were extruded from the mold. Plastic plates were placed on top and bottom of each specimen and a rubber membrane was placed arround the specimen in order to retain the moisture and to protect it from any damage. Specimens of size 6-in. x 4.58-in. were molded in the same way as specimens of size 4-in. x 8-in. except that they were molded in 3 layers instead of 5 layers. After compaction, specimens were cured in a humidity room with a controlled temperature of 21°C (71°F) and a relative humidity of 95%.

4.8 Seismic Modulus Test

This test consisted of placing an accelerometer at one end of the specimen and tapping the other end with a hammer having a load cell attached to it, as shown in Figure 4.7. Both the accelerometer and hammer are connected to a data acquisition system that is connected to a laptop computer. Software has been developed to acquire and process the time records from the accelerometer and the load cell. The response measured with the accelerometer contains an

oscillation that corresponds to the standing wave energy within the specimen (Nazarian et al., 2003a).

The frequency of oscillation was determined by transforming the two signals (acceleration and load) into frequency-domain using the Fast–Fourier Transform (FFT) technique and then normalizing the acceleration amplitude with the load amplitude. The variation of normalized amplitude as a function of frequency, which is called transfer function, contains peaks that correspond to the oscillation of the standing waves. A computer program written by Khanna (2006), in Matlab 7.0, was used to convert the hammer and the accelerometer data into frequency domain. The program is attached in APPENDIX D. A typical plot of the transfer function is shown in Figure 4.8. The transfer function shows two distinct peaks. The first peak corresponds to shear resonance (f_s), while the second peak corresponds to longitudinal resonance (f_p). Knowing the resonant frequency (f_p in Hz), mass density (ρ in lb/in^3), and the length of the specimen (*l* in inches), the seismic modulus (E*), could be determined using the following equation (Nazarian et al., 2003a):

$$E^* = \rho\,(2\,f_p\,L)^2 \qquad (4.1)$$

The seismic modulus tests were performed on only four stabilized-chat specimens of which two were stabilized with 10% CFA (CFA-1 and CFA-2) and the other two with 10% CKD (CKD-1 and CKD-2). Each specimen had a height of 8-in. and a diameter of 4-in., so that the height to diameter ratio was 2, as recommended by Nazarian et al. (2003a). After testing for seismic modulus, these specimens were tested for UCS. This scheme was feasible since the seismic modulus test is a non-destructive technique. A total of 12 hits was performed on each specimen. Figure 4.9 shows a transfer function for a CFA-stabilized chat specimen. The graph shows two clearly visible peaks. The first peak indicates the shear resonant frequency, while the

second peak indicates the resonant frequency with the highest amplitude; these peaks were identified in accordance with the procedure described by Nazarian et al. (2003a). The resonant frequency corresponding to the second peak was used for calculation of seismic modulus (E*), using Eqn. 3.1. Plots of transfer function for all the specimens are attached in APPENDIX E.

Results for each specimen were statistically analyzed to identify the potential of any outliers in accordance with the *box-plot and whiskers method* (McClave et al., 2001). The spread of data was assumed to be in a normal distribution. The box plot is based on the quartiles of a data set. Quartiles are the values that partition the data set into four groups, each containing 25% of the measurements. The lower quartile Q_L is the 25th percentile, the middle quartile is the median Qm (50th percentile), and the upper quartile Q_U is the 75th percentile, as shown in Figure 4.10. Interquartile range (IQR) is determined as IQR = Q_U - Q_L. For construction of the "tails" of the box plot, two sets of limits, called inner fences and outer fences, are used (see Figure 4.10). Inner fences are located at a distance of 1.5(IQR) from the hinges. Emanating from the hinges of the box are lines called whiskers. Two whiskers extend to the most extreme observation inside the inner fences. Values beyond the inner fences are deemed potential outliers because they are extreme values that represent relatively rare occurrence. Less than one-hundredth of 1% (0.1% or 0.0001) of the measurements from mound-shaped distributions are expected to fall beyond the outer fences, which would be considered outliers.

Figures 4.11 to 4.14 show the box plots of CFA-stabilized and CKD-stabilized chat specimens. From these figures, it is evident that the results of CFA-1 and CKD-2 did not show any outliers, while CFA-2 and CKD-1 showed the existence of four and one outliers. Identified outliers were removed, and the results were statistically analyzed. A summary of the statistical analysis for each replicate is presented in Table 4.4 and Table 4.5.

It can be observed from Table 4.6 that the seismic modulus (E*) of CFA-1 varied between 520 ksi and 830 ksi with an average modulus of 766 ksi, whereas the seismic modulus CFA-2 was between 850 ksi to 915 ksi with an average modulus of 904 ksi. Comparatively, CKD-stabilized specimens had lower E* values than CFA-stabilized specimens. Specifically, the E* values of CKD-1 ranged between 103 ksi and 302 ksi with an average modulus of 224 ksi, whereas CKD-2 had a seismic modulus ranging between 103 ksi and 266 ksi with an average modulus of 168 ksi. Heterogeneity in specimens could be partly responsible for such variations.

Additional statistical analyses were performed on the duplicates of the stabilized specimens. A summary is presented in Table 4.6. From Table 4.6, it can be seen that the seismic modulus (E*) of the CFA-stabilized chat was approximately 868 ksi with a standard deviation of about 42 ksi. The E* of CKD-stabilized chat was about 197 ksi with a standard deviation of about 71 ksi. From these results, the seismic modulus of CFA-stabilized chat specimens was approximately 440% higher than that of CKD-stabilized chat specimens. Difference in E* values due to type of stabilizing agent could be attributed to the difference in the chemical reactions in the stabilization process. Similar observations have been reported previously in the literature. For example, Zaman et al. (1998) reported that limestone aggregate stabilized with CFA has a higher modulus compared to the corresponding modulus of CKD-stabilized specimens. In a recent study, Khoury (2005) reported that the difference in the performance of CKD- and CFA-stabilized specimens is attributed to the amount of cementitious hydration and crystal formation in a cementitious mixture. X-ray diffraction (XRD) and scanning electron microscopy (SEM) tests were used by Khoury (2005) to justify such differences in strength due to different stabilizing agents. XRD and SEM tests revealed a higher intensity in hydration and crystal formation in CFA-stabilized specimens than in CKD-stabilized specimens. In this study, SEM

and XRD tests were not performed. Use of such tests would be helpful in explaining the variations in the data.

4.9 Unconfined Compressive Strength (UCS) Test

Unconfined compressive strength (UCS) tests were conducted in accordance with the ASTM D 5102-96 test method. Specimens were loaded in an MTS frame (Figure 4.15) at a constant strain rate of 1% (of sample height) per minute, which is equivalent to 0.08-in. per minute for the specimen configuration used here. Deformation values were recorded during the test using a linear variable differential transformer (LVDT) having a 0.2-in. stroke length. The load values were obtained from the load cell. A specimen is subjected to several unloading-reloading cycles before subjecting it to failure. Figure 4.16 shows a typical stress-strain curve obtained from the UCS test using unloading-reloading cycles. A straight line "AB" is drawn through the first unloading-reloading curve, (see Figure 4.16). Similarly, lines "CD", "FG" and "HI" are drawn through the other three unloading-reloading curves, as shown. The average slope of these lines is treated as the elastic modulus (E_{UCS}) of the stabilized specimen. Typical failure of a CFA-stabilized specimen under compressive loading is shown in Figure 4.17.

Five additional specimens for each stabilizing agent were molded and tested for UCS; specimens tested for seismic modulus were also tested for UCS, as previously mentioned. A summary of the UCS test results for CFA-stabilized and CKD-stabilized specimens is presented in Table 4.7. The UCS values of CFA-stabilized specimens varied between 137 to 197 psi, with an average value of 163 psi and a standard deviation of 18 psi. As for the CKD-stabilized specimens, the UCS values ranged from 56 psi to 94 psi with an average value of approximately 73 psi and a standard deviation of 17 psi. Table 4.8 shows the summary of the statistical analyses of UCS results of CFA-stabilized specimens and CKD-stabilized specimens. From Table 4.8, the

average UCS value of CFA specimens is 163 psi and the average UCS of chat specimens stabilized with CKD is about 73 psi. Similar values have been reported in the literature although different aggregates were utilized. For example, Pandey (1996) reported an average UCS value of 177 psi for Meridian aggregates stabilized with 10% CFA. Zhu (1998) reported a UCS of 166 psi for aggregates stabilized with 10% CKD. Although chat is a much stronger material (based on the L.A. abrasion values) than Meridian aggregates, gradation of the material is an important factor affecting the compressive strength of the material. The maximum aggregate size (MAS) for Meridian aggregates was 1.5-in, whereas for chat the MAS is only about 3/8-in. According to Mindess et al. (2002), a larger MAS can result in reduced void spaces and increased density of a specimen, and hence more strength. The average strain at failure of CFA-stabilized specimens was approximately 0.63%, whereas CKD-stabilized specimens had a strain value of approximately 1.18%. This is consistent with previous studies (see e.g., Pandey, 1996; and Zhu, 1998). Khoury and Zaman (2002) reported a strain level of 0.42% at failure for CFA-stabilized aggregates. Pandey (1996) and Zhu (1998) reported strains of 1.05% and 0.95%, respectively, for CKD-stabilized aggregates.

Efforts were made to evaluate the strength of pile run chat compacted at OMC so that the effect of stabilization could be evaluated. A total of three specimens were molded; however, each specimen failed under its own weight, and the UCS tests could not be performed. The UCS of pile run chat was thus considered negligible due to lack of cohesion. Similar observations were reported by Teredesai et al. (2005), who used chat from the Kenoyer North Pile.

4.10 Modulus of Elasticity (E_{UCS})

Elastic modulus (E) was determined from the unloading-reloading curves from the UCS test on stabilized-chat specimens (Table 4.9). Figures 4.18 and 4.19 show the unloading-

reloading curves of selective CFA-stabilized specimens and CKD-stabilized specimens, respectively. The initial loading part of the curve is concave in nature due to closure of micro-cracks during the loading. Also, the top surface of the specimen on which the platen of the load cell rests, is not completely smooth. This leads to stress concentration in the specimen initially. A summary of the actual modulus results (before removing the outliers) is presented Table 4.10. One outlier was identified in the results of CFA-stabilized specimens using the box-plot method discussed earlier and was removed. The revised results (without outliers) are summarized in Table 4.11. It can be noted that removing outliers from the results of CFA-stabilized specimen reduced the standard deviation from 45 ksi to 17 ksi. The average modulus (E_{UCS}) of CFA-stabilized specimens after removing the outliers was found to be approximately 59 ksi, while CKD-stabilized specimens had an average modulus (E_{UCS}) of approximately 25 ksi. Similar results were reported in the literature pertaining to stabilized aggregate bases. For example, Zenieris (1988) reported that the elastic modulus ranged between 28 ksi to 58 ksi for a variety of aggregates stabilized with fly ash. Also, Pandey (1996) reported an average modulus of 42 ksi for Meridian aggregates stabilized with 10% CFA. Another study by Zhu (1998) reported a modulus of about 24 ksi for aggregates stabilized with 15% CKD.

In addition, from Table 4.11 it is evident that the average (E_{UCS}) of CFA-stabilized specimen is approximately twice the value of CKD-stabilized specimens. One explanation points to more hydration and crystal formation in CFA-stabilized specimens than CKD-stabilized specimens. The hydration and crystal formation are responsible for the strength gain and differences in strength. From the aforementioned results, it can also be observed that the seismic modulus (E*) of CFA-stabilized specimens is approximately 14.6 times higher than the elastic modulus obtained from the UCS test. CKD-stabilized specimens also exhibited a higher seismic

modulus (8 times) than the corresponding elastic modulus (E_{UCS}) obtained from the UCS test. Nazarian et al. (2003a) reported that the seismic modulus obtained from this non-destructive test is approximately twice the resilient modulus of the material. No studies, to the authors' knowledge, have addressed the difference between the seismic modulus and the elastic modulus from UCS test for stabilized aggregate bases.

4.11 Indirect Tensile Strength Test

Indirect tensile strength tests were conducted in accordance with the ASTM D 3967-95 method. These tests were performed on five specimens each of CFA-stabilized chat and CKD-stabilized chat. Two 0.2-in. LVDTs were used to record the axial deformation of the specimen. The specimens were loaded at a constant strain rate of 0.02-in./min and load was registered by a 5,000-lb load cell. The experimental set-up is shown in Figure 4.20. A photographic view of a typical failed specimen is shown in Figure 4.21.

A summary of the indirect tensile strength (ITS) test results is presented in Table 4.12. Results show that the average ITS of CFA-stabilized chat was approximately 19 psi, while CKD-stabilized specimens had an average value of approximately 8 psi. Comparatively, the average ITS value was approximately 1/8.6 (11.6%) of the corresponding UCS of CFA-stabilized specimens. As for CKD-stabilized specimens, the corresponding ratio was 1/9 (11.1%). These results are consistent with those of Weng et al. (1998), Baghdadi et al. (1995) and Thompson (1966a). Weng et al. (1998) reported a ITS to UCS ratio of 1/8 (12.5%) for CFA-stabilized aggregates. Baghdadi et al. (1995) and Thompson (1966b) have reported ITS/UCS ratios of 1/7.7 (13%) and 1/7.5 (13.3%), respectively for CKD-stabilized aggregates. Another study by NCHRP (1992) reported that this ratio for a highly stabilized aggregate base can be 1/10 (10%). Figure 4.22 shows minimum, average and maximum values of UCS and ITS for CFA-stabilized chat

and CKD-stabilized chat. From the aforementioned results, it is clear that stabilized-chat specimens exhibited some tensile strength. Indirect tensile strength is an important parameter in designing a pavement structure containing a stabilized-chat layer.

Table 4.1 Chemical Properties of CFA, CKD, Alite and Belite (Lafarge, 2005; Kamon and Nontananandh, 1991)

Chemical Composition	**CFA**	**CKD**	**Alite (C_3S)**	**Belite (C_2S)**
SiO_2	36.55	14.66	24.83	32.50
Al_2O_3	21.45	3.34	1.24	2.13
Fe_2O_3	6.19	1.38	0.94	1.03
CaO	24.23	47.98	72.23	62.83
MgO	5.37	1.83	0.98	0.52
SO_3	1.17	2.78	-	-
Na_2O	1.42	0.22	0.09	0.2
K_2O	--	1.26	0.14	0.3
Na_2O eq	--	1.04	-	-
LOI (%)	0.16	26.03	-	-
Free Lime	-	7.60	-	-
Hydration Modulus	0.37	2.47	2.67	1.76

Note: Hydration Modulus = CaO/(Al_2O_3+ SiO_2+ Fe_2O_3)

Table 4.2 Summary of OMCs and MDDs

Material	**OMC (%)**		**γ_{dry} (pcf)**
	Oven (w_a)	**Controlled (w_b)**	
Pile Run Chat *	6.0	6.1	127.7
Chat + 10% CFA	6.6	7.1	138.4
Chat + 10% CKD	7.7	8.4	136.7

*Sooner Pile

Table 4.3 Specimen Test Matrix for Laboratory Study

Mix	**Specimen Size**	**Number of Specimens**
Pile Run Chat *	4-in. x 8-in.	7
Chat + 10% CFA	4-in. x 8-in.	7
Chat + 10% CKD	4-in. x 8-in.	7
Pile Run Chat	6-in. x 4.58-in.	5
Chat + 10% CFA	6-in. x 4.58-in.	5
Chat + 10% CKD	6-in. x 4.58-in.	5

*Sooner Pile

Table 4.4 Statistical Analysis of NDT Results (E*) for CFA-Stabilized Specimens

Statistical Parameter	**Seismic Modulus (ksi)**	
	CFA-1	**CFA-2**
Mean	766	904
Median	850	913
Standard Deviation	131	22
Minimum	520	850
Maximum	850	915

Table 4.5 Statistical Analysis of NDT Results (E*) for CKD-Stabilized Specimens

Statistical Parameter	**Seismic Modulus (ksi)**	
	CKD-1	**CKD-2**
Mean	224	168
Median	266	146
Standard Deviation	76	54
Minimum	103	103
Maximum	302	266

Table 4.6 Summary of NDT Test Results (E*)

Aggregate	**Stabilizing Additive**	**% Additive**	**Replicate**	**For Each Replicate**		**Total**	
				E^*_{avg} (ksi)	**Std. Dev**	**E^*_{avg} (ksi)**	**Std. Dev**
Chat*	CFA	10	1	766	131	868	42
			2	904	22		
Chat*	CKD	10	1	224	76	197	71
			2	168	54		

*Sooner Pile

Table 4.7 Summary of UCS Test Results

Aggregate	Stabilizing Additive	% Additive	Replicate	UCS (psi)	UCS_{avg} (psi)	Std. Dev. (psi)
Chat*	CFA	10	1	164	163	22
			2	137		
			3	147		
			4	154		
			5	153		
			6	189		
			7	197		
Chat*	CKD	10	1	60	73	17
			2	62		
			3	62		
			4	56		
			5	88		
			6	94		
			7	89		

*Sooner Pile

Table 4.8 Statistical Analysis for the Results of UCS Test

Statistical Parameter	UCS (psi)	
	CFA	CKD
Mean UCS (psi)	163	73
Median	154	62
Standard Deviation	22	17
Sample Variance	497	273
Minimum	137	56
Maximum	197	94

Table 4.9 Summary of Elastic Modulus (E) Results from UCS Tests

Aggregate	Stabilizing Additive	% Additive	Replicate	E (ksi)	E_{avg} (ksi)	Std. Dev. (ksi)
Chat*	CFA	10	1	40	59	18
			2	39		
			3	71		
			4	58		
			5	150*		
			6	84		
			7	63		
Chat*	CKD	10	1	17	25	11
			2	13		
			3	13		
			4	24		
			5	39		
			6	28		
			7	39		

*Sooner Pile

Table 4.10 Statistical Analysis of Elastic Modulus (E) for CFA-Stabilized Specimens Before Removing The Outliers

Statistical Parameter	E_{CFA} (ksi)	E_{CKD} (ksi)
Mean	71	25
Median	58	24
Standard Deviation	45	11
Sample Variance	2096	125
Minimum	39	12
Maximum	150	39

Table 4.11 Statistical Analysis of Elastic Modulus (E) After Removing The Outliers

Statistical Parameter	Elastic Modulus (ksi)	
	CFA	CKD
Mean E (ksi)	59	25
Median	61	24
Standard Deviation	18	11
Sample Variance	306	126
Minimum	39	13
Maximum	84	39

Table 4.12 Summary of Indirect Tensile Strength Test Results

Aggregate	Stabilizing Additive	% Additive	Sample Name	ITS (psi)	ITS_{avg} (psi)	Std. Dev
Chat*	**CFA**	**10**	1	13	19	5
			2	22		
			3	15		
			4	20		
			5	24		
Chat*	**CKD**	**10**	1	10	8	2
			2	7		
			3	9		
			4	5		
			5	8		

*Sooner Pile

Figure 4.1 Sooner Chat Pile, Looking South

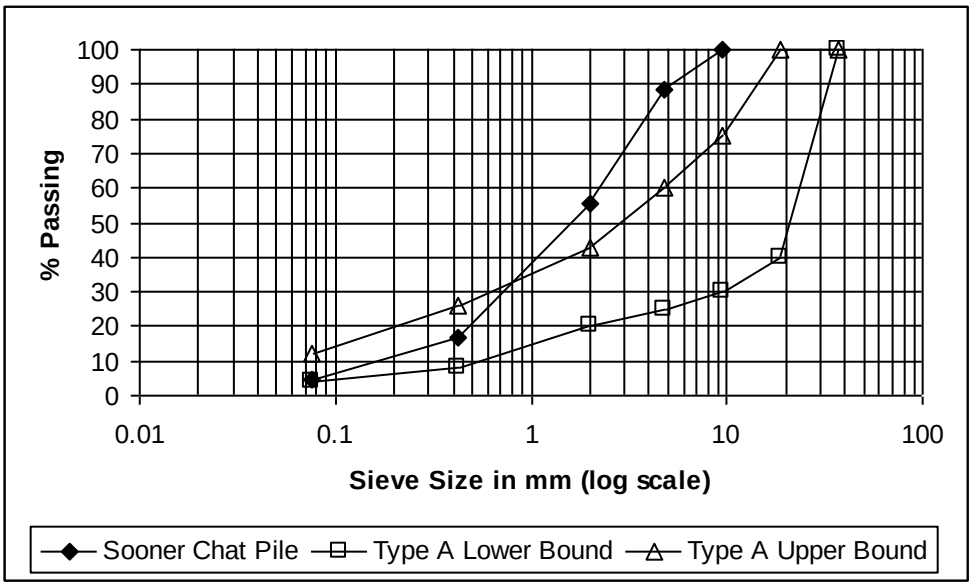

Figure 4.2 Gradation of Pile Run Chat (Sooner Pile)

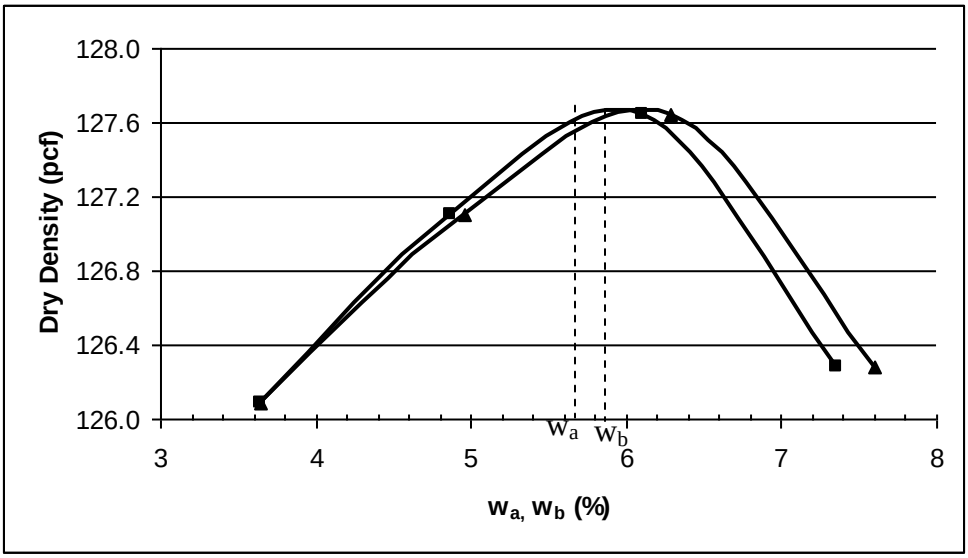

Figure 4.3 Moisture-Density Curve for Pile Run Chat (Sooner Pile); w_a is Moisture Content from Oven Drying, w_b is Moisture Content calculated from Initial Weight of Water and Soil

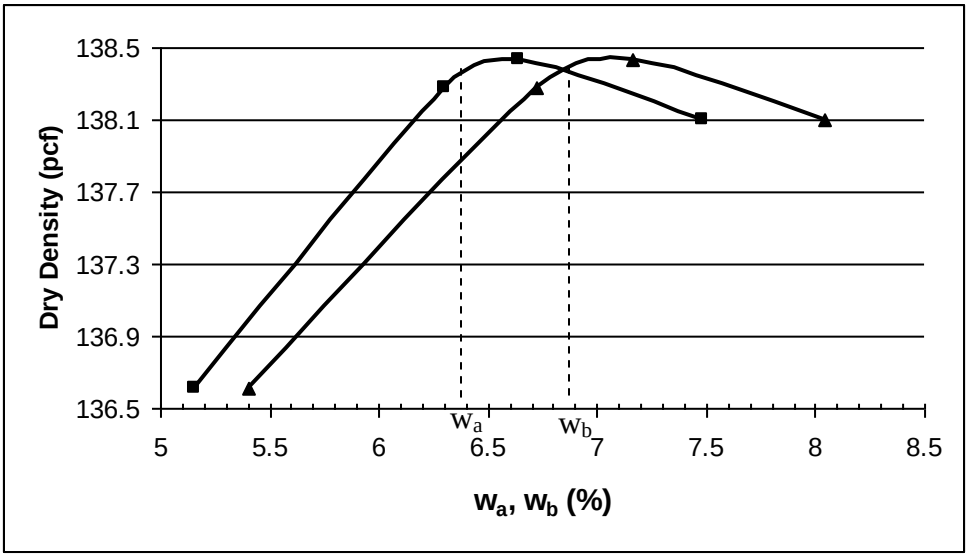

Figure 4.4 Moisture-Density Curve for Chat (Sooner Pile) + 10% CFA

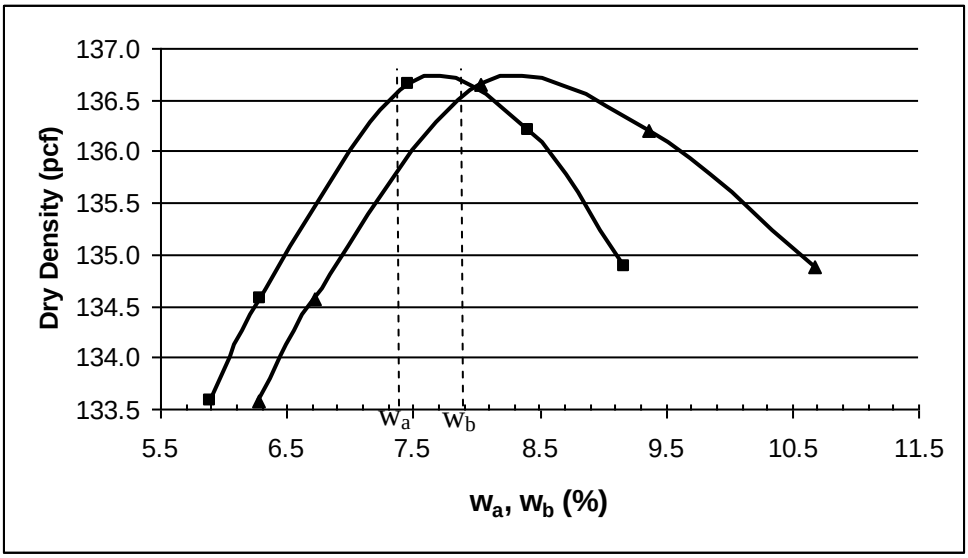

Figure 4.5 Moisture-Density Curve for Chat (Sooner Pile) + 10% CKD

Figure 4.6 Molds and Rammer Used for Specimen Preparation

Figure 4.7 Seismic Test

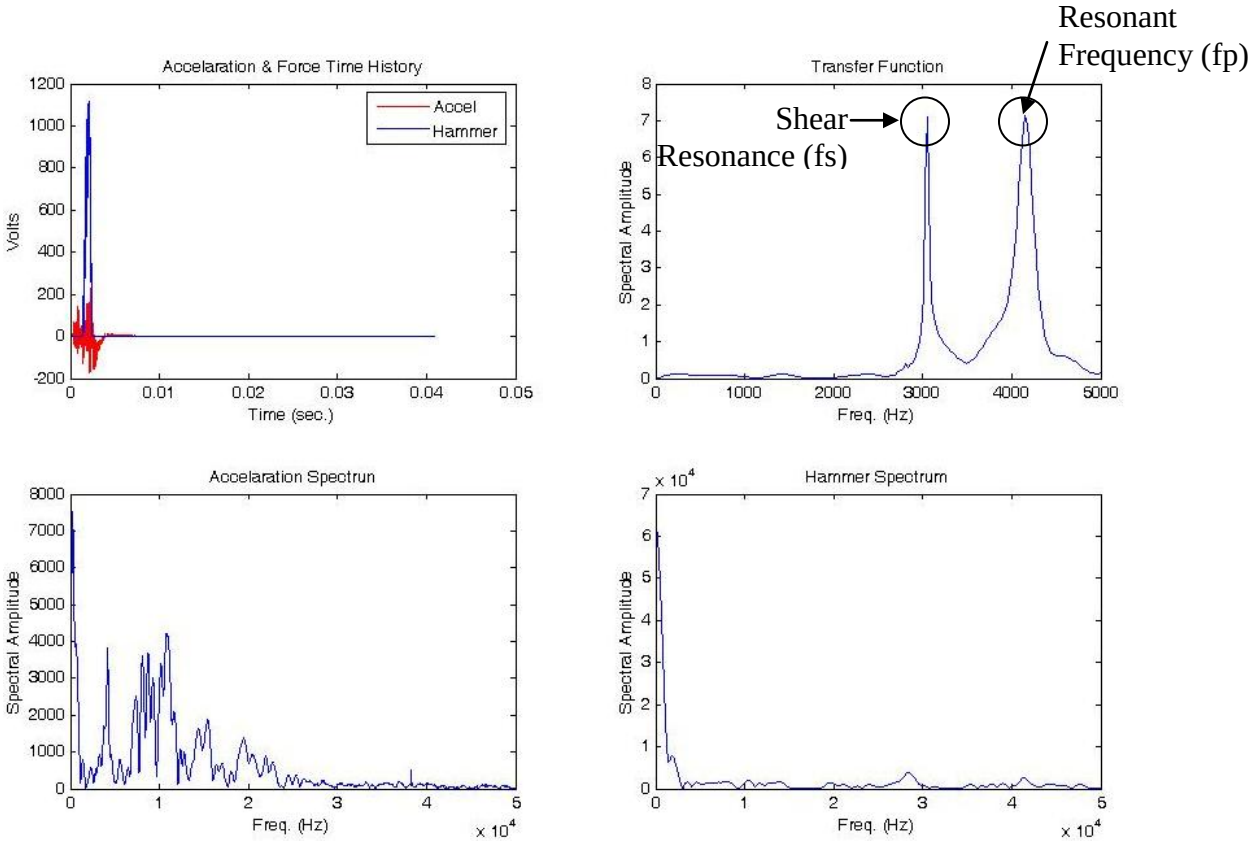

Figure 4.8 Typical Results of a Laboratory Seismic Test

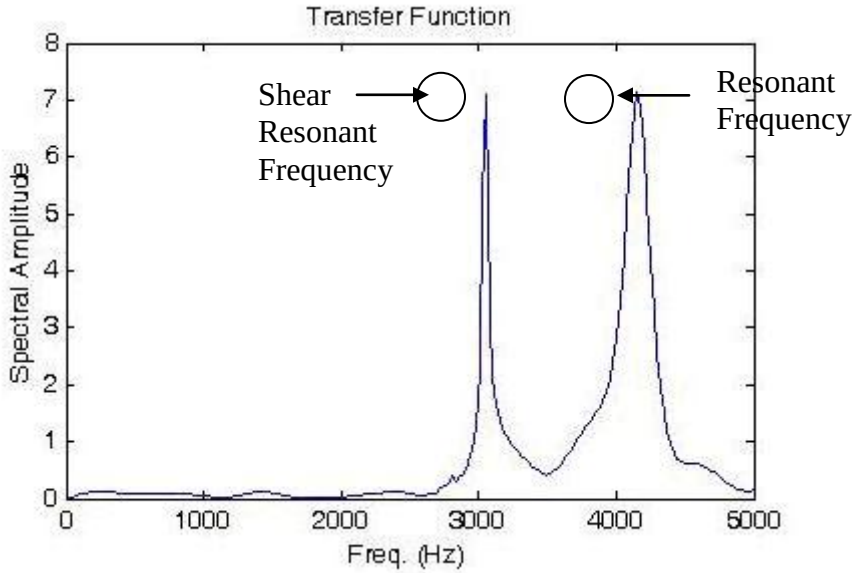

Figure 4.9 Output of NDT for Specimen "CKD-2"

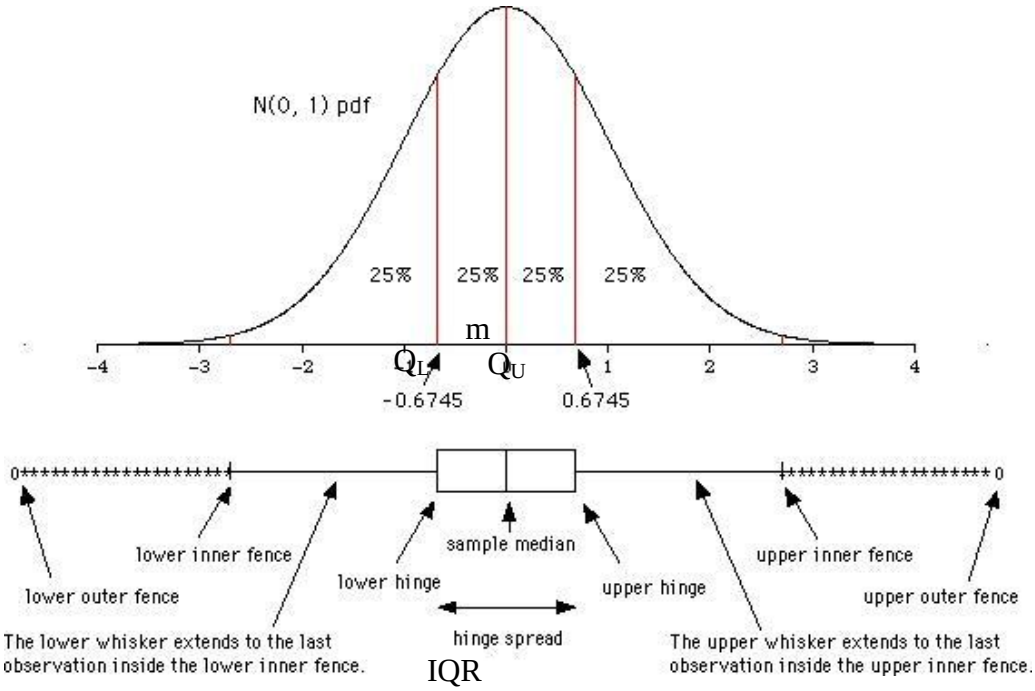

Figure 4.10 Concept of Box Plot (Reproduced from McDonald 1999)

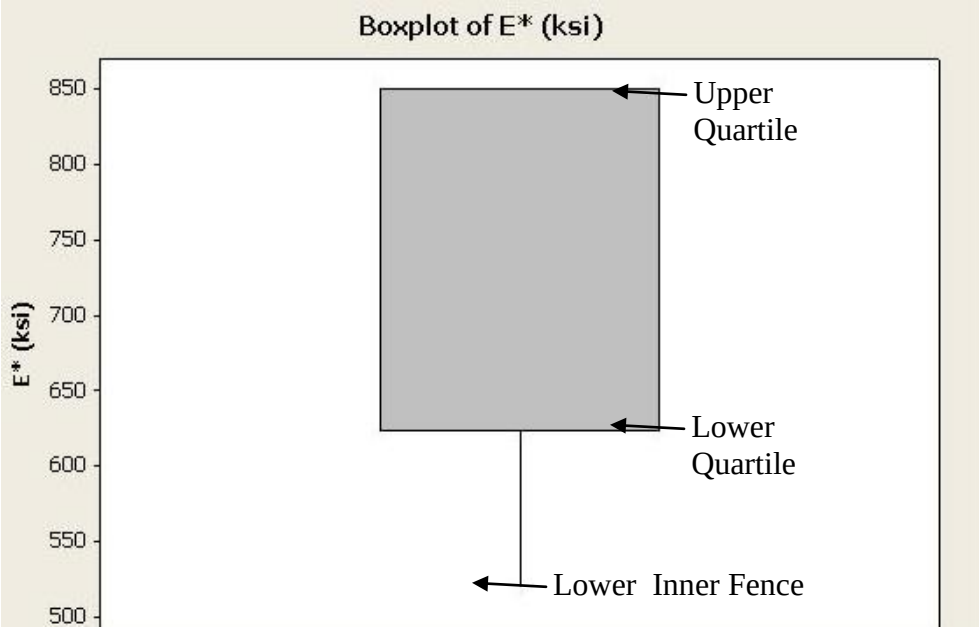

Figure 4.11 Box Plot for CFA-Stabilized Chat Specimen "CFA-1"

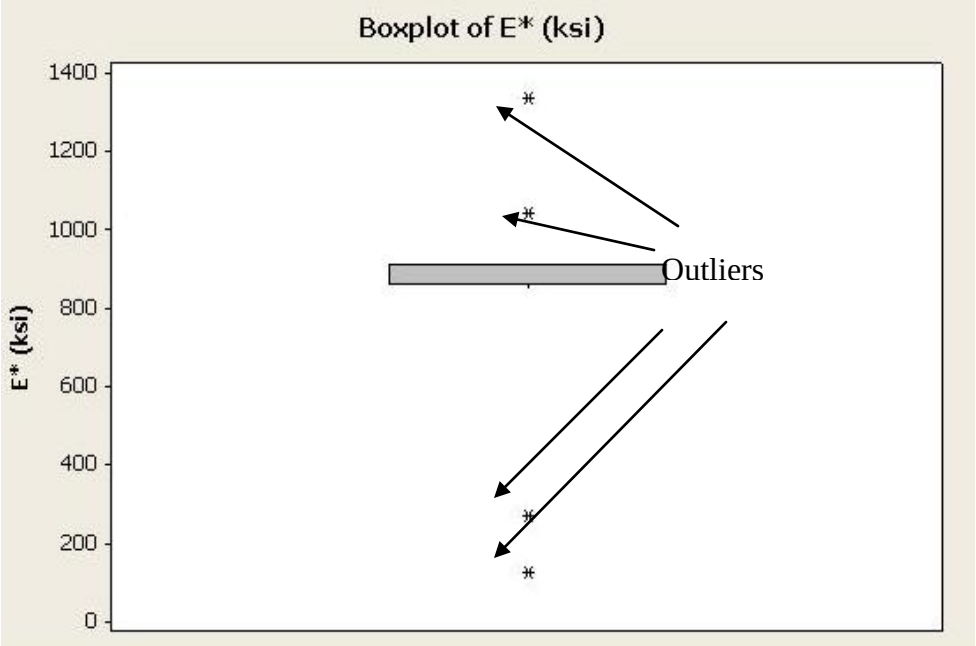

Figure 4.12 Box Plot for CFA-Stabilized Chat Specimen "CFA-2"

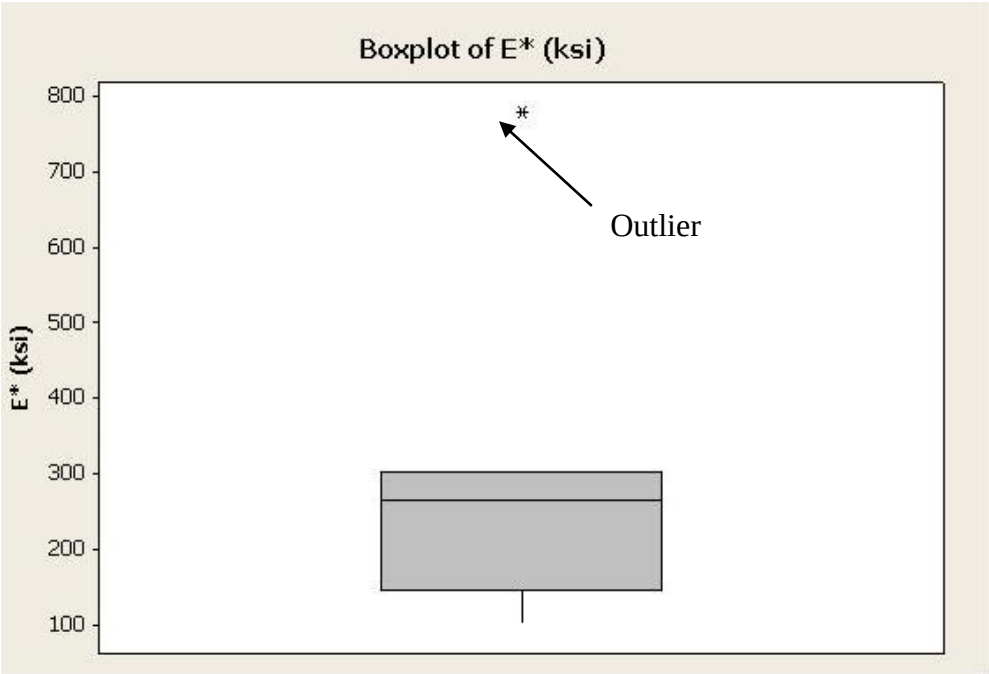

Figure 4.13 Box Plot for CKD-Stabilized Chat Specimen “CKD-1”

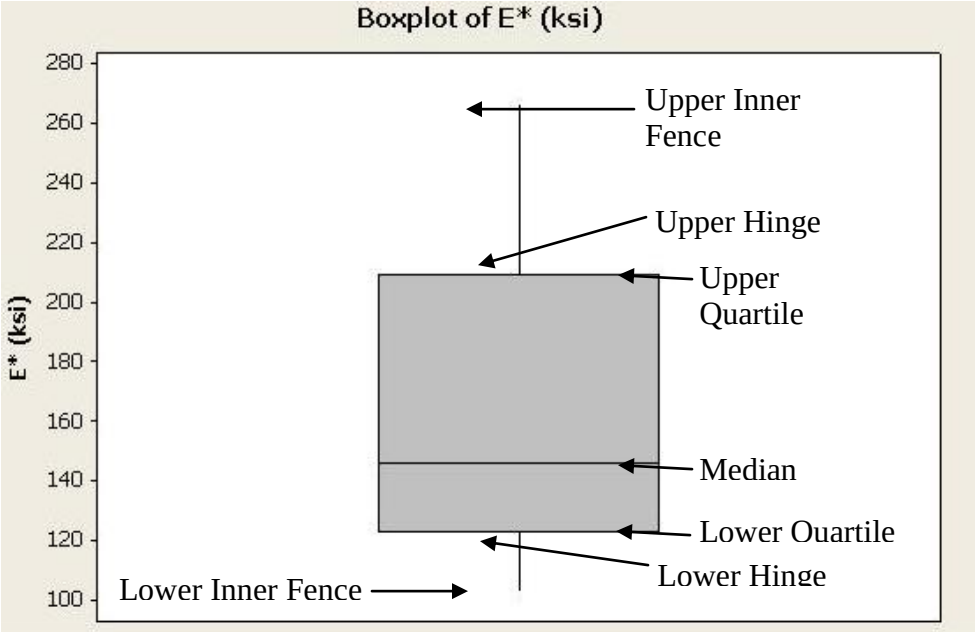

Figure 4.14 Box Plot for CKD-Stabilized Chat Specimen “CKD-2”

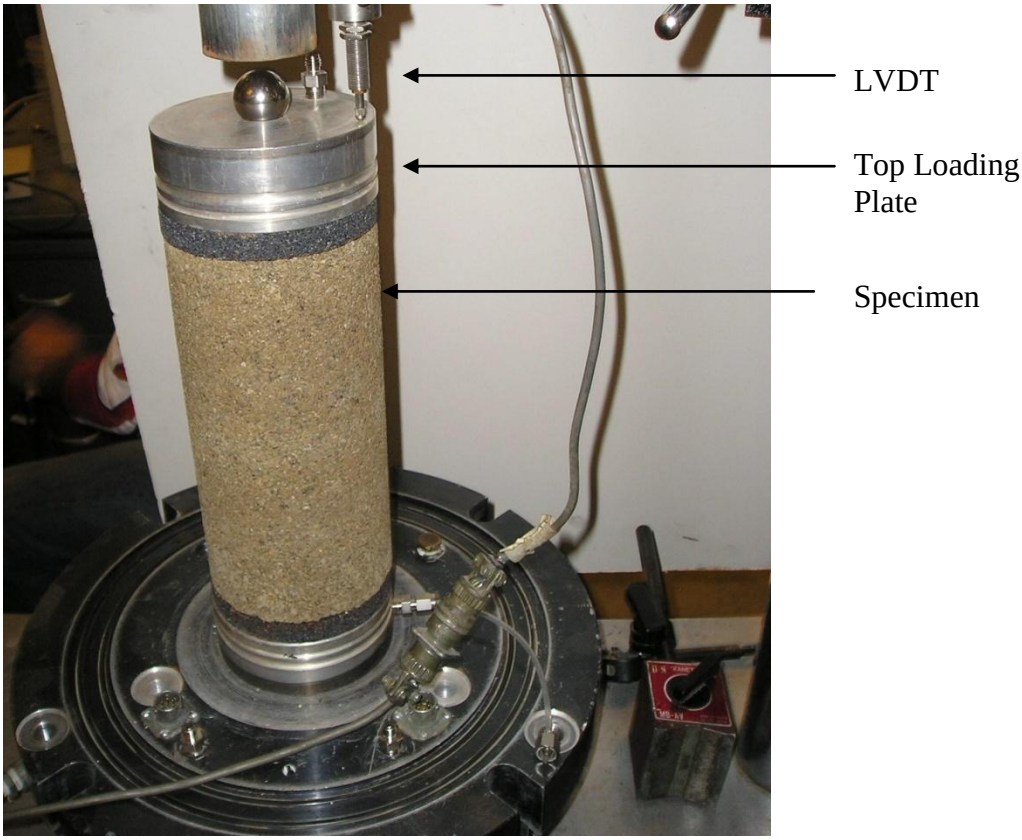

Figure 4.15 Specimen in MTS Frame for UCS Test

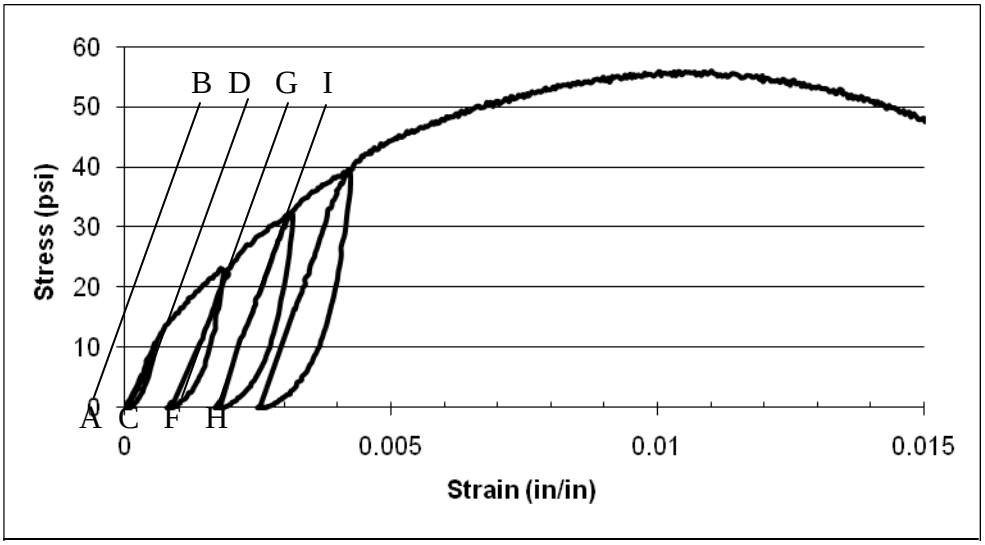

Figure 4.16 Determination of Elastic Modulus from UCS Test Stress-Strain Curve

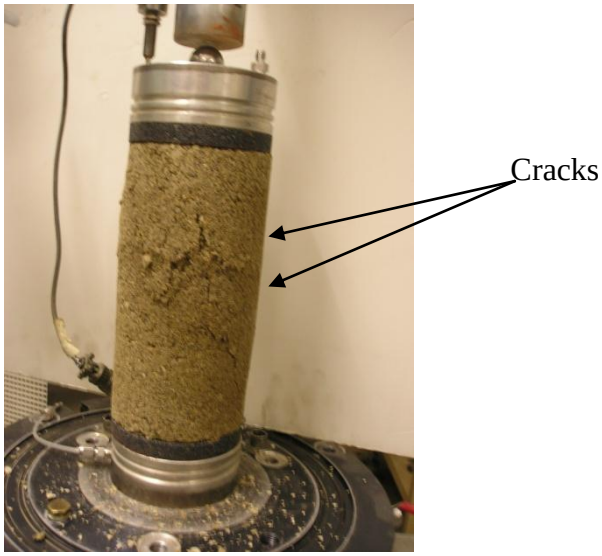

Figure 4.17 CFA-Stabilized Chat Specimen at Failure Showing Cracks During UCS Test

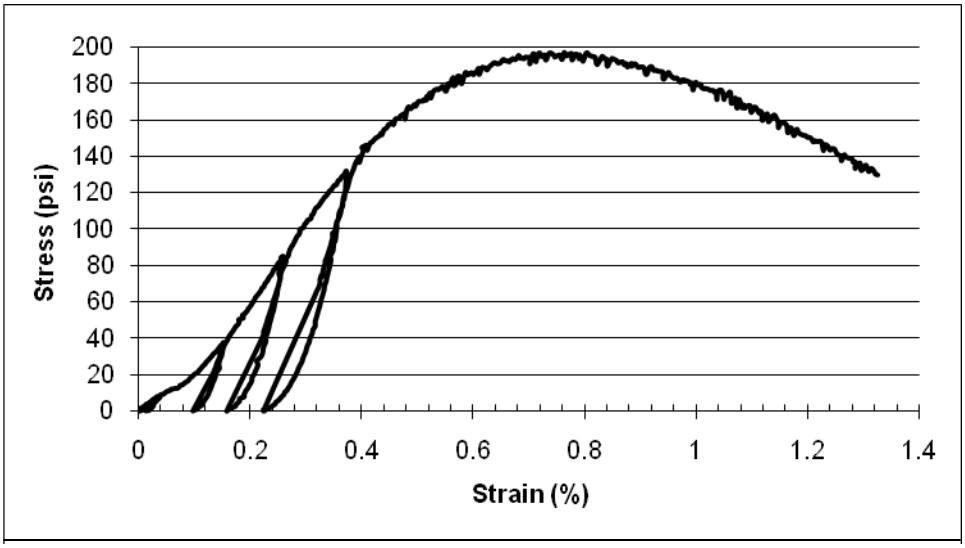

Figure 4.18 Typical Stress-Strain Curve for CFA-Stabilized Chat with Unloading-Reloading Sequence

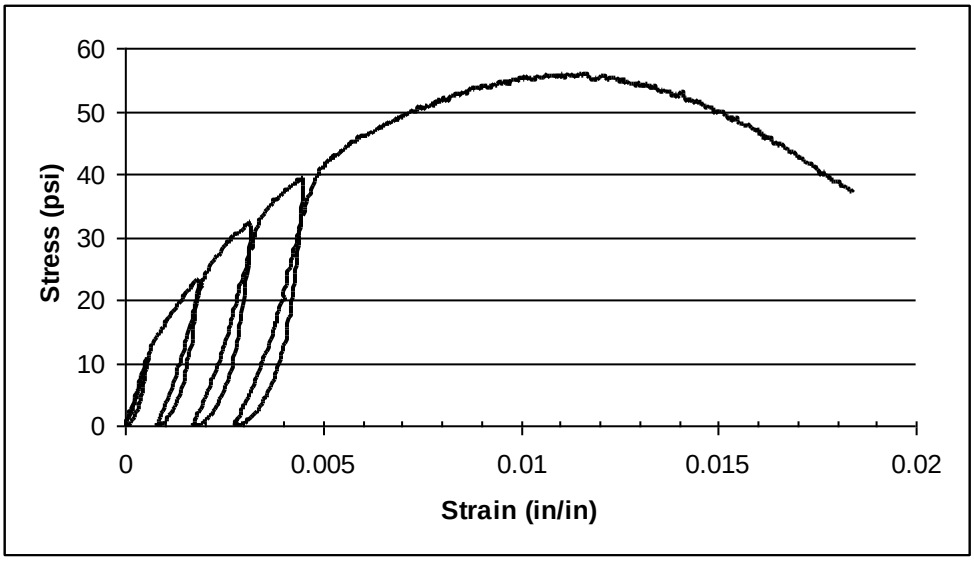

Figure 4.19 Stress-Strain Curve for CKD-Stabilized Chat with Loading and Unloading

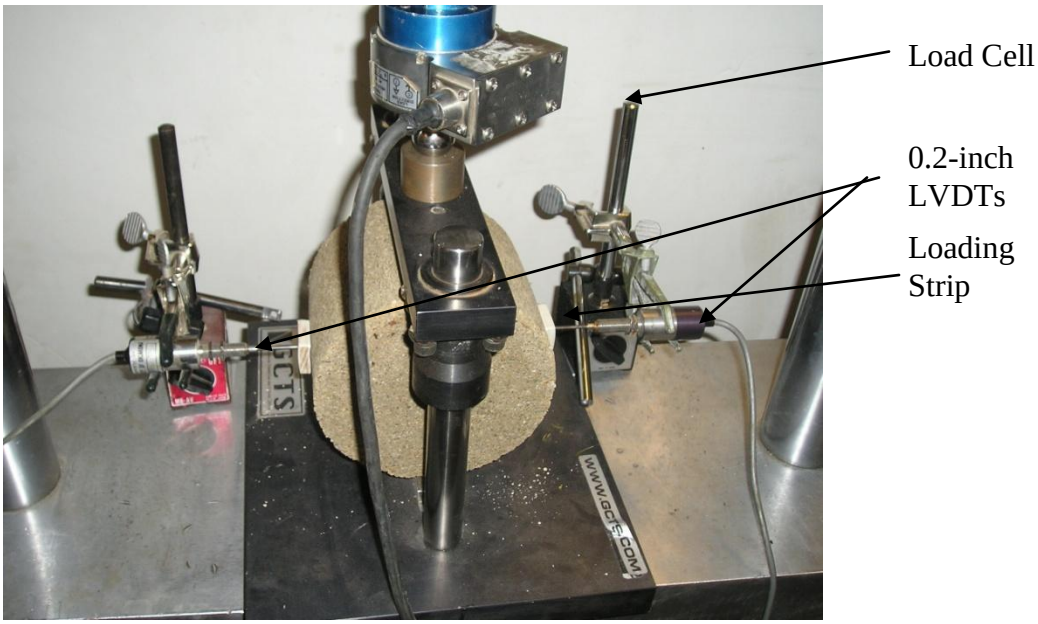

Figure 4.20 Set-up for Indirect Tensile Strength Test

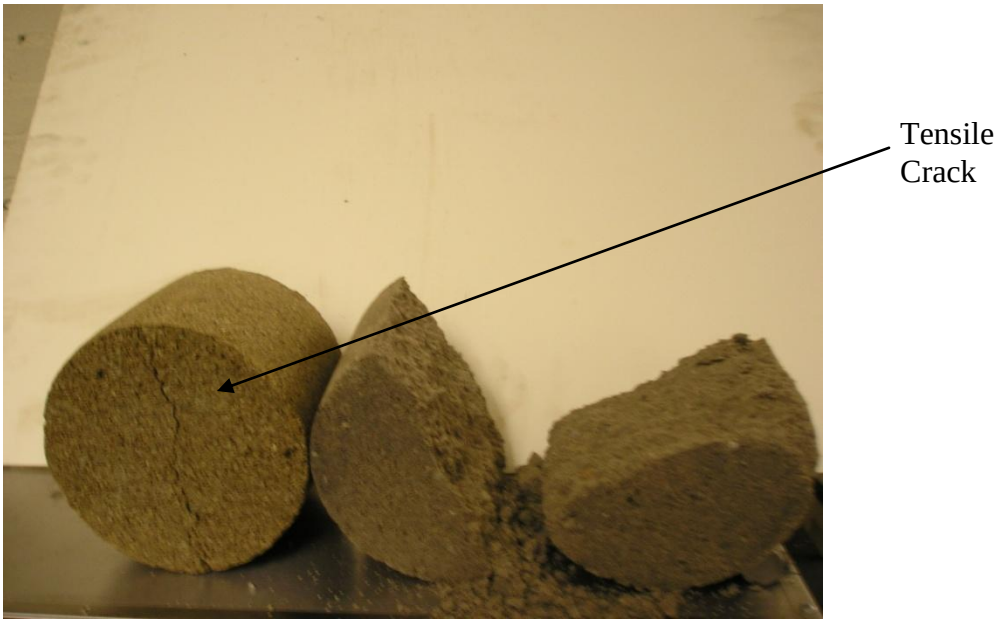

Figure 4.21 Failed Specimens After Indirect Tensile Strength Test

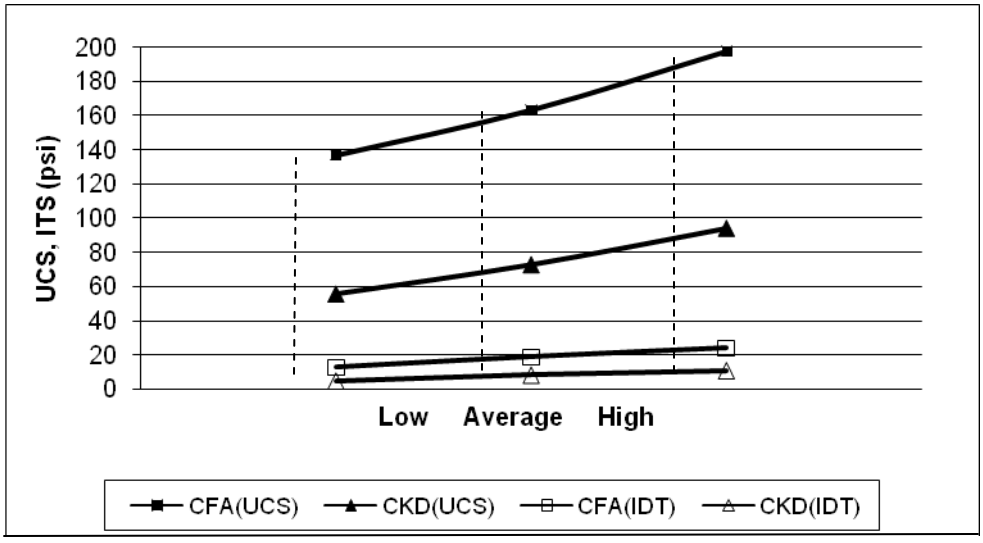

Figure 4.22 Summary of UCS and ITS Results for CFA-Stabilized and CKD-Stabilized Specimens

CHAPTER 5 LABORATOTY TESTING OF CHAT-ASPHALT

5.1. General

As noted previously, chat-asphalt was used to construct the base course and the surface course of the Test Road project. This chapter provides an overview of the mix design for chat-asphalt, using the pile run chat from the Tri-State Asphalt. Specifically, laboratory sample preparation, laboratory test procedure and laboratory test results for chat-asphalt collected from the field but compacted in the laboratory are discussed. The laboratory tests include cyclic indirect tension resilient modulus, APA rut, fatigue and permeability.

5.2 Design of HMA Surface and Base

Wasiuddin et al. (2005) performed a systematic bench-scale testing program for characterization and use of pile run chat in HMA in an environmentally responsible manner. That study revealed that pile run chat is an excellent aggregate in HMA and as much as 80% pile run chat can be used in a S5-type Superpave surface mix. In case of the base mix, a maximum of 50% pile run chat can be used safely as a roadway base material. Based on the recommendation from that study, an HMA surface mix with 80% pile run chat (Tri-State Asphalt) and a HMA base mix with 50% pile run chat (Tri-State Asphalt) were pursued in this study. The various steps for mix design are discussed in the following sections.

5.2.1 Gradation of Chat and Non-Chat Aggregates

Sieving and size separation of pile run chat was performed in accordance with the AASHTO T 27 and AASHTO T 11 methods. Figure 5.1 shows the gradation of different trial blends attempted in this mix design, including the gradation of the pile run chat. The pile run chat contains a small percentage (1%) of 9.5-mm (3/8-in) particles. It contains 6.1% of minus 0.075-mm (#200) materials and slightly passes through the restricted zone (see Figure 5.1) of an

S5 type surface mix. The pile run chat from the Tri-State Asphalt is finer than the chat from the Sooner Pile. The percentages of materials passing #200 sieve are 6.1% and 4.7%, respectively, for the Tri-State Asphalt and the Sooner Pile. The chat used by Wasiuddin et al. (2005) was obtained from the Kenoyer North Pile, called KNRC in this report, which was chosen by the Oklahoma Department of Environmental Quality (ODEQ) for sampling due to the availability of recent data indicating relatively high lead concentrations. It can be seen that KNRC is "cleaner" (3.5% minus 0.075-mm materials) compared to the chat used in this study for chat-asphalt surface and base courses. Table 5.1 shows a comparison of gradations of pile run chat from different sources. It is evident that the gradation of chat from Tri-State Asphalt is similar to some other sources such as Ottawa Pile and Atlas Pile. Figure 5.2 shows the gradation of trial blends used in the design of the base mix, which is a S3 type mix. It can be seen that the pile run chat requires a large amount of coarser particles to meet the gradation requirements of a S3 type base mix.

Three non-chat aggregates, namely 9/16-in. limestone, 1.5-in. limestone and screenings from MidWest Minerals, Miami, Oklahoma were blended with pile run chat to meet the gradation requirements.

5.2.2 Selection of Mix Type and Asphalt Binders

The maximum aggregate size in a S5 mix is ½-in. The pile run chat (Tri-State Asphalt) does not contain this size aggregates. Also, the pile run chat lacks 9.5-mm (3/8-in) particles (coarse aggregate). Coarser aggregates from non-chat sources were blended with the pile run chat to meet the gradation requirements. Among the three commonly used types of base mixes (S1, S2 and S3), S3 is the finest one. Because chat is a finer aggregate, S3 type base mix was selected to maximize the use of pile run chat. Two PG binders, namely a PG 64-22 for the base

mix and a PG 70-28 (Elvaloy® RET) for the surface mix used here, were provided by Valero Refinery, Ardmore, Oklahoma.

5.2.3 Preparation of Trial Blends

Surface Mix with 80% Pile Run Chat (RSM80) – The mix designs were commenced by first preparing two trial blends for RSM80 by varying the gradation of non-chat aggregates, but keeping the pile run chat (Tri-State Asphalt) proportion to 80% (by weight) (see Table 5.2). Percentages of 9/16-in. limestone and screenings were adjusted so as to vary the gradation of non-chat aggregates, keeping the non-chat aggregate to 20% and pile run chat aggregate to 80% (by weight). The following nomenclature was used for the three trial blends prepared for RSM80: *RSM80-N1-N2*, where *RSM* indicates surface mix, N1 indicates trial blend number, and N2 indicates compacted specimen number.

Figure 5.1 shows the two trial blends prepared for RSM80. It is observed that RSM80-2 is finer than RSM80-1. Both the trial blends passed below the restricted zone. The percentages of pile run chat, 9/16-in. limestone and screenings for these trial blends are shown in Table 5.3. The amount of finer aggregates in the trial blends was controlled by the amount of screenings added, while the amount of coarser aggregates was controlled by the amount of 9/16-in. limestone added. The amounts of minus 0.075-mm (passing #200 sieve) materials in RSM80-1 and RSM80-2 were 5.3 4.05% and 64.89%, respectively.

Base Mix with 50% Pile Run Chat (RBM50) – As in the case of RSM80, two trial blends were prepared for the base mix (RBM50) by varyng the gradation of non-chat aggregates, but keeping the pile run chat (Tri State Asphalt) proportion to 50%. Percentages of 1.5-in. limestone, 9/16-in. limestone and screenings were adjusted to vary the gradation of non-chat aggregates, keeping the non-chat aggregate to 50% and pile run chat aggregate to 50% (by

weight). The nomenclature of the trial blends and specimens were essentially the same as that for RSM80.

Figure 5.2 shows the two trial blends prepared for RBM50. It is noted that RBM50-2 is finer than RBM50-1, and both the trial blends pass below the restricted zone. The percentages of pile run chat, 9/16-in. limestone, 1.5-in. limestone and screenings blended to obtain these trial blends are shown in Table 5.3. The amount of minus 0.075-mm (#200 sieve) materials in RBM50-1 and RBM50-2 are 4.05% and 6%, respectively.

5.2.4 Testing of Aggregate Properties

Specific Gravity – Fine and coarse aggregate specific gravity and absorption were determined for each trial blend of both the mixes. Bulk specific gravity of the trial blends was calculated from the weighted average of fine and coarse aggregate specific gravity. It can be seen from Table 5.4 that the bulk specific gravity of the selected trial blends varies between 2.458 and 2.483 for RSM80 and for RBM50 it varies between 2.491 and 2.504.

Coarse Aggregate Angularity – Pile run chat is a crushed material from mining operations. The non-chat aggregates used in this study are also machine-crushed. Therefore, all the aggregate particles have fractured faces. As a result, the coarse aggregate angularity of all the trial blends was found to be 100%. Table 5.5 shows that all the trial blends have a higher angularity than that required by ODOT for roads with 10 to 30 million ESALs.

Fine Aggregate Angularity – As noted above, all the aggregates used in this study resulted from crushing operations. Therefore, the trial blends contain a large amount of voids in the loose aggregate form. The more angular the aggregates the higher the amount of these voids. The uncompacted void content or the fine aggregate angularity of the trial blends was found to

be higher (at least 1%) than that required by ODOT for roads designed for 3 to 30 million ESALs (see Table 5.5). The fine aggregate angularity of all the blends varies between 46% and 47%

Flat or Elongated Particles - The coarse aggregate in pile run chat (materials retained on a 4.75-mm (#4) sieve) has less than 5% flat or elongated particles. It was found that all trial blends for surface and base mixes also possess less than 5% flat or elongated particles, which is less than the maximum allowed by ODOT for roads having more than 0.3 million ESALs (see Table 5.5)

Sand Equivalent - The sand equivalent values (see Table 5.5) of all the trial blends are found to be much higher (at least 30%) than the minimum required by ODOT. The sand equivalent values of all the blends were between 76% and 84%

Los Angeles Abrasion - The L.A. abrasion values of pile run chat and limestone are 18% and 38%, respectively, which are much smaller than the ODOT specification of 40% maximum. Table 5.6 lists the L.A. abrasion values for some trial blends calculated by the weighted average of pile run chat and limestone. The L.A. abrasion value decreases with an increase in the amount of pile run chat and varies between 22% and 28%.

Aggregate Durability Index - ODOT specifies a minimum aggregate durability index of 40%. In this study the aggregate durability index of pile run chat was found to be 78%, which is much higher than what is required (see Table 5.6). The aggregate durability index of limestone (MidWest Minerals, Miami, Oklahoma) was found to be 65% from the ODOT database. Table 5.6 shows the aggregate durability index of all the trial blends calculated by the weighted average of pile run chat and limestone. The aggregate durability index increases with an increase in the amount of pile run chat and varies between 72% and 75%.

Insoluble Residue - The percent insoluble residue of pile run chat (Tri State Asphalt) was found to be 98%. The insoluble residue value of limestone (Midwest Minerals, Miami, OK) was found to be 25% from the ODOT database (see Table 5.6). The minimum requirement for insoluble residue is 40% for pavements designed for 3 million ESALs or more, as set by ODOT. The insoluble residue values of some trial blends calculated by the weighted average of pile run chat and limestone are reported in Table 5.6. As the percent insoluble residue of pile run chat is much higher than that of limestone, the percent of insoluble residue increases significantly with an increase in the amount of pile run chat. The percent insoluble residue varies between 62% and 83%.

5.2.5 Selection of Final Blend

Mixing and Compaction – In order to establish the best blend for each mix (RSM80 and RBM50), two HMA samples were prepared for each of the trial blends. Two trial asphalt binder contents of 6.5%, and 5.75% were used for RSM80 and RBM50, respectively. The samples were compacted at 115 gyrations (maximum gyration).

Specific Gravity of HMA – To evaluate the volumetric properties, the compacted chat-asphalt samples were evaluated for specific gravity (G_{mb}). This measured G_{mb} at maximum gyrations was used to calculate the estimated G_{mb} at design gyrations. The specific gravity test of loose asphalt-coated aggregates, which is also called the theoretical maximum density, was also performed (G_{mm}). Table 5.7 shows the estimated G_{mb} at design gyrations and the G_{mm} values for the trial blends. These values will be used in volumetric analyses.

Selection of Final Blend – Volumetric analyses were performed to evaluate the best blend for each mix. Table 5.8 shows the volumetric properties determined for all the trial blends. Table 5.9 shows the estimated volumetric properties at estimated optimum asphalt binder content

(OAC). It can be seen that both the trial blends of RSM80 fulfill the VMA and VFA requirements. In this case, RSM80-2 was selected as the final blend as it has lower estimated optimum asphalt binder content. Also, RBM50-2 was selected as the final blend for the same reason.

5.2.6 Determination of OAC

Mixing and Compaction – In order to evaluate the OAC for the selected blend (final blend), two HMA samples were prepared at selected asphalt binder contents: one above the estimated OAC, one around the estimated OAC and one below the estimated OAC. For the selected blend of RSM80, 6.25%, 6.75% and 7.25% asphalt binder contents were used. Three asphalt binder contents, namely 5.0%, 5.5% and 6.0%, were used to determine the OAC of RBM50-2. The samples were compacted at 75 gyrations.

Specific Gravity of HMA - Tables 5.10(a) and (b) show the G_{mb} at design gyrations for both mixes. It also shows the theoretical maximum density (G_{mm}) of the selected blends. These values will be used in the volumetric analyses.

Determination of OAC – Volumetric analyses were performed to determine the OAC for each mix. Tables 5.11 (a) and (b) show the volumetric properties determined for both mixes at different asphalt binder contents. Table 5.11 (a) shows that the effective specific gravity values of aggregate (G_{se}) are very close to each other (between 2.607 and 2.603) for both mixes. The asphalt binder absorption of aggregate (P_{ba}) in RSM80-2 is higher than RBM50-2.

The OAC values shown in Table 5.12 for both mixes were obtained from an interpolation for 4% air voids. The OAC values found for RSM80-2 and RBM50-2 were found to be 6.85% and 5.55%, respectively. The corresponding VMA and VFA at OAC are 15% and 73% for RSM80-2 and 13% and 69% for RBM50-2. Both VMA and VFA fulfill the ODOT requirements.

5.3 Collection of Materials

Bulk chat-asphalt mixes were collected from the field during the pavement construction, as shown in Figure 5.3. These bulk mixes were used to prepare specimens in the laboratory. Field cores were also retrieved from the project site for laboratory testing. A summary of mix properties for the collected loose chat-asphalt mixes is shown in Table 5.13. Additional information on the asphalt mixes is presented in the design sheets attached in Appendix B.

5.4 Cyclic Indirect Tension Resilient Modulus Test

In the 2002 AASHTO Pavement Design Guide, resilient modulus is used as an important property (stiffness) of hot mix asphalt. Generally, the higher the resilient modulus, the better the pavement. The resilient modulus is a measure of the elastic modulus of a linear visco-elastic material at a given stress state (Huang, 2004). It is mathematically defined as the applied deviator stress (σ_d) divided by the recoverable (resilient) strain (ε_r) that occurs when the applied load is removed from the test specimen. In this study, resilient moduli of chat-asphalt specimens were determined from cyclic indirect tension test, Figure 5.4. According to Brown et al. (1989), the ASTM D 4123 testing protocol suffers from the lack of accuracy and precision. Therefore, the expression for evaluating diametric or indirect tension M_R, as derived by Tarefder (2003), was used in this study. The following expression was used to determine the resilient modulus, M_R:

$$M_R = \frac{2P}{\Delta h \pi t d}\left\{\frac{(3+\upsilon)d^2 d_g + (1-\upsilon)\left\{d_g^3 - 2d(d^2 + d_g^2)\tan^{-1}\left(\frac{d_g}{d}\right)\right\}}{d^2 + d_g^2}\right\} \quad (5.1)$$

where, P = applied load, ν = Poisson's ratio, t = thickness of the cylinder, and d=diameter of the cylinder.

When using this approach, the diametric vertical load and deformation along vertical and lateral directions are measured using two LVDTs. Each LVDT has a stroke length of 2.54 mm (0.1 in). The M_R value is determined from the deviatoric stress and recoverable horizontal deformation. Assumed Poisson's ratio values of 0.2, 0.35, and 0.5 were used for test temperatures of 5°C (41°F), 25°C (77°F) and 40°C (104°F), respectively, as suggested by Barksdale et al. (1997) and the SHRP Protocol P07 (SHRP, 1992). The Poisson's ratio of each specimen was evaluated from the test results as the ratio of the measured lateral and vertical deformations.

5.4.1 Sample Preparation for M_R Testing

Both laboratory prepared cylindrical specimens and field cores of 100 mm (4 in) diameter and 75 mm (3 in) height were used in the testing program. Figure 5.5 shows a photographic view of coring a specimen in the field. In order to obtain laboratory prepared test specimens, the following steps were followed, as described in the ASTM D 4123 test method. First, the theoretical maximum specific gravity (G_{mm}) test for each asphalt mix was performed on reference samples in accordance with the AASHTO T 209-04 test method. Then, the loose chat-asphalt mix was heated in an oven for approximately two hours at a temperature of 149°C (300°F). The heated loose mix was then compacted in a 150 mm (6-in) diameter cylindrical mold and a height of approximately 100 mm (4 in) using a Superpave gyratory compactor. In order to obtain specimens of a specific height (75 mm or 3in), as shown in Figure 5.6, both ends of the SGC compacted specimens were trimmed using a heavy duty asphalt saw (Figure 5.7). After

trimming, the remaining part was cored using a heavy duty asphalt coring machine, as shown in Figure 5.8.

Field cores were extracted by using a 100 mm (4 in) coring rig. The final test specimens of 75 mm (3 in) thickness were prepared in the laboratory by trimming both ends of the specimen using a heavy duty asphalt saw. For both laboratory prepared specimens and field cores, the bulk specific gravity (G_{mb}) was evaluated by using the CoreLok sealing method, in accordance with the OHD L-45 test method.

5.4.2 M_R Test Procedure

The M_R test procedure consisted of applying six stress sequences, as listed in Table 5.14. Each test sequence consisted of a haversine-shaped load pulse having a duration of 0.1 sec and a rest period of 0.9 sec. An electro-hydraulic test system manufactured by Material Testing System (MTS) was used to load the specimen. The load-deformation response was recorded for 50th and the last 5 cycles of each stress sequence by using a computer-controlled FlexTest SE Test Controller (see Figure 5.9). The FlexTest SE digital servo-controller from MTS is made up of a powerful array of reliable, flexible and easy-to-use controllers designed to address the full spectrum of material and component testing needs (MTS, 2005). Basic capabilities include station configuration editing, the creation of up to four parameters sets per configuration, auto-zeroing, control mode switching with hydraulics on, and adaptive control. The controller provides a self-contained, single-channel control, and can be linked to other controllers for multi-channel testing.

Table 5.14 shows the number of loading cycles used in each sequence. A 22.2 kN (5 kips) load cell was used for samples at 40°C (104°F) and a 97.9 kN (22 kips) load cell was used for samples at 5°C (41°F) and 25°C (77°F). The vertical and horizontal deformations were

measured by two LVTDs having a stroke length of 2.54 mm (0.1 in), attached in the diametrically perpendicular direction of one face of the specimen, as shown in Figure 5.10. A gauge length of approximately 80 mm (3.15 in) was used to mount the LVDTs on one face of the specimen. M_R tests were conducted within a temperature chamber, as shown in the Figure 5.11. The samples were kept in the temperature chamber for a time period of 18 to 24 hours for the specimen to reach and maintain the required test temperature. A set of four samples were prepared for each temperature (5°C, 25°C, and 40°C). One sample was tested for indirect tensile strength and other three samples were tested for resilient modulus at each temperature. The applied stress level was chosen according to the tensile strength of the sample of each set. A load corresponding to 0.10 stress ratio (applied stress divided by tensile strength) was used for the conditioning sequence. For the remaining five sequences, a starting load at the first sequence corresponding to a stress ratio of 0.20 was used and a 0.10 stress ratio increment in each subsequent sequence was applied. In order to make full contact between the specimen and the loading strip, 10% of the peak applied load was used as the seating load in each loading cycle. The resilient modulus values were calculated from the average recoverable deflection and average load from the last five cycles of each sequence. A sample of the MTS test software and a tutorial explaining "How to Run Indirect Tensile Resilient Modulus Test" and "How to Run Indirect Tensile Strength Test" is given by Navaratnarajah (2006).

5.4.3 Accuracy of Deflection Value in M_R Calculation

The accuracy of deflection measurement in M_R calculation depends on the resolution of the data acquisition system and LVDTs. In the current study, using ±2.54 mm (± 0.1 in) LVDTs and 16-bit data acquisition, the resolution of the measured displacement was $0.2/2^{16} = 3 \times 10^{-6}$ in. The expected displacement for HMA specimen is generally between 25.4×10^{-4} (10^{-4} in) to 25.4

x 10^{-3} (10^{-3} in). So, the deviation of displacement or maximum relative error was in the range of 3 x $10^{-6}/10^{-4}$ and 3 x $10^{-6}/10^{-3}$ (3% - 0.3%). Based on these calculations, the possible error associated with the M_R values may be considered negligible.

5.4.4 Variation of Cyclic Indirect Tension Resilient Modulus

The following factors were considered in the cyclic indirect tension resilient modulus (M_R) tests performed in this study: stress ratio, temperature and specific mix properties, namely, air voids, binder content, specific gravity and aggregate sizes. Specimens were tested for three different temperatures, namely, 5°C, 25°C and 40°C (i.e., 41°F, 77°F and 104°F), as recommended by the ASTM D 4123 test method. The following sub-sections summarize the results.

5.4.5 Variation of M_R with Stress Ratio

Previous studies (Hossain et al., 1992; Zhou et al., 1992; Shalaby et al., 2004; Tarefder, 2003; Tarefder and Zaman, 2003) have addressed the variation of resilient modulus of hot mix asphalt with test temperature, air voids, binder content and binder grade, among others. The resilient modulus values were generally evaluated at one specific stress level. Tarefder (2003) and Tarefder and Zaman (2003) reported the resilient modulus at a specific stress level between 10% and 40% of the indirect tensile strength (ITS). In a similar study, Hossain et al. (1992) used an average load of 445 N (100 lb) to calculate the resilient modulus of asphalt pavement cores. In these studies, no attempts were made to examine the variation of M_R with stress levels.

A study by Barksdale et al. (1997) noted that the modulus of asphalt mixes, at a temperature higher than 25°C, is highly influenced by the stress state. In that study, it was also reported that SHRP P07 recommended the evaluation of resilient modulus at different stress levels, namely, 5%, 15% and 30% of the indirect tensile strength. The tests were performed at

three different temperatures 5°C, 25°C and 40°C (i.e., 41°F, 77°F and 104°F). Another study by Brown and Foo (1989) noted that the stress applied to the specimen has a significant effect on the M_R value. In that study, the resilient modulus tests were conducted in accordance with the ASTM D 4123 test method. Specimens were subjected to stress levels corresponding to 10%, 15% and 20% of indirect tensile strength.

In the present study, the variations of resilient moduli under various stress levels were examined for both the chat-asphalt mixes (surface and base). In this chapter the chat-asphalt surface and base mixes are called the Test Road surface and base, respectively, as there are two other HMA mixes. The resilient modulus values for different stress ratios (applied stress/indirect tensile strength), at different temperatures, for all the mixes are summarized in Tables 5.15 through 5.17. It is evident that the resilient modulus, in general, decreases with the increase in stress ratio. For example, the M_R value of Test Road base specimen (TC-B-M_R-6) at 25°C (77°F) exhibited a decrease from approximately 3861 MPa (560 ksi) to 3068 MPa (445 ksi) as the stress ratio increased from 0.21 to 0.35. A similar trend has been reported in the literature. For example, Brown and Foo (1989) reported that the resilient modulus exhibited a decrease with an increase in the stress ratio. Almudaiheem and Al-Sugair (1991) reported a decrease in resilient modulus with increasing stress ratio from approximately 10% to 30%. Also, Boudreau et al. (1992) reported that the resilient modulus depends on the percentages of indirect tensile stress applied.

It has been recognized that the state of stress and deformations at any location within a pavement structure, due to traffic loading, is a function of moduli (Witczak, 2000). Also, the modulus, in turn, is a function of the state of stress. As a result, a predictive model correlating M_R with state of stress is expected to be beneficial to pavement design. These models may also

be useful in the finite element analysis of pavements. Thus, it was decided to evaluate the performance of three potential models in predicting M_R of chat-asphalt and other HMA mixes with the stress ratio, R. The following three models were evaluated:

Linear Model: $M_R = A + B\,R$ *(5.2)*

Semi-Log Model: $M_R = A\,B^R$ or $\log(M_R) = \log(A) + R\log(B)$ *(5.3)*

Log-Log Model: $M_R = A\,R^B$ or $\log(M_R) = \log(A) + B\log(R)$ *(5.4)*

where, "*A*" and "*B*" are model parameters that were evaluated from test data. Each model was then used to predict the resilient modulus values of the 53 test specimens. It is important to note that other studies have used some of these models. For example, Brown and Foo (1989) used a similar linear model to correlate resilient modulus (M_R) with stress ratio. Results showed that M_R values decreased approximately 12% as the stress ratio increased from 10% to 15%, for samples tested at 25°C (77°F). In Huang (2004), the dynamic modulus of HMA mixes under flexural stress was predicted using a similar semi-log model. It was reported that the dynamic stiffness modulus decreases with an increase in dynamic load magnitude, due to relatively large strain in the flexural test.

Tables 5.18 through 5.20 show the model parameters and the R-squared values for both the chat-asphalt surface and base mixes, using the aforementioned models. The R-squared value, also known as coefficient of determination, was used to compare the relative performance of each model in predicting the resilient modulus with stress ratio. Although both models revealed high R-squared values, only the semi-log model was used subsequently to determine the resilient modulus at specific stress ratios, namely, 0.20, 0.35 and 0.50. These stress levels were used since they fall within the range specified by the ASTM D 4123. The resilient modulus at those

specific stress ratios were used to evaluate the performance of the four selected mixes (chat-asphalt surface, base and two new mixes) in the subsequent sections.

5.4.6 M_R Values at Selected Stress Ratio

Behavior of chat-asphalt mixes used in the Test Road project was compared with two other mixes: one from Davis (HW # 7, Davis, OK) and one from OKC (Eastern Ave., Oklahoma City, OK). The details of these mixes are presented in Appendix B. The M_R values for the laboratory mixes at the aforementioned stress ratios, i.e., 0.20, 0.35 and 0.50, are summarized in Table 5.21 and graphically illustrated in Figures 5.12 through 5.17. In comparing these results, laboratory Davis specimens resulted in the highest average resilient modulus values, followed by the OKC specimens, the Test Road base mix specimens, and then the Test Road surface mix specimens, in general. For example, the average M_R value of the Davis specimens (laboratory compacted) at a temperature of 25°C (77°F) and a stress ratio of 0.20 is approximately 26%, 39% and 74% higher than the corresponding values of the OKC base, the Test Road base and the Test Road surface specimens, respectively, as shown in Figure 5.13. The corresponding average M_R values are 9,811 MPa (1423 ksi) for the Davis base, 7,288 MPa (1057 ksi) for the OKC base, 5,992 MPa (869 ksi) for the Test Road base and 2,565 MPa (372 ksi) for the Test Road surface specimens. From Figures 5.12 through 5.17, it is clear that the Davis mix would perform better compared to all the other mixes. While the OKC base and the Test Road base are expected, based on this resilient modulus values, to have similar performance. The Test Road surface mix appears to have the lowest performance compared to the other mixes. The difference in M_R values is believed to be due to the difference in the specific mix properties, namely, binder content, binder grade, air voids, nominal maximum aggregate size (NMAS) and percentage of fines, among others. A summary of the mix properties is presented in Table 5.22. Attempts have

been made to evaluate the effects of individual properties on the behavior of resilient modulus values of these mixes, as discussed in the following such sections. Also, a regression model depicting the combined effect of these properties was developed.

5.4.7 Effect of Binder Content on Resilient Modulus

Figure 5.18 shows the variation of resilient modulus with the binder contents for laboratory compacted specimens. It is evident that the highest resilient modulus corresponds to specimens with a binder content of 4.5%. Specimens with a higher binder contents exhibited lower M_R values, as shown in Figure 5.18. Also evident in this figure is that the resilient modulus of specimens with a binder content of 4.3% have a lower value than the corresponding values at a binder content of 4.5%. A similar qualitative trend was observed for field cores, as shown in Figure 5.19. For example, an increase in M_R values for the Davis cores (binder content 4.3%) relative to the OKC cores (binder content 4.5%) and a decrease in M_R values for the Test Road cores (binder content 5.6%) relative to the Davis cores (binder content 4.5%) are seen.

The increase in resilient modulus as the binder content increased from 4.3% to 4.5% could be attributed to the fact that a slight increase in binder content increases the binder film thickness between aggregate particles, thereby, an increased proportion of asphalt acts to resist the applied stress and thus increase the resilient modulus. A similar explanation was given by Tarefder (2003). A decrease in resilient modulus as the binder content increased beyond 4.5% would be attributed to the fact that additional asphalt (more than the optimum binder content) would increase the binder film thickness between particles excessively and decrease the internal friction of the aggregate, thus making the HMA specimen undergo a large strain with applied load. Materials can flow laterally due to the loss of aggregate interlock (Roberts et al., 1996), thus reducing resilient modulus values. It is also worth noting that the difference in resilient

modulus (increase or decrease) due to the binder content may be attributed to other properties previously listed, because other mix properties are not identical. The effect of various binder contents on the same mix, by fixing the other properties, was not addressed in this study. A future study may be undertaken to address this issue.

5.4.8 Effect of Air Voids on Resilient Modulus

Figure 5.20 and Figure 5.21 show the variation of resilient modulus values with air voids for the laboratory specimens and field cores, respectively. Results showed that no specific trend is evident between the resilient modulus and the air voids. This is consistent for all three temperatures. For example, laboratory specimen with air voids of 6.4% have an average resilient modulus higher than the corresponding values of laboratory specimens with 6.3%, 6.7% and 8.0% air voids. Also, laboratory specimens with air voids of 6.3% have a lower M_R value than the laboratory specimen with 6.7% air voids and a higher M_R value than the laboratory specimen with 8.0% air voids. The range of air void variation within the laboratory specimens are lower (6.0% to 8.0%) in this study. Therefore, a study with changing air voids within a comparatively higher range, keeping other variables unchanged, would give a clear indication of the effect of air voids on resilient modulus.

A trend was observed for resilient modulus between the laboratory specimens and field cores. As one can see from Table 5.23, the laboratory resilient modulus values were higher than those of field cores except for some selected specimens. This is due to the fact that the field core densities are lower than those of the laboratory prepared specimens. Difference in compaction imparted by a laboratory gyratory compactor and a vibratory compactor in the field is the primary reason for this variation. Also, Table 5.23 shows that M_R of laboratory specimens could be as high as 76% of the field cores. Therefore, we can conclude that the increasing air voids

(decreasing density) significantly decreases the resilient modulus values. This suggests that homogeneity is more successfully achieved for specimens compacted in the laboratory than for field cores, which can vary depending upon the compaction quality. This is consistent with the study by Katicha (2003). That study showed that densities of the field cores are much lower than those of laboratory prepared specimens, therefore, the average resilient modulus of field core is lower than that of laboratory prepared specimens. Also, the present study showed that the predicted resilient moduli decrease with increasing void ratios. Similar conclusions were made by Crovetti et al. (2005). That study reported that the resilient modulus values decrease at a given temperature, as the percent air voids increase.

5.4.9 Effect of Aggregate Sizes on Resilient Modulus

With regard to the NMAS of the aforementioned mixes, the OKC and the Test Road base mixes, with an NMAS of 25 mm (1 in), were coarser than the Davis and the Test Road surface mixes. The NMAS was 19 mm (¾ in) for the Davis mix and 12.5 mm (½ in) for the Test Road surface mix. A study by Mindess et al. (2002) reported that the larger the NMAS, the higher the strength. However, in this study, the effect of aggregate size on resilient modulus is not clear and could not be adequately investigated. This is due to the fact that the Davis base mix with a NMAS of 19 mm (¾ in), which is less than the NMAS (25 mm (1 in)) of the Test Road base and the OKC base mixes, exhibited a higher resilient modulus values.

The percentage of aggregate passing No. 200 sieve for the Test Road surface mix and the Davis base mix were higher and are 6.0% and 5.9%, respectively, as shown in Figure 5.22 and Figure 5.23. These values for the Test Road base mix and the OKC mix are comparatively lower and are approximately 4.9% and 4.7%, respectively. But, the resilient modulus for the Test Road surface mix specimens is lower than the Davis mix specimens followed by the OKC mix and the

Test Road base mix specimens. A study by Crovetti et al. (2005) reported that the resilient modulus increases at a given temperature, as the aggregate passing No. 200 sieve increases. In the present study, no clear trend could be identified for variation in resilient modulus with percentage fines. This may be attributed to changes in other mix properties.

5.4.10 Variation of MR with Temperature

The variation of resilient modulus values with temperature for all the mixes is presented in Table 5.21 and graphically illustrated in Figures 5.24 through Figures 5.28. The resilient modulus decreased significantly with increasing temperature for all mixes. For example, resilient modulus (at stress ratio 0.35) decreases from 11,935 MPa (1731 ksi) to 1,103 MPa (160 ksi) as the temperature increased from 5°C to 40°C (41°F to 104°F) for the Test Road base mix. The Davis specimens exhibited a decrease in M_R values from 15,410 MPa (2235 ksi) to 3,172 MPa (460 ksi) as the temperature varied from 5°C to 40°C (41°F to 104°F). It is an indication that the variation in M_R values due to temperature varied from one mix to another. A similar behavior for hot mix asphalt has been reported in previous studies. For example, Katicha (2003) reported that the resilient modulus decreases with increasing temperature and the variation can be best represented by an exponential model. A decrease in M_R values with an increase in temperature was also reported by Tarefder (2003) and by Tarefder and Zaman (2003).

The performance of each mix due to temperature was also examined. Figure 5.29 shows the average percentage reduction (PR) in M_R for all the laboratory specimens and field cores. As depicted in Figure 5.29, the average percentage reductions in M_R for laboratory specimens are 87% for the Test Road base, and the Davis and the OKC base mixes. For the Test Road surface mix, the percent reduction is 89%. For the field cores the average percentage reduction for the Test Road and the Davis cores are 87% and for the OKC cores the reduction is 93%. A similar

percentage reduction for different HMA mixes has been reported in the literature (Salem, 2004; Katicha, 2003; and Ali and Lobez, 1996). For example, Katicha (2003) reported that the percentage reduction due to temperature varied between 78% and 90%. Based on these results, it may be concluded that the Test Road surface mix was more susceptible to temperature than the other mixes, if the percent reduction in M_R is used as an indicator of temperature susceptibility. It is believed that the temperature susceptibility of the HMA specimens may be attributed to the binder content in the mixes, since the Test Road surface mix has the higher binder content compared to the other mixes.

5.4.11 A Model to Predict Resilient Modulus

From the aforementioned results, it is evident that resilient modulus varies with stress level, temperature, material properties and mix properties. This is consistent with Katicha (2003) that the difference in measured resilient modulus is believed to be due to the difference in properties of various mixes, namely, air voids, binder content, specific gravity of materials and percentage fines. To this end, it was decided to develop a general model correlating resilient modulus with stress ratio, temperature and aforementioned specific mix properties. The employed semi-log model (Equation 5.7) includes two model parameters ("A" and "B"). The parameter "A" represents the resilient modulus at a stress ratio of zero, while "B" represents the sensitivity of resilient modulus to stress ratio changes. These model parameters were correlated with temperature, material properties and specific mix properties, namely air voids, binder content, specific gravity and percentage fines. The actual model parameters "A" and "B", shown in Table 5.19, were used to develop a general model as a function of the aforementioned properties. The SAS statistical software was used for this purpose. The stepwise method at a level of 0.15 was used in developing model for "A" and "B". The stepwise method consists of

entering or removing one variable at a time in the regression model, to attain a better R-squared value. The employed stepwise method showed that the model parameter "A" was related to temperature, percentage of air voids, percentage of binder content and percentage of material passing No. 200 sieve. Parameter "B" was found to be only related to temperature and percentage air voids. The relationships for predicted model parameters "A" and "B" are presented in Equations 5.5 and 5.6, respectively.

$$A = 3048.96 - 23.12\,T - 148.36\,A_v - 280.39\,AC + 443.04\,N_{200} \qquad (5.5)$$

$$B = 0.803 - 0.010\,T + 0.053\,A_v \qquad (5.6)$$

where, T = temperature, in ˚F, A_v = air voids, in %, AC = binder content, in %, and N_{200} = aggregate passing No. 200 sieve, in %.

The analysis of variance (ANOVA) of this predicted model parameter yields an F value of 35.1 and an R-squared value of 0.75 with a P_r value less than 0.0001, for parameter "A". Parameter "B" had an F-value of 38.4 and R-squared value of 0.61 with a P_r less than 0.0001, which indicates that the model is considered statistically significant in predicting the variation of model parameters with aforementioned specific mix properties. Comparisons between the calculated and the predicted model parameters "A" and "B" are summarized in Table 5.24 and illustrated in Figure 5.30 and Figure 5.31. From Figure 5.30, the predicted "A" can be correlated with the measured "A" with a straight line regression having a slope of approximately 1.0 and an R-squared value of 0.75. For parameter "B", the predicted "B" is correlated with a line of slope 1.002 and an R-squared value of 0.6, as shown in Figure 5.31. Thus, the proposed model to predict the resilient modulus with other engineering properties can be expressed as follows:

$$M_R = (3048.96 - 23.12\,T - 148.36\,A_v - 280.39\,AC + 443.04\,N_{200}) \times (0.803 - 0.010\,T + 0.053\,A_v)^R \qquad (5.7)$$

From the developed regression model, it is evident that M_R values of HMA mixes depend on the temperature, air voids, binder content and percentage passing No. 200 sieve. The sensitivity of each variable was checked with by increasing each variable by 20% with respect to the reference value shown in Table 5.25. It is evident that the temperature and percentage passing No. 200 sieve are more sensitive variables than the others. A decrease of 34% and an increase of 33% were obtained for temperature and percentage passing No. 200 sieve, respectively.

Finally, the proposed model was used to estimate resilient modulus. The average resilient modulus was compared to the calculated values for all the mixes. The M_R values were plotted with the calculated M_R values shown in Figure 5.32. As a result, the predicted M_R can be correlated with the corresponding actual values with a straight line regression having a slope of approximately 0.98 (fairly close to 1.0) and an R-squared value of 0.84. It is an indication that such a model could be a good indicator in making performance predictions of M_R due to variations of stress level, temperature, material properties and mix properties.

5.5 APA Rut Test

The Asphalt Pavement Analyzer (APA) is a multi-functional Loaded Wheel Tester that has been successfully used for evaluating permanent deformation (rutting), fatigue cracking and moisture susceptibility of HMA mixes (Kandhal and Mallick, 1999). The APA has the capability of testing both rectangular and cylindrical specimens. A typical APA rut test uses three beam specimens or six cylindrical specimens. Each beam specimen is 75 mm (3 in) tall, 125 mm (5 in) wide and 300 mm (12 in) long (see Figure 5.33). Each cylindrical specimen is 150 mm (6 in) in diameter and 75 mm (3 in) in height. Both laboratory compacted samples and field cores can be tested. In this study six laboratory compacted specimens, using a Superpave gyratory compactor (SGC), from each mix and six field cores from each site were used for laboratory rut testing.

Laboratory cylindrical specimens were compacted from each loose HMA mix type. The weight of the loose mix was chosen to obtain 7% air voids, in accordance with the OHD L-43 test method. The compacted specimens were kept overnight at room temperature and then bulk specific gravity tests were performed in accordance with the OHD L-45 test method. Subsequently, the compacted specimens were placed in the molds, as shown in Figure 5.34 and preconditioned at 64°C (147.2°F) for a minimum of 6 hours, inside the APA test chamber. This was done by switching on the APA chamber and setting the duration of preconditioning time. Following preconditioning, the desired vertical wheel load (445 N or 100 lbs) was applied and the hose pressure was set at 690 kPa (100 psi). The APA was allowed to run for 8000 loading cycles in accordance with the OHD L-43 test method. The rut depth was measured as a function of load cycles by the automated rut depth measuring system. Manual measurements were taken by a digital measuring gauge as a check on the automatic system rut depth measurement. The average rut depths of six specimens (three sets) were reported as the rut depth of the mixture, as recommended by the OHD L-43 test method.

The APA rut test results for laboratory prepared samples and field cores are shown in Table 5.26. A total of 42 specimens were tested and the reported APA rut values correspond to 8000 loading cycles. The APA rut values with number of loading cycles are graphically shown in Appendix F. From the test results for all three HMA base mixes it is evident that the Test Road base mix showed a high rut value of 4.9 mm (0.2 in) for specimens with an average air void of 7.0%. Comparatively, the OKC and the Davis base mixes exhibited lower rut values. The average rut value for specimens from the Davis mix was 2.7 mm (0.1 in) with a standard deviation of 0.4 mm (0.02 in). As for the OKC base mix, the average value was 2.4 mm (0.1 in) with a standard deviation of 0.05 mm (0.002 in). The average air voids for the Davis and the

OKC specimens was approximately 7.0%. For all these base mixes, the rut values are less than the Oklahoma Department of Transportation (ODOT) design rut requirement (5 mm or 0.2 in). Only one surface mix (i.e., the Test Road surface mix) was tested in this study for APA rut. An average rut value of 7.6 mm (0.3 in) was obtained for the Test Road surface mix with an average air void of 7.9%. From Table 5.26, one can see that the Test Road cores with an average air void 8.0% had a higher rut depth of 9.5 mm (0.4 in), followed by the OKC cores 5.6 mm (0.2 in) and then the Davis cores 3.1 mm (0.1 in). Consequently, one can conclude that the Test Road mixes are more susceptible to rutting potential than the OKC and the Davis mixes.

5.5.1 Effect of Binder Content on Rut Depth

The binder contents varied from one mix to another. Among the base mixes, the Test Road base mix had a 5.6%, which is higher than the binder content used for the Davis (4.5%) and the OKC (4.3%) HMA base mixes. Eliminating the effects of other properties such as air voids, specific gravity and percentage fines, one can conclude that a higher binder content produces a larger rut depth. This is also true for the Test Road surface mix with a binder content of 6.9%, which gives comparatively higher rut depths than the other mixes. This is consistent with Roberts et al. (1996) that a high binder content is expected to produce higher rut depth. It is due to the fact that an increase in binder content would increase the binder film thickness between particles and would decrease the internal friction of the aggregate, thus, making the mix tender and more susceptible to rutting, because materials can flow laterally due to the loss of aggregate interlock (Roberts et al., 1996). Similar observations were also reported by Tarefder (2003), Tarefder and Zaman (2003) and Wasiuddin et al. (2005). Wasiuddin et al. (2006) reported in a study that a trial blend for a base mix with 70% pile run chat (Kenoyer Pile) had high rut values due to the higher binder content used in the mix. This is consistent with the

current study, the Test Road surface mix contained a higher chat percentage (80%) than the Test Road base mix (50%). The binder content used in the Test Road surface mix was higher than that in the Test Road base mix. The increased binder content led to increased rut depths in the surface mix specimens. The reason for the higher binder content in the Test Road surface mix could be attributed to the higher amount of N_{200} in the mix requiring more binder to coat the aggregate. However, N_{200} is not the only factor. The overall gradation is also an effective factor for higher binder content in the Test Road surface mix. Specifically, although the N_{200} value for the Test Road surface mix and the Davis base mix are approximately the same (6.0% and 5.9%, respectively), overall the Test Road surface mix is finer than the other three mixes, as can be seen from the mix design sheet in Appendix B.

5.5.2 Effect of Air Voids on Rut Depth

From the present study, effects of air voids on the rut depth could not be identified since the laboratory prepared specimens were compacted at average air voids of approximately 7±1 %, as recommended in the OHD L-43 test method. Due to the limited scope of this study, no attempts were made to investigate the variation of rut depths with varying air voids. The air voids of the laboratory specimens varied between 6% to 8%. In similar studies by Tarefder (2003) and by Tarefder et al. (2003), it was reported that there is no significant effect on rut depth for specimens with air voids varying between 6% to 8%. But, the air voids of the Test Road cores varied between 6.9% to 9.6%. Therefore, if we compare the rut depth of the Test Road laboratory compacted chat-asphalt specimens with the Test Road field cores, we can observe that the rut depths are reduced with decreasing air voids. This is due to the fact that specimens having smaller air voids create a more homogeneous binder-aggregate structure.

Therefore, reduced air voids can lead to increased stiffness and reduced rut potential of HMA mixes.

5.5.3 Effect of Percentage Fines on Rut Depth

The variation of rut depth with percentage fines in mixes could not be clearly examined in this study. For example, the percentage fines (passing No. 200 sieve) for the Davis base mix and the Test Road surface mix are approximately the same (5.9% and 6.0%, respectively). However, the average rut depth of the Test Road surface mix specimens is higher (7.6 mm, i.e., 0.3 in) than the average rut depth of the Davis base mix specimens (2.7 mm, i.e., 0.1 in). Also, the Test Road base mix specimens with percentage passing No. 200 sieve of 4.9%, exhibited an average rut depth of 4.9 mm (0.2 in), which is higher than the Davis base mix specimens but lower than the Test Road surface mix specimens. This may be attributed to the variation of other mix properties in these mixes. Therefore, no clear conclusions could be drawn with respect to the effect of percentage fines on rutting potential. A study by Teng (1998) reported that the increase in percentage fines reduces excess binder in the HMA mixes and consequently reduces the rut depth. Overall, the present study supports this observation.

5.5.4 General Model to Predict Rutting Potential

Based on the aforementioned results, it was decided to develop a regression model correlating rutting potential with specific mix properties, namely air voids, binder content and percentage fines. The stepwise method at a 0.15 level was used for this purpose. The following rut model was developed:

$$Log\ (Rut) = 0.676 + 0.179\ AC - 0.178\ N_{200} \qquad (5.8)$$

where, Rut = rut depth, in mm, AC= binder content, in %, and N_{200} = aggregate passing No. 200 sieve, in %.

The ANOVA of this model yielded an F value of 11.6 with a P_r of less than 0.0006 and an R-squared value of 0.56, which indicates that the model may be considered statistically significant in predicting the variation of rut depth with specific mix properties, namely binder content and percentage fines. From this model, it is clear that the increasing binder content increases the rut depth and an increase in percentage fines decreases the rut depth. This observation is consistent with those reported by Tarefder (2003), Tarefder and Zaman (2003) and Teng (1998). Binder content is the only common variable in the rut models reported by Tarefder (2003) and Tarefder and Zaman (2003) and the rut model developed here. The other properties, namely air voids and specific gravity were not included in this model due to statistical insignificance in the model. Table 5.27 shows a summary of measured and predicted rut depths. A comparison between the predicted rut depths and the actual rut depths is illustrated in Figure 5.35.

5.5.5 Correlations between M_R and APA Rut

The average rut depths of the six specimens tested from the laboratory specimens and field cores were correlated with the M_R values at temperatures of 5°C, 25°C and 40°C (i.e., 41°F, 77°F and 104°F). The average value of M_R at three stress levels (R = 0.20, 0.35 and 0.50) was used to develop a model correlating M_R and rut depth. A linear model similar to the one employed by Tarefder (2003) and Tarefder and Zaman (2003) was used. The models were developed using M_R values at different stress ratios and temperatures with the APA rut depths at different numbers of loading cycles, namely 2000 and 8000, as shown in Table 5.28. The linear models along with coefficients of determination (R-squared) are shown in the Table 5.29 and are graphically illustrated in Figures 5.36 through 5.41. From Table 5.29, comparatively a high R-squared value of 0.72 was obtained for rut at 2000 loading cycles and M_R at 40°C (104°F) and a

stress ratio of 0.50. A low R-squared value of 0.54 was obtained for rut at 2000 loading cycles and M_R at 5°C (41°F) and a stress ratio of 0.20. The obtained R-squared values for different temperature and stress levels for M_R and different loading cycles for rut depth did not show a clear trend. This may be due to the testing parameters and mechanisms involved in these two types of testing. Rutting is expected to occur at high temperatures and with large number of load repetitions, whereas modulus should present stress-strain properties of HMA mixes at intermediate temperatures and lower loading cycles (Tarefder, 2003; Tarefder and Zaman, 2003). Also, rutting measures the consolidation and plastic flow characteristics of HMA mixes under repeated loading, whereas resilient modulus represents the elastic stress-strain behavior under cyclic loading. These differences in test parameter and different mechanisms result in different correlation coefficients. This is also evident from the study by Brown and Cross (1989), Tarefder (2003), Tarefder and Zaman (2003) and Bhasin et al. (2005).

Brown and Cross (1989) reported that there is no good relation (R-squared = 0.01) between HMA rutting and indirect tension resilient modulus. That study also noted that there is no reason to expect a good relationship to exist between these parameters since rutting is due to compressive stress and resilient modulus test measures tensile properties of the HMA mixes. Tarefder (2003) and Tarefder and Zaman (2003) conducted a study to correlate APA rut at 8000 loading cycles with the indirect tension resilient modulus at three temperatures (0°C, 23°C and 40°C). The highest R-squared value of 0.27 was obtained for the regression equation relating rutting and resilient modulus at 40°C. Overall, a poor correlation was obtained for each test temperature. The reason stated for this poor correlation was the mechanistic differences (stress level, strain, temperature, loading cycles etc.) between modulus and rut tests. But, comparatively high R-squared values were obtained in the present study. This may be due to the stress levels

used in the resilient modulus testing between these two studies. A stress level of 20 psi to 30 psi was used by Tarefder (2003) and Tarefder and Zaman (2003), while in the present study the stress level varied between 20 psi to 150 psi.

5.6 Fatigue Test

Fatigue failure generally occurs when a pavement is stressed to the limit of its fatigue life by repetitive axle load applications. Fatigue cracking is often associated with loads that are too heavy for the pavement structure or more repetitions of a given load are imposed than provided for in the design. Fatigue cracking is generally considered to be more of a structural problem than just a material problem (Brown et al., 2004). It is usually caused by a number of pavement factors that occur simultaneously. In addition to repeated heavy loads, poor sub-grade drainage can contribute to high deflections in a pavement, which is also one of the principal causes of fatigue cracking.

The Asphalt Pavement Analyzer (APA) is capable of testing fatigue life of asphalt specimens. Fatigue cracking resistance of HMA can be determined by subjecting beam specimens to repeated wheel loads and contact pressures. The automated data acquisition system in APA plots the vertical deformation of the beam from which the fatigue life is evaluated. In this study, a set of three 125 mm x 300 mm x 75 mm (5 in x 12 in x 3 in) beam specimens were prepared from each type of HMA mix. The weight of loose mix was chosen so as to get a targeted air void of 7 ± 1% in these specimens. The compacted specimens were kept over night at room temperature and then a bulk specific gravity test (G_{mb}) was performed in accordance with the AASHTO T166 test method. The APA wheels were calibrated by using a pre-calibrated load cell to a 1113 ± 4.5 N (250 ± 1 lb) load and the cycle counter was preset to 50,000 cycles. Then the specimens were placed in the testing molds and secured in the APA sample tray. The

temperature of the APA was set to the test temperature (20°C) and the specimens were allowed to condition at the test temperature for one hour before starting the test. The APA was started and allowed to run for the preset number of cycles. The APA stops automatically at the end of the test cycle or when all three beams have failed in fatigue. After the APA stopped, the number of cycles completed for each specimen was recorded from the test data sheet and reported as the fatigue life of the HMA mix.

A total of 12 beam specimens (3 specimens from each HMA mix) were tested for APA fatigue. The results are summarized in Table 5.30. From the number of fatigue cycles shown in Table 5.30, it is evident that both the Test Road surface and base mixes show a high fatigue cycle of approximately 49,000. Comparatively, the Davis and the OKC mixes exhibited lower fatigue cycles of approximately 20,000 and 27,000, respectively. The results indicate that the Test Road specimens exhibited a greater fatigue resistance than the Davis and the OKC specimens. This can possibly be attributed to many factors such as air voids, aggregate type and binder content, among others.

Higher binder contents will result in a mix having a greater tendency to deform elastically (or at least deform) rather than fracturing under repeated load. The optimum binder content, as determined by mix design, should be high enough to prevent excessive fatigue cracking. The use of an asphalt binder with a lower stiffness will increase a mixture's fatigue life by providing greater flexibility (Roberts et al., 1996). However, the potential for rutting must also be considered in the selection of the asphalt binder amount. A study by Buchanan (2000) reported that increasing effective binder content is the most likely influential factor in greater fatigue resistance of a granite-HMA mix. In the present study, a similar observation can be made for both the Test Road base and surface mixes. The effectiveness of asphalt content used in these

mixes was higher compared to the Davis and the OKC mixes. Therefore, a greater fatigue resistance was observed for both the Test Road base and surface mixes. A study by Kim et al. (2006) reported that fatigue failure under repeated loading is due to a combination of several mechanisms, among which damage growth, relaxation due to viscoelasticity, and healing of micro cracks play essential roles. The increase in the binder content helps healing of micro cracks. This is also evident from the present study, the increase in binder content in the Test Road mixes increased the fatigue life. A separate study by Tangella et al. (1990) reported that binder content has a significant effect on the fatigue life of HMA mixes. According to that study, the optimum binder content to obtain maximum fatigue life is generally higher than the design based on rutting considerations.

In the present study, it was decided to develop a statistical model to evaluate the effects of specific mix properties, namely air voids, binder content, specific gravity and percentage fines, on the fatigue resistance of HMA mixes. A stepwise method was employed at a 0.15 level. The final model obtained from this effort is given below:

$$N_f = 826568 - 3371\, A_v - 279230\, G_{se} - 3234\, N_{200} \qquad (5.9)$$

where, N_f = number of fatigue cycles, A_v = air voids, in %, G_{se} = specific gravity of aggregate, andN_{200} = aggregate passing No. 200 sieve, in %.

The predicted model yields an R-squared value of 0.98 and an F value of 148.2 with a P_r less than 0.001, which indicates that the predicted model is considered statistically significant. The predicted and calculated fatigue cycles for each specimen tested are shown in Table 5.31. Figure 5.42 shows the predicted fatigue cycles from the model against the calculated fatigue cycles. It can be seen from the model that increasing air voids, specific gravity of aggregate and aggregate passing No. 200 sieve reduces the number of fatigue cycles since all these variables

have a negative coefficient in the model. Inadequate compaction results in increased air voids and subsequently reduced stiffness of HMA specimens (Hughes, 1989). Therefore, the higher the air voids the lower the number of fatigue cycles. This is also evident from the study by Harrigan et al. (2002). That study reported that a 1% increase in air voids will result in a 10% decrease in fatigue life. An increase in percentage fines reduces the effectiveness of the binder in the HMA mixes, therefore it reduces the fatigue life of HMA pavements. This is consistent with the study by Teng (1998). It was reported by Teng (1998) that at low dust to binder ratio values, additional fines act as an asphalt binder extender, and causes the fatigue performance to decline.

5.7 Permeability Test

It is generally agreed that excess moisture in HMA pavements is potentially detrimental to pavement performance because of phenomena such as stripping in the HMA layers and softening or weakening in underlying unbound layers. Most laboratory-based methods for estimating permeability of HMA feature either a constant head or a falling head type test (e.g., Kantipong, et al., 2003; Mohammad, et al., 2003). In this study, a relatively simple laboratory method involving a falling head device, shown in Figure 5.43 and manufactured by Karol-Warner, was used according to the OHD L-44 test method. Two specimens having 150 mm (6 in) diameter and 75 mm (3 in) height were prepared using the Superpave Gyratory Compactor for each type of HMA mix. The weight of loose mix was chosen so as to obtain a target air void of 7 ± 1%. The compacted samples were kept overnight at room temperature and then a bulk specific gravity (G_{mb}) test was performed in accordance with the OHD L-45 test method. Then the permeability test was performed, as described in the OHD L-44 test method. The time taken for the meniscus of water to drop in the graduated cylinder from the initial timing mark (65-cm) to lower timing mark (0-cm) was recorded to nearest 0.1 second. The test was performed three

times for each specimen and the lowest time was recorded. For samples having a test time approaching 30 min during the first run without the water level reaching the lower timing mark, the water level at 30 min was recorded and then the test was performed one more time. The coefficient of permeability (k) was calculated by using the following equation (OHD L-44, 2003):

$$k = \frac{aL}{At} \ln\left(\frac{h_1}{h_2}\right) C \qquad (5.10)$$

where, k = coefficient of permeability, cm/s, a = inside cross-sectional area of the buret, cm^2, L = average thickness of the test specimen, cm, A = average cross-sectional area of the test specimen, cm^2, t = elapsed time between h_1 and h_2, sec, h_1 = initial head across the test specimen, cm, h_2 = final head across the test specimen, cm, C = temperature correction for viscosity of water.

For the permeability calculation, the mark and the time record which results in the highest coefficient of permeability was used and reported as the permeability of that HMA specimen.

The permeability test results for all mixes are summarized in Table 5.32. All of the mixes exhibited the permeability values below the maximum design permeability of 125 x 10^{-5} cm/s (49 x 10^{-5} in/s), as recommended by ODOT. Among the different types of mixes, the Test Road surface mix and the OKC base mix showed higher permeability values. The average permeability value for the Test Road surface mix was 10.8 x 10^{-6} cm/s (4.3 x 10^{-6} in/s). This value is consistent with similar values reported by Wasiuddin et al. (2005). That study reported a permeability value of 12.0 x10^{-6} cm/s (4.7 x 10^{-6} in/s) for a similar type of HMA specimen using pile run chat from the Kenoyer pile. The OKC base mix showed an average permeability value of 14.8 x 10^{-6} cm/s (5.8 x 10^{-6} in/s), which is higher than the corresponding value of the Test

Road surface mix. Comparatively, the Test Road base and the Davis base mixes showed lower permeability values of approximately 2.4 x 10^{-6} cm/s (0.9 x 10^{-6} in/s) and 3.0 x 10^{-6} cm/s (1.2 x 10^{-6} in/s), respectively. It is evident that the gradations of the mixes and the amount of interconnected and opened air voids are the key factors that affect the permeability. The gradation curves for all four HMA mixes are shown in Appendix B along with the mix design sheets. From the lower portion of the gradation curve (the portion representing percentage passing of the smaller particles with size less than 1 mm) the OKC mix is of coarser gradation, followed by the Test Road surface, the Davis and the Test Road base mixes. Therefore, the permeability values of the OKC base mix and the Test Road surface mix are greater than the Davis and the Test Road base mixes.

From the results shown in Table 5.32, even a slight change in air voids, approximately 1% in the Test Road surface mix and the OKC base mix, changes the permeability values approximately by 50%. Therefore, it is evident that the air voids is one of the key factors affecting the permeability of HMA mixes. It is evident that as the size of air voids increase, the potential for interconnected air voids also increases. This is also evident from the study by Mallick et al. (2003) that found a slight change in air voids causes a major change in permeability. Mallick et al. (2003) also reported that mixes with larger NMAS values have more potential to be permeable. But, it depends on whether a gradation is fine or coarse graded for a given NMAS. The combination of larger NMAS and less fine aggregate to fill the air voids likely results in coarse graded mixes having more interconnected voids. This factor is consistent with the results obtained from the present study. The percentage fines in the Test Road surface mix and the OKC base mixes are comparatively lower than the Davis base mix and the Test Road base mix. This leads to an increase in interconnected open air voids in the specimens and it

eventually increases the permeability values.

A statistical model was developed to correlate the permeability with specific mix properties, namely air voids, binder content, specific gravity and percentage fines using the stepwise method. The developed model is shown below:

$$k_{Pred} = 8.10 + 5.48\ A_v - 7.15\ N_{200} \qquad (5.11)$$

where, k_{pred} = permeability, in 10^{-6} cm/s, A_v = air voids, in %, and N_{200} = aggregate passing No. 200 sieve, in %.

As expected, the air voids and percentage passing No. 200 sieve are well correlated with the permeability with an R-squared value of 0.96. From the developed model, it is clear that an increase in air voids increases the permeability, as expected. Also, the lesser the amount of N_{200} particles in the mix, the higher the permeability. This is consistent with the factors discussed previously. The ANOVA of this statistical model yields an F value of 55.3 with a P_r less than 0.0004, which indicates that the model is considered statistically significant in predicting the variation of permeability with mix properties, namely air voids and percentage fines. Table 5.33 shows a comparison between the predicted and calculated permeability values. Also, a comparison between the predicted and obtained permeability is illustrated in Figure 5.44. From this figure, it is evident that the values are close to the 45° line, which indicates that such a model could be a good indicator in making performance predictions of laboratory permeability due to the aforementioned specific mix properties.

Table 5.1 Gradations of Chat from Different Sources

Percent Passing through Different Sieve Sizes					
Sieve Size	Chat* (This Study)	KNRC[1]	KNRC[2]	ATRC[2]	OTRC[2]
12.5-mm (1/2-in.)	100	100	100	100	100
9.5-mm (3/8-in.)	99	100	99.8	99.9	99.9
4.75-mm (#4)	76	79.2	86.1	80.4	82
2.36-mm (#8)	48.5				
2-mm (#10)	43	43.6	65.4	52.7	50.1
1.18-mm (#16)	31.2				
0.6-mm (#30)	20.4				
0.425-mm (#40)	16	11.5	17.3	22.6	18.7
0.30-mm (#50)	12.6				
0.18-mm (#80)	9	8	8.6	14.3	10.3
0.15-mm (#100)	8				
0.075-mm (200)	6.1	3.5	3.9	7.4	5.6

[1]Wasiuddin et al. (2005); [2]Datin and Cates (2002)

*Tri-State Asphalt

Table 5.2 Proportions of Aggregates

Trial Blends	Chat* (%)	Limestone (9/16-in)	Limestone (1.5-in)	Limestone (Screenings)
RSM80-1	80	20	00	00
RSM80-2	80	14	00	06
RBM50-1	50	35	15	00
RBM50-2	50	28	15	07

*Tri-State Asphalt

Table 5.3 Gradations of Trial Blends

Sieve Size	Chat*	Limestone (9/16-in.)	Limestone (1.5-in.)	Limestone (Screenings)	RSM80-1	RSM80-2	RBM50-1	RBM50-2
37-mm (1.5-in.)			100				100	100
25-mm (1-in.)			91				98.65	98.65
19-mm (3/4-in.)	100	100	62	100	100	100	94.3	94.3
12.5-mm (1/2-in.)	100	99	33	100	99.8	99.9	89.6	89.67
9.5-mm (3/8-in.)	99	74	19	100	94	95.6	78.25	80.07
4.75-mm (#4)	76	10	3	93	62.8	67.8	41.95	47.76
2.36-mm (#8)	48.5	3	3	75	39.4	43.7	25.75	30.79
1.18-mm (#16)	31.2	2	2	61	25.4	28.9	16.6	20.73
0.6-mm (#30)	20.4	2	2	46	16.7	19.4	11.2	14.28
0.30-mm (#50)	12.6	2	2	30	10.5	12.2	7.3	9.26
0.15-mm (#100)	8	2	2	20	6.8	7.9	5	6.26
0.075-mm (200)	6.1	2	2	14	5.3	6	4.05	4.89

*Tri-State Asphalt

Table 5.4 Bulk Specific Gravity of Trial Blends

Trial Blends	Specific Gravity
RSM80-1	2.483
RSM80-2	2.458
RSM80-2 (Repeat)	2.465
RBM50-1	2.504
RBM50-2	2.491
RBM50-2 (Repeat)	2.504

Table 5.5 Consensus Aggregate Properties of Trial Blends

Trial Blends	Coarse Aggregate Angularity (%)	ODOT Req. Min. (%)	Fine Aggregate Angularity (%)	ODOT Req. Min. (%)	Flat or Elongated Particles (%)	ODOT Req. Max. (%)	Sand Equivalent (%)	ODOT Req. Min. (%)
RSM80-1	100	95	46	45	<5	10	76	45
RSM80-2	100		46		<5		78	
RBM50-1	100	95	47	45	<5	10	82	40
RBM50-2	100		47		<5		84	

Table 5.6 Source Aggregate Properties

Aggregate	L.A. Abrasion (%)	ODOT Req. Max. (%)	Aggregate Durability Index (%)	ODOT Req. Min. (%)	Insoluble Residue (%)	ODOT Req. Min. (%)
Chat	18	40	78	40	98	40
Limestone	38		65		25	
RSM80-2	22		75		83	
RBM50-2	28		72		62	

Table 5.7 G_{mb} and G_{mm} Values of the Trial Blends

Trial Blends	Trial Asphalt Binder Content (%)	G_{mb}	G_{mm}
RSM80-1	6.50	2.200	2.356
RSM80-2	6.50	2.229	2.349
RBM50-1	5.75	2.237	2.396
RBM50-2	5.75	2.310	2.395

Ta

Table 5.8 Volumetric Properties of the Trial Blends

Mixes	Trial Blends	Effective Specific Gravity Of Aggregate, G_{se}	Asphalt Absorption of Aggregate, P_{ba} (%)	Effective Asphalt Content, P_{be} (%)	Air Voids, V_a (%)	Voids in Mineral Aggregate, VMA (%)	Voids Filled With Asphalt, VFA (%)
RSM80	RSM80-1	2.597	1.794	4.822	6.633	17.138	61.295
	RSM80-2	2.588	2.056	4.577	5.096	15.199	66.473
RBM50	RBM50-1	2.610	1.664	4.182	6.662	15.806	57.850
	RBM50-2	2.608	1.846	4.011	3.559	12.613	71.783

Table 5.9 Estimated Volumetric Properties of the Trial Blends at the Estimated OAC

Mixes	Trial Blends	Est. OAC (%)	Est. VMA at Est. OAC (%)	Req. VMA (%)	Est. VFA at Est. OAC (%)	Req. VFA (%)
RSM80	RSM80-1	7.55	16.61	Min 15	75.92	65-76
	RSM80-2	6.94	14.98	Min 15	73.30	65-76
RBM50	RBM50-1	6.82	15.27	Min 13	73.81	65-76
	RBM50-2	5.57	12.66	Min 13	68.40	65-76

Table 5.10 Specific Gravity and Theoretical Maximum Density of Different Mixes

Selected Blend	Asphalt Binder Content (%)	G_{mb}	G_{mm}
RSM80-2	6.25	2.228	2.373
	6.75	2.256	2.356
	7.25	2.273	2.339
RBM50-2	5.0	2.293	2.416
	5.5	2.303	2.399
	6.0	2.324	2.382

Table 5.11 (a) Volumetric Properties at Different Asphalt Binder Contents

Blend	Asphalt Content (%)	Effective Specific Gravity of Aggregate, G_{se}	Asphalt Absorption of Aggregate, P_{ba} (%)	Effective Asphalt Content, P_{be} (%)
RSM80-2	6.25	2.607	2.233	4.157
	6.75	2.607	2.233	4.668
	7.25	2.607	2.233	5.179
RBM50-2	5.0	2.603	1.555	3.522
	5.5	2.603	1.555	4.030
	6.0	2.603	1.555	4.538

Table 5.11 (b) Volumetric Properties at Different Asphalt Binder Contents

Blend	Asphalt Binder Content (%)	Air Voids, V_a (%)	Voids in Mineral Aggregate, VMA (%)	Voids Filled with Asphalt, VFA (%)
RSM80-2	6.25	6.302	15.283	58.760
	6.75	4.242	14.668	71.077
	7.25	2.855	14.473	80.274
RBM50-2	5.0	5.714	12.993	56.022
	5.5	4.209	13.059	67.766
	6.0	2.443	12.752	80.843

Table 5.12 Volumetric Properties at OAC

Blend	OAC (%)	VMA at OAC (%)	Req. VMA at OAC (%)	VFA at OAC (%)	Req. VFA at OAC (%)	DP
RSM80-2	6.85	15	Min 15	73	65-76	1.26
RBM50-2	5.55	13	Mine 13	69	65-76	1.2

Table 5.13 Summary of Mix Properties for the Collected Loose HMA Mixes

Project Site	Mix Type	Aggregate Type	Binder Type	AC (%)
Test Road	Surface Mix (S5)	Lime Stone with 80% chat	PG 64-22 OK	6.9
	Base Mix (S3)	Lime Stone with 50% chat	PG 64-22 OK	5.6
Davis	Base Mix (S2)	Lime Stone	PG 64-22 OK	4.5
OKC	Base Mix (S2)	Lime Stone	PG 64-22 OK	4.3

Table 5.14 Number of Loading Cycle Used in Each Stress Sequence

Sequence ID	**Number of Cycles**
C	200
S1	100
S2	100
S3	100
S4	100
S5	100

Table 5.15 Measured M_R for Test Road Base Mix Laboratory Specimens

Mix/Core Type	Specimen ID	Temp (°F)	Stress Ratio	Measured M_R (ksi)
Test Road Base Mix	TC-B-MR-9	41	0.21	1506
			0.28	1520
			0.36	1432
			0.41	1364
	TC-B-MR-10	41	0.19	1584
			0.26	1611
			0.32	1614
			0.38	1531
			0.42	1488
	TC-B-MR-11	41	0.19	1523
			0.25	1516
			0.32	1483
			0.38	1418
			0.42	1375
	TC-B-MR-6	77	0.21	560
			0.27	514
			0.35	445
	TC-B-MR-7	77	0.21	781
			0.28	690
			0.35	598
	TC-B-MR-8	77	0.21	924
			0.28	874
			0.35	740
	TC-B-MR-13	104	0.25	145
			0.33	142
			0.41	143
			0.49	130
			0.57	108
	TC-B-MR-14	104	0.28	187
			0.38	195
			0.47	174
			0.57	142
	TC-B-MR-15	104	0.20	239
			0.26	230
			0.33	243
			0.39	229
			0.45	186

Table 5.16 Measured M_R for Test Road Surface Mix Laboratory Specimens

Mix/Core Type	Specimen ID	Temp (°F)	Stress Ratio	Measured M_R (ksi)
Test Road Surface Mix	TC-S-MR-4	41	0.21	1232
			0.28	1225
			0.36	1252
			0.42	1181
	TC-S-MR-5	41	0.20	1302
			0.27	1309
			0.35	1301
			0.41	1207
	TC-S-MR-6	41	0.21	1438
			0.28	1385
			0.36	1423
			0.42	1340
			0.46	1310
	TC-S-MR-1	77	0.23	586
			0.30	569
			0.37	536
			0.45	498
			0.52	453
	TC-S-MR-2	77	0.22	552
			0.29	546
			0.36	522
			0.43	487
			0.50	423
	TC-S-MR-3	77	0.21	477
			0.28	449
			0.35	411
			0.42	381
			0.49	335
	TC-S-MR-7	104	0.23	158
			0.31	146
			0.39	128
			0.46	100
	TC-S-MR-8	104	0.24	170
			0.32	168
			0.39	158
			0.47	136
			0.55	119
	TC-S-MR-9	104	0.23	162
			0.30	162
			0.38	147
			0.45	124
			0.53	102

Table 5.17 Measured M_R for Test Road Cores

Mix/Core Type	Specimen ID	Temp (°F)	Stress Ratio	Measured M_R (ksi)
Test Road Cores	TC-C-MR-3	41	0.21	1465
			0.29	1403
			0.36	1354
			0.44	1346
			0.50	1464
	TC-C-MR-4	41	0.30	994
			0.40	967
			0.51	902
			0.62	897
	TC-C-MR-1	77	0.23	733
			0.30	679
			0.38	642
			0.45	567
			0.53	439
	TC-C-MR-2	77	0.26	733
			0.34	716
			0.43	694
			0.51	612
			0.60	450
	TC-C-MR-5	104	0.31	156
			0.41	144
			0.51	128
			0.61	99
	TC-C-MR-6	104	0.24	177
			0.33	174
			0.41	159
			0.49	138
			0.57	109

Table 5.18 Linear Model Parameters for Test Road Specimens ($M_R = A + BR$)

Mix/Core Type	Sample ID	Temp (°F)	A	B	R-squared
Test Road Base Mix	TC-B-MR-9	41	1694.0	-754.0	0.81
	TC-B-MR-10		1701.6	-433.9	0.54
	TC-B-MR-11		1669.9	-663.9	0.90
	TC-B-MR-6	77	732.1	-818.8	0.99
	TC-B-MR-7		1051.8	-1313.8	1.00
	TC-B-MR-8		1209.5	-1318.0	0.94
	TC-B-MR-13	104	177.8	-107.9	0.77
	TC-B-MR-14		254.4	-166.2	0.74
	TC-B-MR-15		279.7	-167.7	0.55
Test Road Surface Mix	TC-S-MR-4	41	1276.1	-166.9	0.26
	TC-S-MR-5		1407.4	-414.1	0.58
	TC-S-MR-6		1533.9	-446.7	0.71
	TC-S-MR-1	77	697.9	-452.3	0.98
	TC-S-MR-2		663.9	-441.0	0.90
	TC-S-MR-3		587.9	-504.3	0.99
	TC-S-MR-7	104	218.6	-246.5	0.96
	TC-S-MR-8		217.9	-171.9	0.92
	TC-S-MR-9		217.6	-208.4	0.92
Test Road Cores	TC-C-MR-3	41	1436.2	-83.1	0.03
	TC-C-MR-4		1093.7	-334.6	0.91
	TC-C-MR-1	77	962.6	-928.2	0.94
	TC-C-MR-2		977.2	-786.5	0.83
	TC-C-MR-5	104	215.4	-182.3	0.96
	TC-C-MR-6		237.5	-211.2	0.92

Table 5.19 Semi-Log Model Parameters for Test Road Specimens ($M_R = A\ B^R$)

Mix/Core Type	Sample ID	Temp (°F)	A	B	R-squared
Test Road Base Mix	TC-B-MR-9	5	1715.6	0.59	0.81
	TC-B-MR-10		1708.8	0.76	0.55
	TC-B-MR-11		1685.4	0.63	0.89
	TC-B-MR-6	25	791.4	0.19	0.98
	TC-B-MR-7		1163.1	0.15	1.00
	TC-B-MR-8		1306.0	0.20	0.92
	TC-B-MR-13	40	188.0	0.43	0.75
	TC-B-MR-14		265.4	0.37	0.74
	TC-B-MR-15		290.0	0.45	0.55
Test Road Surface Mix	TC-S-MR-4	5	1278.1	0.87	0.26
	TC-S-MR-5		1415.9	0.72	0.58
	TC-S-MR-6		1542.8	0.72	0.71
	TC-S-MR-1	25	729.0	0.42	0.97
	TC-S-MR-2		695.2	0.41	0.88
	TC-S-MR-3		631.9	0.29	0.98
	TC-S-MR-7	40	256.1	0.15	0.94
	TC-S-MR-8		237.5	0.31	0.91
	TC-S-MR-9		247.9	0.21	0.90
Test Road Cores	TC-C-MR-3	5	1436.2	0.94	0.03
	TC-C-MR-4		1105.5	0.70	0.91
	TC-C-MR-1	25	1102.6	0.20	0.91
	TC-C-MR-2		1114.4	0.26	0.79
	TC-C-MR-5	40	252.1	0.24	0.93
	TC-C-MR-6		272.2	0.23	0.89

Table 5.20 Log-Log Model Parameters for Test Road Specimens ($M_R = AR^B$)

Mix/Core Type	Sample ID	Temp (°F)	A	B	R-squared
Test Road Base Mix	TC-B-MR-9	41	1219.9	-0.15	0.73
	TC-B-MR-10		1433.2	-0.07	0.44
	TC-B-MR-11		1255.9	-0.13	0.81
	TC-B-MR-6	77	285.2	-0.43	0.96
	TC-B-MR-7		350.1	-0.51	0.99
	TC-B-MR-8		487.4	-0.42	0.88
	TC-B-MR-13	104	99.9	-0.30	0.65
	TC-B-MR-14		123.6	-0.38	0.65
	TC-B-MR-15		173.5	-0.22	0.45
Test Road Surface Mix	TC-S-MR-4	41	1169.4	-0.04	0.21
	TC-S-MR-5		1148.5	-0.09	0.49
	TC-S-MR-6		1234.5	-0.10	0.66
	TC-S-MR-1	77	387.3	-0.30	0.91
	TC-S-MR-2		369.7	-0.29	0.79
	TC-S-MR-3		262.0	-0.41	0.94
	TC-S-MR-7	104	66.6	-0.62	0.88
	TC-S-MR-8		98.9	-0.42	0.82
	TC-S-MR-9		79.7	-0.53	0.81
Test Road Cores	TC-C-MR-3	41	1365.3	-0.03	0.08
	TC-C-MR-4		825.5	-0.16	0.92
	TC-C-MR-1	77	345.5	-0.55	0.83
	TC-C-MR-2		403.3	-0.50	0.69
	TC-C-MR-5	104	78.9	-0.62	0.87
	TC-C-MR-6		89.6	-0.54	0.81

Table 5.21 Average M_R for the Stress Ratios 0.20, 0.35 and 0.50

Mix/Core Type	Temp (°F)	M_R								
		R = 0.20			R = 0.35			R = 0.50		
		Average (ksi)	Stdev (ksi)	CV (%)	Average (ksi)	Stdev (ksi)	CV (%)	Average (ksi)	Stdev (ksi)	CV (%)
TCB	41	1827	11	0.6	1731	8	0.5	1640	6	0.4
	77	869	11	1.3	745	7	1.0	639	5	0.7
	104	218	16	7.4	160	10	6.1	117	6	4.9
TCS	41	1610	0	0.0	1540	0	0.0	1474	0	0.0
	77	372	19	5.1	340	17	4.9	310	14	4.6
	104	81	26	32.0	61	19	31.0	46	14	30.0
DB	41	2342	81	3.5	2235	58	2.6	2132	37	1.7
	77	1423	48	3.4	1203	20	1.7	1017	2	0.2
	104	627	34	5.4	460	8	1.7	338	9	2.7
OKCB	41	1748	42	2.4	1691	35	2.1	1635	28	1.7
	77	1057	45	4.2	890	26	3.0	750	13	1.7
	104	295	63	21.2	218	37	17.0	161	21	12.9
TCC	41	1311	157	12.0	1294	142	11.0	1277	127	9.9
	77	709	15	2.2	627	12	1.9	555	9	1.7
	104	51	23	44.1	41	18	43.5	33	14	42.8
DC	41	1961	104	5.3	1932	88	4.6	1904	73	3.8
	77	1218	35	2.9	1082	24	2.2	961	16	1.6
	104	656	4	0.6	437	14	3.1	291	16	5.6
OKCC	41	2007	22	1.1	1894	17	0.9	1787	11	0.6
	77	844	37	4.4	746	28	3.8	659	21	3.1
	104	376	7	1.9	225	12	5.3	134	12	8.8

Table 5.22 Materials and Mix Properties

Project Site Site	Mix Type Type	Aggregate					Binder		
		Type	Max. Size (in)	G_{se}	L.A. Abrasion	N_{200} (%)	Type	Content (%)	G_b
Test Road	Surface Mix (S5)	Lime Stone with 80% Chat*	½	2.61	22	6.0	PG 64-22 OK	6.9	1.01
Test Road	Base Mix (S3)	Lime Stone with 50% Chat*	1	2.60	28	4.9	PG 64-22 OK	5.6	1.02
Davis	Base Mix (S2)	Lime Stone	¾	2.70	22	5.9	PG 64-22 OK	4.5	1.01
OKC	Base Mix (S2)	Lime Stone	1	2.71	16	4.7	PG 64-22 OK	4.3	1.01

*Tri-State Asphalt

Table 5.23 Percentage Difference in M_R Values of Field Cores with Respect to Laboratory Specimens

Mix Type	Temp (°F)	M_R Difference with respect to Laboratory Specimen (%)		
		R = 0.20	R = 0.35	R = 0.50
Davis	41	16	14	11
	77	14	10	6
	104	-5	5	14
OKC	41	-15	-12	-9
	77	20	16	12
	104	-28	-3	17
Test Road	41	28	25	22
	77	18	16	13
	104	76	74	72

Table 5.24 Measured and Predicted Model Parameters

Mix Type	Specimen ID	Temp (°F)	A_v (%)	$A_{Measured}$	$B_{Measured}$	$A_{Pred.}$	$B_{Pred.}$
Test Road Base Mix	TC-B-MR-9	41	5.9	1716	0.59	1949	0.70
	TC-B-MR-10	41	5.8	1709	0.76	1964	0.70
	TC-B-MR-11	41	5.7	1685	0.63	1979	0.69
	TC-B-MR-6	77	6.3	791	0.19	1058	0.36
	TC-B-MR-7	77	6.1	1163	0.15	1087	0.35
	TC-B-MR-8	77	6.3	1306	0.20	1058	0.36
	TC-B-MR-13	104	7.2	188	0.43	300	0.14
	TC-B-MR-14	104	6.8	265	0.37	359	0.12
	TC-B-MR-15	104	7.0	290	0.45	329	0.13
Test Road Surface Mix	TC-S-MR-4	41	6.7	1278	0.87	1708	0.74
	TC-S-MR-5	41	6.7	1416	0.72	1708	0.74
	TC-S-MR-6	41	6.7	1543	0.72	1708	0.74
	TC-S-MR-1	77	9.8	729	0.42	415	0.55
	TC-S-MR-2	77	9.6	695	0.41	445	0.54
	TC-S-MR-3	77	9.9	632	0.29	401	0.55
	TC-S-MR-7	104	7.9	257	0.15	73	0.18
	TC-S-MR-8	104	7.4	238	0.31	147	0.15
	TC-S-MR-9	104	7.5	248	0.21	132	0.15
Davis Base Mix	D-MR-9	41	5.6	3706	0.54	2622	0.69
	D-MR-12	41	7.1	2247	0.54	2400	0.77
	D-MR-14	41	6.7	3570	0.61	2459	0.74
	D-MR-6	77	5.9	1801	0.42	1746	0.34
	D-MR-8	77	4.9	2261	0.37	1894	0.29
	D-MR-T2	77	6.2	2699	0.07	1701	0.36
	D-MR-15	104	7.8	658	0.07	839	0.17
	D-MR-16	104	6.9	1074	0.05	973	0.12
	D-MR-17	104	6.5	572	0.30	1032	0.10
OKC Base Mix	OKC-MR-5	41	7.5	1632	1.14	1865	0.79
	OKC-MR-6	41	8.0	1349	1.68	1791	0.81
	OKC-MR-1	77	5.1	1381	0.16	1389	0.30
	OKC-MR-2	77	5.3	1151	0.14	1359	0.31
	OKC-MR-3	77	6.1	1419	0.10	1240	0.35
	OKC-MR-7	104	7.2	1106	0.01	453	0.14
	OKC-MR-8	104	8.1	407	0.20	319	0.19
	OKC-MR-9	104	6.5	985	0.03	557	0.10

Table 5.24 Measured and Predicted Model Parameters (Cont'd)

Mix Type	Specimen ID	Temp (°F)	Av (%)	$A_{Measured}$	$B_{Measured}$	$A_{Pred.}$	$B_{Pred.}$
Test Road Cores	TC-C-MR-3	41	9.2	1436	0.94	1460	0.88
	TC-C-MR-4	41	10.9	1106	0.70	1207	0.97
	TC-C-MR-1	77	7.7	1103	0.20	850	0.44
	TC-C-MR-2	77	7.9	1114	0.26	820	0.45
	TC-C-MR-5	104	8.6	252	0.24	92	0.21
	TC-C-MR-6	104	8.9	272	0.23	48	0.23
Davis Cores	D-C-MR-3	41	9.2	1770	0.72	2088	0.88
	D-C-MR-4	41	10.4	1600	1.47	1910	0.94
	D-C-MR-1	77	7.8	1466	0.23	1464	0.44
	D-C-MR-2	77	8.3	782	0.47	1389	0.47
	D-C-MR-5	104	5.7	330	0.33	1151	0.06
	D-C-MR-6	104	6.0	359	0.27	1106	0.07
OKC Cores	OKC-C-MR-3	41	5.6	1681	0.6	2147	0.69
	OKC-C-MR-4	41	5.3	2925	1.0	2191	0.67
	OKC-C-MR-1	77	7.5	1014	0.2	1033	0.43
	OKC-C-MR-2	77	8.0	622	0.52	958	0.45
	OKC-C-MR-5	104	5.1	485	0.02	764	0.03
	OKC-C-MR-6	104	5.3	376	0.1	735	0.04

$$A_{Pred} = 3048.96 - 23.12\,T - 148.36\,A_v - 280.39\,AC + 443.04\,N_{200}$$
$$B_{Pred} = 0.803 - 0.010\,T + 0.053\,A_v$$

Table 5.25 Sensitivity Check for M_R Model by Changing Each Variable by 20%

Stress Ratio (R)	Temperature T, (°F)	Air Voids (A_V), (%)	Binder Content (AC), (%)	% Passing No. 200 Sieve N_{200}, (%)	M_R (ksi)	Change of M_R (%)
0.20*	77.0*	7.0*	4.0*	5.0*	1104*	-
0.24	77.0	7.0	4.0	5.0	1065	-4
0.20	**92.4**	7.0	4.0	5.0	733	-34
0.20	77.0	**8.4**	4.0	5.0	963	-13
0.20	77.0	7.0	**4.8**	5.0	917	-17
0.20	77.0	7.0	4.0	**6.0**	1474	33

$$M_R = (3048.96 - 23.12\,T - 148.36\,A_v - 280.39\,AC + 443.04\,N_{200}) \times (0.803 - 0.010\,T + 0.053\,A_v)^R$$

Table 5.26 Matrix of APA Rut Results

* - Reference Value

Sample ID	Air Voids (%)	Rut Depth (mm)
Test Road Base Mix		
TC-B-R-1	7.2	3.4
TC-B-R-2	7.5	
TC-B-R-3	7.2	6.1
TC-B-R-4	6.8	
TC-B-R-5	6.7	5.1
TC-B-R-6	6.9	
AVG (STDEV)	***7.0 (0.3)***	***4.9 (1.4)***

Sample ID	Air Voids (%)	Rut Depth (mm)
Test Road Surface Mix		
TC-S-R-1	7.7	7.9
TC-S-R-2	9.5	
TC-S-R-3	7.9	7.7
TC-S-R-4	7.2	
TC-S-R-5	7.9	7.1
TC-S-R-6	7.2	
AVG (STDEV)	***7.9 (0.8)***	***7.6 (0.4)***

Sample ID	Air Voids (%)	Rut Depth (mm)
Test Road Cores		
TC-C-R-1	7.2	8.3
TC-C-R-2	9.6	
TC-C-R-3	7.0	8.5
TC-C-R-4	8.2	
TC-C-R-5	6.9	11.6
TC-C-R-6	8.9	
AVG (STDEV)	***8.0 (1.1)***	***9.5 (1.8)***

Davis Base Mix		
D-B-R-1	7.3	2.9
D-B-R-2	7.6	
D-B-R-3	7.0	2.2
D-B-R-4	7.0	
D-B-R-5	6.3	2.9
D-B-R-6	6.8	
AVG (STDEV)	***7.0 (0.4)***	***2.7 (0.4)***

Davis Cores		
D-C-R-1	8.5	2.4
D-C-R-2	7.8	
D-C-R-3	6.8	3.4
D-C-R-4	6.1	
D-C-R-5	7.8	3.5
D-C-R-6	8.3	
AVG (STDEV)	***7.5 (0.9)***	***3.1 (0.6)***

OKC Base Mix		
OKC-B-R-1	7.3	2.4
OKC-B-R-2	6.9	
OKC-B-R-3	6.9	2.5
OKC-B-R-4	6.6	
OKC-B-R-5	6.5	2.4
OKC-B-R-6	6.4	
AVG (STDEV)	***6.8 (0.3)***	***2.4 (0.05)***

OKC Cores		
OKC-C-R-1	5.8	6.3
OKC-C-R-2	6.6	
OKC-C-R-3	5.0	5.3
OKC-C-R-4	5.3	
OKC-C-R-5	4.5	5.3
OKC-C-R-6	4.4	
AVG (STDEV)	***5.3 (0.8)***	***5.6 (0.6)***

Table 5.27 Predicted Rut Depth from Material and Mix properties

Mix Type	Sample ID	$Rut_{Measured}$ (mm)	Rut_{Pred} (mm)
Test Road Base	1	3.4	6.95
	2	6.1	6.95
	3	5.1	6.95
Test Road Surface	1	7.9	6.38
	2	7.7	6.38
	3	7.1	6.38
Test Road Cores	1	8.3	6.95
	2	8.5	6.95
	3	11.6	6.95
Davis Base	1	2.9	2.70
	2	2.2	2.70
	3	2.9	2.70
Davis Cores	1	2.4	2.70
	2	3.4	2.70
	3	3.5	2.70
OKC Base	1	2.4	4.06
	2	2.5	4.06
	3	2.4	4.06
OKC Cores	1	6.3	4.06
	2	5.3	4.06
	3	5.3	4.06

$$Log\ (Rut_{Pred}) = 0.676 + 0.179\ AC - 0.178\ N_{200} \qquad (R\text{-squared} = 0.56)$$

Table 5.28 Predicted M_R and APA Rut Depth at 2000 and 8000 Loading Cycles

Mix/ Core Type	Rut_{2000} (mm)	Rut_{8000} (mm)	M_R (ksi) at 41°F			M_R (ksi) at 77°F			M_R (ksi) at 104°F		
			R			R			R		
			0.20	0.35	0.50	0.20	0.35	0.50	0.20	0.35	0.50
TCB	3.1	4.8	1827	1731	1640	869	745	639	217	159	117
TCS	4.6	7.6	1610	1540	1473	372	339	310	81	61	46
TCC	5.5	9.7	1310	1293	1277	708	627	554	51	40	32
DB	1.5	2.7	2342	2234	2132	1422	1202	1017	626	460	338
DC	1.9	3.1	1960	1932	1904	1218	1082	961	655	436	290
OKCB	1.5	2.5	1748	1690	1634	1057	890	749	295	217	161
OKCC	3.9	5.6	2007	1893	1786	844	745	658	376	224	134

Table 5.29 Models for Predicted M_R and Rut Depth at 2000 and 8000 Loading Cycles

M_R Test Temperature (°F)	Stress Ratio	Rut - M_R Model	R-squared
41	0.20	Rut_{2000} (mm) = -0.0036 M_R (ksi) + 9.70	0.54
		Rut_{8000} (mm) = -0.0065 M_R (ksi) + 17.02	0.61
	0.35	Rut_{2000} (mm) = -0.0040 M_R (ksi) + 10.24	0.58
		Rut_{8000} (mm) = -0.0072 M_R (ksi) + 17.62	0.64
	0.50	Rut_{2000} (mm) = -0.0045 M_R (ksi) + 10.70	0.62
		Rut_{8000} (mm) = -0.0079 M_R (ksi) + 18.46	0.66
77	0.20	Rut_{2000} (mm) = -0.0039 M_R (ksi) + 6.75	0.71
		Rut_{8000} (mm) = -0.0063 M_R (ksi) + 11.03	0.65
	0.35	Rut_{2000} (mm) = -0.0046 MR (ksi) + 6.83	0.69
		Rut_{8000} (mm) = -0.0075 M_R (ksi) + 11.17	0.63
	0.50	Rut_{2000} (mm) = -0.0053 M_R (ksi) + 6.87	0.66
		Rut_{8000} (mm) = -0.0087 M_R (ksi) + 11.25	0.60
104	0.20	Rut_{2000} (mm) = -0.0052 M_R (ksi) + 4.85	0.62
		Rut_{8000} (mm) = -0.0089 M_R (ksi) + 8.08	0.63
	0.35	Rut_{2000} (mm) = -0.0079 M_R (ksi) + 4.96	0.68
		Rut_{8000} (mm) = -0.0134 M_R (ksi) + 8.20	0.67
	0.50	Rut_{2000} (mm) = -0.0117 M_R (ksi) + 5.01	0.72
		Rut_{8000} (mm) = -0.0194 M_R (ksi) + 8.25	0.68

Table 5.30 APA Fatigue Results

APA Fatigue					
Sample ID	**Air Voids (%)**	**# of Cycles**	**Sample ID**	**Air Voids (%)**	**# of Cycles**
Test Road Base Mix			**Test Road Surface Mix**		
TC-B-F-1	9.6	47,440	TC-S-F-1	10.5	48,080
TC-B-F-2	8.9	49,920	TC-S-F-2	10.0	47,520
TC-B-F-3	8.6	49,680	TC-S-F-3	10.8	49,920
Davis Base Mix			**OKC Base Mix**		
D-B-F-1	10.6	16,240	OKC-B-F-1	8.4	27,040
D-B-F-2	10.7	22,320	OKC-B-F-2	8.2	26,960
D-B-F-3	10.9	16,240	OKC-B-F-3	8.2	26,960

Table 5.31 Measured and Predicted Fatigue Cycles

Mix Type	Sample ID	$N_{f, Cal}$	N_{200} (%)	$N_{f, Pred}$
Test Road Base	1	47,440	6.00	46,852
	2	49,920	6.00	49,211
	3	49,680	6.00	50,222
Test Road Surface	1	48,080	4.90	48,493
	2	47,520	4.90	50,178
	3	49,920	4.90	47,481
Davis Base	1	16,240	5.90	18,953
	2	22,320	5.90	18,616
	3	16,240	5.90	17,942
OKC Base	1	27,040	4.70	26,340
	2	26,960	4.70	27,014
	3	26,960	4.70	27,014

$N_{f, Pred} = 826568 - 3370\ A_v - 279230\ G_{se} - 3234\ N_{200}$ *(R-squared = 0.98)*

Table 5.32 Permeability Test Results

Permeability					
Sample ID	**Air Voids (%)**	**Permeability (10^{-6} cm/s)**	**Sample ID**	**Air Voids (%)**	**Permeability (10^{-6} cm/s)**
Test Road Base Mix			**Test Road Surface Mix**		
TC-B-P-1	6.6	2.315	TC-S-P-1	7.4	13.51
TC-B-P-2	6.5	2.422	TC-S-P-2	6.6	8.10
Davis Base Mix			**OKC Base Mix**		
D-P-1	6.9	3.385	OKC-P-1	6.8	11.87
D-P-2	7.0	1.993	OKC-P-2	7.7	17.79

Table 5.33 Comparison of Measured and Predicted Permeability Values

Mix Type	Sample ID	k_{Calc} (10^{-6} cm/s)	k_{Pred} (10^{-6} cm/s)
Test Road Base	1	2.315	1.352
	2	2.422	0.804
Test Road Surface	1	13.510	13.606
	2	8.100	9.221
Davis Base	1	3.385	3.712
	2	1.993	4.260
OKC Base	1	11.870	11.749
	2	17.790	16.682

$k_{Pred} = 8.10 + 5.48\ A_v - 7.15\ N_{200}$ *(R-squared = 0.96)*

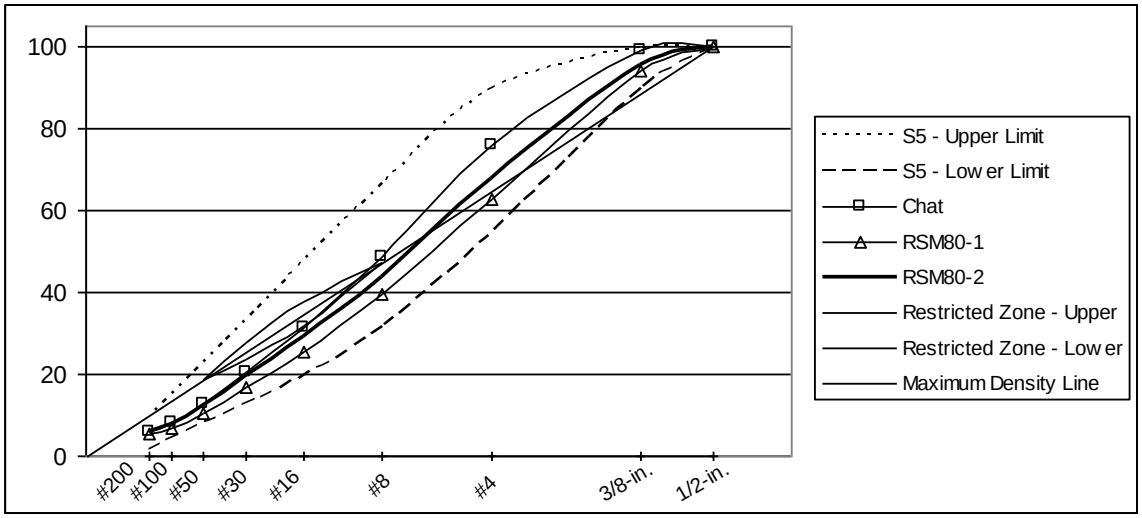

Figure 5.1 Gradation of Trial Blends for Surface Mix
*Chat is Tri-State Asphalt

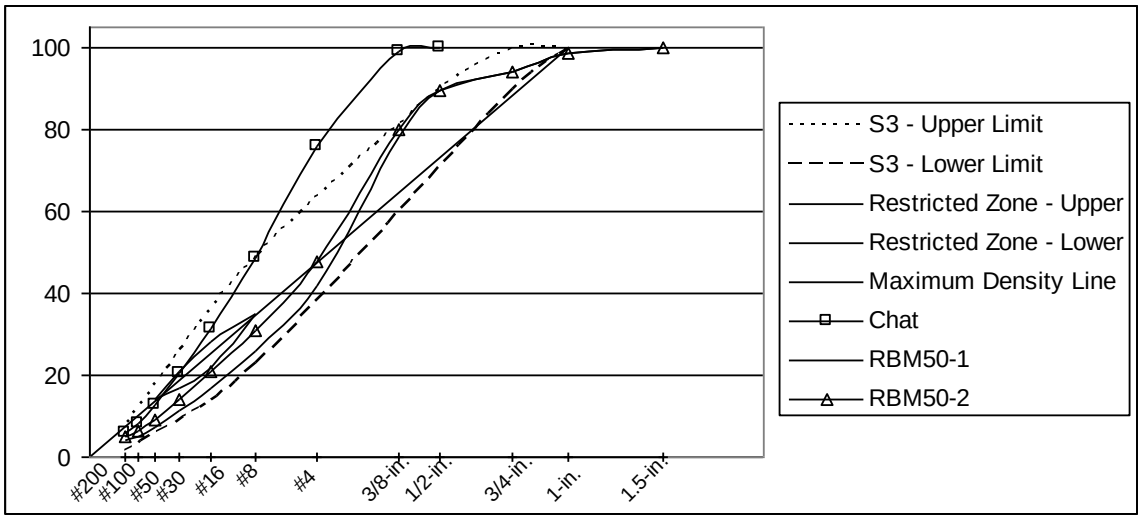

Figure 5.2 Gradation of Trial Blends for Base Mix
*Chat is Tri-State Asphalt

Figure 5.3 Collection of Loose Chat-Asphalt Mix from the Test Road Site

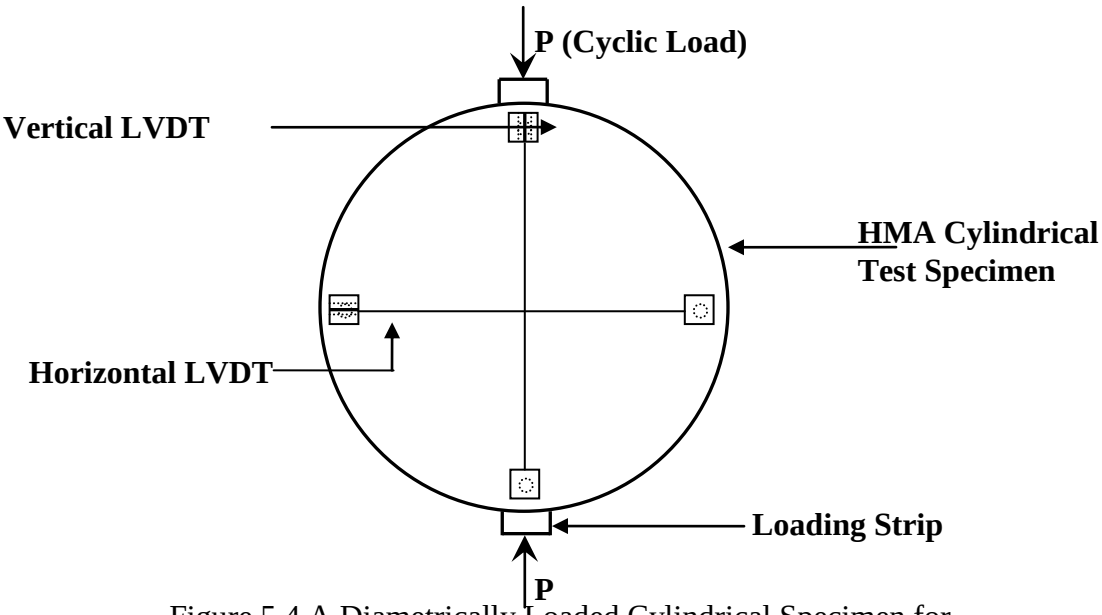

Figure 5.4 A Diametrically Loaded Cylindrical Specimen for Cyclic Indirect Tension Testing

Figure 5.5 Coring for Laboratory Testing of Test Road

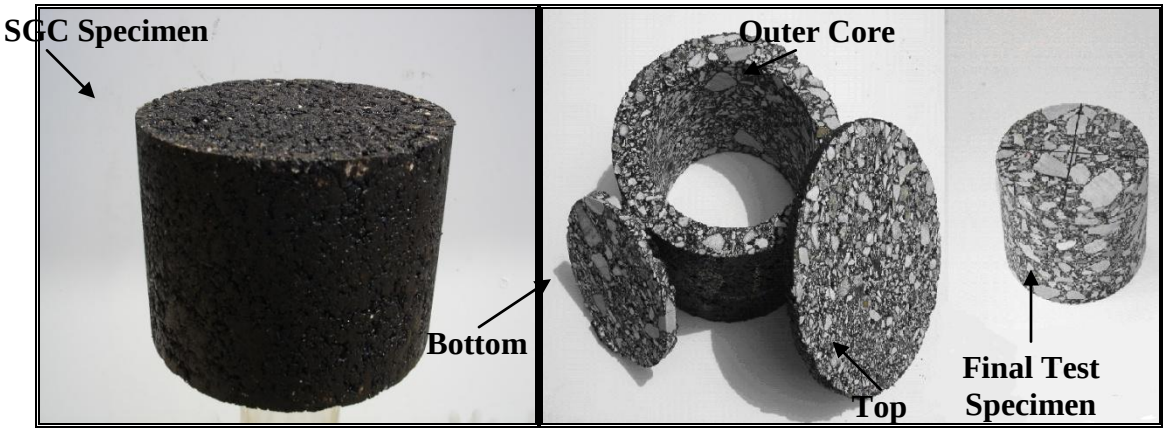

Figure 5.6 Cyclic Indirect Tension Resilient Modulus Test Specimen

Figure 5.7 Heavy Duty Asphalt Saw

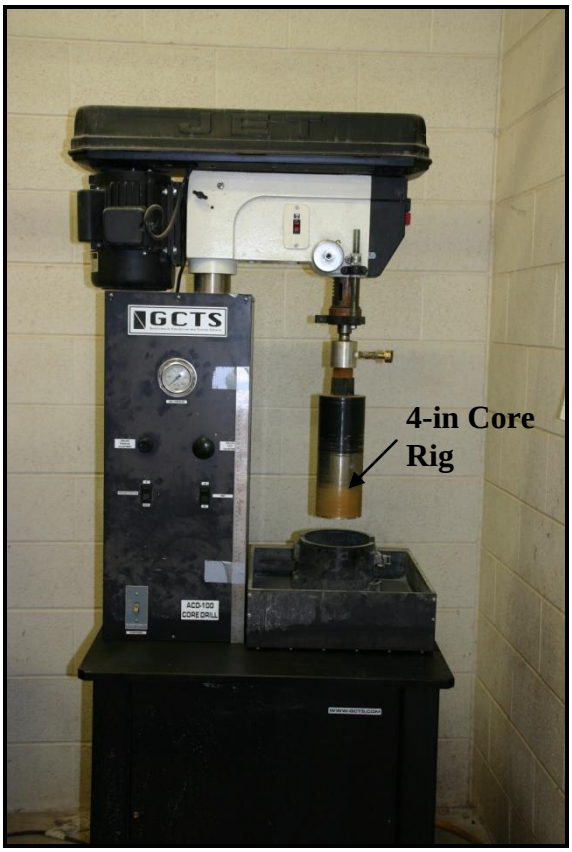

Figure 5.8 Heavy Duty Coring Machine

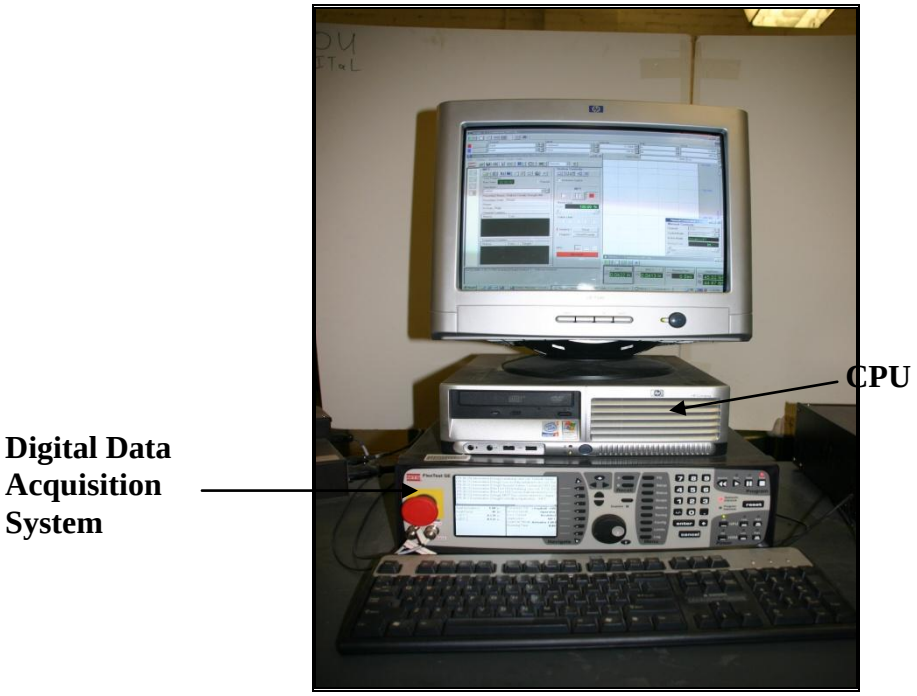

Figure 5.9 Computer Controlled MTS Digital Data Acquisition System

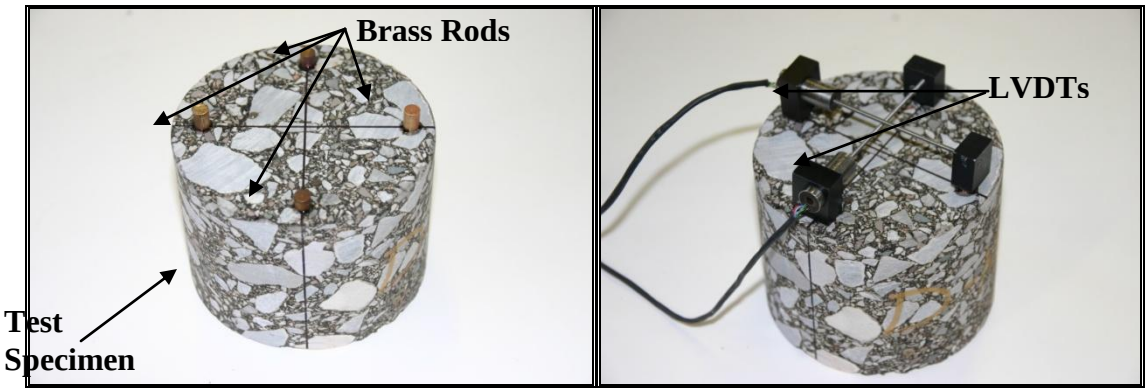

Figure 5.10 LVDTs Attached to the Cyclic Indirect Tension Resilient Modulus Test Specimen

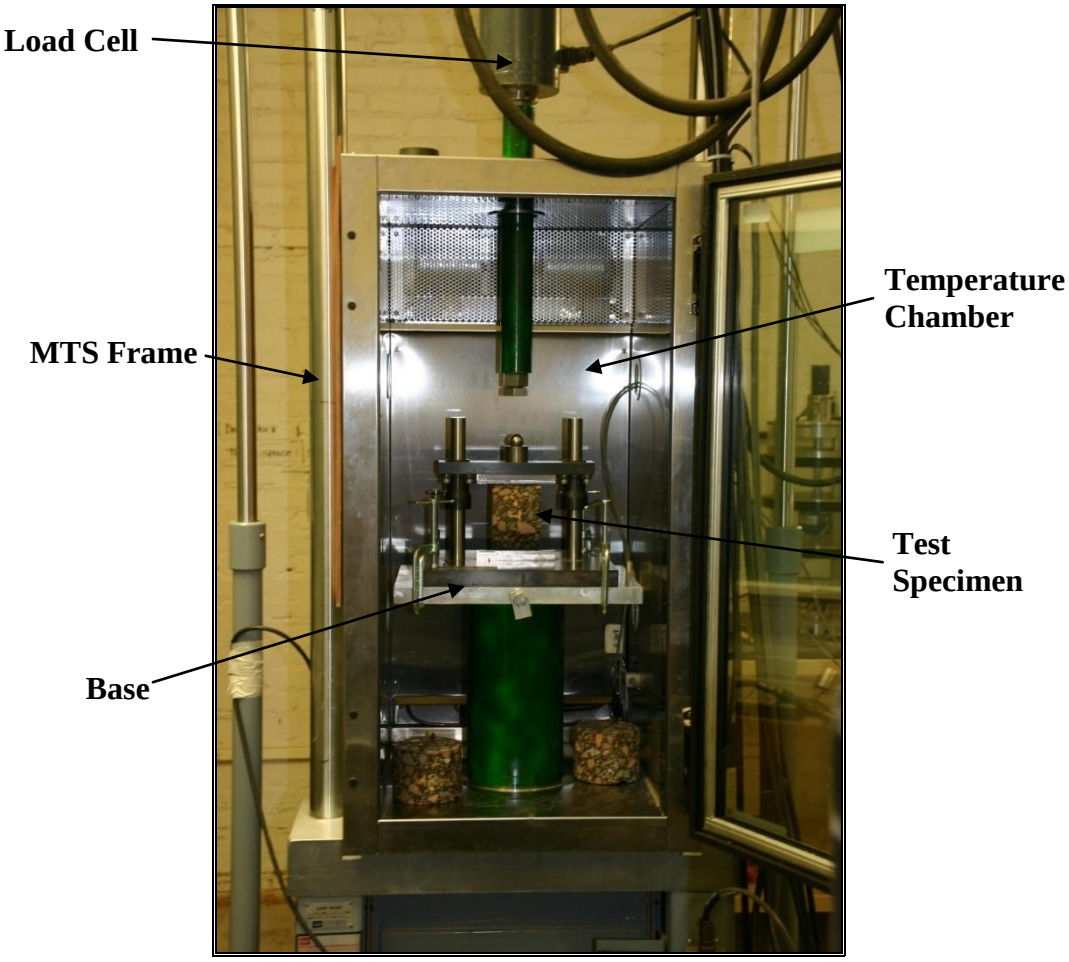

Figure 5.11 Temperature Chamber and Loading Setup Connected with the MTS Frame

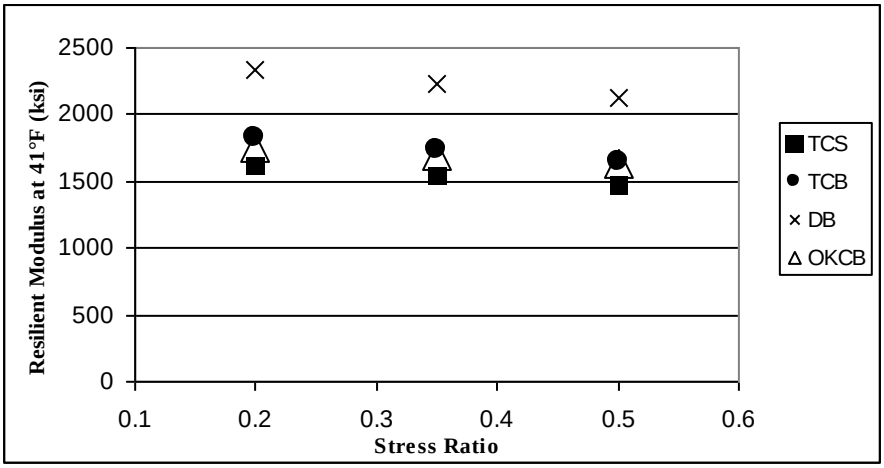

Figure 5.12 Variation of M_R with Stress Ratio for Laboratory specimen at T = 41°F

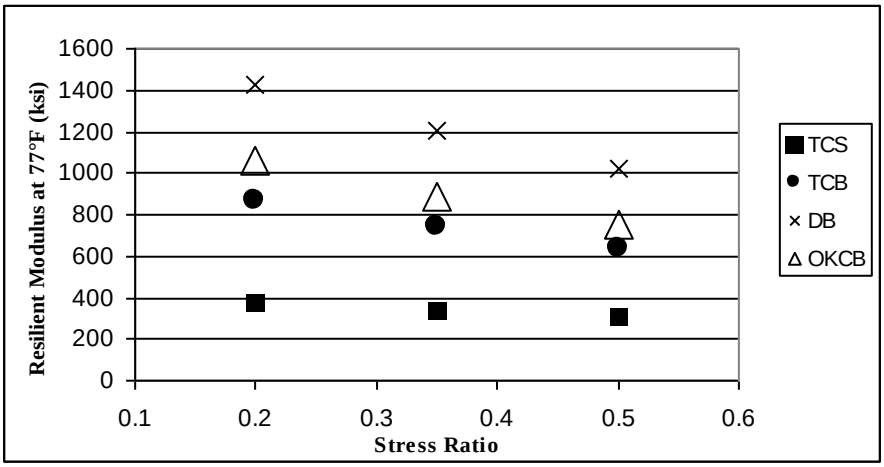

Figure 5.13 Variation of M_R with Stress Ratio for Laboratory specimen at T = 77°F

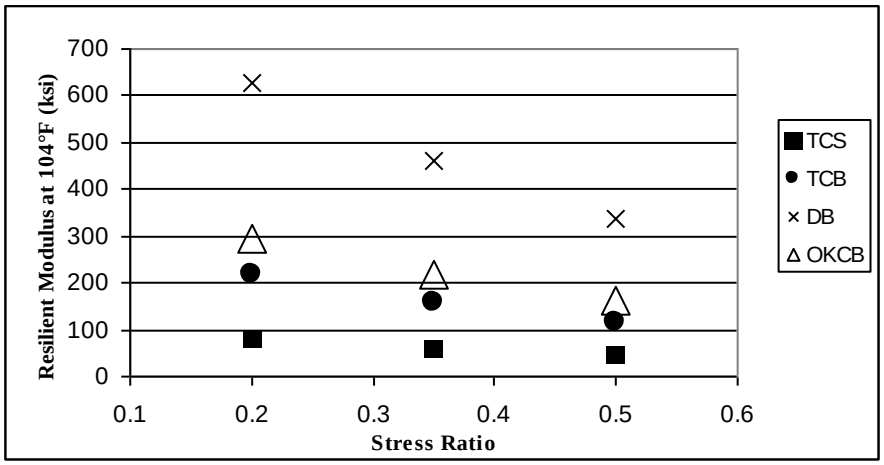

Figure 5.14 Variation of M_R with Stress Ratio for Laboratory specimen at T = 104°F

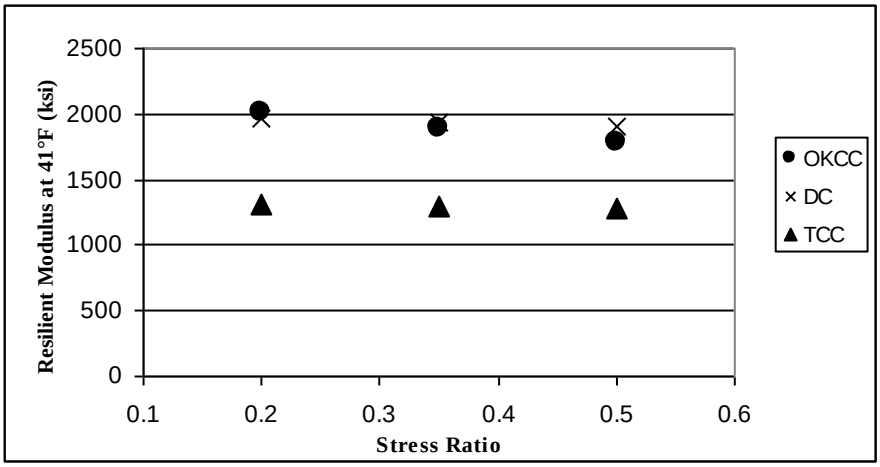

Figure 5.15 Variation of M_R with Stress Ratio for Field Cores at T = 41°F

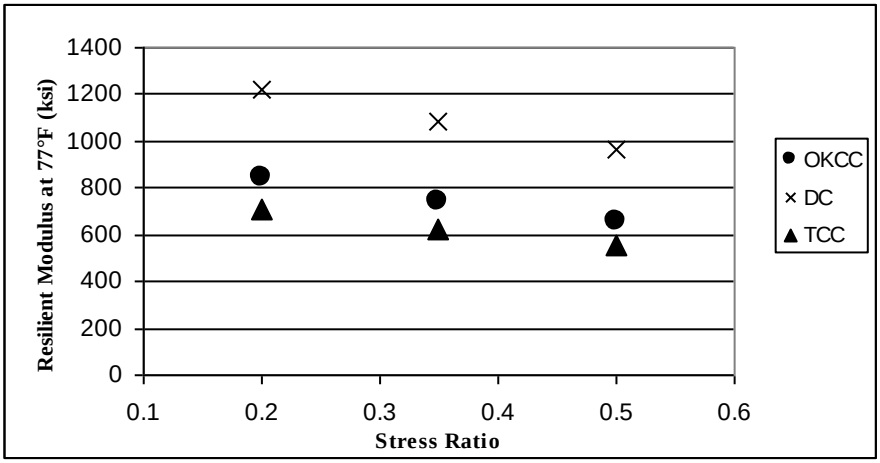

Figure 5.16 Variation of M_R with Stress Ratio for Field Cores at T = 77°F

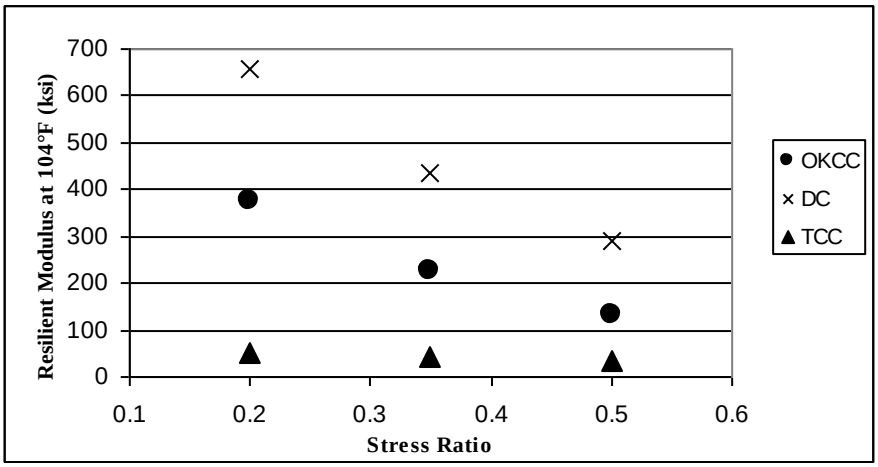

Figure 5.17 Variation of M_R with Stress Ratio for Field Cores at T = 104°F

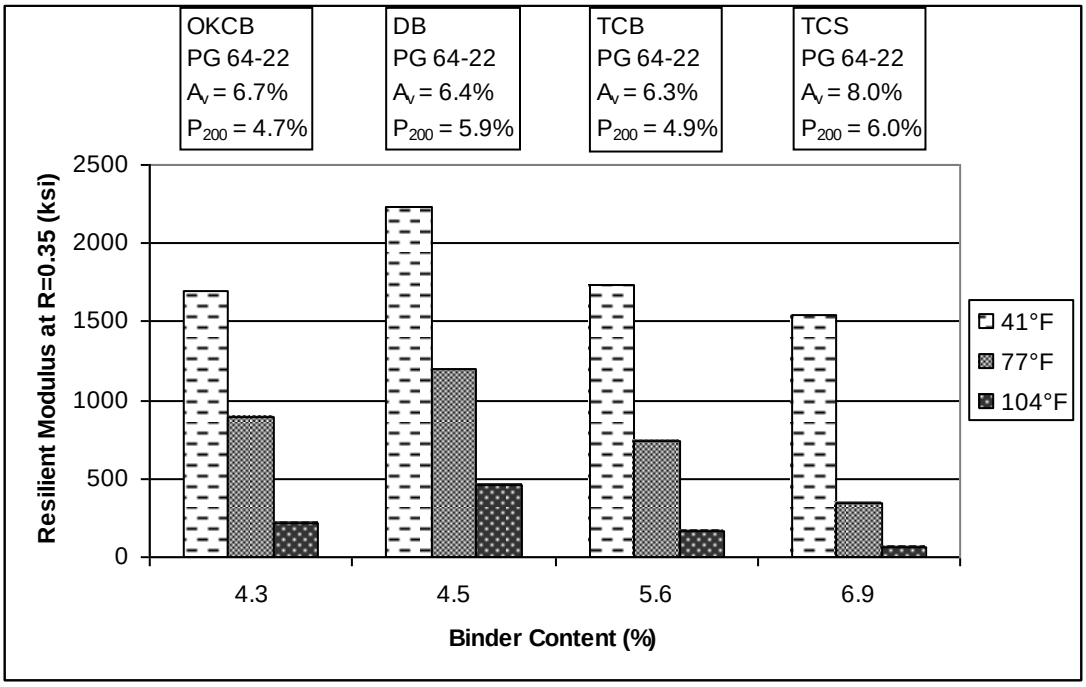

Figure 5.18 Variation of M_R with Binder Content (Laboratory Specimens)

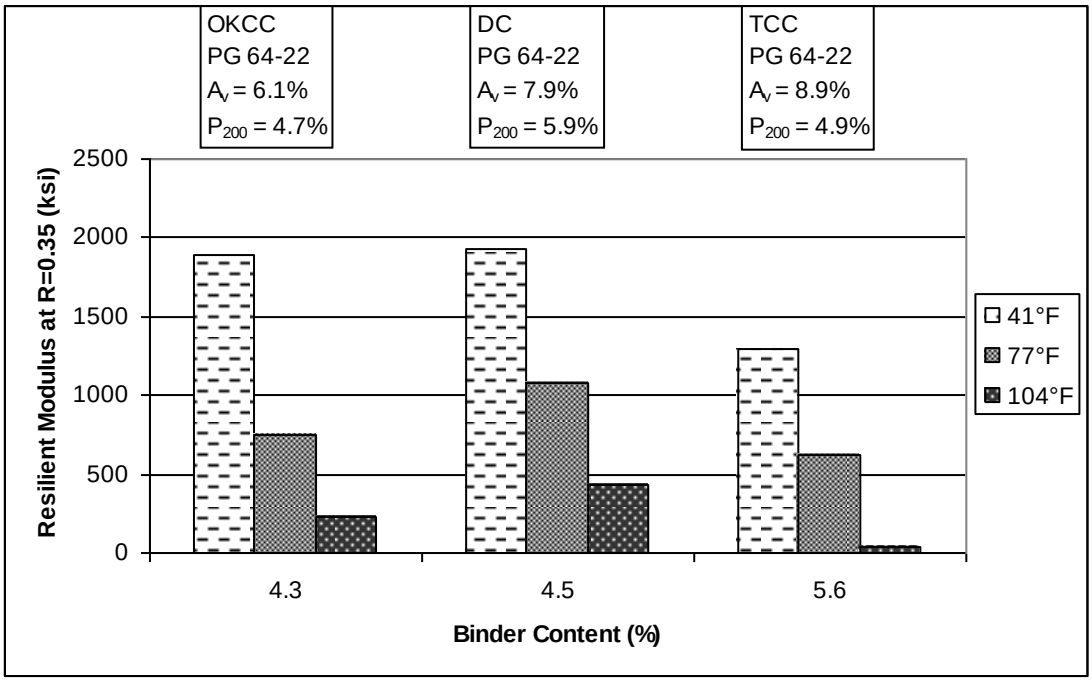

Figure 5.19 Variation of M_R with Binder Content (Field Cores)

(TCB-Tar Creek (Test Road) base mix, TCS-Tar Creek (Test Road) surface Mix, TCC-Tar Creek (Test Road) core, DB-Davis base Mix, DC-Davis core, OKCB-OKC base mix, OKCC-OKC core)

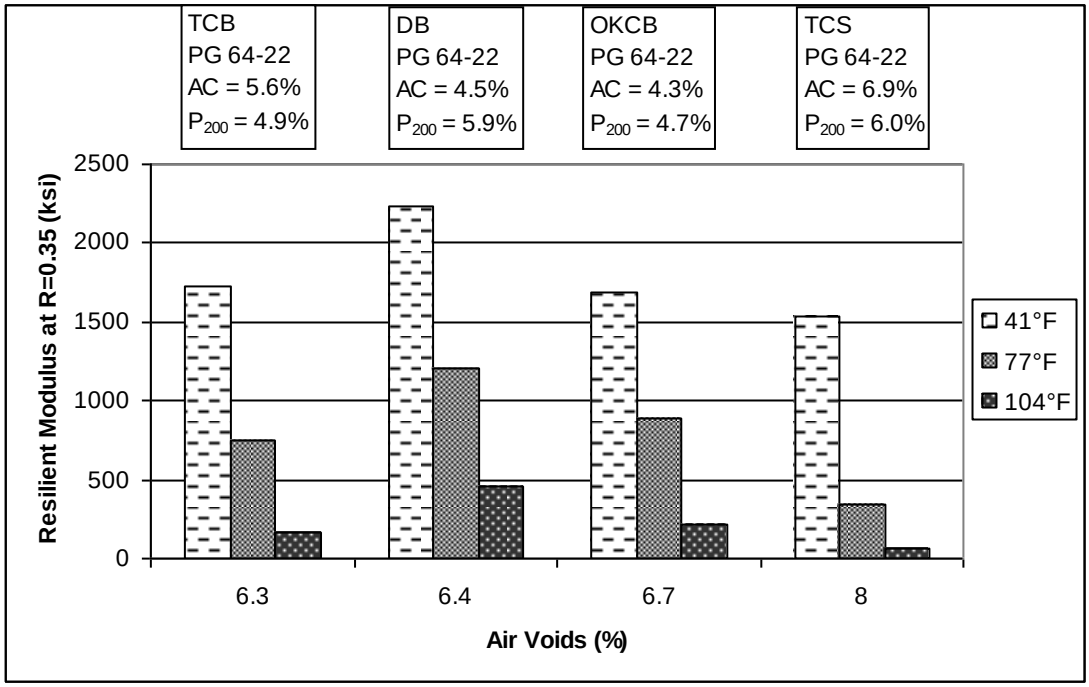

Figure 5.20 Variation of M_R with Air Voids (Laboratory Specimens)

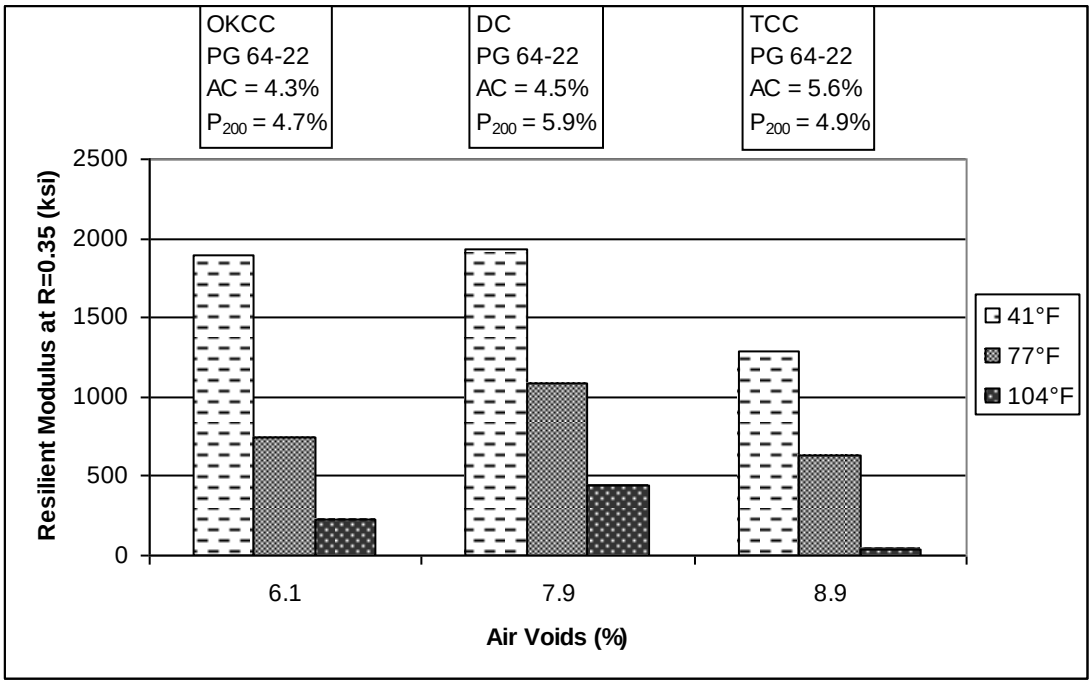

Figure 5.21 Variation of M_R with Air Voids (Field Cores)

(TCB-Tar Creek (Test Road) base mix, TCS-Tar Creek (Test Road) surface Mix, TCC-Tar Creek (Test Road) core, DB-Davis base Mix, DC-Davis core, OKCB-OKC base mix, OKCC-OKC core)

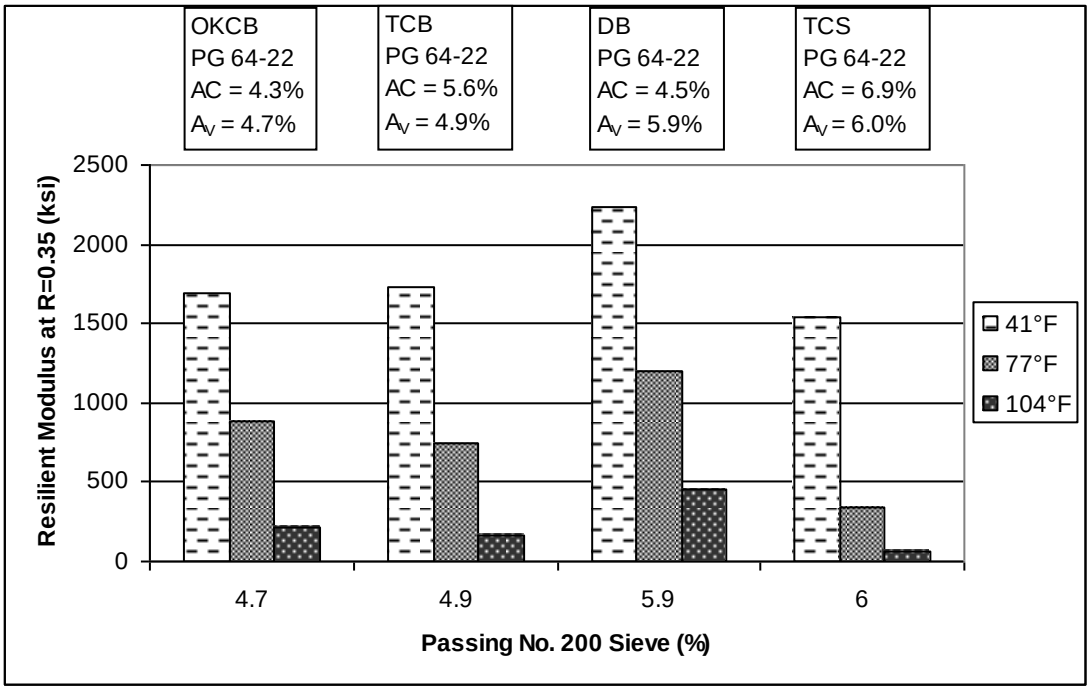

Figure 5.22 Variation of M_R with Percentage Passing No. 200 Sieve (Laboratory Specimens)

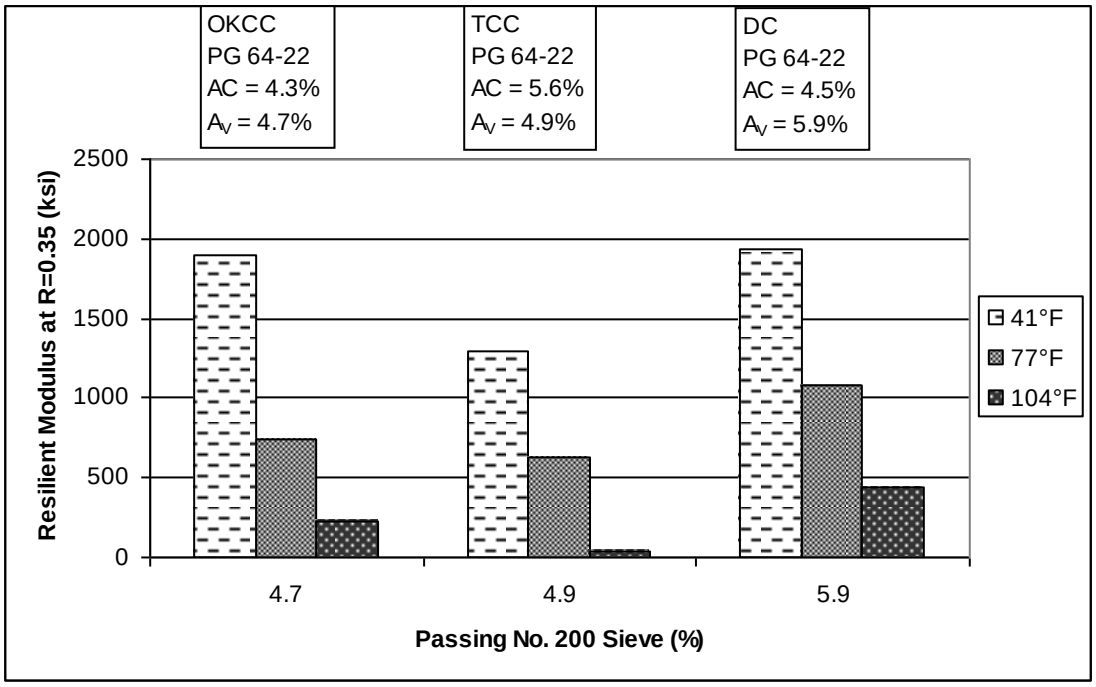

Figure 5.23 Variation of M_R with Percentage Passing No. 200 Sieve (Field Cores)

(TCB-Tar Creek (Test Road) base mix, TCS-Tar Creek (Test Road) surface Mix, TCC-Tar Creek (Test Road) core, DB-Davis base Mix, DC-Davis core, OKCB-OKC base mix, OKCC-OKC core)

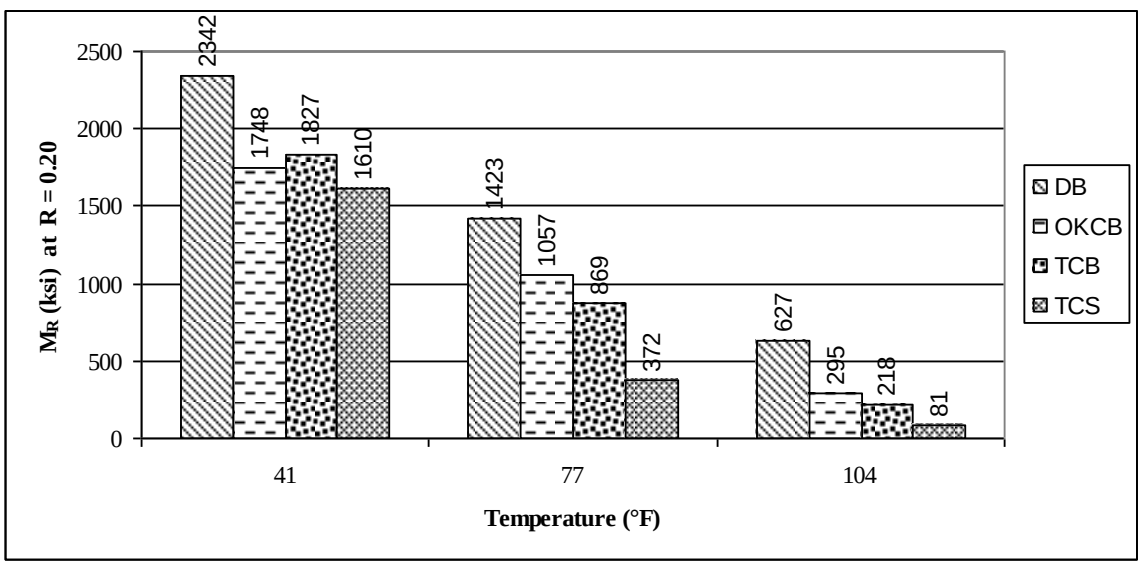

Figure 5.24 Variation of M_R with Temperature for Laboratory specimens at R = 0.20

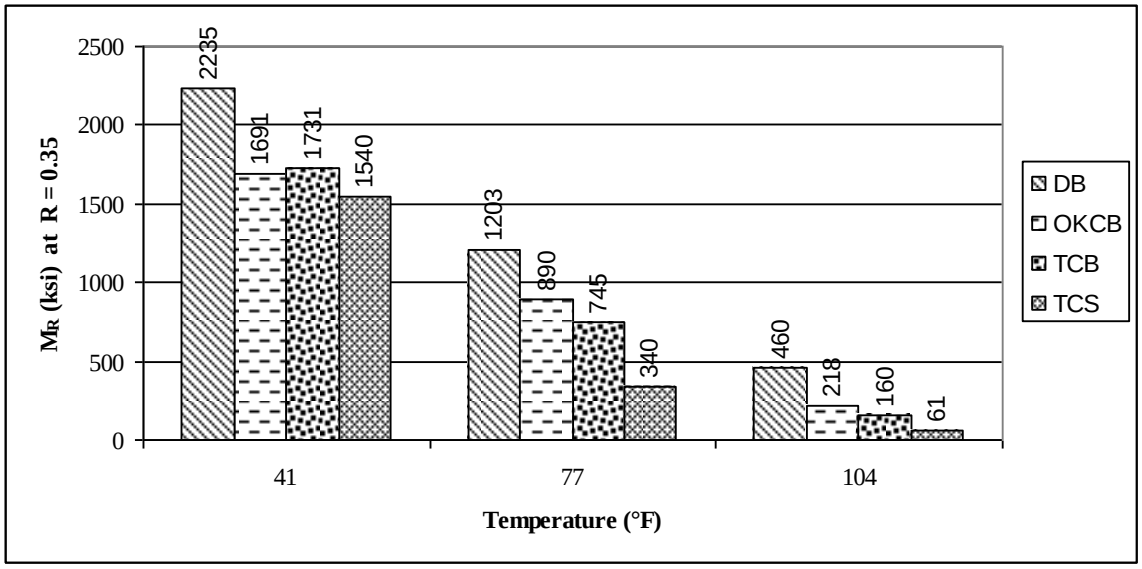

Figure 5.25 Variation of M_R with Temperature for Laboratory specimens at R = 0.35

(TCB-Tar Creek (Test Road) base mix, TCS-Tar Creek (Test Road) surface mix, DB-Davis base mix, OKCB-OKC base mix)

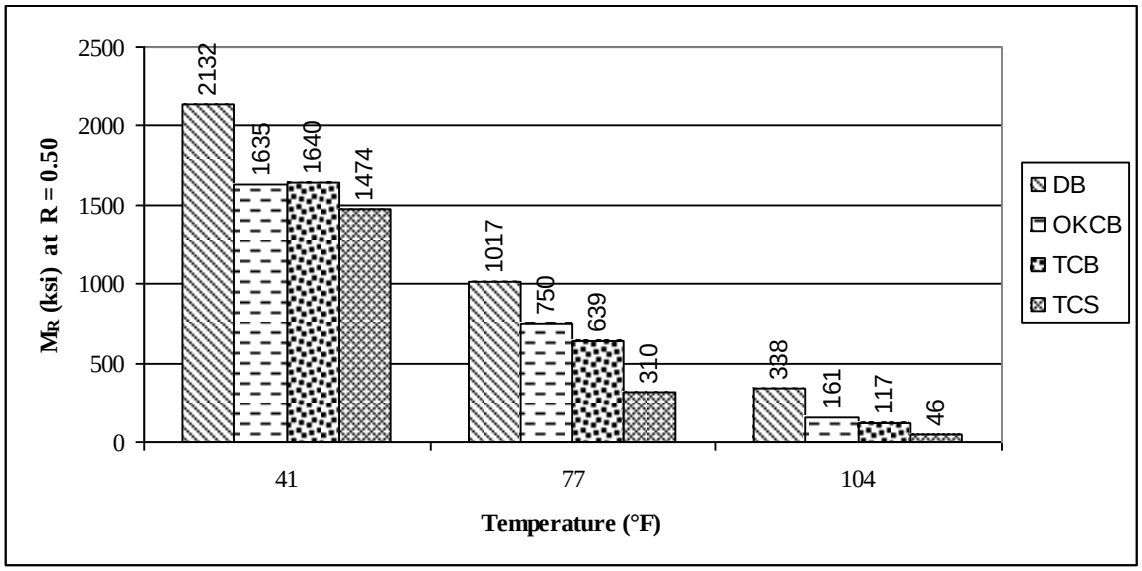

Figure 5.26 Variation of M_R with Temperature for Laboratory specimens at R = 0.50

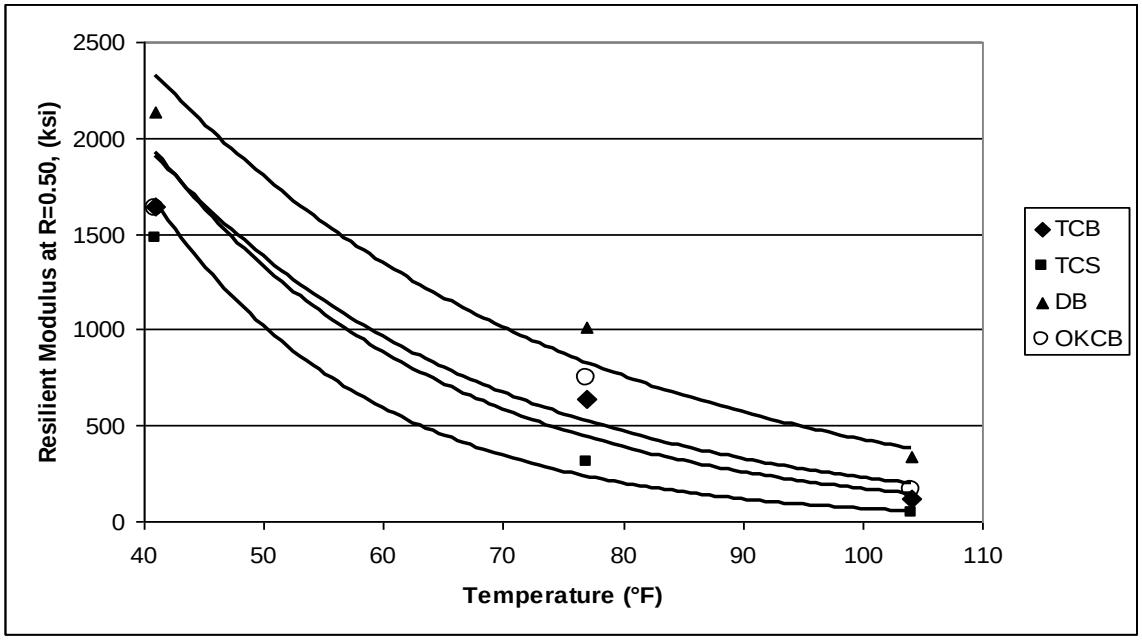

Figure 5.27 Variation of M_R with Temperature at R = 0.35 (Laboratory Specimens)

(TCB-Tar Creek (Test Road) base mix, TCS-Tar Creek (Test Road) surface Mix, TCC-Tar Creek (Test Road) core, DB-Davis base Mix, DC-Davis core, OKCB-OKC base mix, OKCC-OKC core)

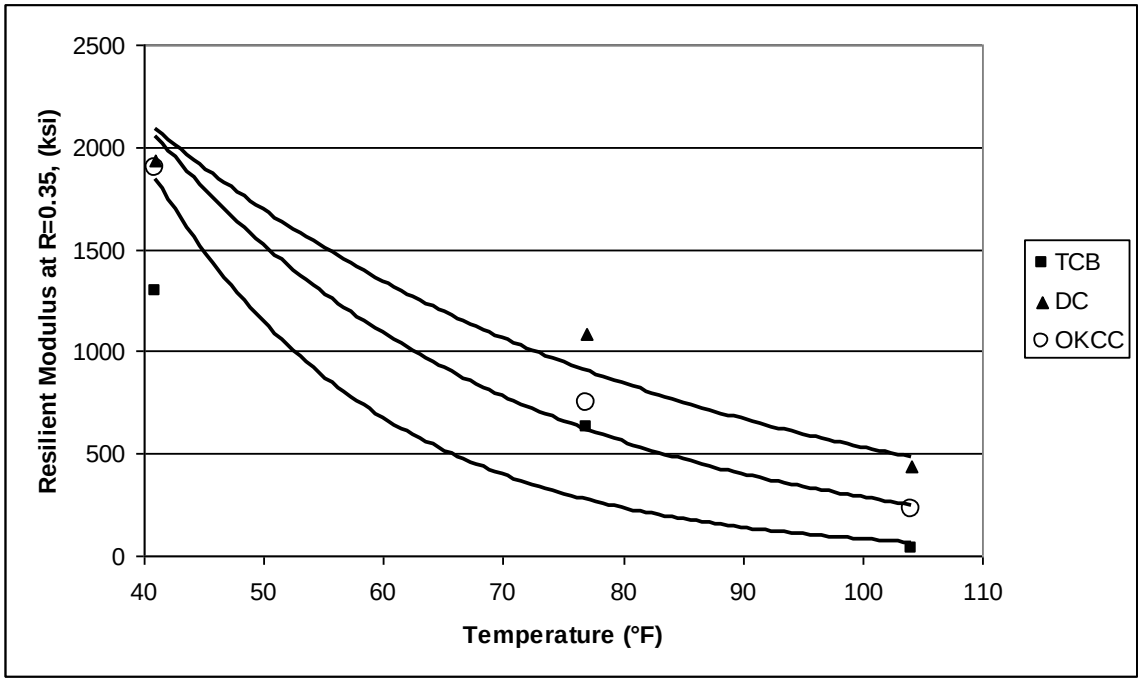

Figure 5.28 Variation of M_R with Temperature at R = 0.35 (Field Cores)

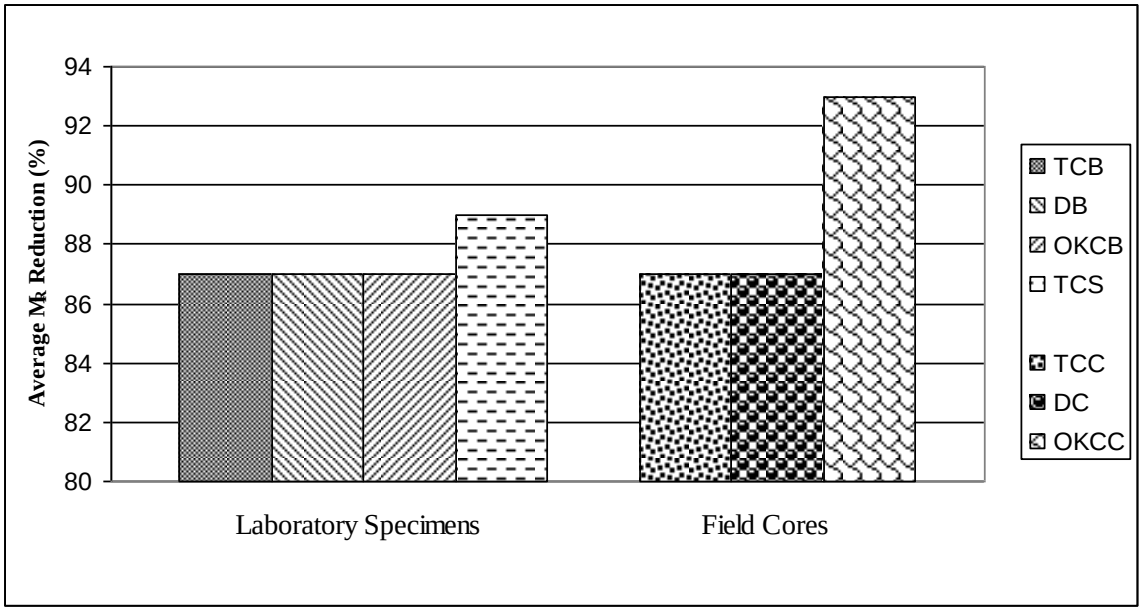

Figure 5.29 Average Decrease of M_R when Temperature increases from 41°F to 104°F

(TCB-Tar Creek (Test Road) base mix, TCS-Tar Creek (Test Road) surface Mix, TCC-Tar Creek (Test Road) core, DB-Davis base Mix, DC-Davis core, OKCB-OKC base mix, OKCC-OKC core)

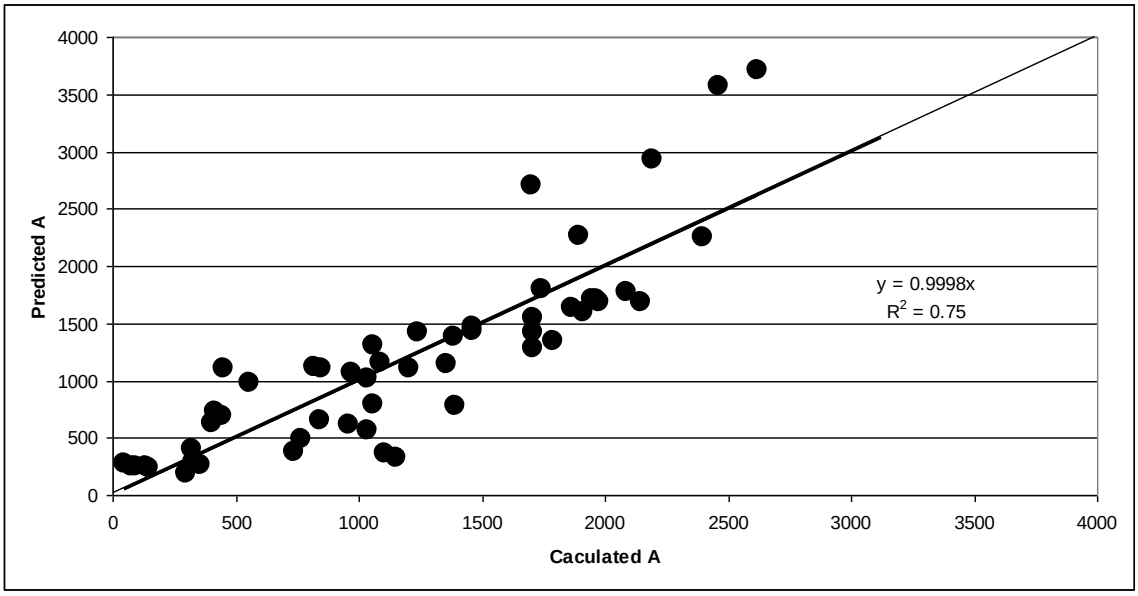

Figure 5.30 Calculated and Predicted Model Parameter A for Power Model

[$A_{pred} = 3048.96 - 23.12\ T - 148.36\ A_V - 280.39\ AC + 443.04\ N_{200}$ *(R-squared* = 0.75)]

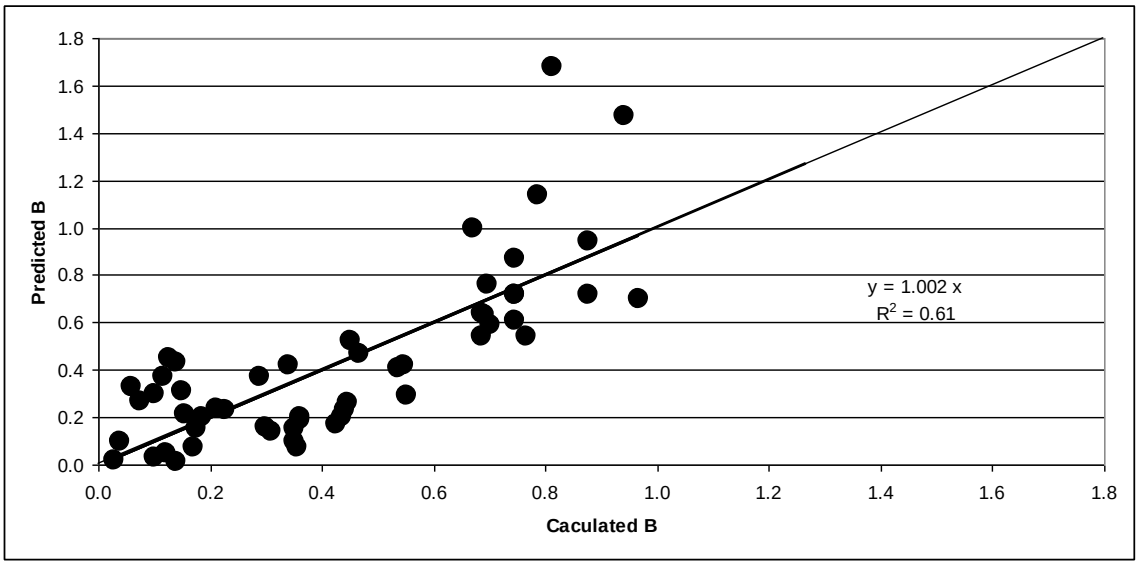

Figure 5.31 Calculated and Predicted Model Parameter B for Power Model

[$B_{pred} = 0.803 - 0.010\ T + 0.053\ A_V$ *(R-squared = 0.61)*]

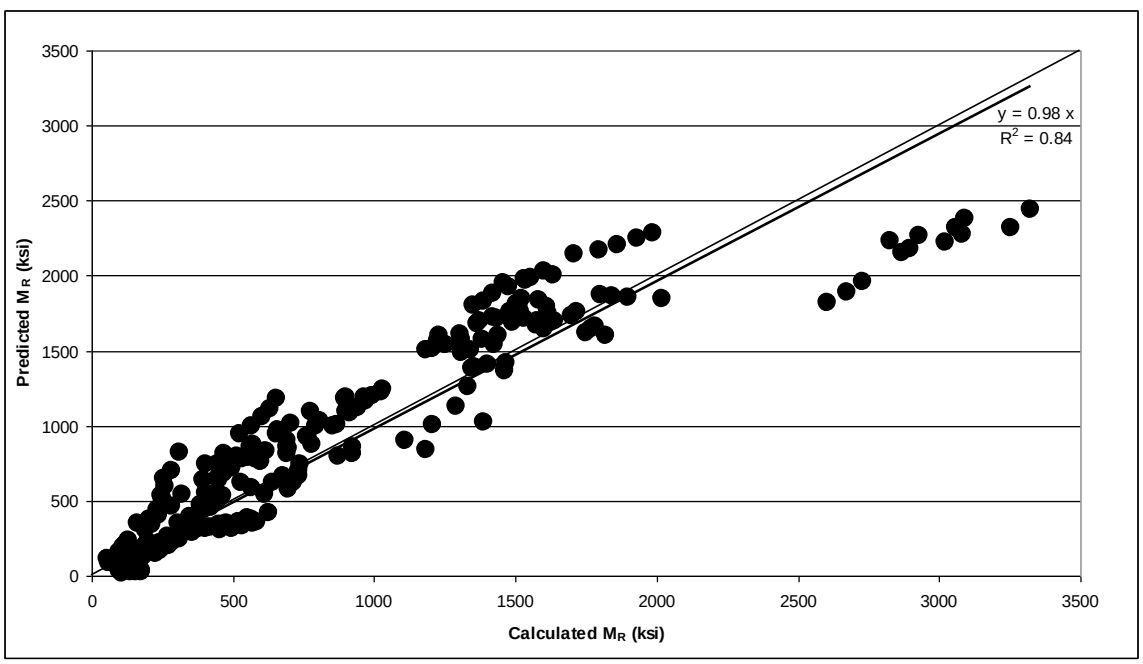

Figure 5.32 Calculated and Predicted M_R from Power Model ($M_R = A\ B^R$)

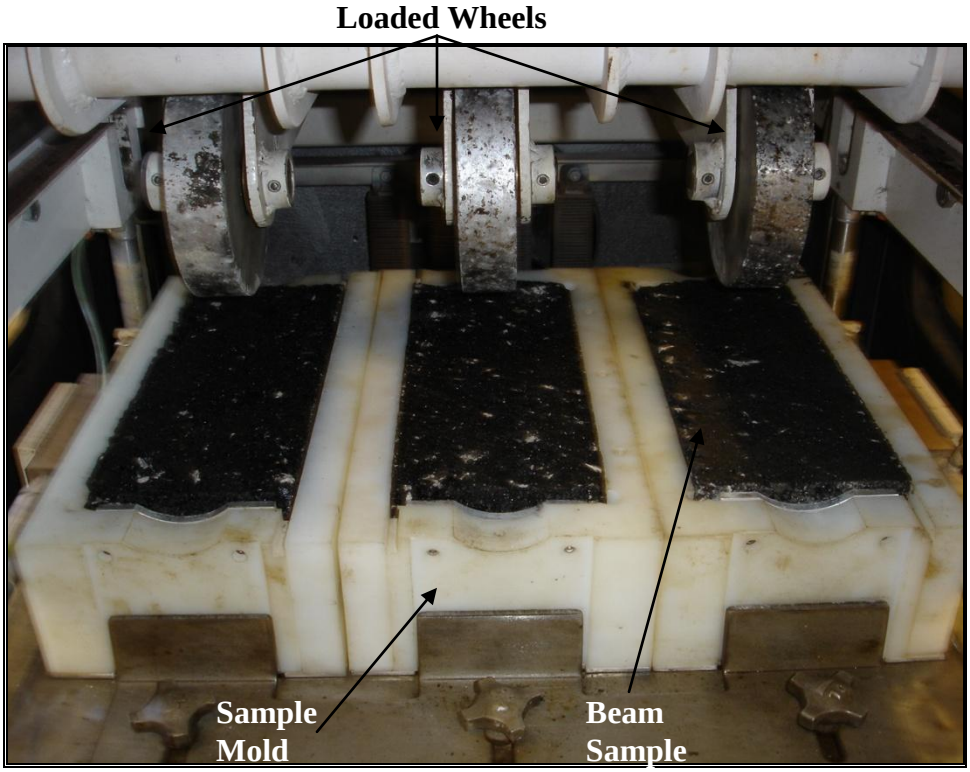

Figure 5.33 APA Fatigue Sample Molds Secured in the Sample Tray

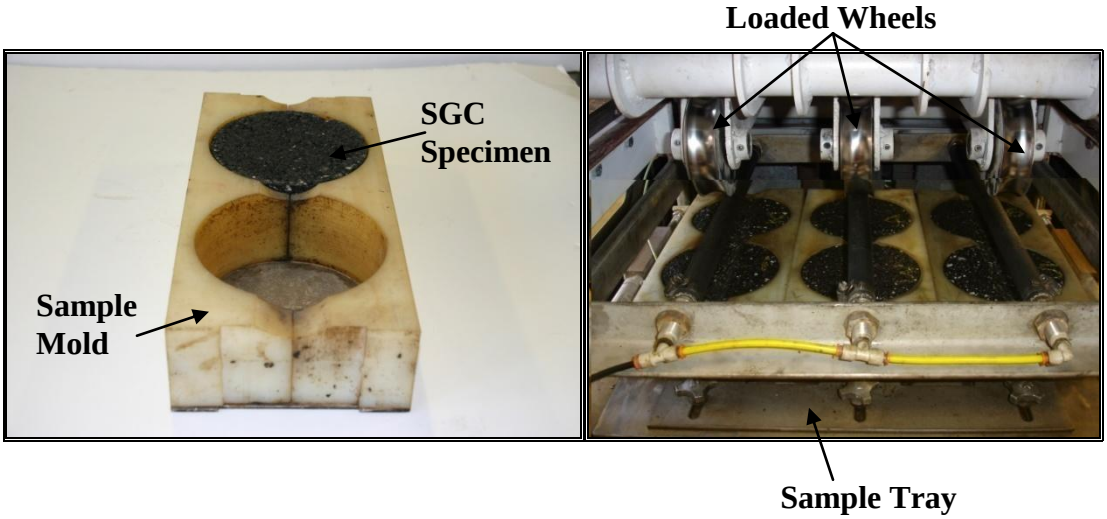

Figure 5.34 APA Rut Sample Mold and Molds Secured in the Sample Tray

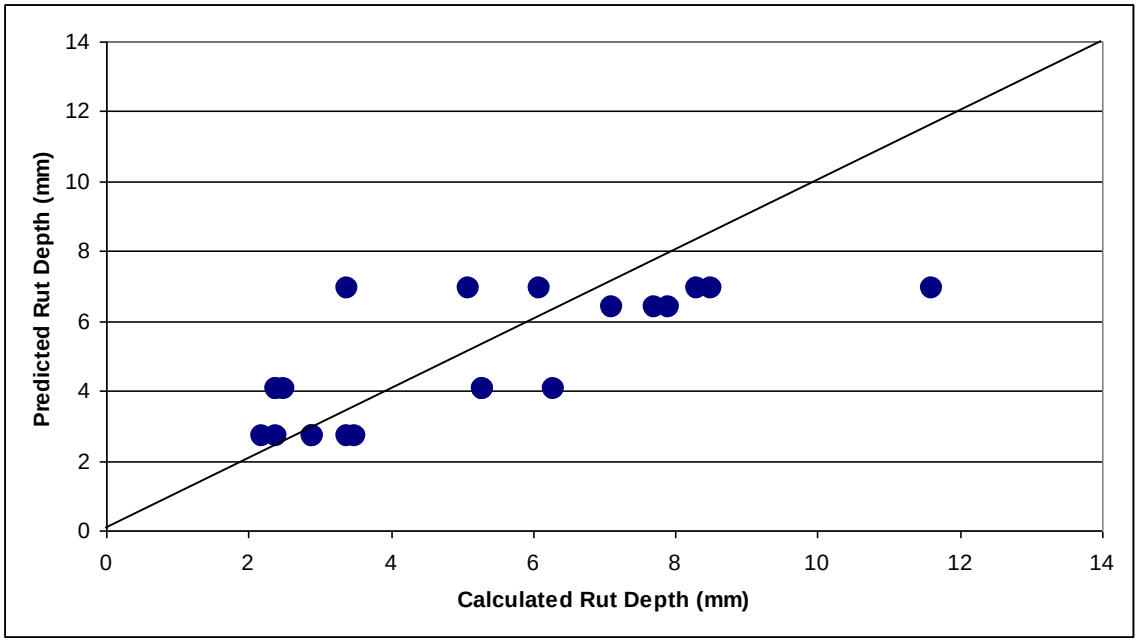

Figure 5.35 Calculated and Predicted Rut Depths
[Log (Rut_{Pred}) = 0.676 + 0.179 AC - 0.178 N_{200} *(R-squared = 0.56)*]

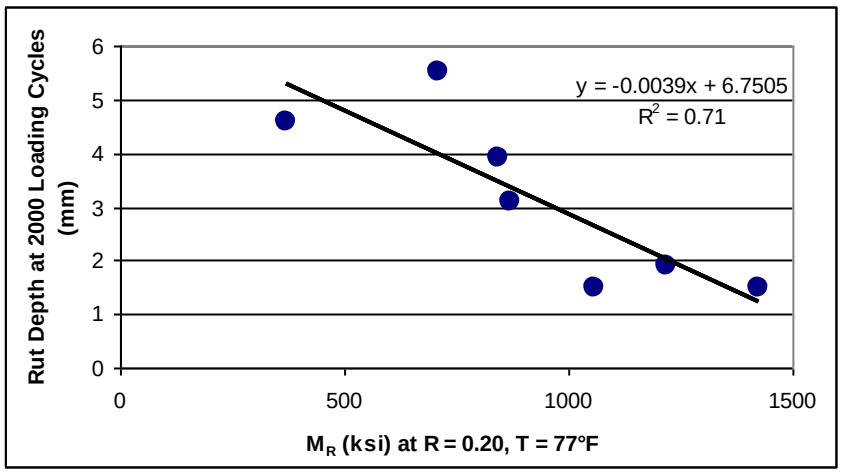

Figure 5.36 Variation of Rut Depth at 2000 Cycles with M_R at R = 0.20 and T = 77°F

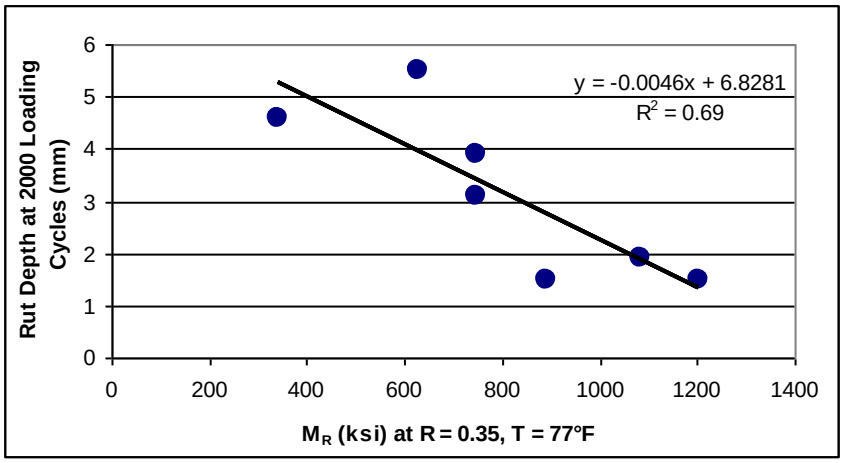

Figure 5.37 Variation of Rut Depth at 2000 Cycles with M_R at R = 0.35 and T = 77°F

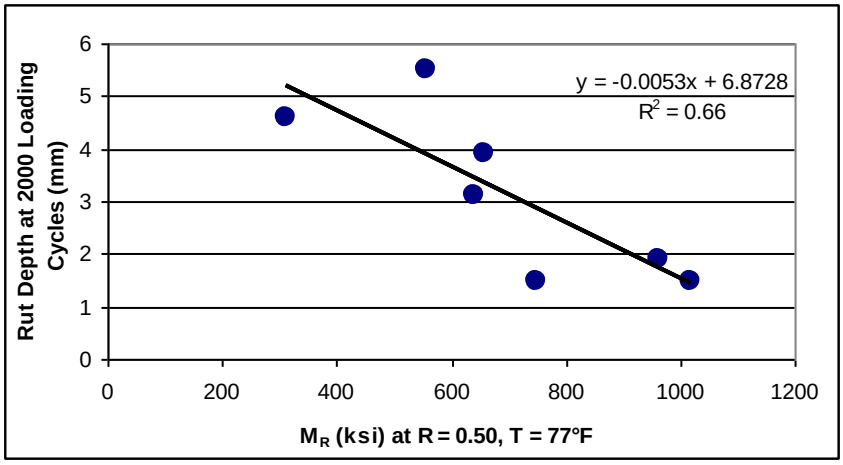

Figure 5.38 Variation of Rut Depth at 2000 Cycles with M_R at R = 0.50 and T = 77°F

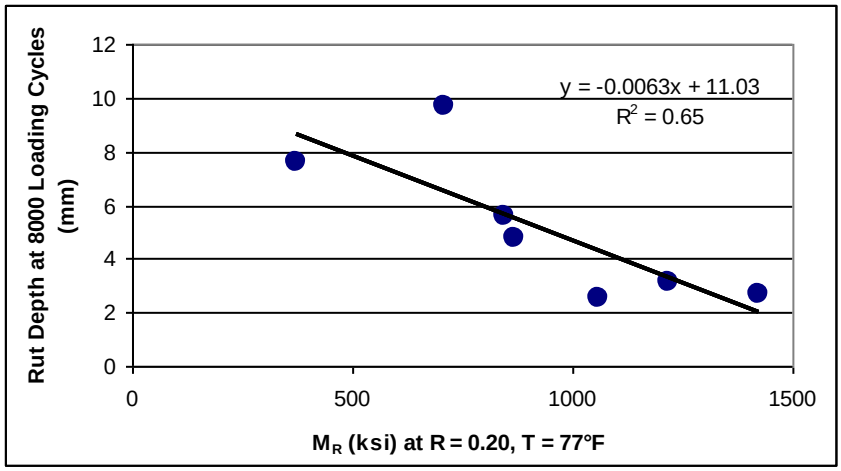

Figure 5.39 Variation of Rut Depth at 8000 Cycles with M_R at R = 0.20 and T = 77°F

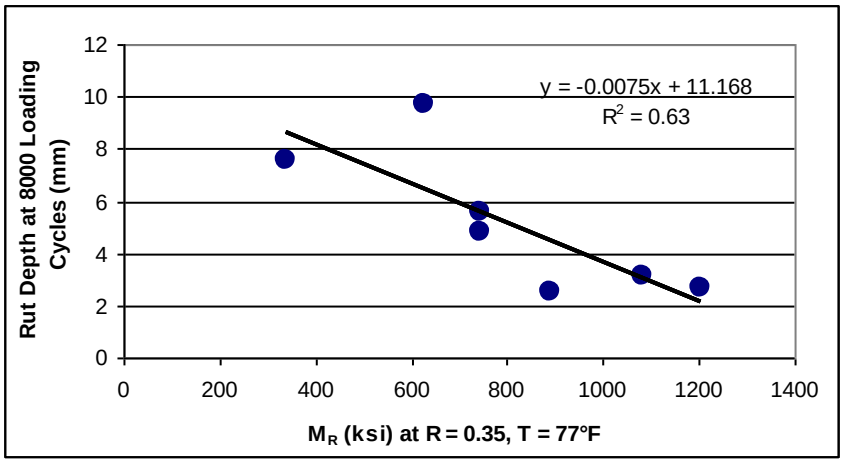

Figure 5.40 Variation of Rut Depth at 8000 Cycles with M_R at R = 0.35 and T = 77°F

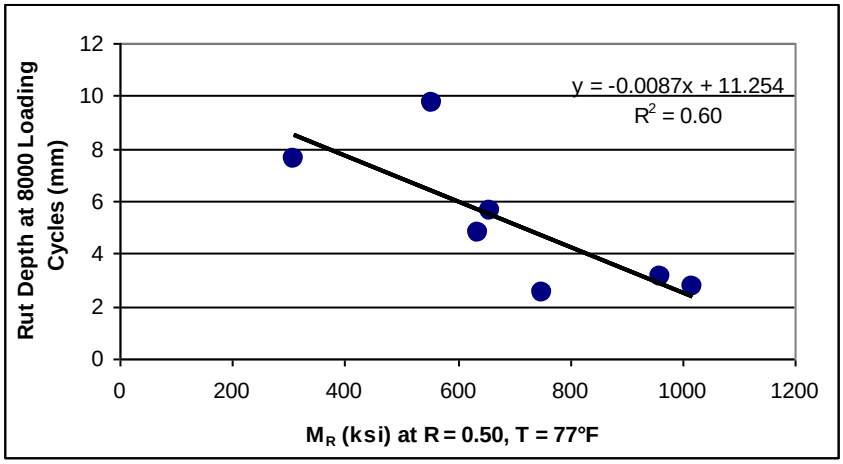

Figure 5.41 Variation of Rut Depth at 8000 Cycles with M_R at R = 0.50 and T = 77°F

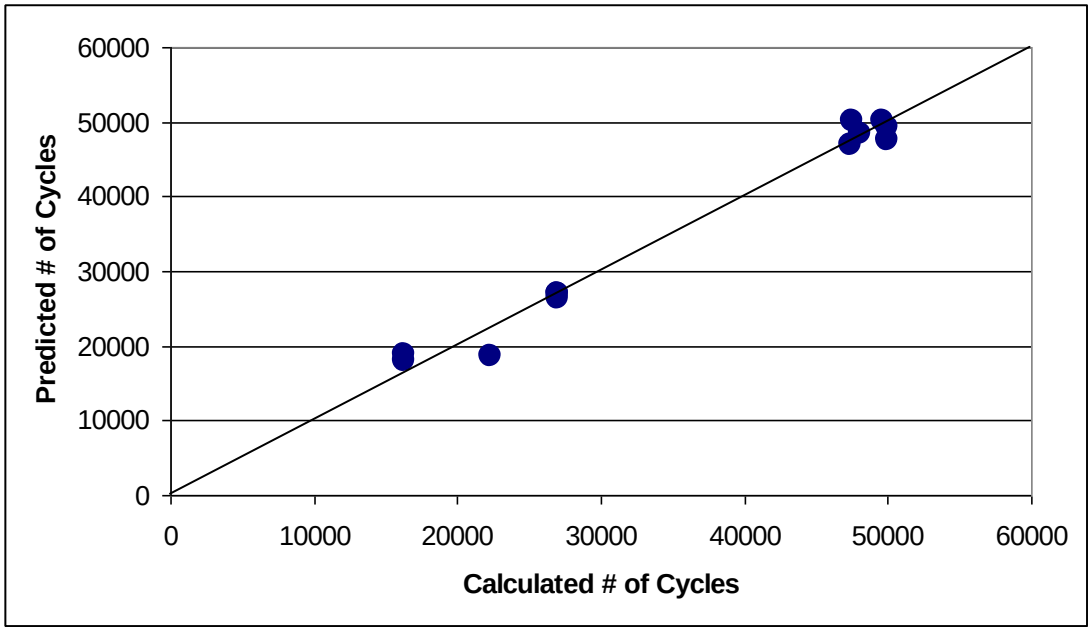

Figure 5.42 Comparison Between Calculated and Predicted Fatigue Cycles

[$N_{f,\ Pred}$ = 826568 - 3370 AV - 279230 G_{se} - 3234 N_{200} *(R-squared = 0.98)*]

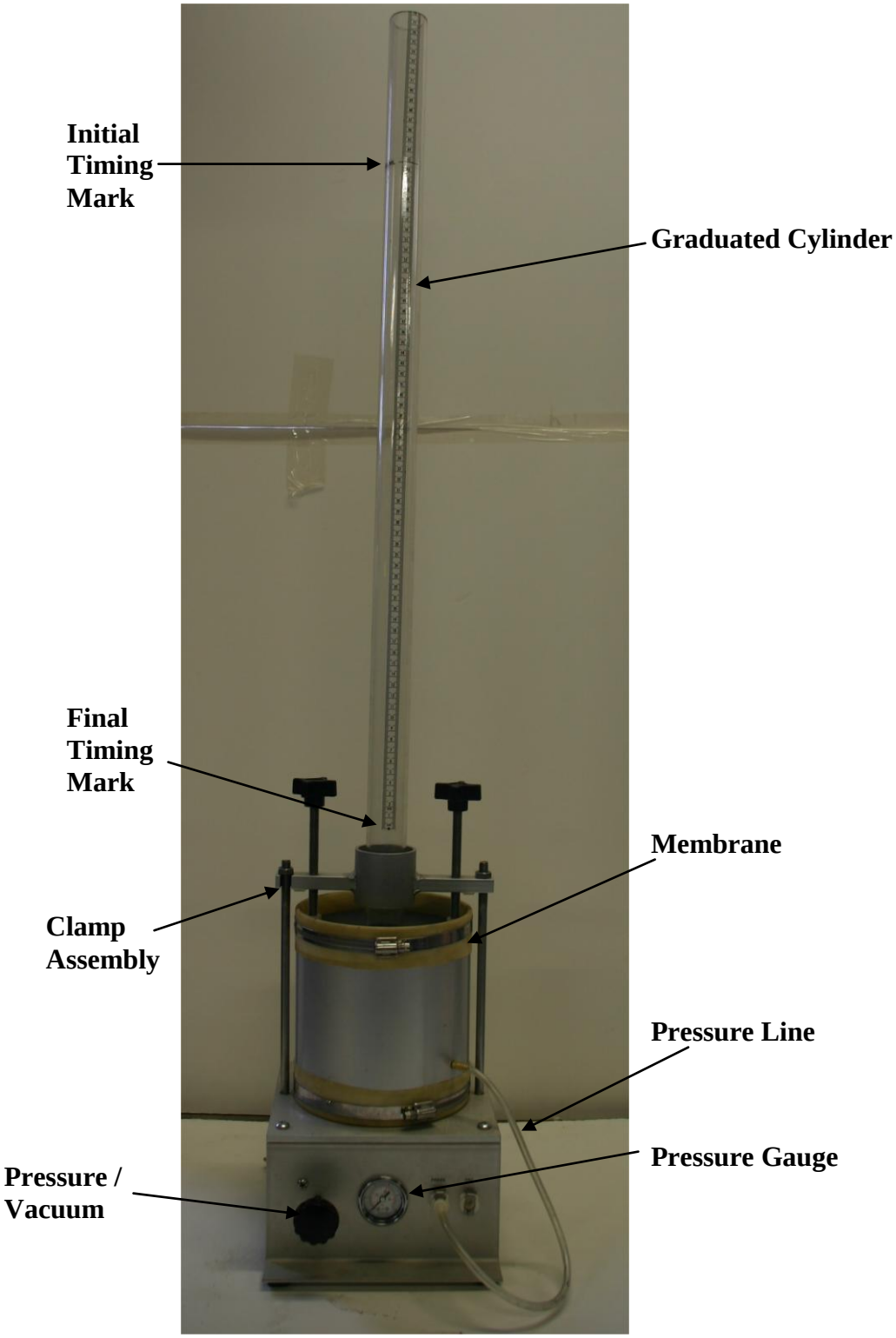

Figure 5.43 Karol-Warner's Falling Head Permeameter

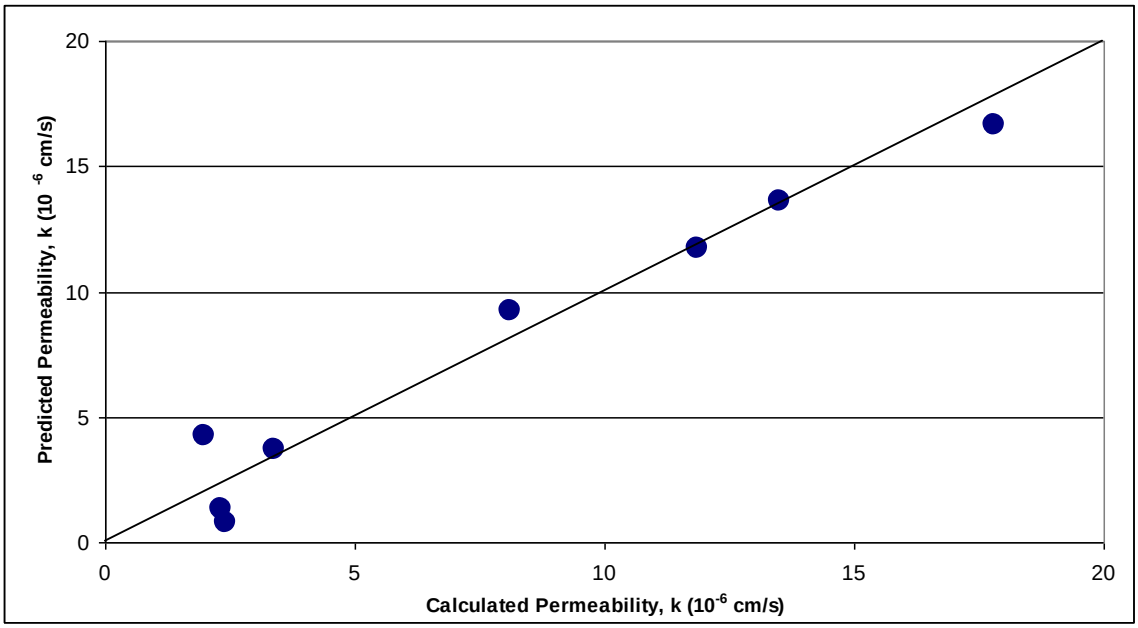

Figure 5.44 Comparison Between Calculated and Predicted Permeability Values

[k_{Pred} = 8.10 + 5.48 AV - 7.15 N_{200} *(R-squared = 0.96)*]

CHAPTER 6 FIELD TESTING OF STABILIZED-CHAT BASE

6.1 General

A number of field tests were conducted to evaluate in-situ properties of the stabilized-chat bases. The following field tests were conducted: spectral analysis of surface waves (SASW), falling weight deflectometer (FWD), ground penetrating radar (GPR) and dynamic cone penetration (DCP). The results of these field tests are presented in this chapter.

6.2 Spectral Analysis of Surface Waves (SASW)

Spectral Analysis of Surface Waves (SASW) is a non-destructive field test to evaluate the in-situ modulus of different layers in a pavement. It can also be used to determine the profile of a pavement structure. The SASW method is based on the dispersive characteristic of Rayleigh waves when traveling through a layered medium (Geovision, 2005). The SASW test is performed on the surface, allowing for less costly measurements than with traditional borehole methods (Bandara and Briggs, 2004).

The SASW test was performed at three selected locations on the Test Road, as shown in Figure 6.1. The test consisted of striking the surface of a pavement with a hammer and recording the resultant stress wave-time histories using two receivers (geophones) at known offsets or known distances. Figure 6.2 shows a photographic view of a SASW test in progress. It is important to note that different sizes of hammers were used for different source-receiver geometries so as to achieve different wavelengths. Also, spacing between the receivers was varied to identify different pavement layers. The wave arrival histories at different spacings were analyzed to determine the pavement layer thicknesses and moduli (Nazarian and Stokoe, 1989). Once the shear wave velocity profiles are determined, shear and Young's modulus (modulus of elasticity) of the materials (E_{SASW}) are calculated through the use of mathematical equations. The

equations are incorporated in WinSASW, a program developed at the University of Texas at Austin, which was used in this study to evaluate the aforementioned properties. Figure 6.3 shows the position of sources (hammer) and receivers (accelerometer and geophones) used to perform the SASW test.

As mentioned previously, the SASW tests were performed at three selected locations of the Test Road, as shown in Figure 6.1. A summary of the test results is presented in Table 6.1. It is seen that the modulus (E_{SASW}) values of 3.5-in. and 6-in. CFA-stabilized layers were 452 ksi and 415 ksi, respectively. The CKD-stabilized layer had a lower value of approximately 233 ksi. Comparatively, the overall modulus of the CFA-stabilized layer was twice the modulus of the CKD-stabilized layer. A comparison between the laboratory and field test results showed that the modulus values from the SASW tests were significantly higher (about one order of magnitude) than the modulus from the unconfined compression strength (UCS) tests. For example, the average modulus of the CFA-stabilized-chat specimens were 59 ksi from the UCS test compared to 415 ksi at Section TS-1 and 452 ksi at Section TS-2 from the SASW test. Another observation from comparing both laboratory and field results is that the modulus (E_{SASW}) of the CKD-stabilized base was 233 ksi, which is also approximately 10 times the modulus of the CKD-stabilized specimens from the UCS test (E_{UCS}). This is consistent with observations by Nazarian et al. (1998) that showed the modulus values from the field are normally higher than the laboratory values by anywhere from 10 to several hundred percent. In addition, results from the laboratory tests show that the modulus (E*) of the CFA-stabilized specimens obtained from the seismic modulus test were higher than the SASW modulus (E_{SASW}). On the other hand, the CKD-stabilized specimens exhibited a lower seismic modulus (E*) than the field modulus obtained from the SASW test (E_{SASW}).

From the aforementioned observations, one can conclude that the field moduli (E_{SASW}) were, in general, higher than the moduli from the laboratory seismic test (E*) or the UCS test (E_{UCS}), except for E* values of the CFA-stabilized specimens. One explanation for such differences (in the laboratory moduli and field moduli) could be attributed to different conditions (curing, boundary conditions, loading rate, etc.). The laboratory test specimens were prepared and cured in a controlled environment. However, in the field it is not possible to have the same level of control for mixing and curing. It is also important to note that the field tests were performed approximately six months after construction, compared to 28 days of curing in the laboratory. Also, the moisture contents and dry densities in the laboratory and field settings could have been different. Moreover, the level of strain at which the seismic tests were performed in the laboratory and field are different. The confining condition for a specimen in the laboratory and stabilized base in the field are different which can yield differences in the modulus obtained from the laboratory and field. No field tests to evaluate the moisture content and dry density during field testing were performed due to the limited scope of this study.

6.3 Falling Weight Deflectometer (FWD)

Falling Weight Deflectometer (FWD) is an impulse deflection method used widely for pavement deflection measurement and evaluation of in-situ moduli of different layers in a pavement. In the present study, FWD tests were carried out in accordance with the ASTM 4694-96 and ASTM D4695-03 test methods at the same locations as the SASW for comparison purposes.

Figure 6.4 shows the device used for performing the FWD test. The test consisted of applying two different loads: one 10-kip and the other 18-kip, falling from two different heights of 4-in. and 15.6-in., respectively. Each load is repeated five times at each location. The resulting

load pulse is transmitted to the pavement as a half sine wave. A time-history plot of a Falling Weight Deflectometer load pulse is shown in Figure 6.5. The peak deflections and load magnitude were captured, reported and automatically stored by the system. Deflections were measured with seven velocity transducers (sensors) that are mounted on a bar, as illustrated in Figure 6.6. They are automatically lowered to the pavement surface during testing. One transducer is located in the center of the loading plate and others are spaced at 0.2, 0.3, 0.5, 0.6, 0.9 and 1.5-m (8, 12, 18, 24, 36 and 60-in.) from the center, as recommended by the Federal Highway Administration (see Figure 6.6; Bandara and Briggs, 2004). The resulting deflections form a "basin" whose depth and shape were used to calculate the moduli (E_{FWD}) of the constituent pavement layers (Bandara and Briggs, 2004). The results of the FWD tests were processed using a computer program, Modulus 5.0, developed by Liu et al. (2000).

FWD tests were also performed at the same locations as the SASW test for comparison purposes. The results were analyzed using the Modulus 5.0 program (Liu and Scullion, 2000) and are summarized in Table 6.1. From Table 6.1 it can be observed that the modulus obtained from the FWD test results (E_{FWD}) for Section TS-1 was approximately 134 ksi (with a standard deviation of approximately 71 ksi), 45 ksi for Section TS-2 (with a standard deviation of approximately 20 ksi), and 56 ksi for Section TS-4 (with a standard deviation of approximately 29 ksi). From these results it is evident that the TS-2 (3.5-in CFA-stabilized base) has a lower modulus than Section TS-1 (6-in. CFA-stabilized base) and Section TS-4 (6-in. CKD-stabilized base). However, Scullion (2005) recommended that the Modulus 5.0 program not be used for back calculation of modulus if the thickness is less than 6-in, because of the fact that the deflection bowls generated are essentially insensitive to the stiffness changes in thin layers, and hence fail to generate reliable results. Therefore, it was decided that the modulus value obtained

for Section TS-2 by the Modulus 5.0 program would not be considered in the final analysis. From Table 6.1, one can see that the modulus (E_{FWD}) for the CFA-stabilized base was about 2.4 times the modulus of the CKD-stabilized base, which is consistent with modulus values from the UCS tests. It is also evident that the moduli values from the FWD tests were lower than the corresponding values from the SASW tests. For example, the modulus values from the FWD tests (E_{FWD}) at Sections TS-2 and TS-4 are approximately 224% and 316% lower than the corresponding SASW test results (E_{SASW}), respectively. The difference in the test setup and performance of each test may be responsible for such variations in the modulus. A summary of all the results (field and laboratory) is plotted in Figure 6.7. It is interesting to note that the modulus values reduce with increasing strain level, except for seismic modulus of CKD-stabilized chat.

6.4 Ground Penetrating Radar (GPR)

Ground Penetrating Radar (GPR) was used to determine the thicknesses of the pavement structure, specifically the chat-asphalt layer and the stabilized base course. GPR is a pulse-echo method for measuring pavement layer thicknesses (USDOT, 2005b). It works like ultrasound, but uses radio waves rather than sound waves to penetrate the pavement (USDOT, 2005b). Antennas mounted on a moving truck are used to transmit short pulses of radio wave energy into the pavement, as shown in Figure 6.8. As this energy travels down through the pavement structure, echoes are created at boundaries of dissimilar materials (such as chat-asphalt base and stabilized-chat base). The arrival time and strength of these echoes can be used to calculate pavement layer thickness. Figure 6.9 shows a typical transmitted radio wave and a reflected wave. It is important to note that GPR is one of the most rapid techniques for data collection among all the geophysical methods in terms of both wave propagation and sampling rates

(scans/second) (USDOT, 2005c). A GPR analysis can be performed at walking or slow driving speeds for quality assurance (QA) assessments and condition assessments of a pavement structure.

The results obtained from GPR tests for both north and south lanes are shown graphically in Figure 6.10 and Figure 6.11, respectively. Table 6.2 shows a numerical summary of the GPR results. The thickness of the stabilized base obtained from the north and south lane was averaged for each of the four sections of the Test Road. The average thicknesses of the stabilized base were found to be 3.7-in., 6.0-in., 6.7-in., and 6.0-in. for sections TS-2, TS-4, TS-1 and TS-3, respectively. The design thickness for the TS-2 section was 3.5-in. and 6-in. for the remaining sections (TS-4, TS-1 and TS-3). From these results, it can be concluded that the thicknesses of the base course obtained from the GPR data were fairly consistent and close to the respective design thickness. Therefore, thicknesses obtained from GPR tests were used in processing the FWD data.

6.5 Dynamic Cone Penetration Test on Stabilized-Chat Base

A total of eighteen cores (twelve cores of 6-in. diameter and six cores of 4-in. diameter) were collected from the chat-asphalt course at the Test Road on October 19, 2005. Figure 6.12 shows the location of the cores. Cores M1 thru M12 are 6-in. diameter and are used for resilient modulus testing, while cores R1 thru R6 are 6-in. diameter and are used for APA rut testing. Volumetric and material properties of these cores were discussed in Navaratnarajah (2006). DCP tests were carried out at four locations namely M1, M11, M10, M6 located in sections TS-2, TS-4, TS-1, and TS-3, respectively. The DCP tests were carried out on the stabilized-chat base (in Sections TS-2, TS-4, and TS-1) and on the unbound aggregate base (in section TS-2) after the cores were removed from the chat-asphalt layer.

Figure 6.13 shows the variation of ICI versus the depth. For all four test locations, a prominent increase in ICI was observed. This increase in the ICI value in the top 0.01-m (0.4-in.) may be due to the disturbance caused by coring. In section TS-2 (at location M1), the ICI value of 5 mm/blow was observed to a depth of 0.2-m (7.9-in.). The ICI values show a continuous increase from 5 mm/blow to 33 mm/blow over the next 0.05-m (2-in.) depth. No variation in the ICI value was observed at the interface of CKD-stabilized-chat base and existing compacted subgrade soil. In Section TS-4 (at location M11), the ICI value of approximately 5 mm/blow was observed to a depth of 0.15-m (5.8-in.), beyond which the average ICI value was observed to be 10 mm/blow. Changes in the ICI value at a depth of 0.15-m (5.8-in.) may indicate a change in the soil stratum. From GPR results, the thickness of the CFA-stabilized chat base in Section TS-4 at location M11 was 0.15-m (5.8-in.), which matches with the observation from the DCP test. ICI values at location M10 in Section TS-1 were approximately 10 mm/blow to a depth of 0.05-m (2-in.). The ICI values showed little variation with depth after 0.05-m (2-in.) with an average value of 5 mm/blow. The ICI value at the location M6 (in Section TS-3) was found to be 5 mm/blow to a depth of 0.11-m (4.4-in.) and 10 mm/blow beyond 0.15-m (5.9-in.). The GPR test results also showed that the thickness of the unbound aggregate base in Section TS-3 was 0.13-m (5.1-in.) which is reasonably close to the observation from the DCP test.

CBR values were calculated from the ICI values using the method described earlier. The CBR of the CFA-and CKD-stabilized chat base was found to be in the range of 100-200 with an average of approximately 150. Compared to the CBR values of existing subgrade (in the range of 20 to 50), the stabilized-chat base was a much stronger base for the Test Road.

Table 6.1 Summary of Modulus from SASW Test (E_{SASW}) and FWD Test (E_{FWD})

Location	Length (ft.)	E_{SASW}	E_{FWD}
TS-1: 6-in CFA-stabilized aggregate base	1,650	415 ksi	134 ksi (71*)
TS-2: 3.5-in CFA-stabilized aggregate base	500	452 ksi	45 ksi (20*)
TS-4: 6-in CKD-stabilized aggregate base	500	233 ksi	56 ksi (29*)

* Values denote the standard deviation

Table 6.2 Summary of GPR Results

Lane	**Base Thickness (in.)**			
	TS-2	**TS-4**	**TS-1**	**TS-3**
North Lane	3.9	5.8	6.3	5.8
South Lane	3.5	6.3	7.0	6.2
Field Average	3.7	6.0	6.7	6.0
Design	3.5	6	6	6

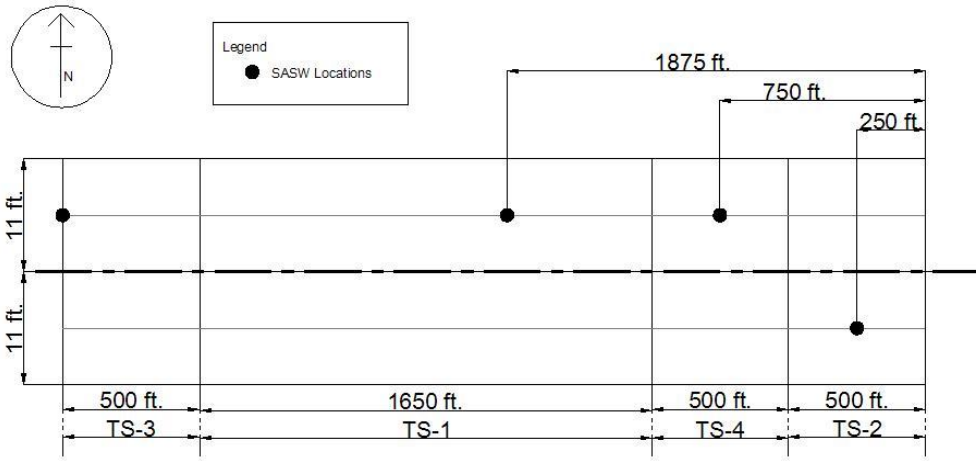

Figure 6.1 Plan of the Test Road Showing the Locations of SASW Tests

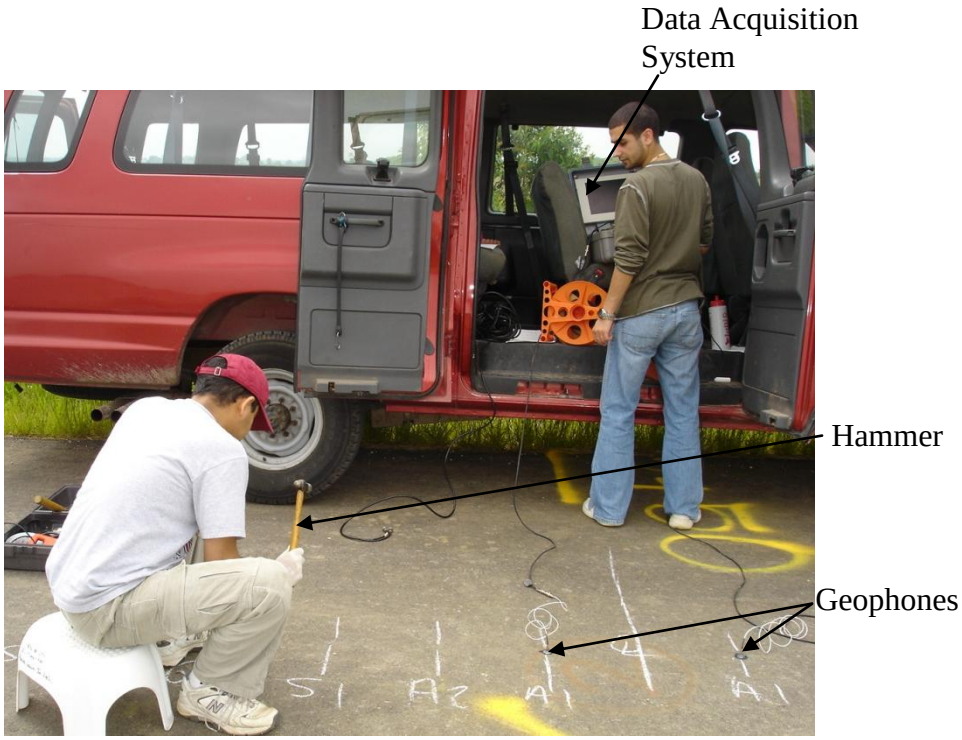

Figure 6.2 SASW Test in Progress at Test Road

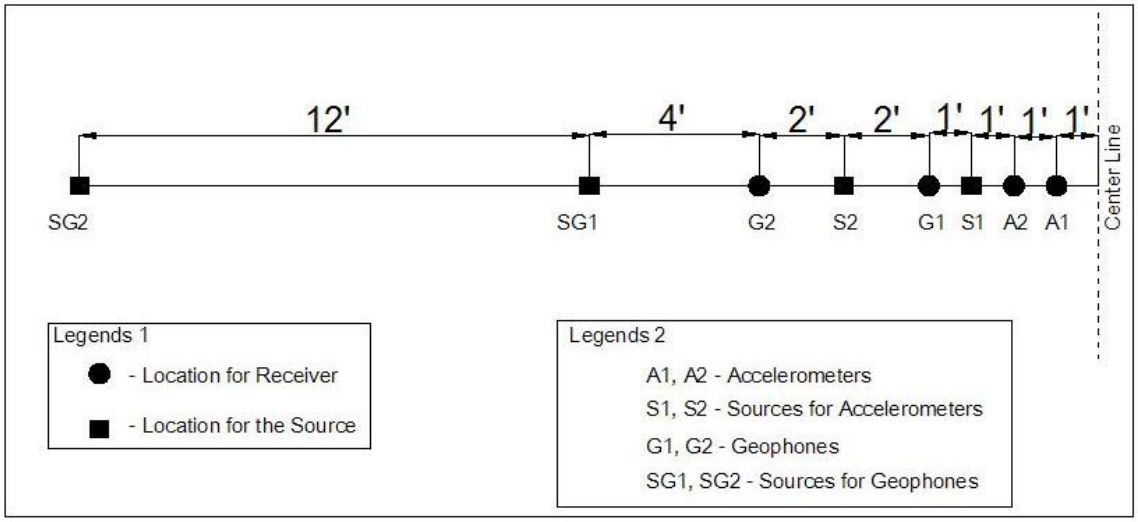

Figure 6.3 Plan View of The SASW Test Set Up

Figure 6.4 FWD Testing Equipment

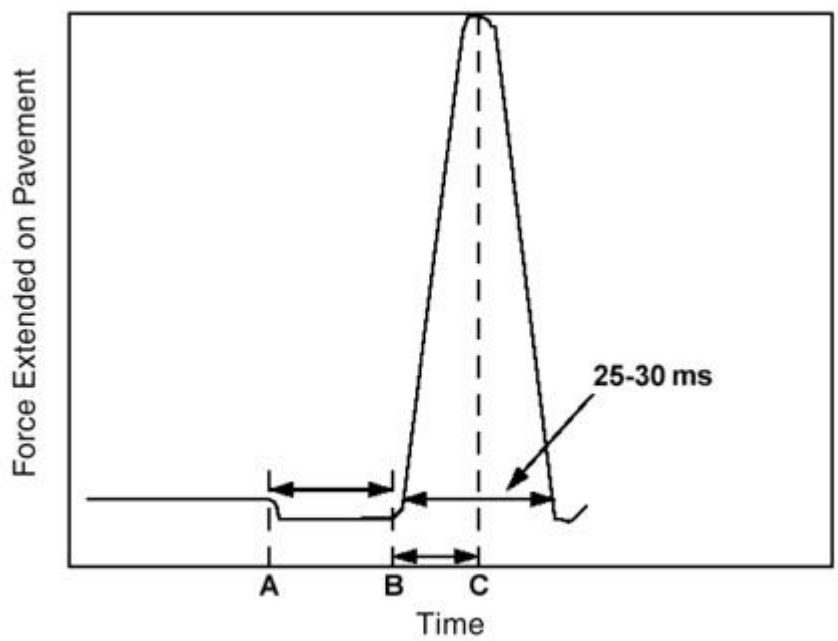

Figure 6.5 Typical Force Output from FWD (time from A to B is variable, depending on drop height): A = time at which weights are released; B = time at which weight package makes first contact; C = peak load reached (Bandara and Briggs, 2004)

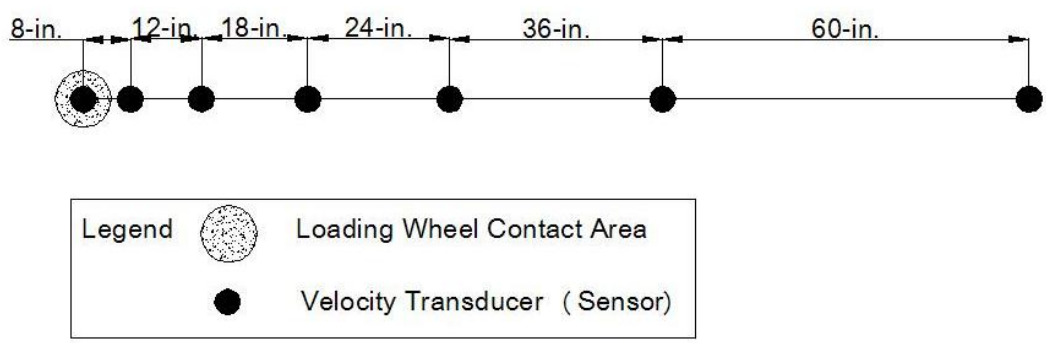

Figure 6.6 Typical Location of Loading Plate and Deflection Sensors for FWD Testing (Bandara and Briggs, 2004)

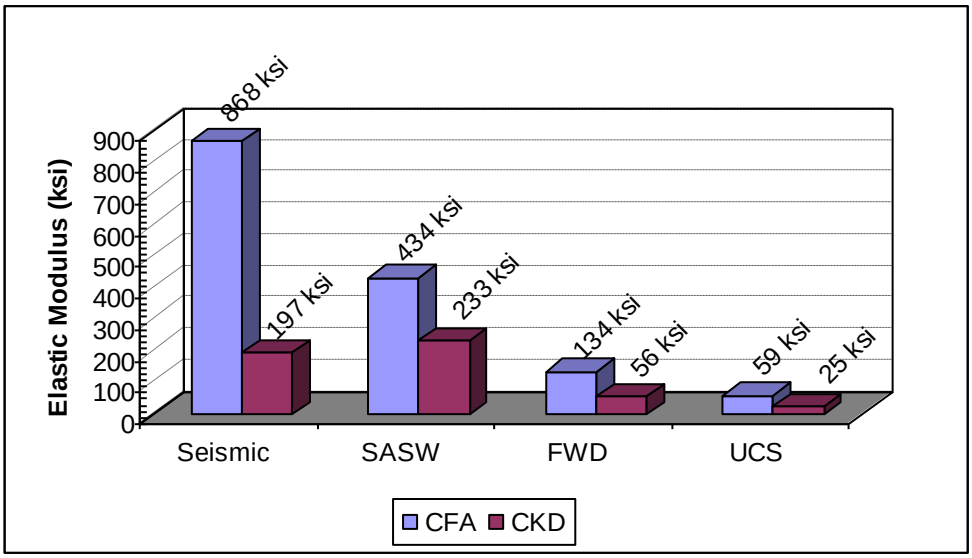

Figure 6.7 Summary of Modulus Values Obtained From Different Tests

Figure 6.8 GPR Testing at the Test Road Site

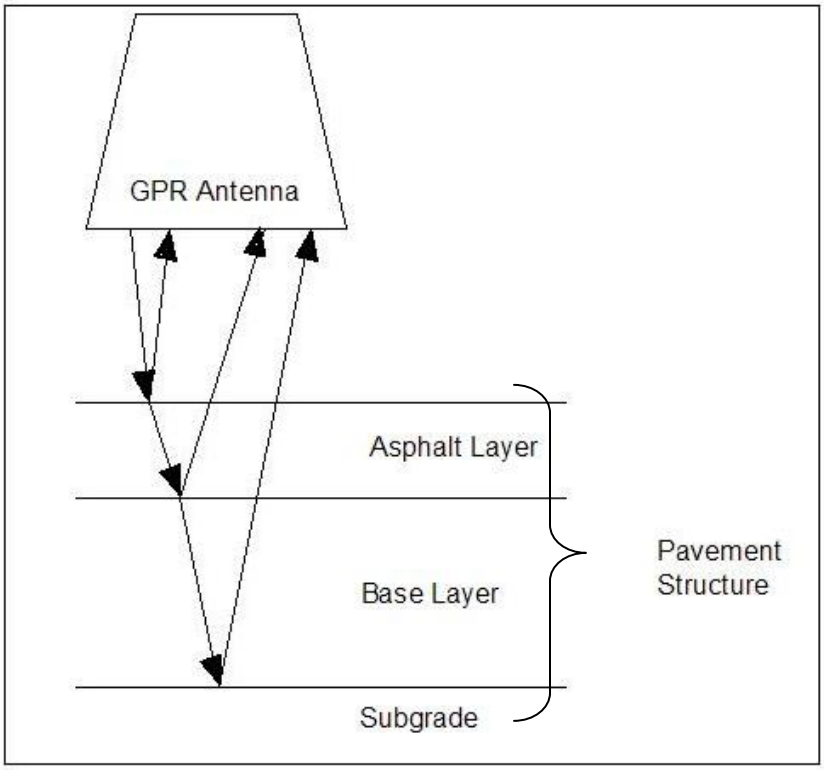

Figure 6.9 Principle of GPR (after USDOT, 2005b)

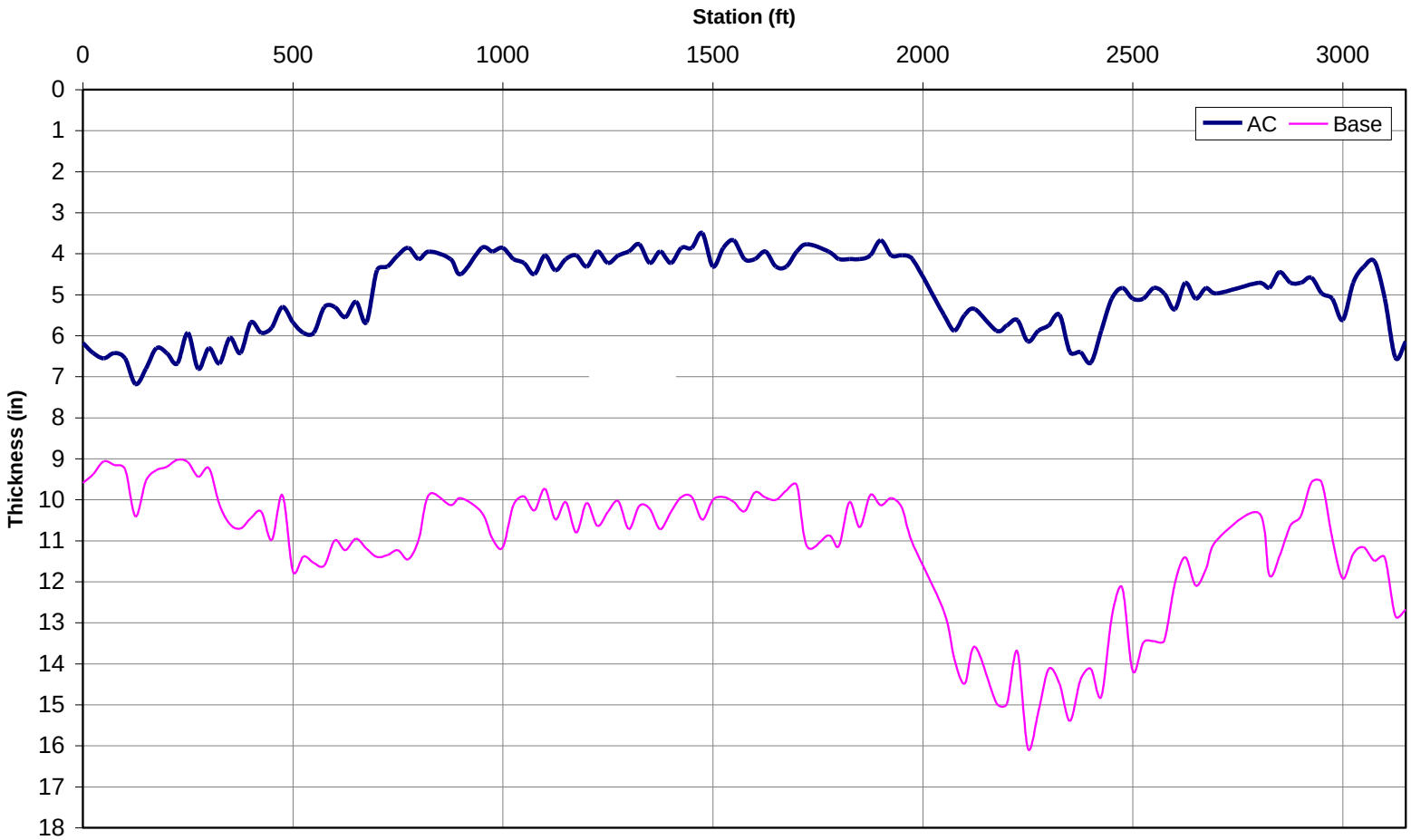

Figure 6.10 GPR Results for South Lane

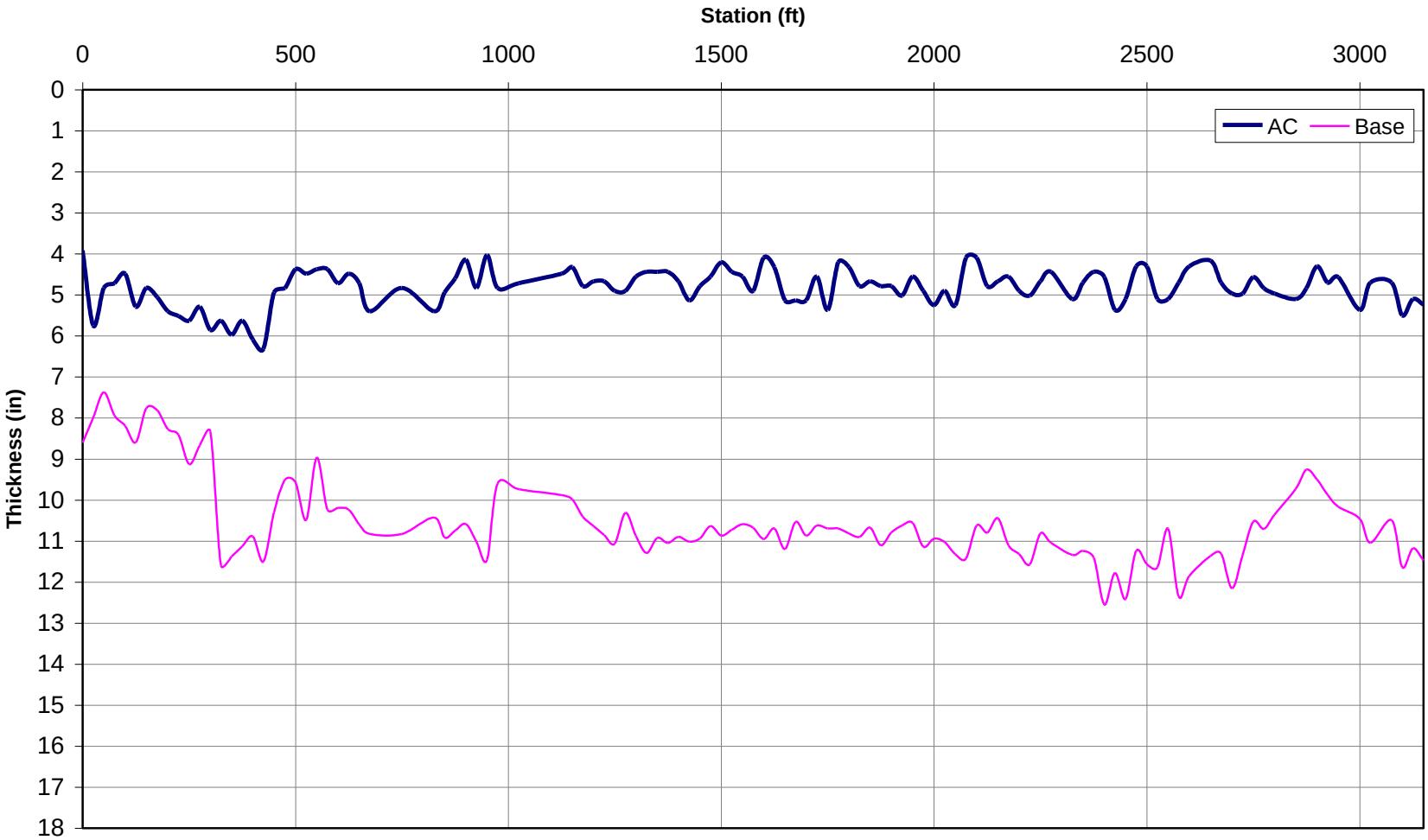

Figure 6.11 GPR Results for North Lane

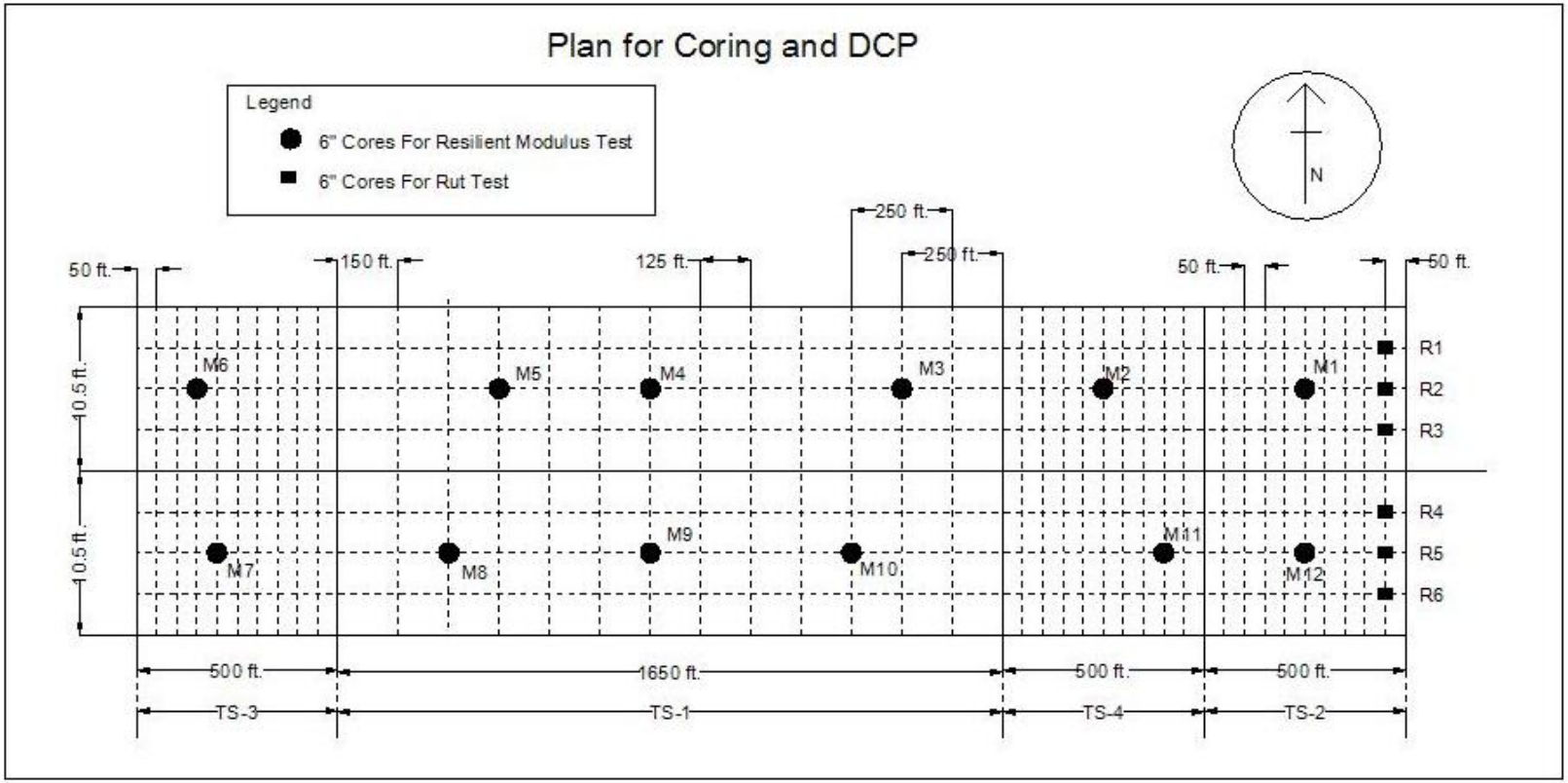

Figure 6.12 Locations for Post-Construction Coring and DCP Test

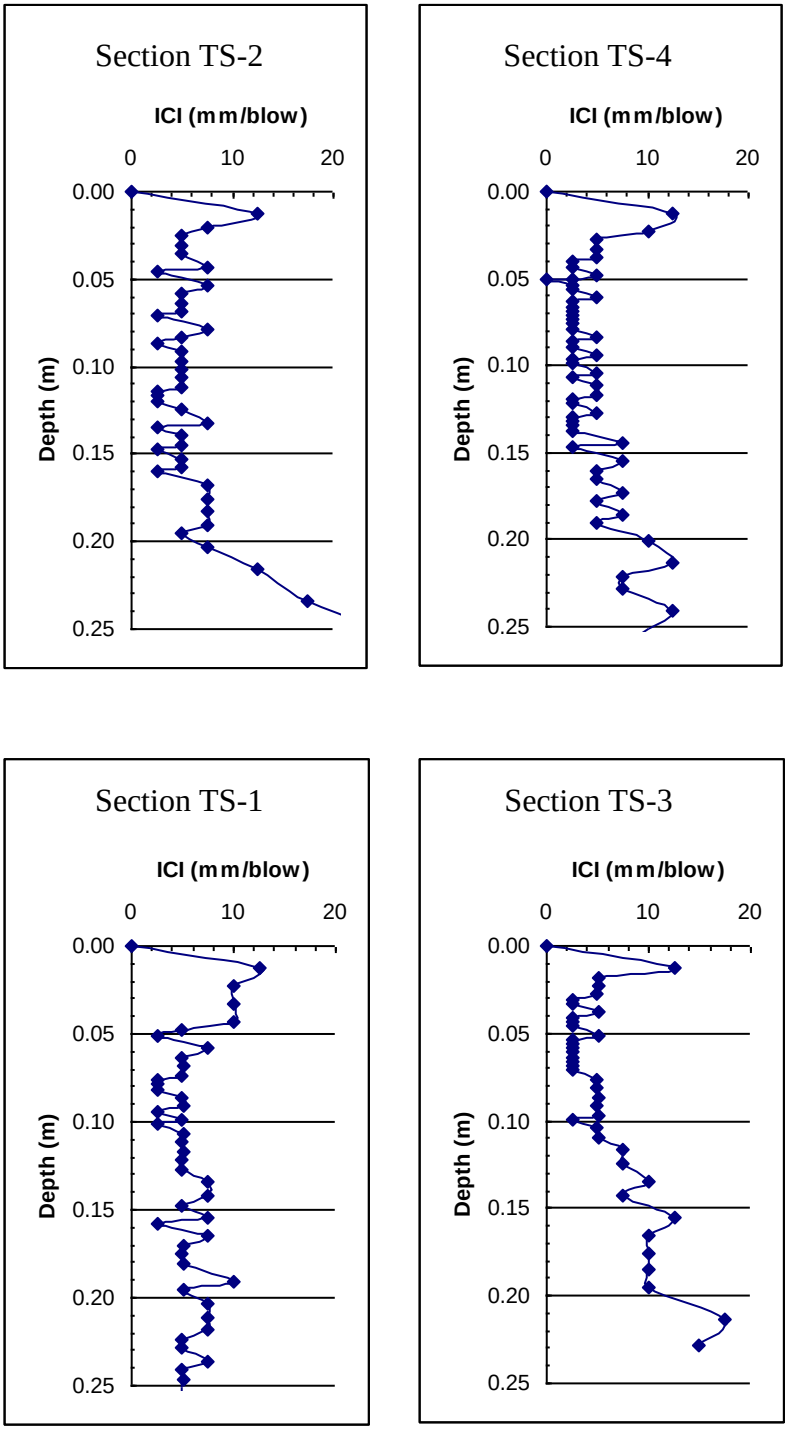

Figure 6.13 Summary of Post-Construction DCP Results

CHAPTER 7 FIELD TESTING OF CHAT-ASPHALT BASE AND SURFACE

7.1 General

Field testing was conducted to evaluate the in-situ properties of chat-asphalt base and surface courses. As in the case of stabilized base (Chapter 6), the field tests included the following: spectral analysis of surface waves (SASW), falling weight deflectometer (FWD) and ground penetrating radar (GPR). Results are presented and discussed in this chapter.

7.2 Falling Weight Deflectometer Test

The procedure for conducting the falling weight deflectometer (FWD) tests is discussed in Chapter 6. The test results were analyzed using a commercially available software, *Modulus 5.0*. The discussion in this section focuses on the FWD results for the chat-asphalt base and surface courses. Because the thickness of the chat-asphalt surface course was relatively small and the flexural behavior of the chat-asphalt base and surface was not distinctly different, the FWD modulus in Table 7.1 is an average modulus of these two layers. The overall FWD back-calculated moduli for the Test Road site are presented in Table 7.1 and graphically illustrated in Figure 7.1, along with the pavement sections. The modulus values vary between 689 MPa (100 ksi) and 2,413 MPa (350 ksi) with an average value of 1,400 MPa (203 ksi) and a standard deviation (SD) of 490 MPa (71 ksi). From Table 7.1, it can be observed that the modulus obtained from FWD data (E_{FWD}) for Section TS-1 was approximately 1,751 MPa (254 ksi) (with a SD of approximately 283 MPa i.e., 41 ksi), 1,255 MPa (182 ksi) for Section TS-2 (with a SD of approximately 310 MPa i.e., 45 ksi), 841 MPa (122 ksi) for Section TS-3 (with a SD of approximately 186 MPa i.e., 27 ksi) and 1,668 MPa (242 ksi) for Section TS-4 (with a SD of approximately 538 MPa i.e., 78 ksi).

To examine the changes in in-situ modulus with time, falling weight deflectometer test (FWD) was conducted at the same locations (Table 7.1) on October 30, 2007. The back-calculated moduli, E_{FWD}, are summarized in Table 7.1A. The E_{FWD} values are adjusted (to 68° F) for the purpose of comparison. Comparing Table 7.1 and Table 7.1A, the E_{FWD} values of chat-asphalt (surface and base layer combined) show an increase with time, meaning the 2007 values are higher than the corresponding 2005 values. The level of increase varies between 29% to more than 700%, the eastbound lane generally showing larger increase than the westbound lane. Additional compaction of chat-asphalt due to traffic could be responsible for increased modulus. However, since FWD tests are very sensitive, one should not look at the actual moduli rather consider the trend while interpreting these results. The subgrade moduli did not change substantially between the two testing periods.

For comparison purposes, the FWD results for two other sites (Davis and Oklahoma City) are also included here. Table 7.2 presents the E_{FWD} results for the Davis site. The results are also plotted along with the pavement length in Figure 7.2. The values vary between approximately 2,758 MPa and 4,481 MPa (400 ksi and 650 ksi) with an average of 3,378 MPa (490 ksi) and a SD of 62 MPa (9 ksi).

The FWD test results for the Oklahoma City (OKC) site are presented in the Table 7.3. Figure 7.3 shows the variation of modulus along the pavement length. The values vary between 552 MPa (80 ksi) and 6,895 MPa (1000 ksi). Inconsistently high values were obtained in three locations at 42.4 m (139 ft), 100.6 m (330 ft) and 122.8 m (403 ft) from the south end. This was possibly due to the surface irregularities and debris at the site due to the construction work. Therefore, these three values were removed. The resulting average was 3,875 MPa (562 ksi), with a SD of 1,889 MPa (274 ksi).

From the aforementioned results, it is evident that the Test Road site shows a comparatively lower FWD modulus than the Davis and the OKC sites. This is consistent with the laboratory indirect tension test results presented in Chapter 5. Consequently, one can conclude that the Davis mix is expected to perform better than the OKC, followed by the chat-asphalt mixes from the Test Road.

7.3 Relative Comparison between M_R and E_{FWD}

Field cores were retrieved from locations where FWD tests were performed. Resilient modulus (cyclic indirect tensile) tests were conducted in the laboratory on these cores. Since M_R tests were performed at different stress levels and at different temperatures, it was decided to calculate the M_R values at three stress ratios (0.20, 0.35 and 0.50) from the developed semi-log model by using the model parameters corresponding to the FWD test temperature. The results are summarized in Tables 7.4, 7.5 and 7.6 for the Davis, the Test Road and the OKC sites, respectively. From Table 7.4, the FWD results for the Davis site compare well with the laboratory moduli. The ratio of laboratory M_R at R = 0.2 to FWD modulus at a load of 40 kN (9 kip) is approximately one (0.92 to 1.09) with an R-squared value of 0.67, as shown in Figure 7.4. This is consistent with the observation by Hossain et al. (1992) who reported that the average ratio of laboratory moduli to back-calculated moduli varied between 1.10 and 1.22. The Test Road and the OKC results, on the other hand, show scattered behavior. Various factors could lead to such behavior including pavement thickness. The HMA thicknesses for both the Test Road and the OKC sites are 100 mm (4 in), while the HMA thickness for the Davis site is 267 mm (10.5 in). As noted by Teredesai (2005), a thickness less than 150 mm (6 in) may produce unreliable back-calculated moduli.

7.4 Spectral Analysis of Surface Waves (SASW)

The procedure for conducting the spectral analysis of surface waves (SASW) test was discussed in Chapter 6. The results of the SASW test for chat-asphalt base and surface course are presented in this section. A summary of the test results is presented in Table 7.7. It is observed that the HMA base layer modulus is higher than the surface layer modulus. This is consistent with the indirect tension M_R test results which show higher modulus values for the chat-asphalt base mix. From Table 7.7, it can be observed that the Section TS-2 showed a comparatively high E_{SASW} 8,618 MPa (1,250 ksi) for the chat-asphalt surface mix and 9,308 MPa (1,350 ksi) for the chat-asphalt base mix. While sections TS-1 and TS-4 showed similar SASW moduli, 4,895 MPa (710 ksi) and 4,275 MPa (620 ksi) for the surface mix and 6,412 MPa (930 ksi) and 5,309 MPa (770 ksi) for the base mix, respectively.

A comparison of both FWD and SASW field moduli are presented in Table 7.8. The results show that E_{SASW} is approximately 4 times higher at Section TS-4 and 6 times higher at Section TS-2 than the E_{FWD}. This is consistent with the study by Nazarian et al. (1988) who reported that the moduli of HMA layers obtained from FWD data exhibit, in general, greater variation than those of SASW test data. Nazarian et al. (1988) also reported that the difference is due to the lack of sensitivity of the FWD test method to the stiffness of the top thin layer, while the SASW method is quite sensitive in this region. Further, Nazarian et al, (1988) reported that the strain level is an important factor in this variation of test results. Moduli from SASW tests are low-strain moduli. On the other hand, moduli back-calculated from FWD deflection basins may contain manifestations of nonlinear behavior induced by the heavy loads imparted to the pavement surface.

7.5 Ground Penetrating Radar (GPR)

As noted in Chapter 6, ground penetrating radar (GPR) tests were performed at the Test Road site to determine the thickness profile of the pavement. The results from both the south and the north lanes are shown graphically in Figure 7.5 and Figure 7.6, respectively. The layer thicknesses calculated from the GPR data depend on the dielectric constant of the medium. For relatively similar mixes, the GPR data could not differentiate between the chat-asphalt surface and base layers (Roddis et al., 1992). Therefore, the results shown in these figures represent the combined thickness of the chat-asphalt surface and base layers. The thickness profile of the south lane varies between 100 mm (4 in) to 150 mm (6 in), while that of the north lane varies between 100 mm (4 in) to 140 mm (5.5 in). By combining both south and north lanes, the average thicknesses of chat-asphalt base and surface layers were found to be 11.8 mm (4.7 in), 147.3 mm (5.8 in), 124.5 mm (4.9 in) and 119.4 mm (4.7 in) for sections TS-1, TS-2, TS-3 and TS-4, respectively. The design thickness for section TS-3 was 125 mm (5.0 in), while for the remaining sections (TS-1, TS-2 and TS-4) the design thickness was 100 mm (4 in). From these results, it can be concluded that the thicknesses of the chat-asphalt base and surface layers obtained from the GPR data were fairly consistent and comparable to the respective design thicknesses. Only section TS-2 showed a high variation. This may be due to the inconsistencies of thickness profile during construction.

The HMA thickness profile of the Test Road site was also obtained from the SASW analysis. The results are shown in Table 7.7. From the thicknesses reported in this table, other than the chat-asphalt base thickness of Section TS-2, the thickness values of each layer in sections TS-2, TS-4 and TS-1 compared favorably with the SASW results.

Ground penetrating radar (GPR) test was conducted again on October 30, 2007. The corresponding thickness profiles for westbound and eastbound lanes are shown in Figure 7.7 and Figure 7.8, respectively. By comparing Figures 7.5 and 7.7 and Figures 7.6 and 7.8, the thickness profiles obtained from the GPR tests in 2005 and 2007 match closely.

Table 7.1 FWD Back-Calculated Moduli for Chat-Asphalt Base and Surface Course

Section ID	Dist. From East End (ft)	E_{FWD} of HMA Layer (ksi) East Bound 10 kip	East Bound 18 kip	West Bound 10 kip	West Bound 18 kip	Average (ksi)	Std. Dev. (ksi)
Section TS-2	50	252	220	157	165	182	45
	100	171	159	-	-		
	150	145	148	140	128		
	200	132	138	-	-		
	250	198	221	190*	191*		
	300	185	185	-	-		
	350	-	-	311	259		
	400	186	157	-	-		
	450	-	-	161	157		
Section TS-4	550	-	-	314	302	242	78
	600	353*	323*	-	-		
	650	-	-	261	338		
	700	251	243	-	-		
	750	-	-	180*	161*		
	800	177	234	-	-		
	850	-	-	137	154		
	900	317	324	-	-		
	950	-	-	134	152		
Section TS-1	1125	269	217	-	-	254	41
	1250	-	-	270	238		
	1375	190	202	-	-		
	1500	-	-	230	192		
	1625	217	230	-	-		
	1750	-	-	261	245		
	1875	268	269	-	-		
	2000	-	-	342	295		
	2125	262	277	-	-		
	2250	-	-	242*	227*		
	2375	323*	340*	-	-		
	2500	-	-	251	247		
Section TS-3	2700	-	-	86	94	122	27
	2750	94	100	-	-		
	2800	-	-	119	127		
	2850	138	143	-	-		
	2900	-	-	108	121		
	2950	137	151	-	-		
	3000	-	-	116	124		
	3050	95	97	-	-		
	3100	-	-	165	183		

* Field cores were retrieved at this locations and preformed laboratory M_R test

Table 7.1A Comparison of Moduli from FWD Tests

Section ID	Station	Lane	Asphalt Thickness	Base Thickness	Asphalt E_{FWD} @ 68°F (2005)	Asphalt E_{FWD} @ 68°F (2007)	Subgrade E_{FWD} (2005)	Subgrade E_{FWD} (2007)
(ft)			(in)	(in)	(ksi)	(ksi)	(ksi)	(ksi)
Section TS-2	50	WB	5.12	3.12	237	643	12.0	11.0
	50	EB	6.32	3.41	322	2138	18.3	17.9
	100	EB	6.32	3.41	286	2348	10.1	13.8
	150	WB	5.12	3.12	244	461	10.5	14.3
	150	EB	6.32	3.41	261	1220	10.6	13.6
	200	EB	6.32	3.41	203	556	11.0	12.4
	249	EB	6.32	3.41	347	452	9.1	14.0
	250	WB	5.12	3.12	316	1696	10.0	11.1
	300	EB	6.32	3.41	339	1013	10.9	12.3
	350	WB	5.47	5.26	415	641	7.9	9.1
	400	EB	6.32	3.41	312	894	8.5	10.2
	450	WB	5.47	5.26	239	489	6.2	8.1
Section TS-4	550	WB	4.68	5.80	520	1047	10.1	12.8
	600	EB	5.10	6.24	685	3044	8.4	10.7
	650	WB	4.68	5.80	3380	3140	10.2	20.4
	700	EB	5.10	6.24	508	1420	7.8	12.2
	750	WB	4.68	5.80	260	423	7.5	10.6
	800	EB	4.05	6.23	519	1144	13.8	15.9
	850	WB	4.68	5.80	573	1840	10.3	18.1
	900	EB	4.05	6.23	775	1028	15.0	17.9
	950	WB	4.68	5.80	197	305	6.8	7.9
Section TS-1	1250	WB	4.61	5.64	411	843	9.9	13.2
	1500	WB	4.69	6.22	330	510	7.4	8.1
	1750	WB	4.69	6.22	404	820	8.1	10.0
	2000	WB	4.69	6.22	542	729	7.6	9.7
	2250	WB	4.69	6.22	404	616	8.6	10.3
	2500	WB	4.75	6.74	408	772	6.4	10.3
Section TS-3	2700	WB	4.75	6.74	221	680	6.3	10.5
	2750	EB	4.98	6.30	167	706	7.7	12.3
	2800	WB	4.75	6.74	299	681	6.8	11.9
	2850	EB	4.98	6.30	230	684	8.7	14.5
	2900	WB	4.92	5.51	229	520	4.9	10.5
	2950	EB	4.98	6.30	226	736	6.7	11.2
	3000	WB	4.92	5.51	239	438	4.9	9.6
	3050	EB	4.98	6.30	156	463	7.1	11.6
	3100	WB	4.92	5.51	284	487	3.7	8.8

Table 7.2 FWD Back-Calculated Moduli for Davis Site

Dist. From East End (ft)	E_{FWD} of HMA Layer (ksi) Load		
	9 kip	12 kip	15 kip
50*	554	543	526
100	387	400	421
150*	634	620	628
200	464	468	534
250*	580	602	579
300	414	417	420
350*	528	487	497
400	386	372	438
450*	460	464	467
500	499	482	531
550*	448	447	459

Average = 490 ksi
Std. Dev.= 9 ksi

* Field cores were retrieved at this locations and preformed laboratory M_R test

Table 7.3 FWD Back-Calculated Moduli for OKC Site

Dist. From South End (ft)	E_{FWD} of HMA Layer Load		
	9 kip	12 kip	18 kip
0	890	684	674
52	221	322	384
139	1726	1686	1714
330*	1892	3004	3296
403*	1747	1777	1740
475	618	931	1053
540	400	288	246
630*	325	288	287
701	810	760	811
810*	928	888	845
881*	932	853	942
957	492	425	448
1026	84	91	94
1105	804	687	699
1174	432	404	450
1266	537	436	463

Average = 562 ksi
Std. Dev.= 274 ksi

* Field cores were retrieved at this locations and preformed laboratory M_R test

Table 7.4 Comparison of Modulus from FWD Test and M_R by Semi-Log Model (Davis Site)

Modulus from FWD Test			**M_R at FWD Test Temperature**		
9 kip	**12 kip**	**15 kip**	**R = 0.20**	**R = 0.35**	**R = 0.50**
554	543	526	604	524	446
528	487	497	521	447	377
580	602	579	536	462	390
460	464	467	476	407	340
448	447	459	449	382	318

Table 7.5 Comparison of Modulus from FWD Test and M_R by Semi-Log Model (Test Road)

Modulus from FWD Test		**M_R at FWD Test Temperature**		
10 kip	**18 kip**	**R = 0.20**	**R = 0.35**	**R = 0.50**
323	340	399	354	293
190	191	504	453	384
353	323	399	354	293
180	161	504	453	384
242	227	475	426	359

Table 7.6 Comparison of Modulus from FWD Test and M_R by Semi-Log Model (OKC Site)

Modulus from FWD Test			**M_R at FWD Test Temperature**		
9 kip	**12 kip**	**15 kip**	**R = 0.20**	**R = 0.35**	**R = 0.50**
325	288	287	461	375	306
1892	3004	3296	445	360	291
928	888	845	461	375	306
932	853	942	445	360	291
1747	1777	1740	461	375	306

Table 7.7 Moduli and HMA Thicknesses from SASW Test for the Test Road Site

Layer	Modulus, E_{SASW} (ksi)			Thickness (in)		
Profile	**TS-2**	**TS-4**	**TS-1**	**TS-2**	**TS-4**	**TS-1**
HMA Surface	1257.5	617.5	707.5	1.44	1.44	1.44
HMA Base	1350.0	772.5	930.0	4.8	2.4	2.4

Table 7.8 Comparison of FWD and SASW Moduli for the Test Road Site

Location	E_{FWD} (ksi)			E_{SASW} (ksi)		
ID	**Load**		**Avg**	**Surface**	**Base**	**Avg**
	10 kip	**18 kip**				
8 (TS-4)	180	161	171	618	773	695
38 (TS-2)	198	221	210	1258	1350	1304

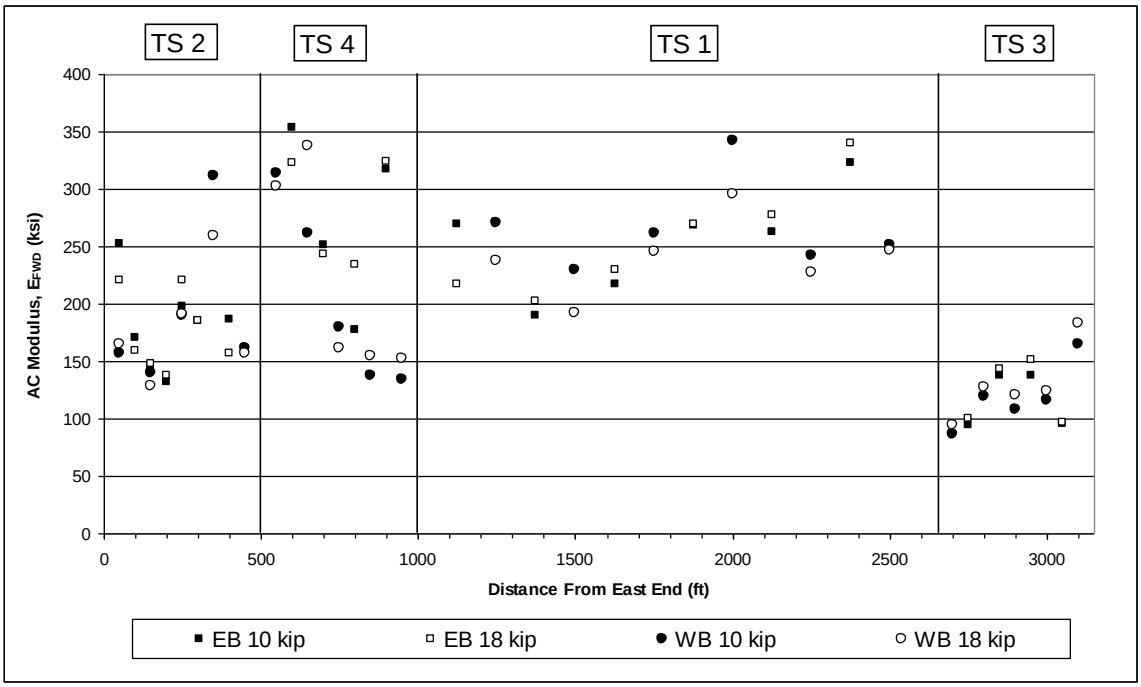

Figure 7.1 FWD Back-calculated Modulus for Tar Creek Site

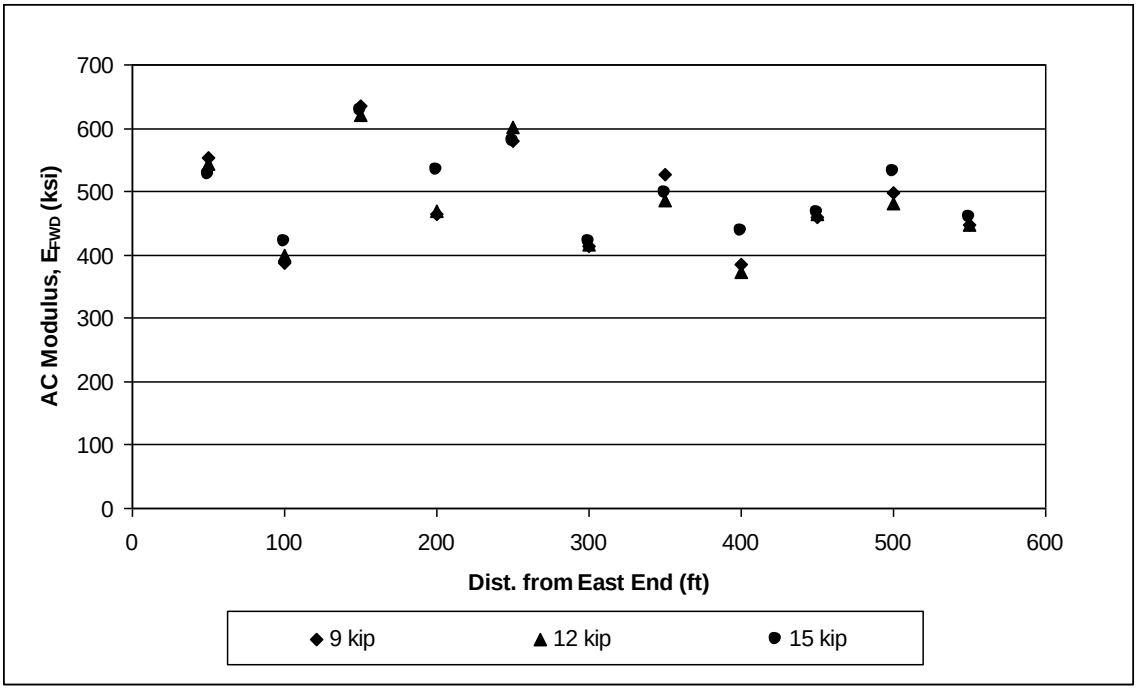

Figure 7.2 FWD Back-calculated Modulus for Davis Site

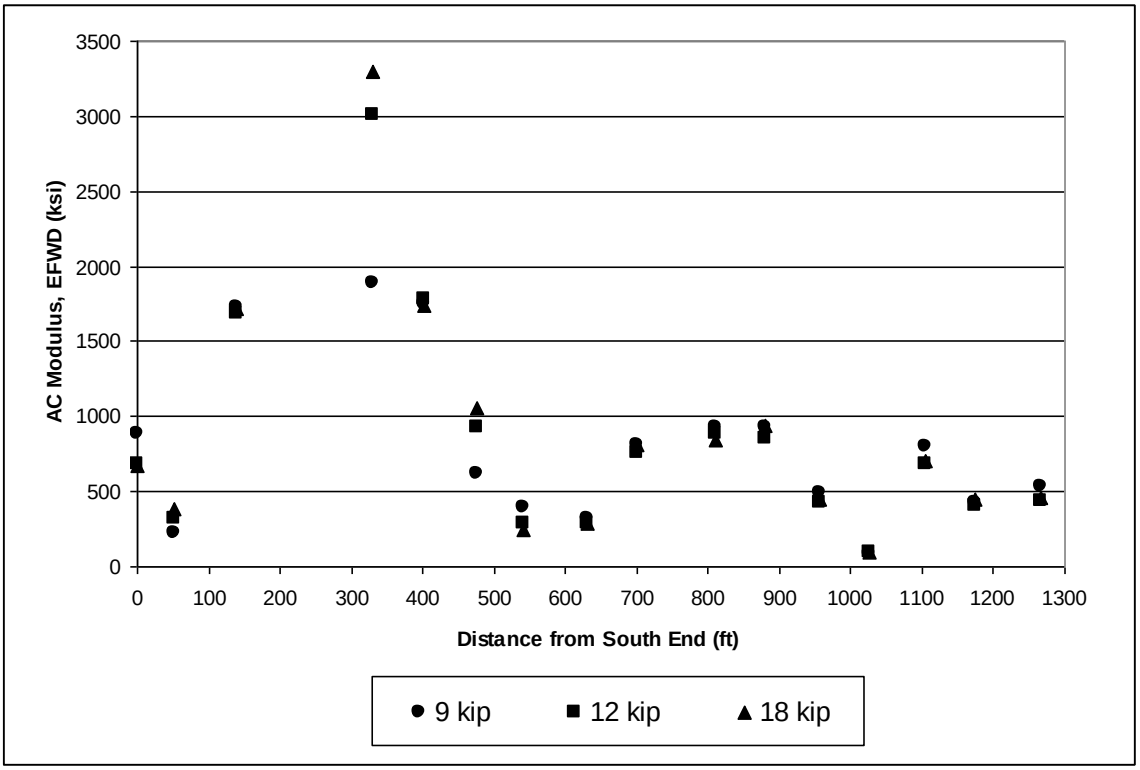

Figure 7.3 FWD Back-calculated Modulus for OKC Site

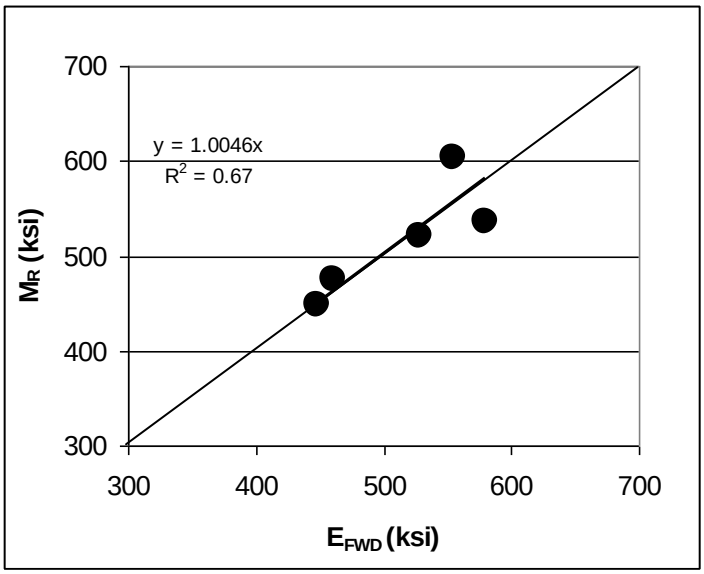

Figure 7.4 Comparison of Laboratory M_R at R = 0.20, E_{FWD} at 9 kip Load for Davis Site

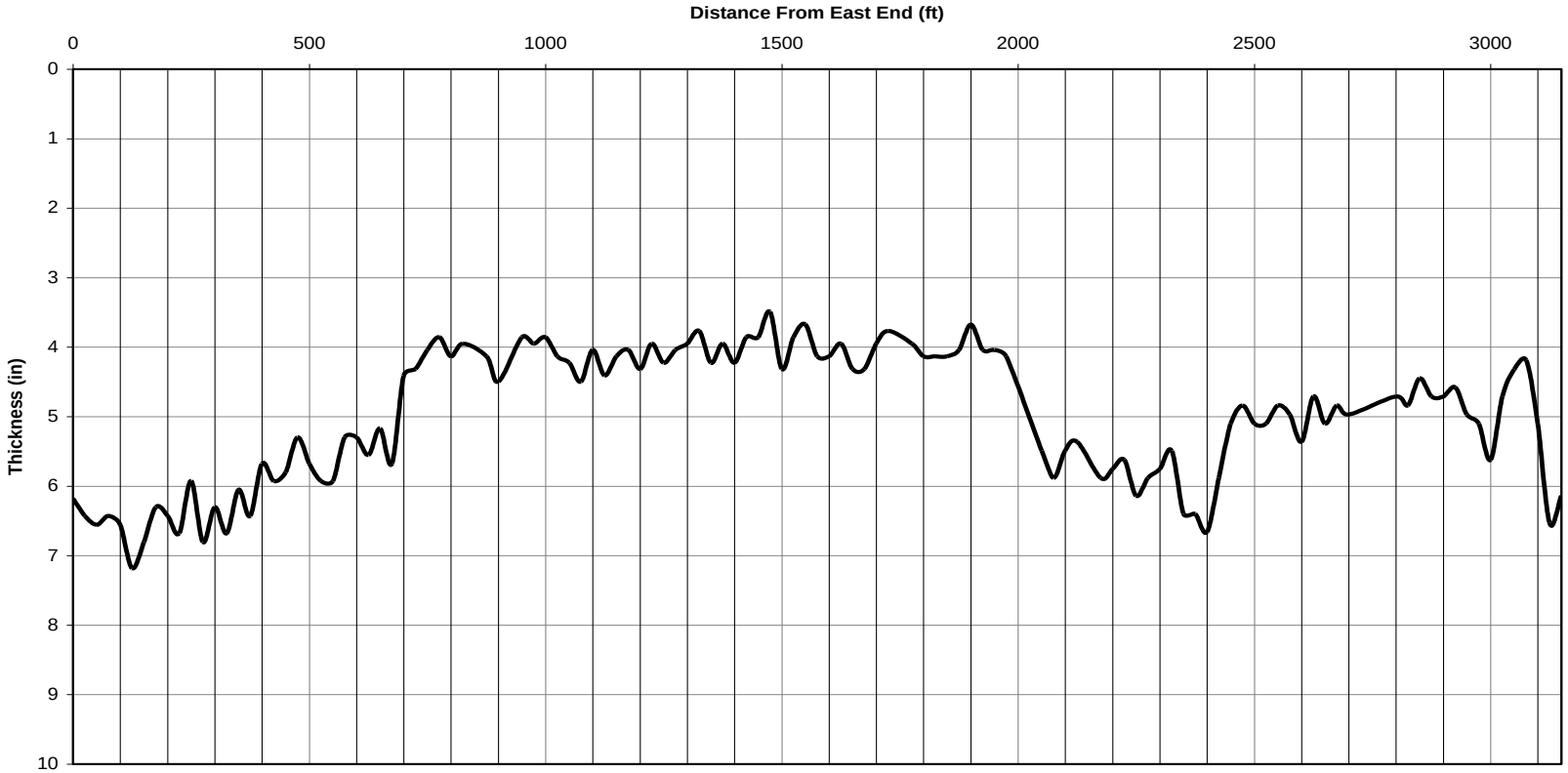

Figure 7.5 GPR Thickness Profile for South Lane, Test Road Site

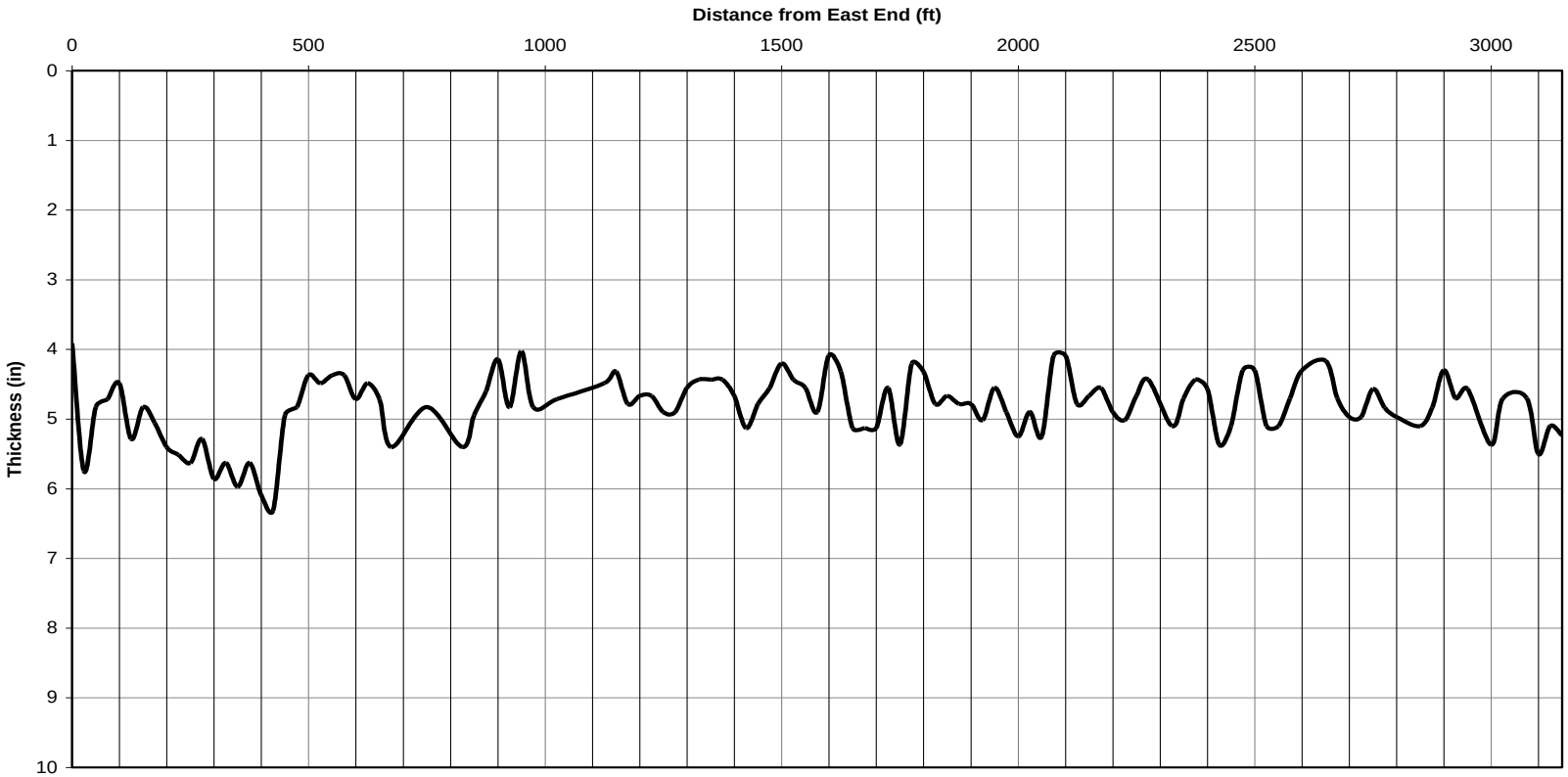

Figure 7.6 GPR Thickness Profile for North Lane, Tar Creek Site

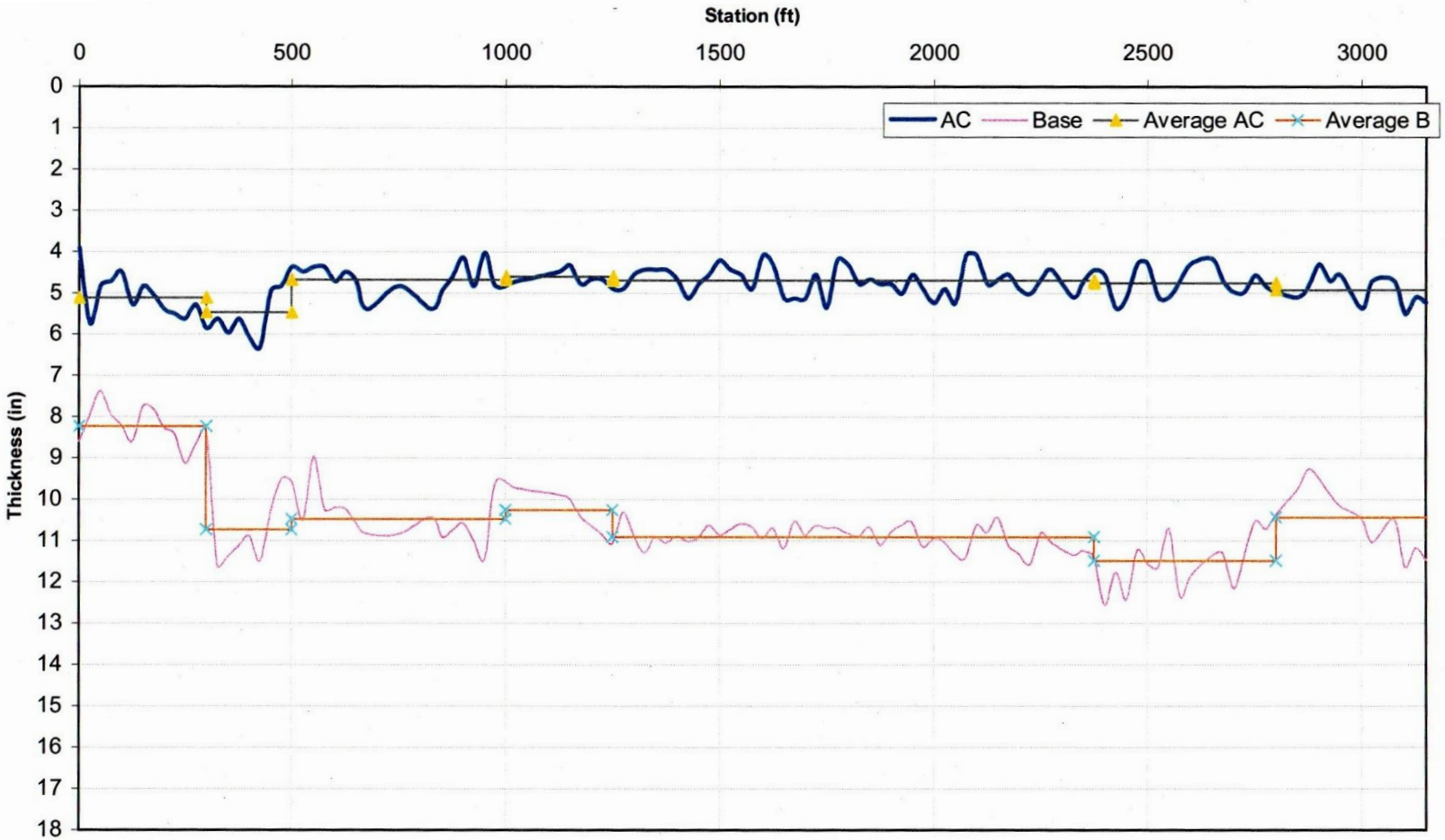

Figure 7.7 Layer Profiles (Westbound Lane) from GPR Test (October 2007)

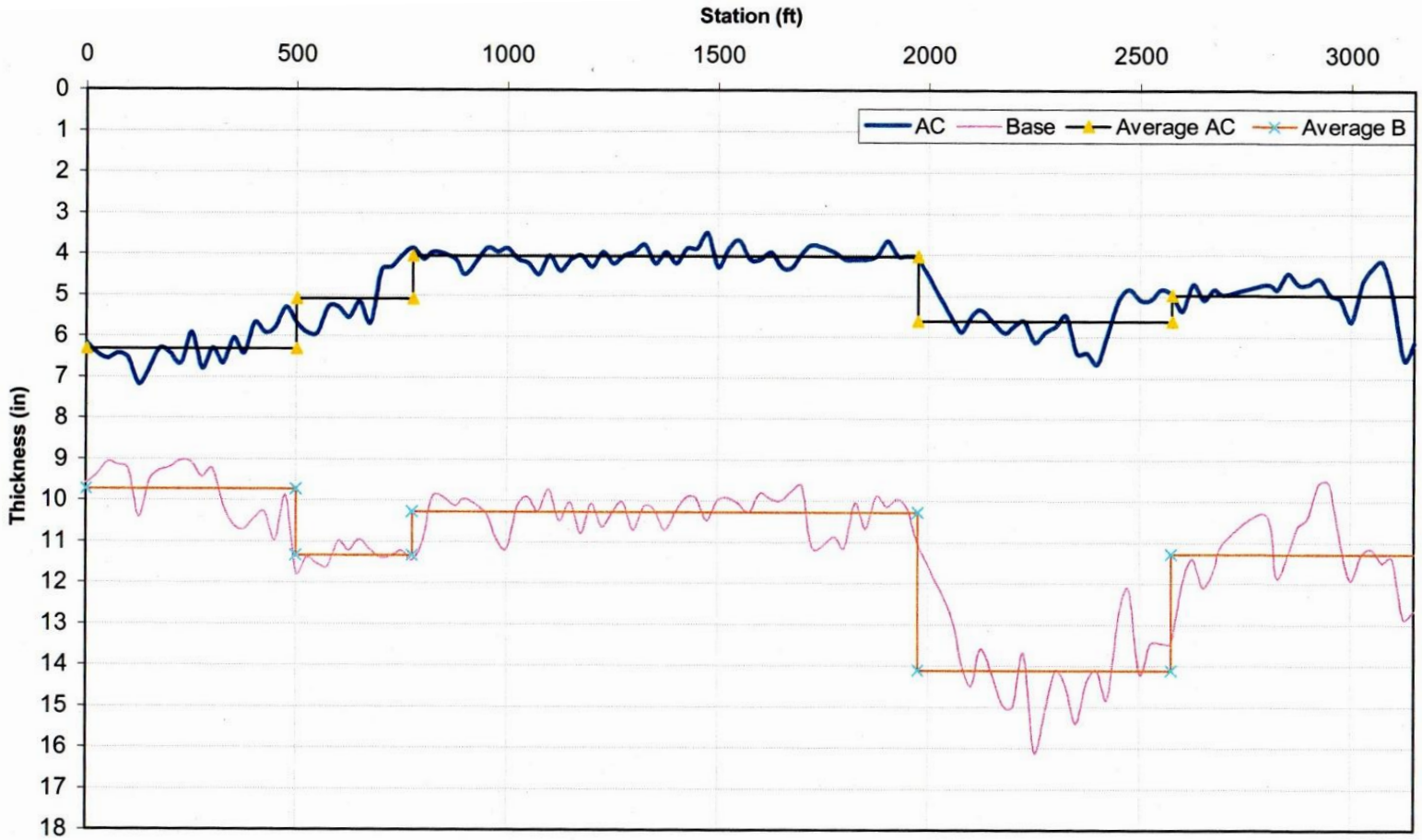

Figure 7.8 Layer Profiles (Eastbound Lane) from GPR Test (October 2007)

CHAPTER 8 MILLING, REPAVING AND DISTRESS SURVEYING

8.1 General

To evaluate the environmental effects of milling, a portion of the Test Road was milled and repaved. This chapter describes the milling and repaving operations performed in this study and some laboratory tests on the millings and the mix used in repaving. This chapter also presents the distress survey of the Test Road after more than two and a half years in service.

8.2 Milling and Repaving

8.2.1 Pavement Inspection (March 2006)

Before milling and repaving a portion of the Test Road, the pavement was inspected for any visible distress. Photographs were taken at some of these locations. Overall, the pavement was in a very good condition and did not exhibit any major distress. Some longitudinal cracks were observed between 1455 and 1475, 1830 and 1850, 2484 and 2500 and 2506 and 2600 feet from the East end, (Figures 8.1 through 8.4). Some permanent deformation was observed in the North lane between 350 and 375 feet. Between 1780 and 1800 feet, edge cracks and potential settlement were observed (Figure 8.5).

8.2.2 Milling

Milling was performed on March 27, 2006, after the road was in service for about 16 months since its construction in November 2004. About 100 feet of the Test Road, starting at 11.3 feet from the East end (Figure 8.6) was milled. A ROTO-MILL Pavement Profiler (CMI Corporation) was used for milling as seen in Figures 8.7-8.10. The milling width was 7.1 feet. In the East bound lane, the milling depth was variable during the first 25 feet. The milling depth was kept at 2.5 inches between 25 and 75 feet and the depth was changed to 2.0 inches for the last 25 feet. For the West bound lane, again during the first 25 feet the milling depth was

variable, as adjustments were being made. During the next 25 feet, the milling depth was increased to 2.5 inches, and for the remaining 50 feet it was reduced to 2.0 inches. The East bound lane (South lane) was milled first, followed by the West bound lane. Two runs of the ROTO-MILL were needed for each of the two lanes. The first run covered 7.1 feet from the centerline of the road and the second run covered the rest from the edge of the East bound lane. The same milling pattern was followed for the West bound lane (third and fourth runs). Figures 8.11 to 8.14 show the four runs of the ROTO-MILL in a progressive manner. During milling the pavement temperature was 68°F as measured using a temperature gun. Samples of millings were collected from the first and third runs at 25 foot intervals (Figures 8.15-8.16).

8.2.3 Repaving

The millings were not used for repaving. Freshly prepared RSM80 (as used in the initial paving in 2004) was used for repaving on March 27 and 28, 2006. Prior to laying the new chat-asphalt surface course, the milled surface was first cleaned with the help of a mechanical broom, as shown in Figures 8.17-8.18. Repaving was performed with a paver manufactured by Barber Greene (model number BG 260B) having a hopper capacity of 21-cu ft. An Extend-A-Mat B Screed (Model 10-20B) was used to achieve a paving width of 10-ft (Figures 8.19-8.20). The chat-asphalt was laid first on the East bound lane and then on the West bound lane (Figures 8.21-8.22). Some loose chat-asphalt mix was collected from the second truck as shown in the Figure 8.23. The temperatures of chat-asphalt mix in the 1st, 2nd and 3rd trucks were 135°C, 139.8°C and 137.8°C, respectively. After laying the mix, a vibratory roller, having a compaction width of 5.8 feet, (see Figures 8.24-8.25) was used for compaction. A pattern of four passes with heavy vibratory mode and two passes with static mode (no vibration) was followed by the vibratory roller, to achieve the desired density. The roller is manufactured by Ingersoll-Rand (Model

number: DD 90). A calibrated PQI gauge was used to check the level of compaction (Figure 8.26). Figure 8.27 shows the road after milling, repaving and compaction.

8.2.4 Asphalt Content of Millings

Asphalt contents of the millings were determined by a NCAT ignition oven (AASHTO T 308). Five samples were tested for asphalt content. Samples were collected from the East bound lane between 0 and 25 feet, 25 and 50 feet, 75 and 100 feet, and from the West bound lane between 0 and 25 feet and 50 and 75 feet. Table 8.1 shows the results of the asphalt content tests. The asphalt content was found to vary between 6.57% and 7.8%, with an average of 7.2%. Comparatively, the design optimum asphalt content was 6.9%. Some variability in asphalt content is introduced during the plant production of the hot mix asphalt.

8.2.5 Rut Test on Repaving Mix (OHD L 43)

Although the repaving mix is the same mix as the original (RSM80), it was collected and compacted for APA rut test according to the OHD L 43 test method. A total of six specimens were prepared and the percent air voids were measured using the Corelok method (OHD L 45). The air voids varied between 6.8 % and 7.6 %. The rut test was performed at 64°C. It was observed that the rut depth varies between 5.3 mm and 6.9 mm, with an average of 5.8 mm (Table 8.2). The maximum allowable rut depth by the ODOT is 5 mm for pavements subjected to 0.3 to 3 million ESALs. As mentioned previously, the high rut depth of the chat-asphalt mixes are due to their high asphalt binder contents. Comparatively, the rut depths are higher in the case of the original mix as mentioned in Table 5.26 in Chapter 5. A total of eight cores were collected from the repaving, section and rut depths were observed between 6.1 mm and 7.2 mm. These rut depths are also lower than those observed for cores from the original mix.

8.2.6 Moisture Susceptibility Test on Repaving Mix (AASHTO T 283)

Moisture susceptibility tests were performed on samples with air voids between 6% and 8%. Table 8.3 shows the results of the moisture susceptibility tests. It can be seen that the tensile strength ratio (TSR) is very high (0.99 > 0.8). Akili (1993) reported that the percent TSR increases with an increase in the asphalt binder content above optimum asphalt content due to the increase in the thickness of the asphalt binder coating over aggregates. The repaving chat-asphalt mix has a very high optimum asphalt binder content (6.9%). Therefore, the TSR can be related to the high optimum asphalt binder content.

8.3 Pavement Inspection (January, 2007)

No maintenance work was performed on the Test Road between construction in October 2004 and January 2007. An inspection was conducted in January 2007. In general, the Test Road was found to do well after more than two years in service. It is noteworthy that the maximum distress occurred in Section TS-2 (Figures 8.28-8.31). While the total base thickness is 8.5 inches, if we consider the chat-asphalt mix as more belonging to the surface than the base, TS-2 has the thinnest stabilized base sections, 3.5 in versus 6.0 inches. Therefore, it is reasoned that the traffic-induced stresses had a higher damaging effect on the subgrade in TS-2 than in the other sections, and this was reflected on the surface as transverse cracking. There was no standing water in the ditches. In addition to the original seeding there was plenty of Woody Panicum, a native species that is very common, some Foxtail, and some Bermuda.

8.4 Pavement Distress Survey (June and July, 2007)

After the Test Road was in service for about two and a half years, a detail distress survey was conducted in June and July, 2007 (Gierhart, 2007). Findings of this survey are summarized in this section. Specifically, the survey was focused on:

(1) Evaluation of the smoothness of the pavement; and

(2) Evaluation of the levels of distress present, if any.

8.4.1 Evaluation of Smoothness

The profilograph, shown in Figure 8.32, measures roadway smoothness. It forms a reference plane using a 25 foot long beam. A separate movable wheel located in the center of the beam measures the vertical deviations from the reference plane. The deviations are accumulated and converted to a reading in inches per mile.

Special Provision 430-2QA provides specifications for the equipment, the testing procedure, and the smoothness requirements for different classes of roadways. The smoothness was tested according to the requirements of Special Provision 430-2QA.

The profilograph test was conducted on June 22, 2007, in collaboration with Claremore Residency, Oklahoma Department of Transportation (ODOT). The profilograph was calibrated on-site, and one pass was made in the inside wheel path in both directions. Because the initial meeting at the job site on June 11th was in the rain and the roadway was almost totally under water at the time, the starting and stopping points were estimated and marked with stakes at the roadside. Therefore, the profilograph traces actually ran from station 1+10 to station 31+77. The traces did not include the 101.5 foot long milled and replaced section on the east end of the project.

Table 8.4 summarizes the results of the profilograph testing. The profilograph data was analyzed using a standard 0.2 inch blanking band, as shown in Figure 8.33. In other words, there is a 0.2 inch acceptable tolerance in the surface deviations from the reference plane. The high point in each bump and the low point of each dip is measured by the profilograph. Deviations over 0.2 inches from plane are summed for each 0.1 mile section. For each trace, the

profilograph software shows the sum for each 0.1 mile section and at the end returns the average deviation for the entire project.

Although the average Profile Index is very similar for each direction, it appears that there is little correlation between the smoothness in the eastbound and westbound inside wheel paths. In addition to the extent and section profile indices, there were no unacceptable bumps, defined as those with vertical deviations in excess of 0.6 inch.

ODOT Special Provision 430-2QA includes a table (Table 8.5), which gives pay factor equations for Profile Indices for roadways classified I through III. The Class III group is for the lowest volume roadways, but would still be a much higher classification than a low volume county road.

Although the average measured profile indices were in excess of the ODOT "unacceptable" range, it must be reiterated that the Test Road pavement is not the type of project to which smoothness specifications would ever apply. Furthermore, since there were no smoothness specifications in place at the time of construction, the extra level of care in subgrade preparation was not taken into account by the contractor. For county roads, the motor grader operator typically prepares the subgrade by visual estimate only. In highway construction, a survey crew would be dispatched to set stakes marking the exact grading elevations. This operation is referred to as "blue-topping." The important evaluation is that the project feels smooth when simply driven over at normal speed, especially in comparison to the surrounding gravel roads.

8.4.2 Pavement Distress Survey

A distress survey was performed on July 6th and 7th by Danny Gierhart, ODOT Materials Division. The distress survey was performed according to Federal Highway Administration

(FHWA) publication FHWA-RD-03-031, *Distress Identification Manual for the Long-Term Pavement Performance Program* (FHWA, 2003). The first part of the survey involved laying out a visible reference system.

A Roll-a-Tape was used to measure out stations in 10 foot intervals for the length of the project. Three of the painted station numbers from previous research were still faintly visible. The Roll-a-Tape was used to confirm the distances between the three existing station marks. These marks were then used to locate and mark station 0+00. The stations were marked in 10 foot intervals with fluorescent spray paint at the distances indicated by the Roll-a-Tape (Figure 8.34).

After the stations were marked, rut measurements were taken at 50 foot intervals as specified by FHWA-RD-03-031 (FHWA, 2003). A rut measurement device was used, which consisted of a 10 foot straight edge and a notched wedge (Figure 8.35). The notches were cut at 0.1 inch intervals to allow quick measurement of the rut. Using 50 foot intervals, ruts were measured at 64 stations along the Test Road. At each station, ruts were measured in 4 places: the inside and outside wheel path of the eastbound lane, and the inside and outside wheel path of the westbound lane. Therefore, a total of 256 individual rut measurements were obtained along the length of the project.

Overall, the roadway had very little rutting after over two and a half years in service. Historically, pavements receive the vast majority of their rutting during the first two summers in place. The general shape of the ruts indicates that they were caused by subgrade consolidation rather than plasticity of the chat-asphalt.

The eastbound lane exhibited much less rutting than the westbound lane, with an average of 0.08 inches, or 2 millimeters in each wheel path. The deepest rut measured in the eastbound

lane was 0.2 inches (5.1 mm). There were only 2 stations having a rut over 0.1 inches (2.5 mm). Out of the 64 stations measured, 15 had no discernable rutting in either wheel path.

The westbound lane averaged 0.19 inches (4.8 mm) of rutting in the inside wheel path and 0.13 inches (3.3 mm) of rutting in the outside wheelpath. The deepest rut found was in the inside wheel path at station 30+50, measuring 0.5 inches (12.7 mm). While there were only 2 stations in the westbound lane that exhibited no discernable rutting, there were 23 in which the ruts were no deeper than 0.1 inches (2.5 mm).

The disparity between the measured rut depths can likely be attributed to the construction sequence. Back in November of 2004, the project was constructed on the first dry day after several days of rain. The conditions were wet, and the chat-asphalt was laid in the eastbound lane first. That means that the westbound lane received more construction traffic, in the form of dump trucks loaded with 15 tons of chat-asphalt each, on its prepared subgrade. The subgrade had a small degree of rutting in the westbound lane before any HMA was ever laid.

According to the Oklahoma Department of Transportation the maximum allowable rut for pavements with less than 0.3 million ESALs is 0.32 inches. Ninety-nine percent of the actual rut measurements met this criterion. All of the rut measurements can be found in Appendix G.

The final part of the distress survey involved walking the project and drawing every distress described in FHWA-RD-03-031 on grid sheets which were previously prepared. The pavement temperature was measured with an infrared gun at the beginning and end of the 50 foot length covered by each grid sheet. Each distress encountered is drawn to scale on the grid sheet, marking the exact location of the distress. Each distress type has an associated code which is noted on the grid sheet next to the drawing of the distress. Along with the code, the length or area covered by the distress is noted in the “Sheet Summary” section. On the final sheet, a

summary of all the distresses found and their total area is noted in the "Section Summary" box. At 50 foot per sheet, there are a total of 64 grid sheets which can be found in Appendix H.

In Table 8.6, three types of distress were noted. The distress guide designates longitudinal cracks as "4." The location of the crack is the next character in the code. Cracks primarily in the wheel path are designated "a" and the rest are designated "b." The last character in the code designates the severity of the crack. Cracks with a mean width less than 6 mm are coded "L" for "Low." Cracks with a mean width greater than 6 mm, but less than 19 mm are coded "M" for "Moderate." Cracks with a mean width greater than 19 mm are coded "H" for "High." Therefore, the 24.9 foot longitudinal crack located between the inside wheel path was designated "4bL" because of the small mean crack width.

Edge cracks are designated "3" in the FHWA Manual. Because by definition they are located at the pavement edge, there is no "a" or "b" designation. The severity levels are designated "L" for cracks with no breakup or loss of material, "M" for cracks with some breakup and loss of material for up to 10% of its length, and "H" for cracks with considerable breakup or loss of material for more than 10% of its length.

Although not addressed in the FHWA manual, locations where cores had been previously obtained were marked as well. Most of the core holes had been sufficiently refilled, but some were refilled either inadequately or not at all. If the core holes exhibited some problem, it was noted on the comment line at the bottom of the page.

Of the types designated in the FHWA manual, two additional distresses were present to some extent. A very small amount of transverse cracking was present, 2.4 feet in total. This type of distress is coded "6." The severity level was designated in exactly the same way as the longitudinal cracks.

Patching was also encountered on the project, which the Distress Manual designates as "7." The severity level is also designated as "L" if the patch has, at most, low severity distress of any type and pumping of water is not evident. The level of "M" is designated if the patch exhibits any moderate severity distresses, rutting of 6 to 12 mm, and pumping is not evident. The level of "H" is designated if the patch has any high severity distresses, rutting over 12 mm, or evidence of pumping. Almost all of the patching on the project was an intentional mill and fill as part of the environmental research on the project.

Distress types which are designated in the FHWA Distress Manual, but not present in the project include fatigue cracking, block cracking, reflection cracking, potholes, shoving, bleeding, polished aggregate, raveling, lane-to-shoulder dropoff, water bleeding and pumping. Some distresses were shown on the grid maps which were not included in the Manual. These included core holes, gouges, and segregated areas. Slightly scraped areas which most likely resulted from snow and ice removal were numerous and not shown on the grid maps (Figure 8.36). Table 8.6 summarizes the distresses found on the entire project and quantified on the grid sheets:

8.4.3 Conclusive Remarks on Distress Survey

- The project is in good overall shape after over two and a half years in service.
- ODOT's smoothness standards for highways are not applicable to this project, but can be used as a reference tool.
- Although the overall smoothness would be unacceptable according to ODOT's highway standards, the smoothness was very good in comparison to surrounding county roads.
- The level of rutting is low for this type of roadway after nearly two and a half years in service.
- The average rut in both wheel paths of the eastbound lane is 0.08 inches.

- The average rut in the inside wheel path of the westbound lane is 0.19 inches.
- The average rut in the outside wheel path of the westbound lane is 0.13 inches.
- The number and severity of distresses is relatively low for this type of roadway after nearly two and a half years in service.

Table 8.1 Asphalt Content by Ignition Method

Sample Identity	Asphalt Binder Content (%)
[0+75] [1+00] EB	6.57
[0+50] [0+75] WB	7.22
[0+25] [0+50] EB	7.20
[0+00] [0+25] WB	7.22
[0+00] [0+25] EB	7.80

Table 8.2 Rut Depths for Repaving Mix

Laboratory Compacted Samples	Rut Depth (mm)	Field Cores	Rut Depth (mm)
L1	5.3	R1	6.8
L2	5.3	R2	7.1
L3	5.5	R3	6.1
L4	5.7	R4	6.8
L5	6.8	R5	7.2
L6	6.9	R6	6.3
		R7	6.6
		R8	6.3
Average	5.9		6.6.5

Table 8.3 Moisture Susceptibility Test Results

Sample ID	Air Void (%) (Surface Saturated)	Tensile Strength (kPa)	Tensile Strength Ratio
M1	7.03	1070	0.99
M2	6.99	1037	
M3	7.29	1110	
M4	6.88	1104	
M5	7.12	1034	
M6	6.77	1087	

Table 8.4 Results of Profilograph Testing

Direction	From	To	Distance (feet)	Profile Index (inches/mile)
Eastbound	31+77	26+49	528	19.30
	26+49	21+21	528	17.90
	21+21	15+93	528	17.90
	15+93	10+65	528	23.50
	10+65	5+37	528	19.90
	5+37	1+10	427	33.63
			Average	**21.64**
Westbound	31+77	27+50	427	31.51
	27+50	22+22	528	17.20
	22+22	16+94	528	12.20
	16+94	11+66	528	17.70
	11+66	6+38	528	30.60
	6+38	1+10	528	15.90
			Average	**20.51**

Table 8.5 ODOT Special Provision 430-2QA Smoothness Pay Factors

For Newly Constructed or Milled and Overlaid Surfaces

Profile Index (in/mi)	Pay Factor Equation
Class I	
3.0 or less	PF = 1.03
3.1 through 12.0	PF = 1.059 – 0.0097* PI
12.1 through 16.0	PF = 1.480 – 0.0445*PI
More than 16.0	Unacceptable
Class II	
5.0 or less	PF = 1.03
5.1 through 12.0	PF = 1.083 – 0.0106* PI
12.1 through 18.0	PF = 1.320 – 0.0302*PI
More than 18.0	Unacceptable
Class III	
7.0 or less	PF = 1.03
7.1 through 14.0	PF = 1.083 – 0.0106* PI
14.1 through 20.0	PF = 1.320 – 0.0302*PI
More than 20.0	Unacceptable

Table 8.6 Distress Summary

Code	Distress Type	Total Quantity
3L	Edge cracking, low severity	202.2 feet
3M	Edge cracking, moderate severity	10.2 feet
4bL	Longitudinal cracking outside of wheel path, low severity	70.1 feet
6L	Transverse cracking, low severity	2.4 feet
7L	*Patching, low severity	2234.5 square feet
n/a	4” cores	13
n/a	6” cores	22

* *All but 1.5 square feet of patching was an intentional mill and fill.*

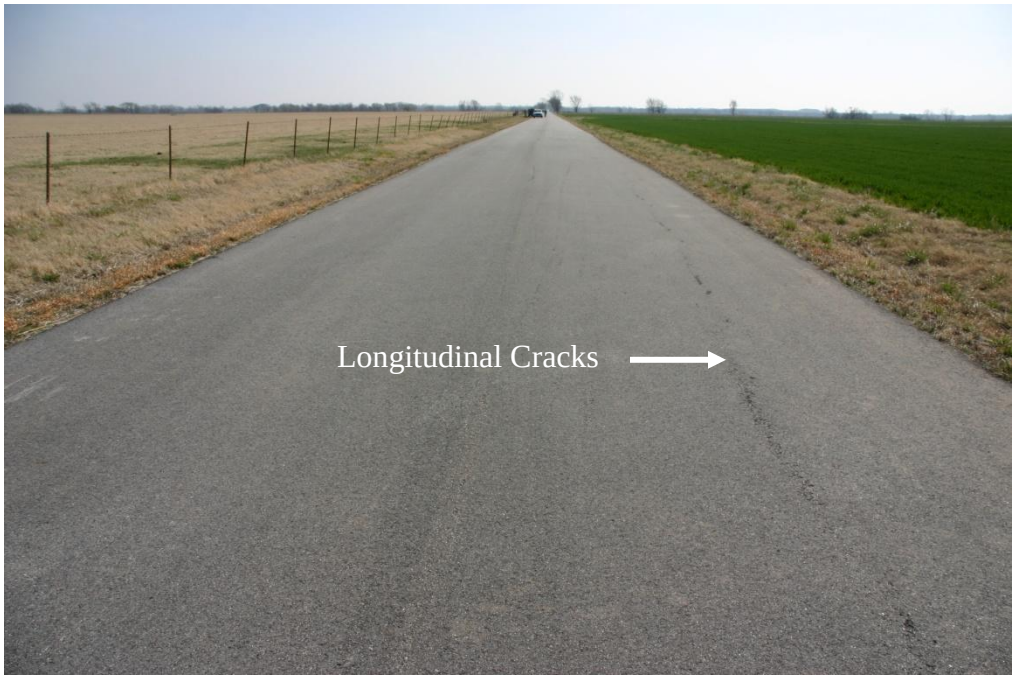

Figure 8.1 Longitudinal Cracks (South Lane)

Figure 8.2 A Close-Up View of a Longitudinal Crack (South Lane)

Figure 8.3 Growing Longitudinal Crack (South Lane)

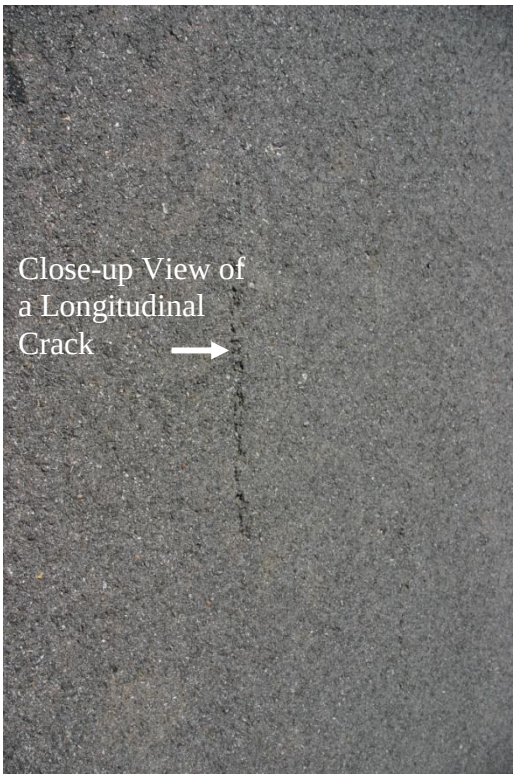

Figure 8.4 Close-Up Shot of a Growing Longitudinal Crack (South Lane)

Figure 8.5 Settlement on the Sides

Figure 8.6 Milling Started from the East End of the Test Road

Figure 8.7 The ROTO-MILL Pavement Profiler

Figure 8.8 Milling Teeth of the ROTO-MILL Pavement Profiler

Figure 8.9 The Teeth of the ROTO-MILL are in Action

Figure 8.10 ROTO-MILL Throws Out Millings into a Truck

Figure 8.11 Completion of the First Run of the ROTO-MILL

Figure 8.12 Second Run of the ROTO-MILL

Figure 8.13 Completion of the Third Run of the ROTO-MILL

Figure 8.14 Fourth Run of the ROTO-MILL

Figure 8.15 Collection of Millings After First Run

Figure 8.16 Collection for Millings After Fourth Run

Figure 8.17 The Mechanical Broom Used for Cleaning After Milling

Figure 8.18 Cleaning with a Mechanical Broom

Figure 8.19 Asphalt Paver Manufactured by Barber Greene

Figure 8.20 Paver is Accepting Asphalt Mix from a Truck

Figure 8.21 Paving the East Bound Lane

Figure 8.22 Paving the West Bound Lane

Figure 8.23 Collected Loose Asphalt Mix from the Second Truck

Figure 8.24 The Ingersoll-Rand Roller

Figure 8.25 Compaction of the East Bound Lane

Figure 8.26 Measurement of the Level of Compaction Using a PQI Gauge

Figure 8.27 Finished Road after Milling, Repaving and Compaction

Figure 8.28 Crack-Free Section of TS-3

Figure 8.29 Edge Deterioration in TS-3

Figure 8.30 Small Longitudinal Crack in TS-1

Figure 8.31 Transverse Crack in TS-2

Figure 8.32 Ames Profilograph

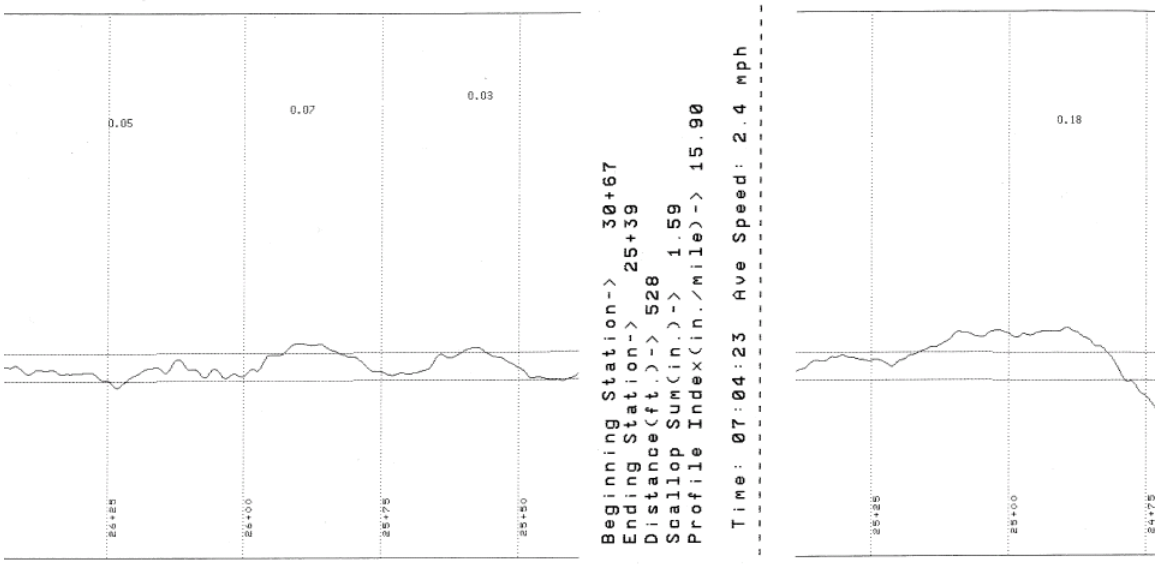

Figure 8.33 Sample Profilograph Printout

Figure 8.34 Marked Station Number at Previous Station

Figure 8.35 Rut Measuring Devices

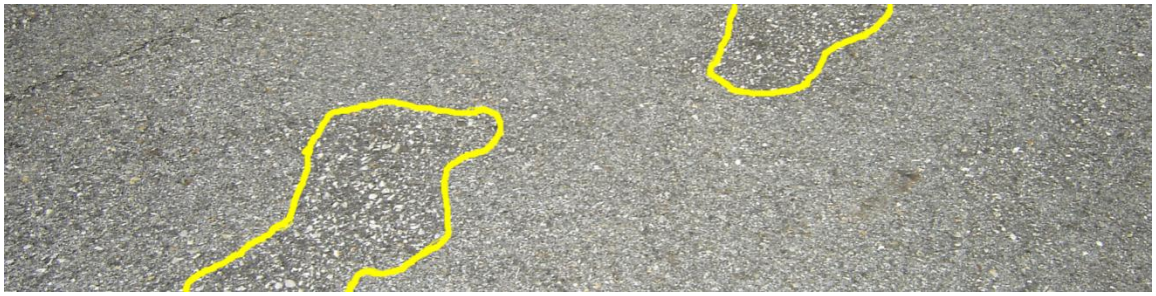

Figure 8.36 Snow and Ice Removal Scraped Areas

CHAPTER 9 CONCLUSIONS AND RECOMMENDATIONS

9.1 Summary

The major objective of this field demonstration project was to evaluate the performance of chat-asphalt and stabilized-chat as paving materials, particularly for the paving of county chat roads in the Tar Creek Superfund Site region. An unpaved chat road segment, county road E30 between S530 and S550, was selected in cooperation with the Oklahoma Department of Environmental Quality. A field survey was conducted to examine the existing profile, right of way, drainage and other pertinent data. Dynamic cone penetration (DCP) tests were conducted at selected locations and laboratory tests were conducted on soil samples collected from DCP boreholes to characterize the subgrade soils. Also, a bench scale laboratory test was conducted to evaluate the feasibility of using stabilized-chat, without any non-chat aggregates, as a base. Moreover, two mix designs, one for chat-asphalt surface course and the other for chat-asphalt base course, were performed. A 3100-ft long Test Road was constructed with four different sections. The stabilizing agents used (CFA and CKD), as well as the thicknesses of the chat-asphalt surface and base courses, varied from one section to the other. Density of the compacted pavement was measured, and field mixes and cores were collected for laboratory testing. In addition, field tests were conducted to evaluate the performance of the Test Road. A segment of the Test Road was milled after sixteen months in service and repaved with chat-asphalt. A distress survey, including drainage inspection, cracking, and rutting, was conducted after more than two and a half years in service. Finally, falling weight deflectometer and ground penetrating radar tests were conducted a few months after the distress survey.

The laboratory assessment of CFA- and CKD-stabilized chat bases was based on elastic modulus (E) and unconfined compressive strength (UCS) determined from uniaxial compressive

strength tests. The seismic modulus (E*) was measured using a non-destructive technique, Spectral Analysis of Surface Waves (SASW). Unlike stabilized bases, one type of modulus test, namely cyclic indirect tension resilient modulus (M_R) test, was performed on chat-asphalt surface and base courses. The resilient modulus (M_R) test was performed with varying stress ratios ranging from 0.15 to 0.70 and three selected test temperatures, namely 5°C, 25°C and 40°C (i.e., 41°F, 77°F and 104°F). The resilient moduli obtained for these mixes were compared with two other sites, Davis and Oklahoma City. Other important performance characteristics of chat-asphalt, namely, APA rut, APA fatigue and permeability, were also performed in the laboratory. Selected field tests (i.e., falling weight deflectometer, Spectral Analysis of Surface Waves, Ground Penetrating Radar, and Dynamic Cone Penetration) were conducted and the results were compared with the laboratory results, whenever possible. To evaluate the environmental effects of milling, a portion of the Test Road was milled and repaved with chat-asphalt. Also, a distress survey of the Test Road was conducted after more than two and a half years in service.

9.2 Conclusions

From the laboratory and field data, and their analyses presented in the preceding chapters, the following conclusions can be drawn:

1. Pile run chat alone should not be used as a base because of the lack of cohesion and aggregate interlock due to the absence of large particles required to meet particle gradation requirements. CFA and CKD, if used as stabilizing agents, react with water leading to hydration products which eventually crystallize to yield strength to the stabilized-chat. Both CFA and CKD-stabilization produced sufficient increases in unconfined compressive strength and elastic modulus that made them a suitable material for roadway base.

2. Laboratory seismic modulus (E*) values of CFA-stabilized chat range between 766 ksi and 904 ksi with an average modulus of approximately 868 ksi. CKD-stabilized chat specimens had E* values ranging between 168 ksi to 224 ksi, with an average modulus of approximately 197 ksi. The average E* of CFA-stabilized chat is approximately four times the E* of CKD-stabilized chat.
3. Elastic modulus (E) of the pile run chat, determined from the unloading-reloading stress-strain curve of a UCS test, exhibited an increase after stabilization using CFA and CKD. The elastic modulus of chat stabilized with 10% CFA ranged between 40 ksi to 84 ksi, with an average modulus of approximately 59 ksi. The elastic modulus of chat stabilized with 10% CKD ranged between 13 ksi to 39 ksi, with an average value of approximately 24 ksi. Comparatively, the E* of the CFA-stabilized chat specimens is about 15 times higher than the corresponding E value from the UCS test. The E* of CKD-stabilized chat specimens was approximately 8 times the value from a UCS test.
4. The average Unconfined Compressive Strength (UCS) of chat stabilized with 10% CFA was approximately 163 psi after 28 days of curing. For CKD-stabilized chat specimens, the UCS ranged between 56 psi to 94 psi, with an average of approximately 73 psi. The average UCS of CFA-stabilized chat was about twice the corresponding value of CKD-stabilized chat. For pile run chat without any stabilizing agents, the specimens failed under their own weight due to lack of cohesion and thus, the UCS of pile run chat could not be determined. Although small, CFA-stabilized and CKD-stabilized chat specimens exhibited some tensile strength. The indirect tensile strengths (ITS) of CFA-stabilized chat ranged between 13 psi to 24 psi, with an average value of approximately 19 psi. For CKD-stabilized chat, the average ITS value was only 8 psi. Also, it was found that the average

ITS value was approximately 1/8.6 (11.6%) for the UCS of CFA-stabilized specimens. As for CKD-stabilized specimens, the corresponding value was 1/9 (11.1%).

5. Pile run chat (e.g., Kenoyer North Pile, Tri-State Asphalt, etc.) alone cannot meet the gradation requirements of the Superpave S5 type surface mix or Superpave S3 type base mix. Therefore, 80% pile run chat was blended with 20% locally available limestone to prepare a S5 type surface mix and 50% pile run chat was blended with 50% limestone to prepare a S3 type base mix.

6. The indirect tension resilient modulus test was performed on chat-asphalt surface and base mixes. The test results suggest that the indirect tension resilient modulus depends on the applied load (stress ratio) and temperature. Based on the test results, the resilient modulus decreases with increases in stress level and temperature. An average resilient modulus values at a stress ratio of 0.20 and a test temperature of 25°C (77°F) are 5,992 MPa (869 ksi) for the Test Road base and 2,565 MPa (372 ksi) for the Test Road surface. The specific mix properties, namely air voids, binder content, specific gravity of aggregates and sizes of aggregates, were identified as the influential factors in the test results. A statistically significant model for resilient modulus with test parameters (stress ratio and temperature), specific mix properties (air voids, binder content and aggregate percentage passing No. 200 sieve) was developed. The APA rut test results suggest that the Test Road mixes are susceptible to rutting. An average rut depth of the Test Road surface mix is 7.6 mm (0.3 in) and that of the base mix is 4.9 mm (0.2 in). The APA test results for field cores also suggest that the Test Road mixes are susceptible to rutting. The average rut depths are 9.5 mm (0.4 in) for Test Road cores. The correlations based on the limited results show that the rut depth are functions of binder content and aggregate percentage passing No. 200 sieve.

APA rut test results from this limited study show that resilient modulus may be correlated with rut depths. A comparatively high R-squared value of 0.72 was obtained for rut at 2000 loading cycles and laboratory M_R at 40°C (104°F) and a stress ratio of 0.50. However, this correlation may not be applicable to other mixes because it depends on associated test parameters and mechanisms.

7. The APA fatigue test results indicate that the Test Road has a greater fatigue resistance than the Davis and the OKC mixes used for comparison in this study. The fatigue cycles for the Test Road base and surface mixes are approximately 49,000. On the other hand, the fatigue cycles for the Davis and the OKC mixes are 20,000 and 27,000, respectively. The difference in number of fatigue cycles for different mixes suggests that the fatigue resistance for mixes depends on specific mix properties. Based on the four different mixes tested in this study, the number of fatigue cycles can be correlated with air voids, specific gravity of aggregates and aggregate percentage passing No. 200 sieve.

8. The average permeability value for the Test Road surface mix is 10.8×10^{-6} cm/s (4.3×10^{-6} in/s) and that of the base mix is 2.4×10^{-6} cm/s (0.9×10^{-6} in/s). Based on the permeability values of four mixes tested in this study, there is a strong correlation of permeability with air voids and aggregate percentage passing No. 200 sieve.

9. In the field three non-destructive tests, namely spectral analysis of surface waves (SASW), falling weight deflectometer (FWD) and ground penetrating radar (GPR) were performed to analyze the performance of the stabilized bases. SASW and FWD tests measure the moduli of different layers in the pavement while GPR measures their thicknesses. The SASW technique (for *in-situ* determination of modulus) yielded an average modulus (E_{SASW}) of 432 ksi in sections with CFA-stabilized base and an average modulus of

approximately 233 ksi in the section with CKD-stabilized base. The modulus (E_{SASW}) obtained from the SASW test is approximately 7.5 and 9.5 times the elastic modulus (E) obtained from the UCS test, for CFA-stabilized and CKD-stabilized chat, respectively. The modulus obtained from the FWD test for CFA-stabilized base was approximately 134 ksi, which is about twice the modulus for CFA-stabilized chat obtained from the UCS test. The modulus obtained from the FWD test for CKD stabilized base was approximately 56 ksi, which is approximately twice the modulus for CKD-stabilized chat obtained from the UCS test. Also, it was found that the CFA-stabilized chat base had a modulus of approximately 2.4 times the modulus of the CKD-stabilized chat base.

10. The two types of moduli determined for the stabilized bases were also determined for chat-asphalt surface and base courses. The pavement layer thicknesses were determined using GPR. The average FWD back-calculated modulus for the Test Road is approximately 1,751 MPa (254 ksi) for Section TS-1, 1,255 MPa (182 ksi) for Section TS-2, 841 MPa (122 ksi) for Section TS-3, and 1,668 MPa (242 ksi) for Section TS-4. The SASW modulus for Section TS-2 of the Test Road is approximately 8,618 MPa (1,250 ksi) for the surface course and 9,308 MPa (1,350 ksi) for the base course. The corresponding values for Sections TS-1 and TS-4 are 4,895 MPa (710 ksi) and 4,275 MPa (620 ksi) for the surface course and 6,412 MPa (930 ksi) and 5,309 MPa (770 ksi) for the base course, respectively. Overall, the results show that E_{SASW} is approximately 4 times higher at Section TS-4 and 6 times higher at Section TS-2 than the corresponding E_{FWD} values. The HMA layer thicknesses obtained from the GPR data are fairly consistent and close to the respective design thicknesses. Only the Section TS-2 showed a high variation.

11. Lack of drainage caused significant problems at the Test Road site. Specifically, it led to significant rutting, increased moisture and reduced strength in Section TS-3, requiring an additional unbound aggregate base. Also, lack of drainage led to partial flooding of Section TS-3. The overall success of the Test Road was greatly hampered by poor drainage. A functional drainage system is needed to prevent flooding and increases in moisture contents in subgrade soils.
12. Different tests on millings and the repaving mix, namely asphalt content, APA rut and moisture sensitivity were performed. It was observed that the millings have an average asphalt content of 7.2% although the optimum asphalt binder content was 7%. The APA rut depths are higher for the field cores than the laboratory compacted samples. In moisture susceptibility tests, it was observed that the tensile strength ratio (TSR) is very high (0.99 > 0.8).
13. After the Test Road was in service for about two and a half years, a detail distress survey was conducted. Although the overall smoothness would be unacceptable according to ODOT's highway standards, the smoothness was very good in comparison to surrounding county roads. The level of rutting is low for this type of roadway. Also, the number and severity of distresses is relatively low.
14. Premature use of the Test Road by farm machinery and fire trucks led to base failures at three locations in TS-2 and localized rutting at many locations in Section TS-3. Cementitious stabilization requires a minimum curing period without traffic.
15. Based on gradation requirements, pile run chat by itself is not a viable option. However, CFA-stabilization and CKD-stabilization of the chat-asphalt surface and chat-asphalt base

appear to make them suitable for roads with low to moderate traffic (< 0.3 million ESAL) based on this study.

9.3 Recommendations

Based on the results of this study, the following recommendations are presented for future studies in this area:

1. Permeability plays an important role in drainage and consequently the strength of the stabilized base. Permeability of stabilized base has not been addressed in the past. It would be interesting to study permeability of stabilized-chat base in order to evaluate its drainage characteristics.
2. Flexural strength is an important parameter influencing the structural response and fatigue performance of a stabilized aggregate base. Flexural strength of stabilized-chat can be an interesting property to study.
3. According to Nazarian (2003a), the seismic modulus results are sensitive to moisture content, curing time and method of specimen preparation. It would be interesting to analyze the results of NDT on the field cores. Also, it would be of interest to observe the variation of seismic modulus with moisture content and curing time.
4. There are several chat piles in the Test Road area, having chat with different gradations. It would be helpful if studies similar to this are carried out on pile run chat from different sources (with different gradations) to assess differences in the properties of stabilized-chat due to differences in gradation.
5. The field component associated with this study involved construction of a county road with very low traffic volume. A future study to explore the possibility of using a stabilized-chat base in roadway pavements with high traffic volumes would be beneficial.

References

American Coal Ash Association, "*Soil and Pavement Base Stabilization with Self-Cementing Coal Fly Ash*," Report, prepared by GeoSystems Engineering Inc, 1999.

Abdallah, I., Yuan, D., and Nazarian, S., "*Integrating Seismic and Deflection Methods to Estimate Pavement Moduli*," Transportation Research Record 1755, pp. 43-50, Washington, D.C., 2001.

Ali, H., and Lobez, A., "*Statistical Analyses of Temperature and Moisture Effects on Pavement Structural Properties Based on Seasonal Monitoring Data*," Transportation Research Record 1540, Washington, D.C., 1996.

Almudaiheem, J.A., and Al-Sugair, F.H., "*Effect of Loading Magnitude on Measured Resilient Modulus of Asphaltic Concrete Mixes*," Transportation Research Record 1317, pp. 139-144, Washington, D.C., 1991.

Ashworth, L., "F*actors Affecting Rutting Potential of Superpave Asphalt Mixtures in New Brunswick*," M.S. Thesis, The University of New Brunswick, USA, August, 2003.
ASTM D 4123, "*Indirect Tension Test for Resilient Modulus of Bituminous Mixtures*," American Society of Testing Materials, Vol. 04.03, 1995.

Azad, S., "Soil *Stabilization of Three Different Soils Using Cement Kiln Dust*," M.S._Thesis, University of Oklahoma, Norman, OK, 1998.

Baghdadi, Z., and Rahman, A.," *The Potential of Cement Kiln Dust For the Stabilization of Dune Sand in Highway Construction*," Journal of Building And Environment, Vol. 4, No. 25, pp. 285-289, 1990.

Baghdadi, Z. A., and Fatani, M. N., and Sabban, N. A., "*Soil Modification by Cement Kiln Dust*," Journal of Materials in Civil Engineering, Vol. 7, No. 4, pp. 218-222, 1995.

Bandara, N., and Briggs, R., "*Nondestructive Testing of Pavement Structures*," American Society for Nondestructive Testing, Inc. Publication, 2004. URL: http://www.asnt.org/publications/materialseval/basics/jul04basics/jul04basics.htm

Barksdale, R.D., Khosla, P., Kim, R., Lambe, P., and Rehman, M., "*Laboratory Determination of Resilient Modulus for Flexible Pavement Design*," Final Report, NCHRP Project 1-28, USA, 1997.

Bhasin, A., Button, J.W., and Chowdhury, A., "E*valuation of Simple Performance Tests on HMA Mixtures,*" Project summary report 9-558-S, Texas Transportation Institute, The Texas A&M University System, August, 2005.

Bin-Shafique, M. S., Benson, C. H., and Edil, T. B. , "*Leaching from Heavy Metals in Fly Ash Stabilized Soils Used in Highway Pavements*," Geo-Engineering Report No. 02-14, Geo Engineering Program, University of Wisconsin-Madison, Madison, WI, 2002.

Blakey, F.A., and Beresford, F.D., "*Tensile Strain in Concrete*," Part II, Report No. C2. 2-2, Division of Building Research, Melbourne, 1955.

Boudreau, R.L., Hicks, R.G., and Furber, A.M., "*Effects of Test Parameters on Resilient Modulus of Laboratory-Compacted Asphalt Concrete Specimens*," Transportation Research Record No. 1353, pp. 46-52, Washington, D.C., 1992.

Brandon, J.M., Jared, D.M., Wu, P.Y., and Geary, G.M., "*Field and Laboratory Investigation of Permeable Asphalt Mixes on Georgia Highways*," Transportation Research Record 1891, pp. 32-39, Washington, D.C., 2004.

Brown, E.R., and Cross, S.A., "*A Study of In-Place Rutting of Asphalt Pavements*," NCAT Report 89-02, National Centre for Asphalt Technology, Auburn, AL, April, 1989.

Brown, E.R., and Foo, K.Y., "*Evaluation of Variability in Resilient Modulus Test Results (ASTM D 4123)*," NCAT Report, No 91-6, USA, 1989.

Brown, E.R., Prowel, B., Cooley, A., Zhang, J., and Powell, R.B., "*Evaluation of Rutting Performance on the 2000 NCAT Test Track*," Asphalt Paving Technology: v 73, Association of Asphalt Paving Technology 2004, pp. 287-336, 2004.

Buchanan, M., "*Evaluation of the Effect of Flat and Elongated Particles on the Performance of Hot Mix Asphalt Mixtures*," NCAT Report 00-03, National Centre for Asphalt Technology, May, 2000.

Christopher, W.R., and Prowell, B.D., "*Comparison of Laboratory Wheel Tracking Test Results with WesTrack Performance*," Transportation Research Record 1681, Washington, D.C., 1999.

Choubane, B., Page G.C., and Musselman J.A., "*Investigation of Water Permeability of Coarse graded Superpave Pavements*," Journal of the Association of Asphalt Paving Technologists, Vol. 67, pp. 254-276, 1998.

Choubane, B., Page, G.C., and Musselman, J.A., "*Suitability of Asphalt Pavement Analyzer for Predicting Pavement Rutting*," Transportation Research Record 1723, pp. 107-115, Washington, D.C., 2000.

Christensen, W. D., Bonaquist, R., and Jack, D.P., "*Evaluation of Triaxial Strength as a Simple Test for Asphalt Concrete Rut Resistance*," Final Report, Pennsylvania Department of Transportation, 2000.

Collins, R., Watson, D.E., and Cambell, B., "*Development and Use of Georgia Loaded Wheel Tester*," Transportation Research Record 1492, Washington, D.C., 1995.

Cooley L.A., Brown, E.R., and Maghsoodloo, S., "*Developing Critical Field Permeability and Pavement Density Values for Coarse-graded Superpave Pavements*," Transportation Research Record 1761, pp. 41-49, Washington, D.C., 2001.

Cooley, L.A., and Brown, E.R., "*Selection an Evaluation of a Field Permeability Device for Asphalt Pavements*," Presented at the 79th Annual Meeting of the Transportation Research Board, Washington, DC, 2000.

Crovetti, J., Hall, K.T., and Williams, C., "*Wisconsin Highway Research Program #0092-03-14 Development of Modulus to Temperature Relations for HMA Mixtures Used in Wisconsin*," Final Report, Wisconsin Department of Transportation, September 2005.

Cruz, J. "*Permeability of Hot-Mix Asphalt Concrete*," M.S. Thesis, University of Arkansas, Fayetteville, May 2000.

Dames and Moore, "*Final Remedial Investigation for Cherokee County, Kansas, CERCLA Site Baxter Springs, Treece Sub-Sites*", Volume I and II, 1993.

Datin, D.L. and Cates, D.A., "*Sampling and Metal Analysis of Chat Piles in the Tar Creek Superfund Site*," Report, Prepared for the Oklahoma Department of Environmental Quality, 2002.

Drake, K. D., "*Leachability of Size-fractioned Mine Tailings from the Kansas Portion of the Tri-State Mining District*," Masters Thesis, University of Missouri, Kansas City, Missouri, 1999.

Epps. J.A., and Monismith, C.L., "*Fatigue of Asphalt Concrete Mixtures – Summary of Existing Information*," STP 508, ASTM, pp. 19-45, 1972.

Federal Highway Administration. *Distress Identification Manual for the Long-Term Pavement Performance Program*. Publication No. FHWA-RD-03-031, 2003.

Finn, F., and Epps, J., "*Compaction of Hot Mix Asphalt Concrete*," Research Report 214-21, Texas Transportation Institute, August 1980.

Gary, M. Jr. McAfee, R. and Wolf, C. L., "*Glossary of Geology*." American Geological Institute (AGI), Washington, D.C., 1977.

Geovision, Geovision Geophysical Services, Corona, CA 92882, 2005
URL: http://www.geovision.com/seismic.htm

Gierhart, D., "Pavement Distress Survey on Tar Creek Chat-Asphalt Road Constructed in Miami, Oklahoma", Internal report submitted to University of Oklahoma, 2007.
Hall, K.D., "*Comparison of Falling –Head and Constant Head Techniques*," Transportation Research Record 1891, pp. 23-31, Washington, D.C., 2004.

Hasset, D.J., Zacher, E.J., and Heebink, L.V., "*Determination of Expansion Potential of Coal Combustion By-Products*," Ash Library Conference Papers, 2001.

Healow, S.P., "*Analysis and Development of Performance Models for WesTrack*," M.S. Thesis, University of Nevada, Reno, May 1998.

Hensley, M.J., and Rose, J.G., "Design, Construction and Performance of Hot Mix Asphalt for Railway Trackbeds," Asphalt Institute, Executive Offices and Research Center, 1st World Conference of Asphalt Pavements, Sydney, Australia, 2005. URL: http://www.asphaltinstitute.org/upload/Design_Construction_Performance_HMA_RR_Trackbeds.pdf

Hondros, G., "*The Evaluation of Poisson's Ratio and the Modulus of Materials of a Low Tensile Resistancy by the Brazilian (Indirect Tensile) Test with Particular Reference to Concrete*," Australian Journal of Applied Science, Vol. 10, No. 3, pp. 243-268, 1959.

Hossain, M., and Scofield, L.A., "*Correlation between Back Calculated and Laboratory-Determined Asphalt Concrete Moduli*," Transportation Research Record 1377, pp. 67-76, Washington, D.C., 1992.

Huang, Y.H., "*Pavement Analysis and Design*," 2nd Edition, Prentice Hall Inc, NJ, USA, 2004.

Huang, B., Mohammad, L., Raghavendra, A., and Abadie C., "*Fundamentals of Permeability in Asphalt Mixtures*," Journal of the Association of Asphalt Paving Technologists, Vol. 68, pp. 479-500, 1999.

Huber, G., and Heiman, G., "*Effects of Asphalt Concrete Parameters on Rutting Performance: A Field Investigation*," Proceedings of the Association of Asphalt Paving Technologists, Vol. 56, 1987.

Hughes, M., "*Sub-grade Stabilization Using Unwashed Mine Tailings From The Tar Creek Superfund Site*," A Report Submitted to Oklahoma Department of Transportation, Oklahoma State University, Stillwater, OK, 2002.

Kamon, M., and Nontananandh, S., *"Combining Industrial Waste with Lime for Soil Stabilization,"* Journal of Geotechnical Engineering, Vol. 117, No. 1, pp. 1-17, 1991.

Kandhal, P.S., and Mallick, R.B., "*Evaluation of Asphalt Pavement Analyzers for HMA Mix Design*," National Center for Asphalt Technology, NCAT Report No. 99-4, pp. 34, Auburn, AL, 1999.

Kandhal, P.S., and Cooley, L.A., "*Evaluation of Permanent Deformation of Asphalt Mixtures using Loaded Wheel Tester*," Asphalt Paving Technology: Association of Asphalt Paving Technologists-Proceedings of the Technical Sessions, Vol. 71, pp. 739-753, 2002.

Kanitpong, K., Bahia, H.U., Benson, C.H., and Wang, X., "*Effect of Lift Thickness and Flow Direction on Hydraulic Conductivity (Permeability) of Laboratory Compacted Asphalt Mixtures*," Presented at the 81st Annual Meeting of the Transportation Research Board, Washington, D.C., 2002.

Kanitpong, K., Bahia, H.U, Benson, C., and Wang, X., "*Measuring and Predicting Hydraulic Conductivity (Permeability) of Compacted Asphalt Mixtures in the Laboratory*," 82nd Annual Meeting of the Transportation Research Board. Washington, D.C., 2003.

Katicha, S.W., "*Development of Laboratory to Field Shift Factors for Hot Mix Aspahlt Resilient Modulus*," M.S. Thesis, Virginia Polytechnic Institute and State University, November 2003.

Kennedy, T.W., and Hudson, W.R., "*Application of the Indirect Tensile Test to Stabilized Materials*," Highway Research Record 235, Highway Research Board, Washington, D. C., 1968.

Khanna, V., "Advancing airport pavement management-development of a web-based IMS for Oklahoma's general aviation airports and exploring the use of SASW and IR for pavement health monitoring," Ph.D. Dissertation, University of Oklahoma, Norman, OK, 2007.

Khoury, N., "*The effect of Freeze-Thaw And Wet-Dry Cycles on Resilient Modulus of Class C Fly Ash Stabilized Aggregate Base*," M.S. Thesis, University of Oklahoma, Norman, OK, 2001.

Khoury, N., and Zaman, M. M.,*"Effect of Wet-Dry Cycles on Class C Fly Ash Aggregate Base,"* Journal of The Transportation Research Board, Geomaterials, No. 1787, pp. 13-21, 2002.

Khoury, N., "*Durability of Cementitiously Stabilized Aggregate Bases for Pavement Application*," Ph.D. Dissertation, University of Oklahoma, Norman, OK, 2005.

Kim, Y.R., Allen, D.H., and Little, D.N., "*A Computational Model to Predict Fatigue Damage Behavior of Asphalt Mixtures Under Cyclic Loading*," Transportation Research Board, TRB 2006 Annual Meeting, Washington, D.C., 2006.

Lafarge, "Properties of CFA and CKD", Material Information Sheet, Lafarge Inc., Tulsa, OK, 2005.

Laguros, J.G. and Zenieris, P., "Feasibility of Using Fly Ash as a Binder in Coarse and Fine Aggregates for Bases," Report No. ORA 155-404, University of Oklahoma, Norman, OK, 1987.

Liu, W., and Scullion, T. (2000), "MODULUS 5.0 FOR WINDOWS," Software Program Texas Transportation Institute, Texas Department of Transportation, Austin, TX.

Mallick, R.B., Cooley, Jr., L.A., Teto, M.R., Bradbury, R.L., and Peabody, D., "*An Evaluation of Factors Affecting Permeability of Superpave Designed Pavements*," NCAT Report 03-02, National Center for Asphalt Technology, June, 2003.

Maupin, Jr., G.W., "*Asphalt Permeability Testing in Virginia*," Presented at the 79th Annual Meeting of the Transportation Research Board, Washington, DC, 2000.

McClave, J., Benson, G., and Sincich, T.,"Statistics for Business and Economics," Prentice Hall, Upper Saddle River, NJ, 2001.

McDonald, P.D.M., "How to Interpret a Box Plot in Terms of a Normal Distribution," 1999. URL: http://www.math.mcmaster.ca/peter/s2ma3/s2ma3_9798/boxplots.html

McWilliams, C.E., "*Air and Water Permeability related to Asphalt Mix Characteristics*," M.S. Thesis, University of Arkansas, Fayetteville, 1986.

Mindess, S., Young, J. F., and Darwin, D. (2002), "Concrete," 2nd Edition, Prentice Hall Inc., Englewood Cliffs, NJ.

Miller, G. A., Zaman, M. M., Rahman, J., and Tan, N. K., "Laboratory and Field Evaluation of Soil Stabilization using Cement Kiln Dust," Report, Item 2144, ORA 125-5693, submitted to Oklahoma Department of Transportation, 1999.

Mohammad, L. N., Herath, A., and Huang, B., "*Evaluation of Permeability of Superpave Asphalt Mixtures*," Transportation Research Record 1832, pp. 50–58, Washington, D.C., 2003.

MTS "*User Information and Software References,*" MTS System Corporation, 100-077-223 J, Eden Prairie, MN, 2005.

Navaratnarajah, S.K., "Performance Characteristics of Selected Asphalt Mixes: A Laboratory and Field Study," Thesis submitted to the School of Civil Engineering and Environmental Science, University of Oklahoma, Norman, Oklahoma, 2006.

Nazarian, S., Stokoe, K.H., Briggs, R.C, and Rogers, R., "*Determination of Pavement Layer Thicknesses and Moduli by SASW Method*," Transportation Research Record 1196, pp. 133-150, Washington, D.C., 1988.

Nazarian, S., and Stokoe, K. H. I. (1989), "Nondestructive Evaluation of Pavements by Surface Wave Method," Nondestructive Testing of Pavements and Back-calculation of Moduli, ASTM STP 1026, pp. 119-137.

Nazarian, S., Rojas, J., Pezo, R., Yuan, D., Abdallah, I., and Scullion, T., "*Relating Laboratory and Field Moduli of Texas Base Materials*," Transportation Research Record, No. 1639, pp. 1-11, 1998.

Nazarian, S., Yuan, D., and Williams, R. R., *"A Simple Method for Determining Modulus of Base and Subgrade Materials,"* Resilient Modulus of Testing for Pavement Components, ASTM STP 1437, G.N. Durham, W.A. Marr, and W.L. DeGroff, Eds., ASTM International, West Conshohocken, West Conshohocken, PA, 2003a.

Nazarian, S., and Yuan, D., *"Comprehensive Mechanistic-based Quality Control of Flexible Pavements with NDT Methods,"* International Symposium (NDT-CE), Berlin, Germany, 2003b.

Nazarian, S., Abdallah, I., and Yuan, D., "*Neural Networks for Rapid Reduction Interpretation of Spectral Analysis of Surface Waves Results*," Transportation Research Record 1868, pp. 150-155, Washington, D.C., 2004.

National Research Council Canada (2001), "Building Envelope and Structure," Construction Envelope, Vol. 6, No. 2,
URL: http://irc.nrc-cnrc.gc.ca/pubs/ci/v6no2/v6no2_10-print_e.html

Oklahoma Department of Environmental Quality (ODEQ*), "Summary Report of Washed and Unwashed Mine Tailings (Chat) from the Tar Creek Superfund Site Area,"* Oklahoma City, Oklahoma, 2000.

ODOT, *"Standard Specifications for Highway Construction,"* Oklahoma Department of Transportation, 1999.

Oklahoma Department of Transportation (ODOT), *"Specifications for Base Course and Surface Course,"* Oklahoma City, Oklahoma, 2001.

Oklahoma Department of Transportation (ODOT), Material Division Mix Design Database, Oklahoma City, Oklahoma, 2002.

Pandey, K.K., *"Evaluation of Resilient Moduli and Layer Coefficients of a Coal Ash Stabilized Marginal Aggregate Base for AASHTO Flexible Pavement Design,"* Ph.D. Dissertation, University of Oklahoma, Norman, OK, 1996.

Prowell, B.D., and Dudley, M.C., "*Evaluation of Measurement Techniques for Asphalt Pavement Density and Permeability*," Transportation Research Record 1789, pp. 36-45, Washington, D.C., 2002.

Roberts, F.L., Kandhal, P.S., Brown, E.R., Lee, D.Y., and Kennedy, T.W., "*Hot mix asphalt materials, mixture design and construction*," 2nd ed. Lanham, MD: NAPA Research and Education Foundation, 1996.

Roddis, W.M.K., Maser, K., and Gisi, A.J., "*Radar Pavement Thickness Evaluation for Varying Base Conditions*," Transportation Research Record 1355, pp. 90-98, Washington, D.C., 1992.

Salem, H.M., "*Quantification of Environmental Impacts on the Performance of Asphalt Pavements*," Ph.D. Dissertation, University of Idaho, June 2004.

Saskatchewan Highways and Transportation (1992), "Evaluation of Bearing Capacities of Subbase and Subgrade Using Dynamic Cone Penetration Test," Standard Test Procedure Manual, STP 240-20,
URL: http://www.highways.gov.sk.ca/docs/reports_manuals/manuals/STP_DOC/stp240-20.pdf

Schmidt, R.J., "*A Practical Method for Measuring the Resilient Modulus of Asphalt Treated Mixes*," Highway Research Record 404, National Research Council, Washington, D.C., 1972.

Shalaby, A., Liske, T., and Kavussi, A., "*Comparing Back Calculated and Laboratory Resilient Moduli of Bituminous Paving Mixtures*," Canadian Journal of Civil Engineering, v 31, No. 6, pp. 988-996, December, 2004.

SHRP Protocol P07, "*Resilient Modulus of Asphalt Concrete*," Long Term Pavement Performance (LTPP) Program Directive M-1, November 1992.

Srinivasan, G., "*Evaluation of Indirect Tensile Strength to Identify Asphalt Concrete Rutting Potential*," M.S. Thesis, West Virginia University, Morgantown, West Virginia, 2004.

Tangella, S.C.S.R., Craus, J., Deacon, J.A., and Monismith, C.L., "*Summary Report on Fatigue Response of Asphalt Mixtures*," TM-UCB-A-003A-89-3, Prepared for Strategig Highway Research Program, Project A-003-A, February, 1990.

Tarefder, R.A., "*Laboratory and Model Prediction of Rutting in Asphalt Concrete*," Ph.D. Dissertation, University of Oklahoma, December 2003.

Tarefder, R.A. and Zaman, M., "*Correlating Asphalt Concrete Modulus with Rut Potential,*" Proc. Third International Symp. on Maintenance and Rehabilitation of Pavements and Technological Control, held on July 7-10, 2003 in Portugal, Vol. 1, pp. 207-217, 2003.

Teng, T.P., "*Performance of Coarse-Graded Mixes at WesTrack Premature Rutting*," Federal Highway Administration, Final Report, June, 1998.

Teredesai, R.V., Zaman, M., Miller, G., and Nairn, R., "*A Study to Optimize Use of Raw Chat in Stabilized Base Construction,*" A Report Prepared for Oklahoma Department of Environmental Quality, Oklahoma City, OK, 2005.

Teredesai, R.V., Stabilization of Pile Run Chat for Roadway Base Application, A thesis submitted to the School of Civil Engineering and Environmental Science, University of Oklahoma, Norman, Oklahoma, 2005.

Timoshenko, S., and Goodier, J., "*Theory of Elasticity*," McGraw Hill Book Company, September 1970.

Thompson, M., "Lime Reactivity of Illinois Soil," Journal of Soil Mechanics and Foundation Divisions, Vol. 92, No. SMS, 1966.

Turner-Fairbank Research Center, *"Coal Fly Ash,"* Online User Guidelines, 2005.

Transportation Research Board, *"Lime Stabilization: Reactions, Properties, Design, and Construction,"* Transportation Research Board, National Research Council, Washington, D.C. 1987. URL: http://www.tfhrc.gov/hnr20/recycle/waste/cfa55.htm

University of Oklahoma, *"Survey on Chat Use in Asphalt Pavement,"* School of Civil Engineering and Environmental Science, 2003.

U.S. Department of Transportation (2005a), "Fly Ash Facts for Engineers," U.S. Department of Transportation- Federal Highway Administration,
URL: http://www.fhwa.dot.gov/pavement/recycling/fach01.cfm

U.S. Department of Transportation (2005b), "Ground Penetrating Radar for Measuring Pavement Layltpper Thickness," U.S. Department of Transportation-Federal Highway Administration, Pub. No. FHWA-HIF-00-015.

U.S. Department of Transportation (2005c), "Ground Penetrating Radar (GPR)," Federal Lands Highway Program, U.S. Department of Transportation- Federal Highway Administration,
URL: http://www.cflhd.gov/agm/engApplications/Pavements/411GroundPenetrationRadar.htm

U.S. Department of Transportation (2005d), "Long Term Pavement Performance," Long Term Pavement Performance Organization by U.S. Department of Transportation- Federal Highway Administration,
URL: http://www.ltpp.org/fwd_temp/faq.htm

Valley Forge Laboratories, *"Kiln Dust Ash Systems for Highway Bases and Subbases,"* U.S. Department of Transportation and U.S. Department of Energy, Devon, PA, 1982.

Wallace, K., and Monismith, C.L., "*Diametral Modulus Testing on Nonlinear Pavement Materials*," Proceedings, Association of Asphalt Paving Technologists, Vol. 49, Louisville, Kentucky, 1986.

Wasiuddin, N., Zaman, M., and Nairn, R., *"A Laboratory Study to Optimize the Use of Raw Chat in Hot Mix Asphalt for Pavement Application,"* A Report Prepared for Oklahoma Department of Environmental Quality, Oklahoma City, OK, 2005.

Wasiuddin, N., Zaman, M., Nairn, R., and Kolothody, N., "*Characteristics of Chat-Asphalt for Road Base Application,*" Journal of Solid Waste Technology and Management, Vol. 32, No. 3, pp. 125-137, 2006.

Weng, Y., and Vipulanandan, C. (1998), "A Study on Controlled Low Strength Material (CLSM)," Department of Civil and Environmental Engineering, University of Houston, Houston, TX.

Williams, C.R., and Prowell, B.D., "*Comparison of Laboratory Wheel-Tracking Test Results to WesTrack Performance*," Transportation Research Record No. 1681, pp. 121-128, Washington, D.C., 1999.

Witczak, M.W., "*Harmonized Test Methods for Laboratory Determination of Resilient Modulus for Flexible Pavement Design*," Transportation Research Board, NCHRP 1-28A, Vol. I, June, 2000.

Wright, P.J.F., "*Comments on an Indirect Tensile Test for Concrete Cylinders*," Magazine of Concrete Research, Vol. 7, No. 20, pp. 87-96, 1955.

Zaman, M. M., Laguros, J. G., Tian, P., Zhu, J., and Pandey, K. K.*), "Resilient Moduli of Raw and Stabilized Aggregate Bases and Evaluation of Layer Coefficients for AASHTO Flexible Pavement Design,"* Final Report, Submitted to ODOT, Item 2199, ORA 125-4262, 1998.

Zenieris, P., *"Fly Ash-Aggregate Mixes for Roadway Bases,"* MS Thesis, University of Oklahoma, Norman, OK, 1988.

Zhou, H., Huddleston, J., and Lundy, J., "*Implementation of Back-calculation in Pavement Evaluation and Overlay Design in Oregon*," Transportation Research Record 1377, pp. 150-158, Washington, D.C., 1992.

Zhu, J., *"Characterization of Cement Kiln Dust Stabilized Base/Subbase Aggregate,"* Ph.D. Dissertation, School of Civil Engineering and Environmental Science, University of Oklahoma, Norman, OK, 1998.

APPENDIX: A
SAMPLE CALCULATION OF WATER APPLICATION RATE FOR SECTION TS-2

Consider the section TS-2 as a rectangular box of dimensions 500-ft. (length of the section) × 25-ft. (width of the section) × 3.5-in. (thickness of the compacted stabilized-chat base) as shown in Figure A.1:

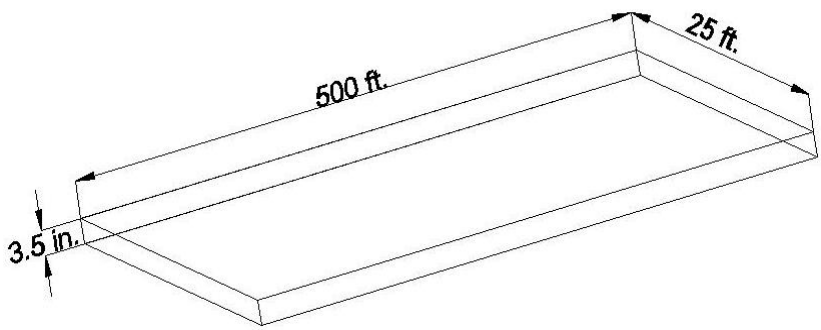

Figure A.1 Section TS-2 (CFA-Stabilized Chat Base)

Area of the section = 1388 sq. yd.

Amount of chat "C" required in this section is calculated as below:

C = Volume of the compacted stabilized base × MDD for 10% CFA-stabilized chat

C (tons) = [Thickness (ft.) × Width (ft.) × Length (ft.)] × MDD (pcf) × $\frac{1}{2000}\frac{tons}{lb}$

$$C = \left(\frac{3.5}{12} \times 25 \times 500\right) \times \frac{138}{2000} = 260 \text{ tons}$$

Considering for losses and chat required for the construction of windrows, 266 tons of chat was laid on this section in the field. To fulfill the criterion for OMC (6.6%), the amount of water to be added to this section "w" was calculated as follows:

$$w \text{ (gallons)} = \frac{\text{Weight of Chat (tons)} \times 2000 \text{ (lb/ton)} \times \text{Water Content (\%)}}{2.2 \text{ (lb/liters)} \times 3.785 \text{ (liters/gallon)}}$$

$$w = \frac{266 \times 0.066 \times 2000}{2.2 \times 3.785} = 4{,}145 \text{ gallons}$$

The rate of application of water "R" to the section was calculated as follows:

$$R = \frac{\text{Weight of Water to be Added}}{\text{Area of the Section}}$$

$$R = \frac{4145}{1388} = 2.986 \text{ gallons/sq.yd.}$$

Sheet B.1: Mix Design Sheet for Tar Creek Base Mix

STATE OF OKLAHOMA
DEPARTMENT OF TRANSPORTATION
MATERIALS DIVISION

Prj. No. 125- S3 **Design No.** 3073-OU-RBM50
Project No. Chat-Asphalt Road **Hwy.** County Road **ESAL** 0.3M+
Contractor Glover Const. Co. **Producer** Glover Const. Co.

MATERIAL	SOURCE	%USED
1-1/4" Limestone	Midwest Minerals @ Miami, OK (5801)	15
9/16" Limestone	Midwest Minerals @ Miami, OK (5801)	28
Screenings (CS-2)	Midwest Minerals @ Miami, OK (5801)	7
Raw Chat	Tri-State Asphalt @ Miami, OK	50
Asphalt Cement (PG 64-22OK)	Valero @ Ardmore, OK	

Laboratory No.

Aggregate Percent Passing	1-1/4" Limestone	9/16" Limestone	Scrns CS-2	Raw Chat	Combined Aggregate	Job Formula	JMF Tolerance
1"	97				100	100	± 0
3/4"	62	100			94	94	± 7
1/2"	33	99		100	90	90	± 7
3/8"	19	74	100	99	80	80	± 7
No. 4	3	10	93	76	48	48	± 7
No. 8	3	3	75	49	31	31	± 5
No. 16	2	2	61	31	21	21	± 4
No. 30	2	2	46	20	14	14	± 4
No. 50	2	2	30	13	9	9	± 4
No. 100	2	2	20	8	6	6	± 3
No. 200	2.0	2.0	14.0	6.1	4.9	4.9	± 2
%AC (PG64-22OK)						5.6	± 0.4
Mix Temperature @ discharge from Mixer, °F						305	± 20
Optimum Roadway Compaction Temperature, °F						290	

Tests on Asphalt Cement:

	Found	Required
Spec. Grav. @ 77 °F	1.02	

Tests on Compressed Mixtures (at Design AC Content):

	SGC	Dens. % of Gmm	Dens. % of Gmm Req'd
Nini	7	85.0	< 90.5
Ndes	75	96	96
Nmax	115	97.8	< 98

Tests on Aggregates:

	Found	Required
F.A.A. %U	47.0	40 Min.
Sand Equivalent	84	40 Min.
L.A. Abrasion	28.0	40 Max.
Durability (DC)	72.0	40 Min.
IOC	0.50	
Insoluble Residue	62.0	30 Min.
Fractured Faces	100/100	75/75 Min.
Gse	2.603	
Gsb	2.504	
Specimen Wt	4500	

Tests on Compressed Mixtures:

Percent Asphalt	Gmb	Gmm	Dens. % of Gmm	Dens. % of Req'd of Gmm	V.M.A. (%)	V.M.A. (Min.%)	%VFA	%VFA Req'd	%DP	%DP Req'd
5.0	2.293	2.416	94.9		13.0		61.0		1.39	
5.5	2.303	2.398	96.0	95-97	13.1	13	69.6	65-78	1.21	0.6-1.6
6.0	2.324	2.381	97.6		12.8		81.2		1.08	

Mix Layer Depth < 4 in.
Compacted mass 105.4 lbs/sq.yd/1" thickness

Sheet B.2: Mix Design Sheet for Tar Creek Surface Mix

STATE OF OKLAHOMA
DEPARTMENT OF TRANSPORTATION
MATERIALS DIVISION

Prj. No. 125- S5 **Design No.** 3075-OU-RSM80
Project No. Chat-Asphalt Road **Hwy.** County Road **ESAL** 0.3M+
Contractor Glover Const. Co. **Producer** Glover Const. Co.

MATERIAL	SOURCE	%USED
9/16" Limestone	Midwest Minerals @ Miami, OK (5801)	14
Screenings (CS-2)	Midwest Minerals @ Miami, OK (5801)	6
Raw Chat	Tri-State Asphalt @ Miami, OK	80
Asphalt Cement (PG 64-22OK)	Valero @ Ardmore, OK	

Laboratory No.

Aggregate Percent Passing	9/16" Limestone	Scrns CS-2	Raw Chat	Combined Aggregate	Job Formula	JMF Tolerance
1/2"	99		100	100	100	± 7
3/8"	74	100	99	96	96	± 7
No. 4	10	93	76	68	68	± 7
No. 8	3	75	49	44	44	± 5
No. 16	2	61	31	29	29	± 4
No. 30	2	46	20	19	19	± 4
No. 50	2	30	13	12	12	± 4
No. 100	2	20	8	8	8	± 3
No. 200	2.0	14.0	6.1	6.0	6.0	± 2
%AC (PG70-28OK)					6.9	± 0.4
Mix Temperature @ discharge from Mixer, °F					325	± 20
Optimum Roadway Compaction Temperature, °F					305	

Tests on Asphalt Cement:

	Found	Required
Spec. Grav. @ 77 °F	1.01	

Tests on Compressed Mixtures (at Design AC Content):

	SGC	Dens. % of Gmm	Dens. % of Gmm Req'd
Nini	7	86.0	< 90.5
Ndes	75	96	96
Nmax	115	96.6	< 98

Tests on Aggregates:

	Found	Required
F.A.A. %U	47.0	40 Min.
Sand Equivalent	78	40 Min.
L.A. Abrasion	22.0	40 Max.
Durability (DC)	75.0	40 Min.
IOC	0.38	
Insoluble Residue	83.0	30 Min.
Fractured Faces	100/100	75/75 Min.
Gse	2.607	
Gsb	2.465	
Specimen Wt	4500	

Tests on Compressed Mixtures:

Percent Asphalt	Gmb	Gmm	Dens. % of Gmm	Dens. % of Req'd of Gmm	V.M.A. (%)	V.M.A. (Min.%)	%VFA	%VFA Req'd	%DP	%DP Req'd
6.3	2.228	2.373	93.9		15.3		60.1		1.44	
6.8	2.256	2.356	95.8	95-97	14.7	15	71.2	65-78	1.29	0.6-1.6
7.3	2.273	2.339	97.2		14.5		80.5		1.16	

Mix Layer Depth < 4 in.
Compacted mass 103.4 lbs/sq.yd/1" thickness

Sheet B.3: Mix Design Sheet for Davis Base Mix

STATE OF OKLAHOMA
DEPARTMENT OF TRANSPORTATION
MATERIALS DIVISION

A.D. No. 010-024-002 S2 Recycle **Design No.** 3072-BCC-02140
Project No. BHFY-21N(04) 16231(04) **Hwy.** SH-7 **ESAL** 3M+
Contractor Plains Bridge Contracting of OK **Producer** Broce Construction Co.

MATERIAL	SOURCE	%USED
1-1/2" Rock	Dolese @ Davis, OK(5002)	32
3/8" Chips	Dolese @ Davis, OK(5002)	11
Screenings	Hanson @ Davis, OK(5008)	8
Stone Sand	Dolese @ Davis, OK(5002)	28
M.A.P.	Stockpile @ Plantsite	21
Asphalt Cement (PG64-22OK)	Valero @ Ardmore, OK	

Laboratory No.

Aggregate Percent Passing	1 1/2" Rock	3/8" Chips	Scrns	Stone Sand	M.A.P.	Combined Aggregate	Job Formula	JMF Tolerance
1 1/2"	100					100	100	± 0
1"	100				100	100	100	± 7
3/4"	74				93	90	90	± 7
1/2"	36	100			90	77	**88	± 7
3/8"	21	99	100	100	86	72	**82	± 7
No. 4	2	17	83	99	82	54	**61	± 7
No. 8	1	4	56	69	75	40	**41	± 5
No. 16	1	3	39	35	70	28	**24	± 4
No. 30	1	3	28	16	62	20	**16	± 4
No. 50	1	2	21	6	54	15	*11	± 4
No. 100	1	2	16	5	24	8	8	± 3
No. 200	1.1	2.0	12.3	3.9	9.0	4.6	**5.9	± 2
%AC (PG64-22OK)					5.2		**4.5	± 0.4

Mix Temperature @ discharge from Mixer, °F ..... 305 ± 20
Optimum Roadway Compaction Temperature, °F 290

Tests on Asphalt Cement:

	Found
Spec. Grav. @ 77 °F	1.01 Est.

Tests on Aggregates:

	Found	Required
F.A.A. %U	44.2	40 Min.
Sand Equivalent	84	45 Min.
L.A. Abrasion	22.2	40 Max.
Durability (DC)	71	40 Min.
IOC	0.12	
Insoluble Residue	N/A	N/A
Fractured Faces	100/100	75/75 Min.
Gse	2.696	
Gsb	2.641	
Specimen Wt.	4750	

Tests on Compressed Mixtures (at Design AC Content):

	SGC	Dens. % of Gmm	Dens. % of Gmm Req'd
Nini	8	85.5	< 89
Ndes	100	96	96
Nmax	160	97.4	< 98

Tests on Compressed Mixtures:

Percent Asphalt	Gmb	Gmm	Dens. % of Gmm	Dens. % of Req'd of Gmm	V.M.A. (%)	V.M.A. (Min.%)	%VFA	%VFA Req'd	%DP	%DP Req'd
3.8	2.360	2.536	93.1		14.0		50.4		1.49	
4.3	2.380	2.517	94.6	95-97	13.8	12	60.5	65-76	1.28	0.6-1.6
4.9	2.400	2.494	96.2		13.6		72.3		1.09	

Mix Layer Depth: > 4 in. TSR: 0.80 0.80 Min. (0.75 Min. Field) Required
Compacted Wt. 110.7 lbs/sq.yd/1" thickness
Lab Permeability Test(cm/sec) - 0.1×10^{-5} (Required: 125×10^{-5} Max.)
APA Rut Test Depth(mm) - 3.985 (Required: 5 mm Max.)
Recommended **3.4% New Asphalt Cement
*REVISED(GRAD.) per Contractor's request effective 8/25/04.
**REVISED(GRAD. & AC) per Contractor's request effective 8/30/04. ✳

MEETS SPECIFICATION REQUIREMENTS for 708-16(a-g)99 Rev. 10/29/03
708-5(a-b)99 Rev. 9/26/02

Sheet B.4: Mix Design Sheet for OKC Base Mix

STATE OF OKLAHOMA
DEPARTMENT OF TRANSPORTATION
MATERIALS DIVISION

A.D. No. 010-029-003 S2 Recycle **Design No.** 3072-OAEST-03145
Project No. STP-055B(802)AG 14364(04)C **Hwy.** City Street **ESAL** 0.3M+
Contractor Allen Contracting, Inc. **Producer** PMI, Inc.

MATERIAL	SOURCE	%USED
1 ½" Rock	Hanson Aggregates @ Davis, OK(5008)	42
Screenings	Hanson Aggregates @ Davis, OK(5008)	15
Wash Shot	Dolese @ Davis, OK(5002)	10
Sand	G.M.I. Meridian Pit @ Oklahoma City, OK	8
M.A.P.	Stockpile @ Plantsite	25
Asphalt Cement (PG64-22OK)	Wynnewood Refining @ Wynnewood, OK	

Laboratory No.

Aggregate Percent Passing	1 1/2" Rock	Scrns	Washed Shot	Sand	M.A.P.	Combined Aggregate	Job Formula	JMF Tolerance
1 1/2"	100					100	100	± 0
1"	98				100	99	99	± 7
3/4"	77				99	90	90	± 7
1/2"	41				95	74	74	± 7
3/8"	27	100	100		92	67	67	± 7
No. 4	8	84	87	100	77	52	52	± 7
No. 8	4	56	10	99	61	34	34	± 5
No. 16	3	37	2	98	48	27	27	± 4
No. 30	3	25	2	90	39	22	22	± 4
No. 50	2	16	1	72	30	17	17	± 4
No. 100	2	12	1	19	16	8	8	± 3
No. 200	1.6	8.4	1.1	2.0	10.0	4.7	4.7	± 2
%AC (PG64-22OK)					4.7		4.3	± 0.4
Mix Temperature @ discharge from Mixer, °F							305	± 20
Optimum Roadway Compaction Temperature, °F							290	

Tests on Asphalt Cement:

	Found	Required
Spec. Grav. @ 77 °F	1.01 Est.	

Tests on Compressed Mixtures (at Design AC Content):

	SGC	Dens. % o Gmm	Dens. % of Gmm Req'd
Nini	7	89.4	85.5 - 90.5
Ndes	75	96	96
Nmax	115	97.4	< 98

Tests on Aggregates:

	Found	Required
F.A.A. %U	46.1	40 Min.
Sand Equivalent	76	40 Min.
L.A. Abrasion	16.3	40 Max.
Durability (DC)	73.0	30 Min.
IOC	0.43	
Insoluble Residue		N/A
Fractured Faces	100/100	65/65 Min.
Gse	2.710	
Gsb	2.678	
Specimen Wt.	4935	

Tests on Compressed Mixtures:

Percent Asphalt	Gmb	Gmm	Dens. % of Gmm	Dens. % of Req'd of Gmm	V.M.A. (%)	V.M.A. (Min.%)	%VFA	%VFA Req'd	%DP	%DP Req'd
4.3	2.428	2.527	96.1	95-97	13.2	12	70.4	65-78	1.21	0.6-1.6

Mix Layer Depth: > 4"
TSR: 1.00 0.80 Min. (0.75 Min. Field) Required
Compacted Wt. 111.2 lbs./sq.yd./1" thickness
Lab Permeability Test(cm/sec) - $2x10^{-5}$ (Required: $12.5x10^{-5}$ Max.)
APA Rut Test Depth(mm) - 4.163 (Required: 6 mm Max.)
Recommended 3.2% New Asphalt Cement (PG 64-22OK)
TIED: STP-055B(803)AG

MEETS SPECIFICATION REQUIREMENTS for 708-3(a-g)99 Rev. 6/3/04
708-5(a-b)99 Rev. 6/3/04

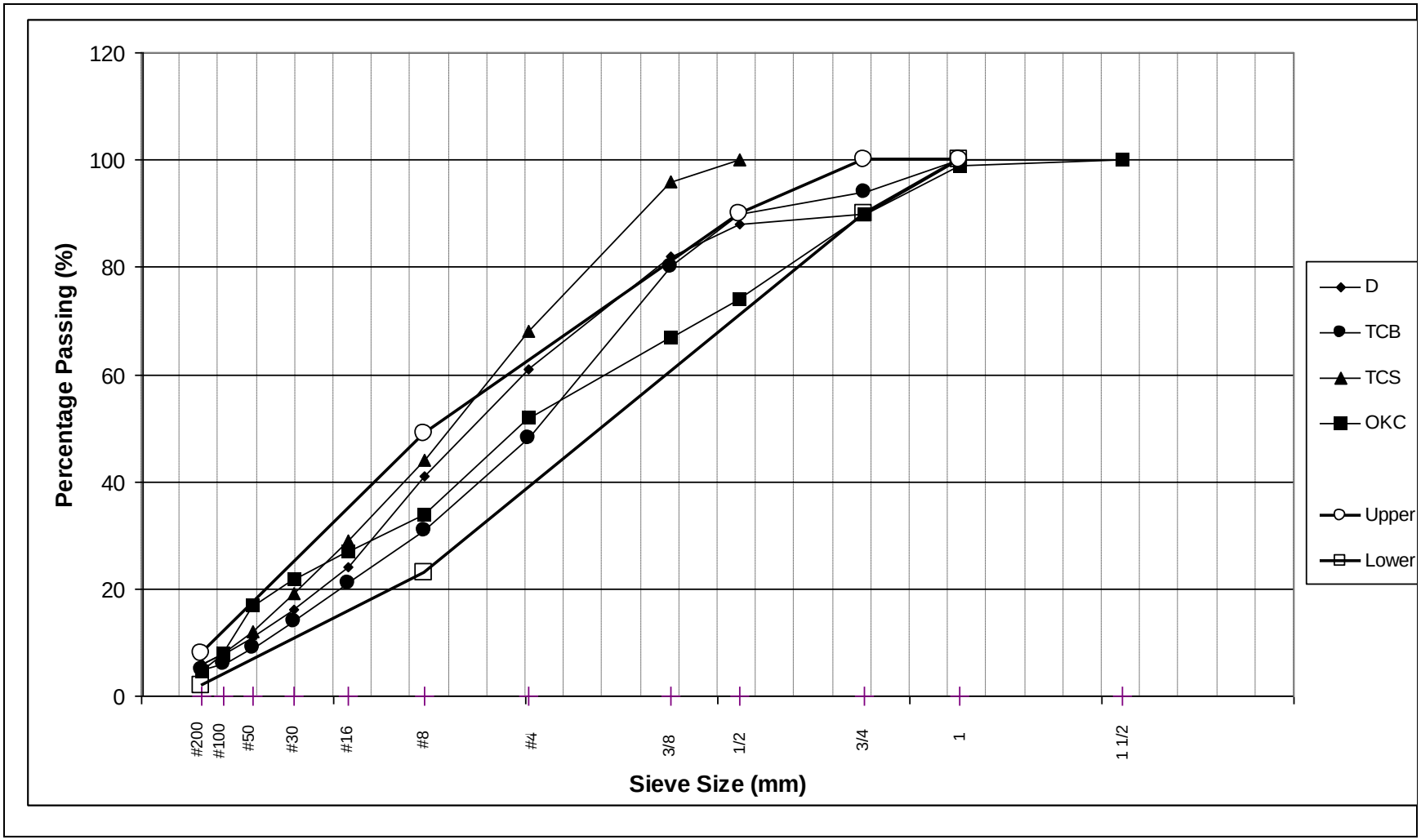

Figure B.1: Gradation Curve for All Four HMA Mixes

APPENDIX: C
COMPACTION LEVEL MEASUREMENTS ON CHAT*-ASPHALT COURSE

1. Compaction Level Readings for Chat-Asphalt Base Course

Rd. No.	R (%)	Rd. No.	R (%)	Rd. No.	R (%)
1	91	**50**	92	**99**	93
2	90	**51**	92	**100**	94
3	90	**52**	92	**101**	94
4	90	**53**	92	**102**	93
5	91	**54**	91	**103**	96
6	92	**55**	88	**104**	98
7	92	**56**	91	**105**	96
8	92	**57**	91	**106**	98
9	93	**58**	92	**107**	93
10	92	**59**	94	**108**	91
11	92	**60**	91	**109**	95
12	92	**61**	91	**110**	93
13	92	**62**	92	**111**	91
14	93	**63**	92	**112**	90
15	91	**64**	88	**113**	90
16	91	**65**	93	**114**	90
17	91	**66**	93	115	91
18	91	**67**	93	**116**	91
19	89	**68**	92	**117**	91
20	90	**69**	89	**118**	96
21	85	**70**	90	**119**	86
22	89	**71**	90	**120**	92
23	91	**72**	90	**121**	95
24	90	**73**	90	**122**	90
25	91	**74**	88	**123**	90
26	90	**75**	90	**124**	90
27	91	**76**	91	**125**	89
28	91	**77**	87	**126**	89
29	92	**78**	90	**127**	88
30	91	**79**	91	**128**	89
31	91	**80**	93	**129**	91
32	90	**81**	89	**130**	89
33	91	**82**	93	**131**	89
34	91	**83**	93	**132**	97
35	91	**84**	88	**133**	93
36	91	**85**	90	**134**	91
37	91	**86**	88	**135**	90
38	90	**87**	88	**136**	92
39	91	**88**	85	**137**	92
40	91	**89**	93	**138**	90
41	90	**90**	93	**139**	89
42	91	**91**	92	**140**	88
43	91	**92**	92	**141**	87
44	90	**93**	94	**142**	89
45	91	**94**	93	**143**	87
46	91	**95**	94	**144**	87
47	92	**96**	92	**145**	94
48	91	**97**	93	**146**	94
49	99	**98**	92	**147**	93

Rd. No.: *Reading Number,* ***R(%):*** *Relative Compaction*
*Tri-State Asphalt

Max. Density	146.4 pcf
Min. Density	117.4 pcf
Avg. Density	132.3 pcf
Target Density	137.9 pcf

Note1: Target density is calculated on the basis of 6% air voids.

Note2: All the 147 locations were selected randomly throughout the length of the Test Road.

Compaction Level Readings for Chat*-Asphalt Surface Course

Rd. No.	R (%)	Rd. No.	R (%)	Rd. No.	R (%)
1	94	**47**	80	**93**	88
2	96	**48**	88	**94**	84
3	94	**49**	92	**95**	89
4	94	**50**	94	**96**	86
5	94	**51**	93	**97**	88
6	90	**52**	89	**98**	88
7	90	**53**	88	**99**	89
8	91	**54**	90	**100**	90
9	89	**55**	90	**101**	86
10	90	**56**	94	**102**	88
11	95	**57**	91	**103**	87
12	94	**58**	91	**104**	88
13	88	**59**	92	**105**	88
14	96	**60**	92	**106**	89
15	92	**61**	91	**107**	92
16	90	**62**	91	**108**	100
17	89	**63**	90	**109**	89
18	89	**64**	90	**110**	88
19	91	**65**	89	**111**	86
20	90	**66**	88	**112**	87
21	91	**67**	90	**113**	89
22	92	**68**	93	**114**	88
23	92	**69**	93	**115**	89
24	89	**70**	94	**116**	86
25	90	**71**	93	**117**	86
26	91	**72**	92	**118**	86
27	90	**73**	94	**119**	86
28	90	**74**	87	**120**	86
29	91	**75**	90	**121**	89
30	91	**76**	88	**122**	88
31	91	**77**	90	**123**	88
32	91	**78**	91	**124**	87
33	90	**79**	90	**125**	88
34	91	**80**	87	**126**	89
35	90	**81**	89	**127**	92
36	90	**82**	90	**128**	92
37	91	**83**	96	**129**	92
38	92	**84**	92	**130**	94
39	88	**85**	89	**131**	90
40	92	**86**	89	**132**	89
41	91	**87**	99	**133**	88
42	89	**88**	89	**134**	88
43	91	**89**	98	**135**	88
44	91	**90**	86	**136**	89
45	88	**91**	92	**137**	93
46	90	**92**	94	**138**	92

Rd. No.: *Reading Number,* ***R(%):*** *Relative Compaction*
*Tri-State Asphalt

Max. Density	146.4 pcf
Min. Density	117.4 pcf
Avg. Density	132.3 pcf
Target Density	137.9 pcf

Note1: Target density is calculated on the basis of 6% air voids.

Note2: All the 138 locations were selected randomly throughout the length of the Test Road.

APPENDIX: D

MATLAB PROGRAM FOR PROCESSING SASW DATA

(This Program is reproduced from Khanna, 2006)

```
clear all
%
% CHANGE DATA FILE FOR EVERY ANALYSIS
%
fid = fopen('F42.txt','r');
A = fscanf(fid,'%f %f',[3 inf]);
A = A';
t = A(:,1);
ham=A(:,2);
accel = A(:,3);
Fs = 100000;
n = 4096;
Ts = 1/Fs;
T = n*Ts;
%t = 0:Ts:(n-1)*Ts;
df=1/(n*Ts);
F=0:df:df*(n-1);
%
%FFT to transform to frequency domain
%
accelf = fft(accel,n);
hamf=fft(ham,n);
%
%DETERMINE THE MAGNITUDE
%
magaccelf = abs(accelf);
maghamf=abs(hamf);
acmag = real(accelf);
hammag = real(hamf);
%
%NORMALIZE ACCELARATION WITH FORCE
%
accham = magaccelf./maghamf;
acha = accelf./hamf;
magacha = abs(acha).^2;
div = acmag./hammag;
%
%PLOT THE TIME HISTORIES of ACCELARATION & FORCE
%
%figure(1)
subplot(2,2,1)
plot(t,accel,'r',t,ham,'b')
```

```
legend('Accel','Hammer')
title('Accelaration & Force Time History')
xlabel('Time (sec.)')
ylabel('Volts')
%
%PLOT TRANSFER FUNCTION
%
%figure(2)
subplot(2,2,2)
%plot(F(1:0.5*n),accham(1:0.5*n))
%figure(3)
plot(F(1:0.5*n),accham(1:0.5*n))
title('Transfer Function')
xlabel('Freq. (Hz)')
ylabel('Spectral Amplitude')
% figure(4)
% plot(F(1:0.5*n),div(1:0.5*n))
%
%PLOT ACCELARATION SPECTRUM
%
%figure(4)
subplot(2,2,3)
plot(F(1:2048),magaccelf(1:2048))
title('Accelaration Spectrun')
xlabel('Freq. (Hz)')
ylabel('Spectral Amplitude')
%
%PLOT HAMMER SPECTRUM
%
%figure(4)
subplot(2,2,4)
plot(F(1:2048),maghamf(1:2048))
title('Hammer Spectrum')
xlabel('Freq. (Hz)')
ylabel('Spectral Amplitude')
```

APPENDIX: E

PLOTS OF TRANSFER FUNCTION

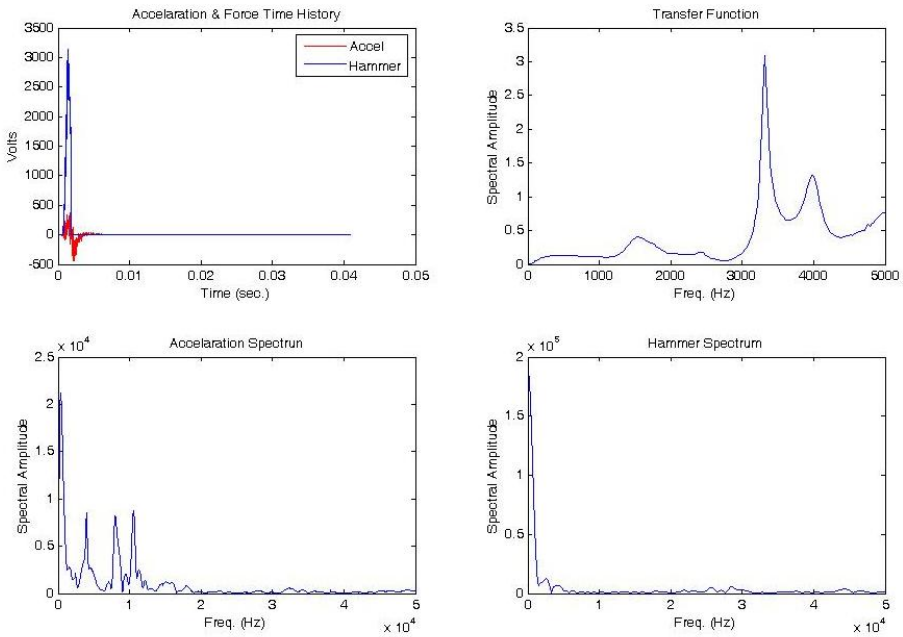

Figure E.1 Transfer Function for Specimen CFA-1 (Hit-1)

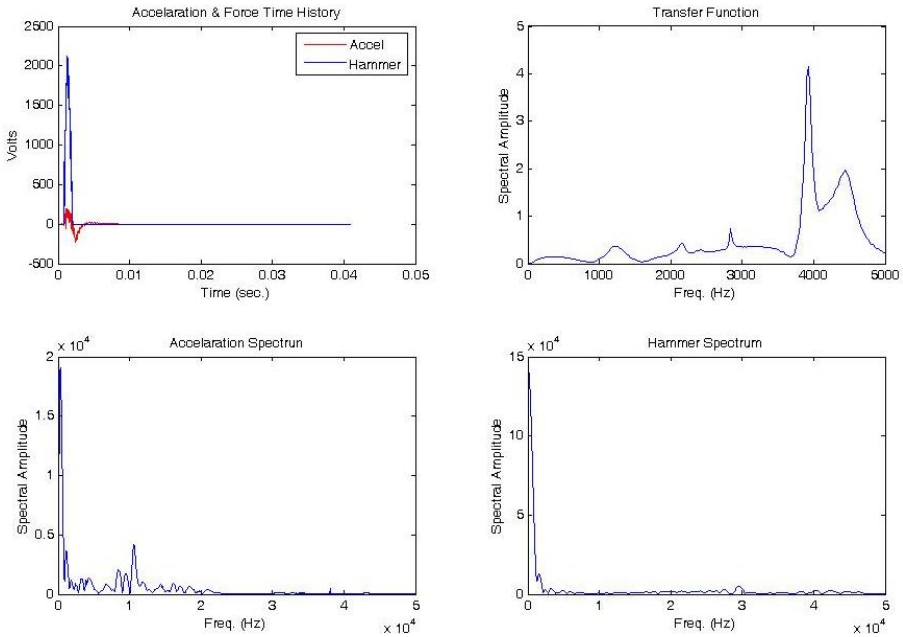

Figure E.2 Transfer Function for Specimen CFA-1 (Hit-2)

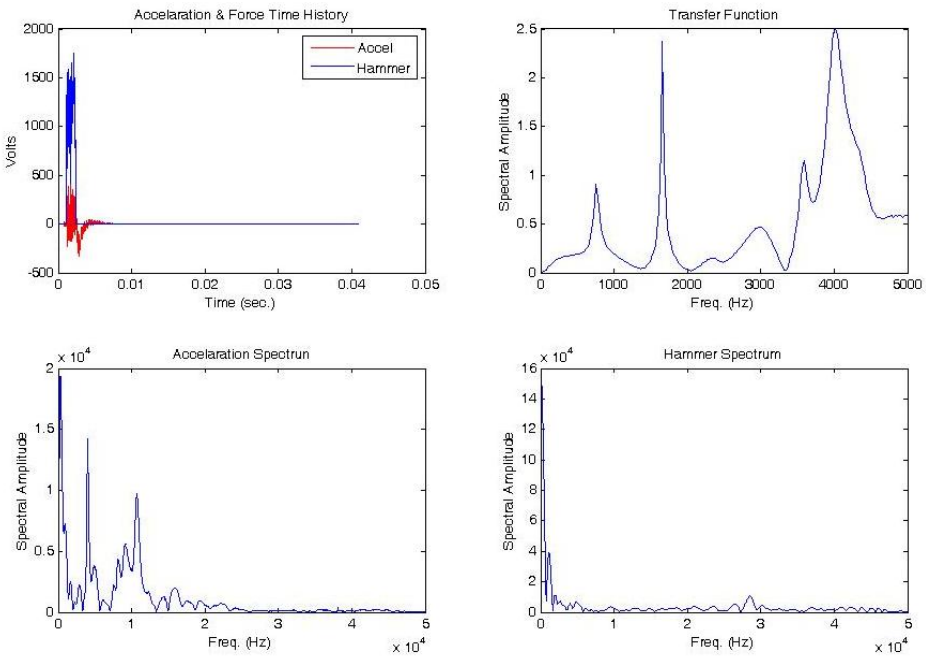

Figure E.3 Transfer Function for Specimen CFA-1 (Hit-3)

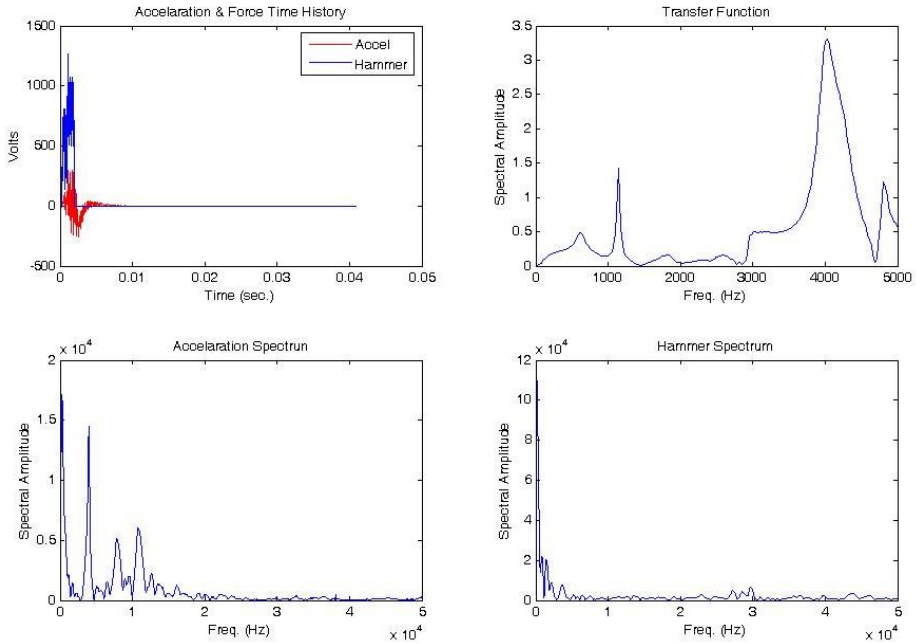

Figure E.4 Transfer Function for Specimen CFA-1 (Hit-4)

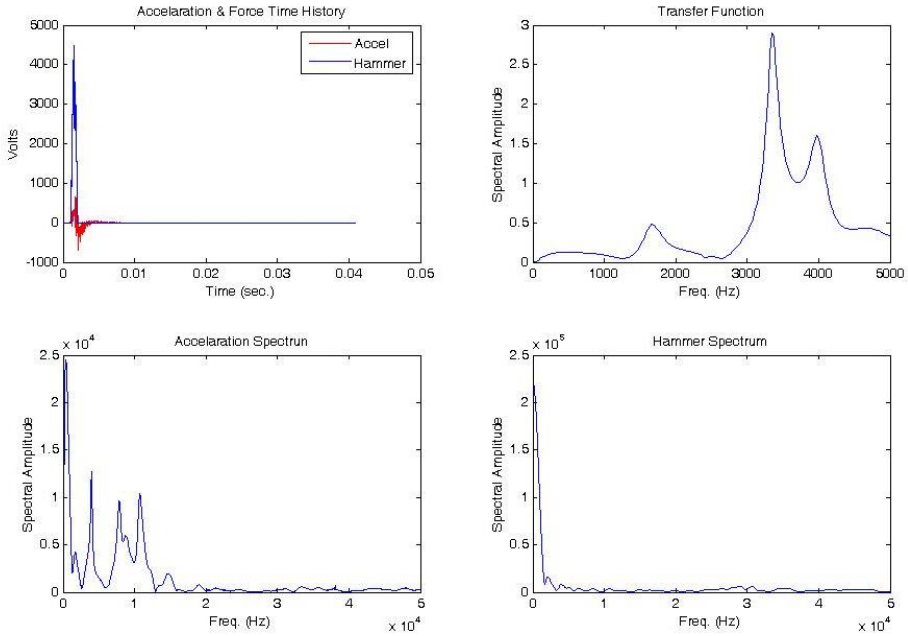

Figure E.5 Transfer Function for Specimen CFA-1 (Hit-5)

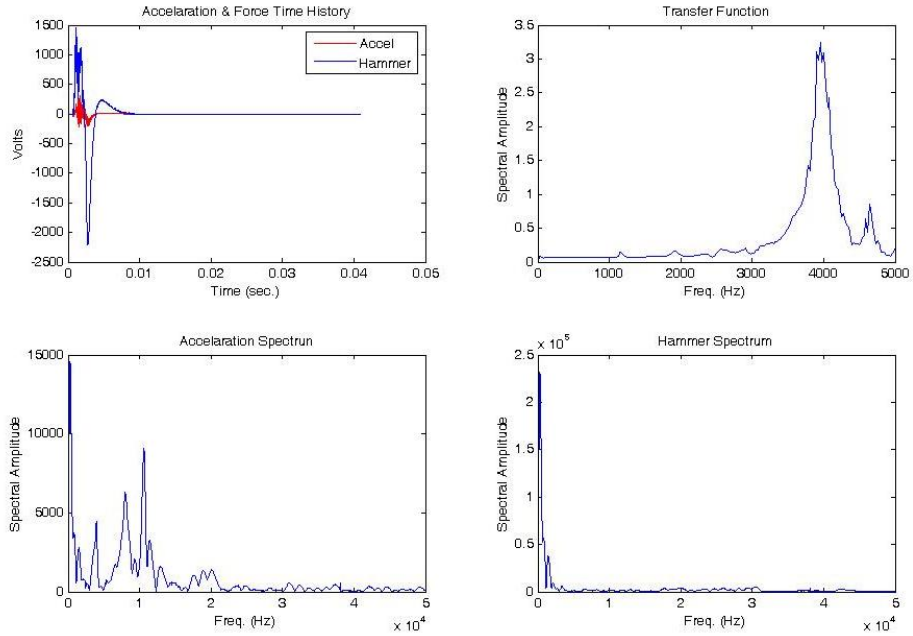

Figure E.6 Transfer Function for Specimen CFA-1 (Hit-6)

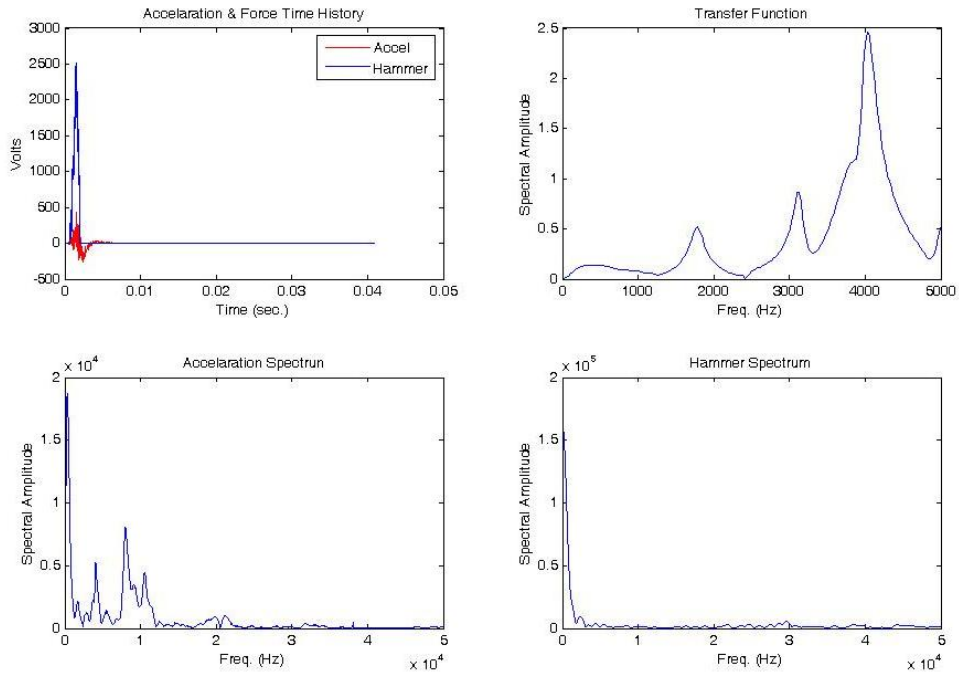

Figure E.7 Transfer Function for Specimen CFA-1 (Hit-7)

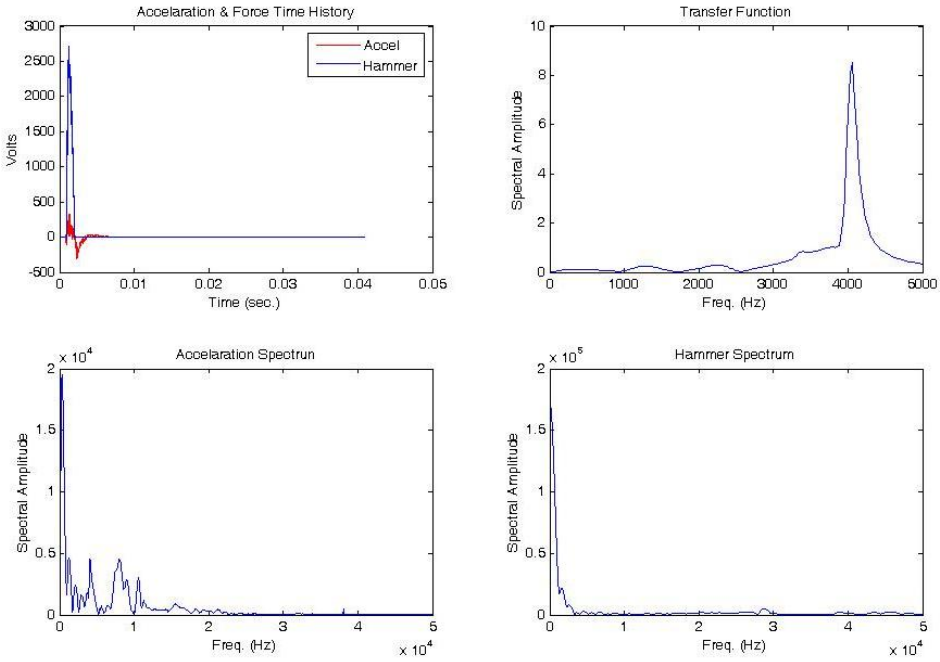

Figure E.8 Transfer Function for Specimen CFA-1 (Hit-8)

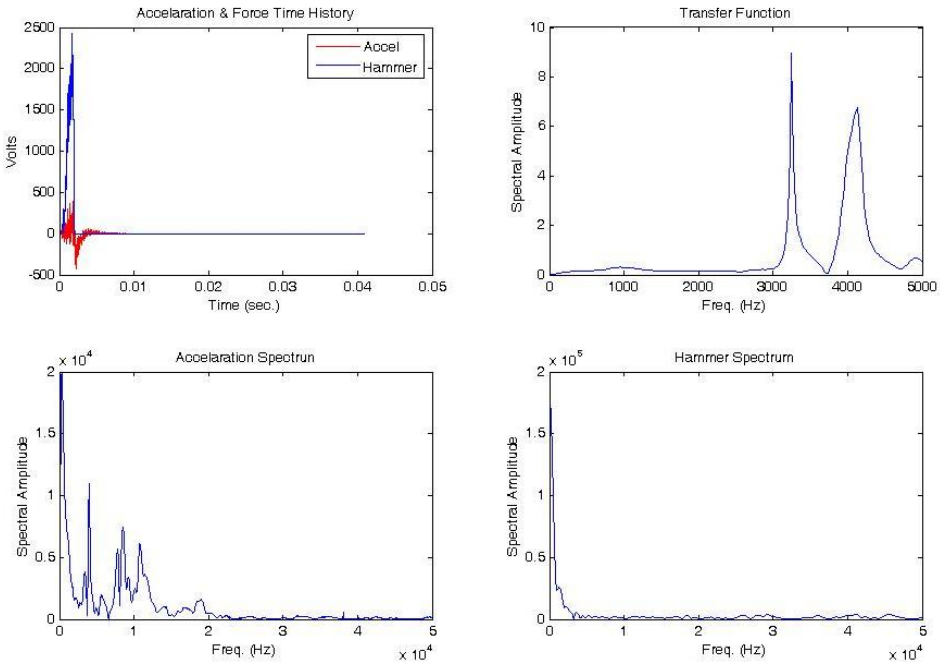

Figure E.9 Transfer Function for Specimen CFA-1 (Hit-9)

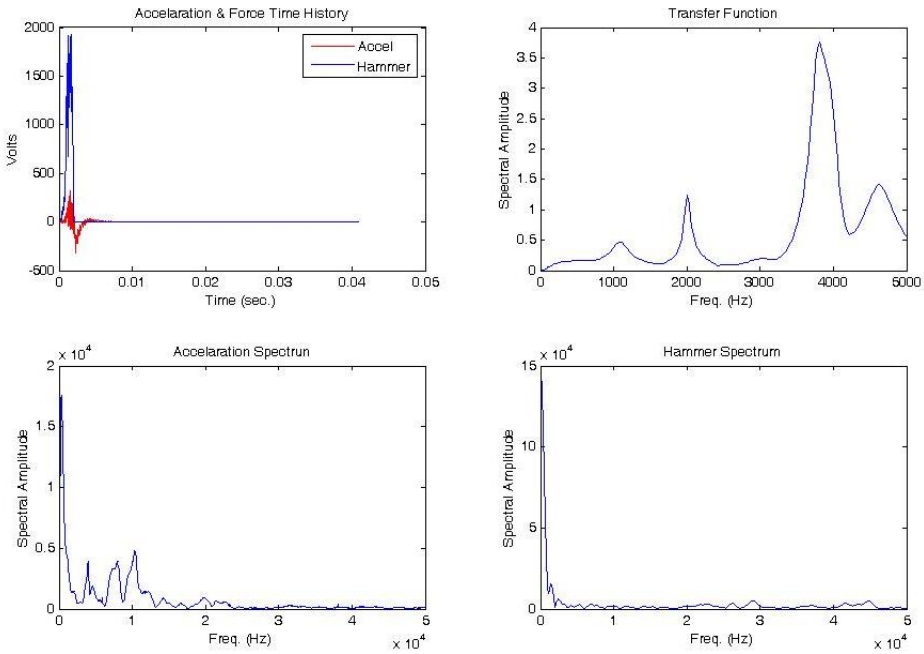

Figure E.10 Transfer Function for Specimen CFA-1 (Hit-10)

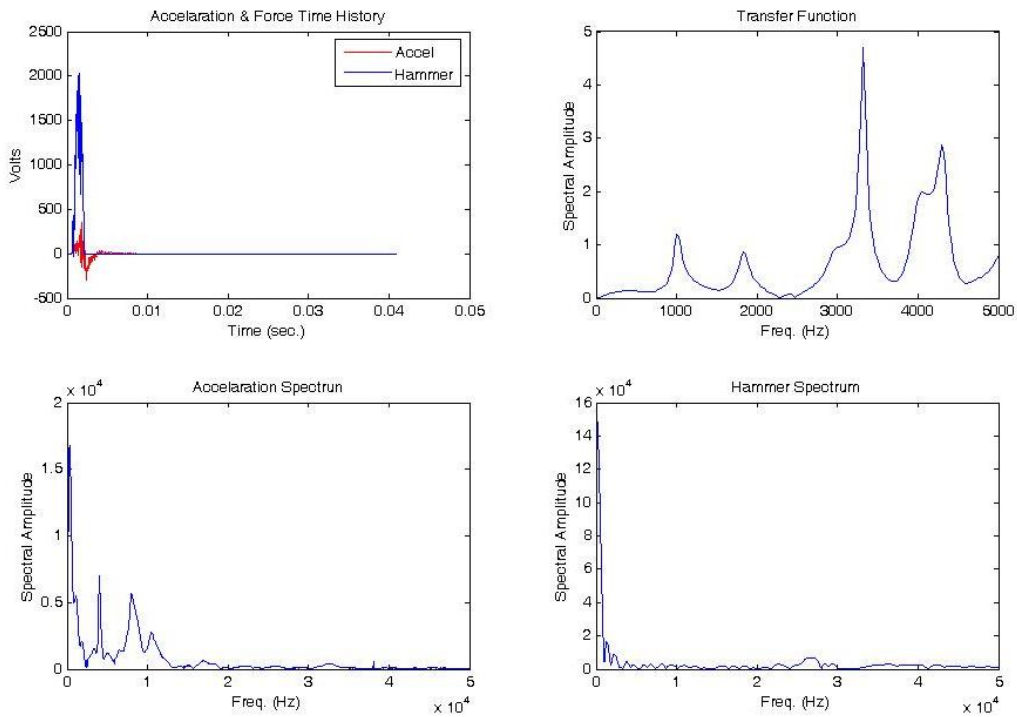

Figure E.11 Transfer Function for Specimen CFA-1 (Hit-11)

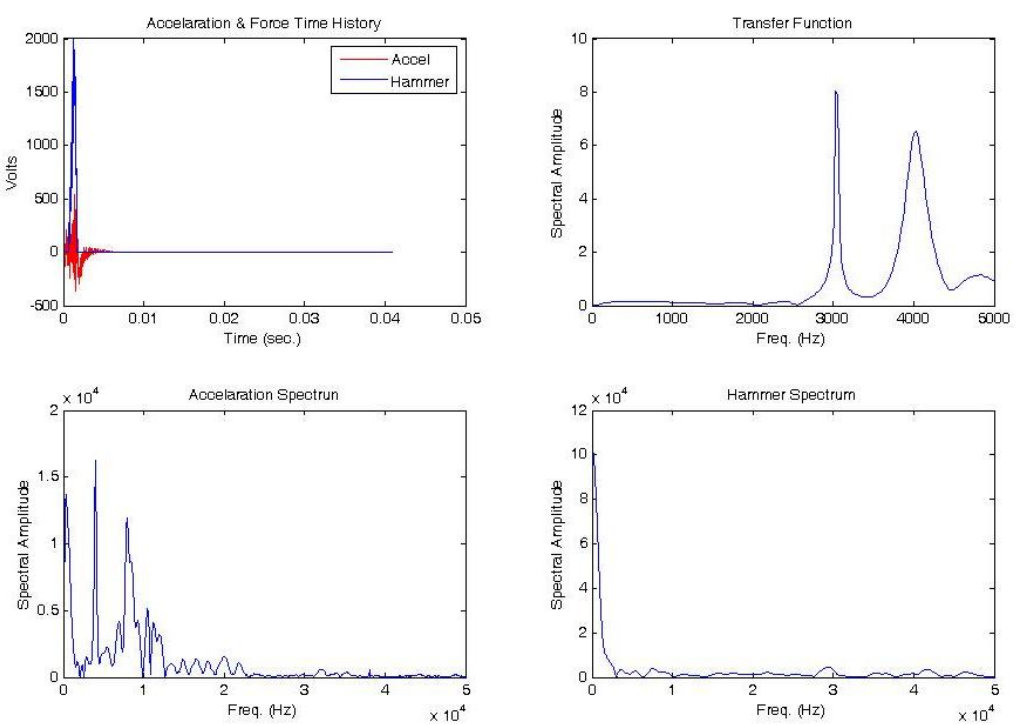

Figure E.12 Transfer Function for Specimen CFA-1 (Hit-12)

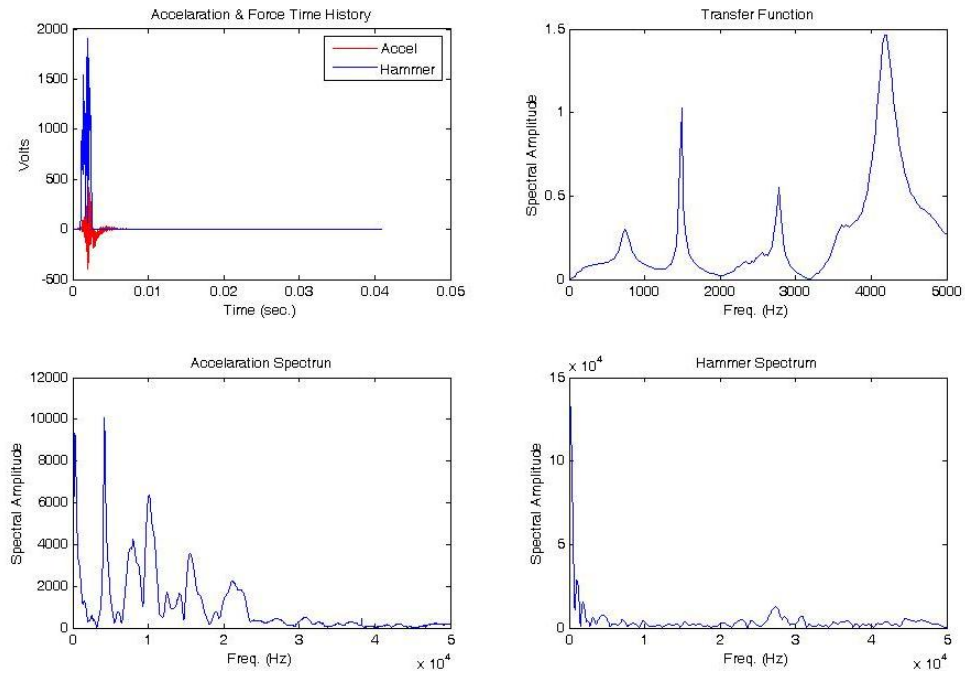

Figure E.13 Transfer Function for Specimen CFA-2 (Hit-1)

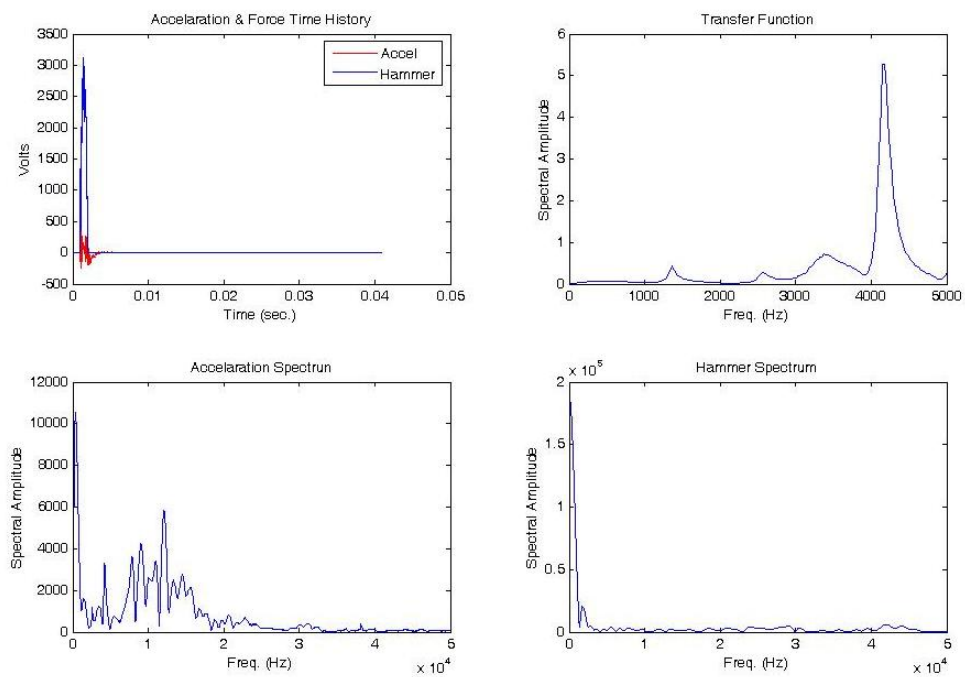

Figure E.14 Transfer Function for Specimen CFA-2 (Hit-2)

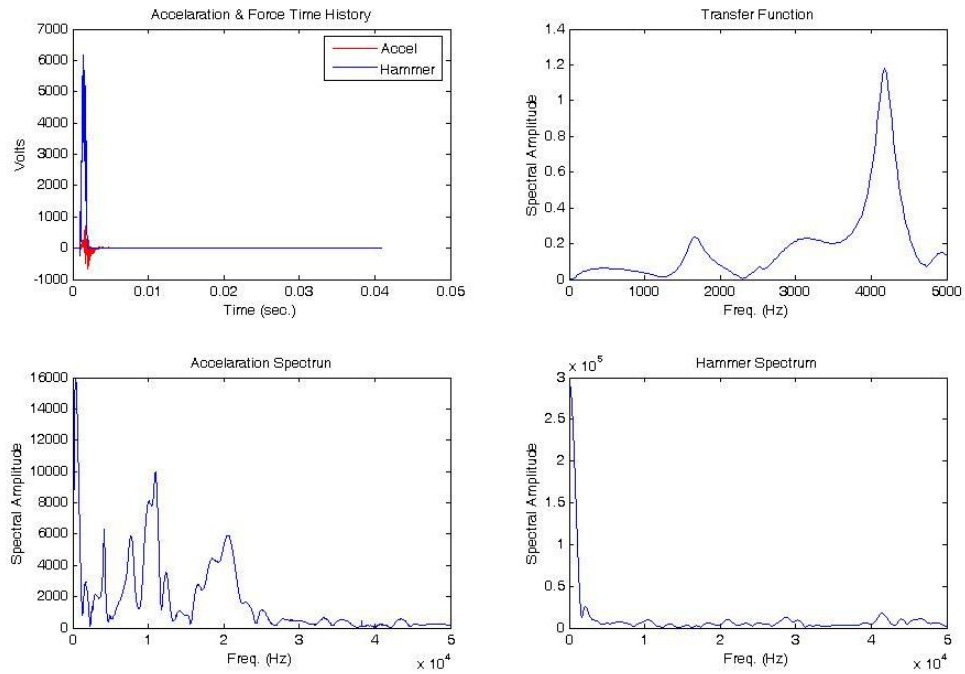

Figure E.15 Transfer Function for Specimen CFA-2 (Hit-3)

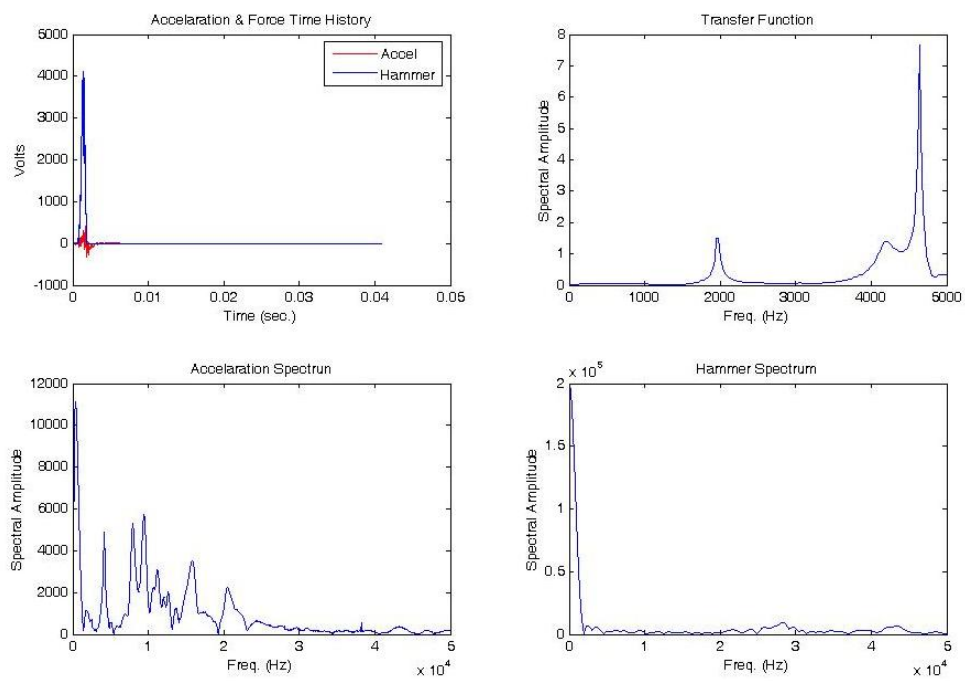

Figure E.16 Transfer Function for Specimen CFA-2 (Hit-4)

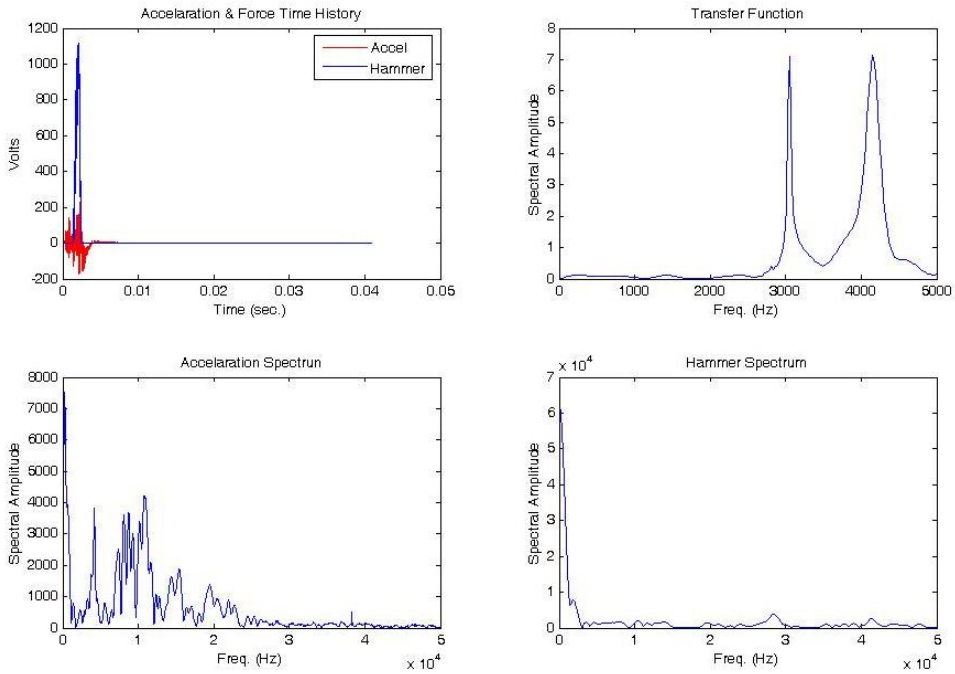

Figure E.17 Transfer Function for Specimen CFA-2 (Hit-5)

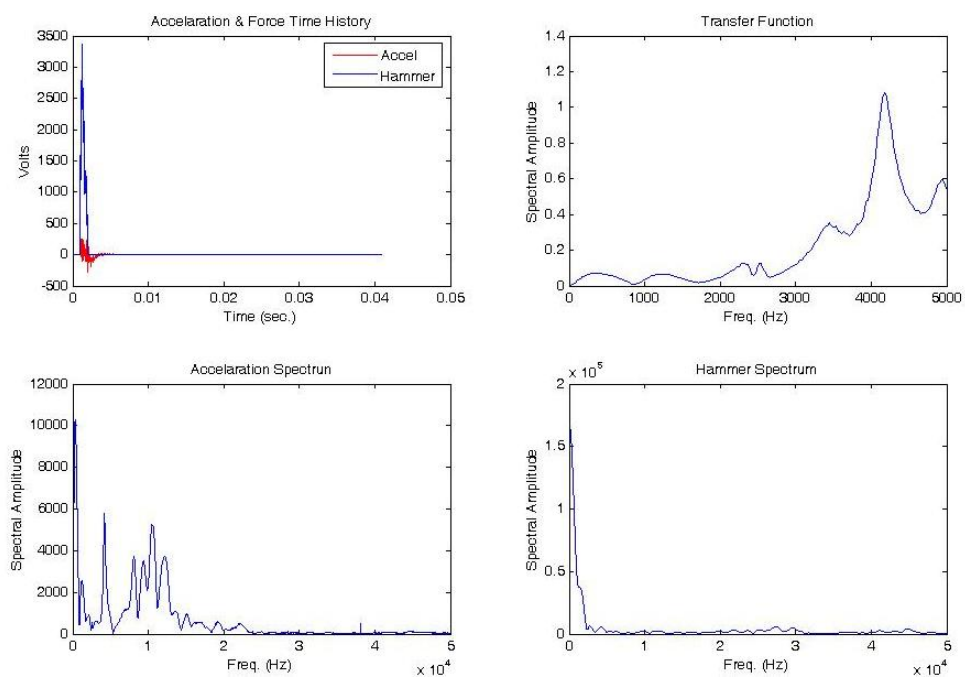

Figure E.18 Transfer Function for Specimen CFA-2 (Hit-6)

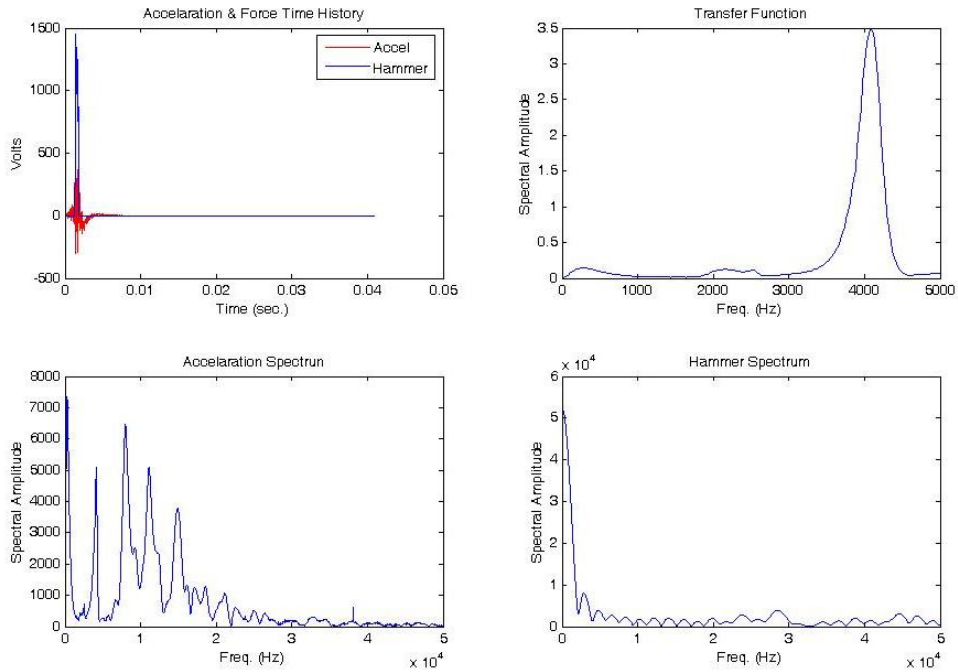

Figure E.19 Transfer Function for Specimen CFA-2 (Hit-7)

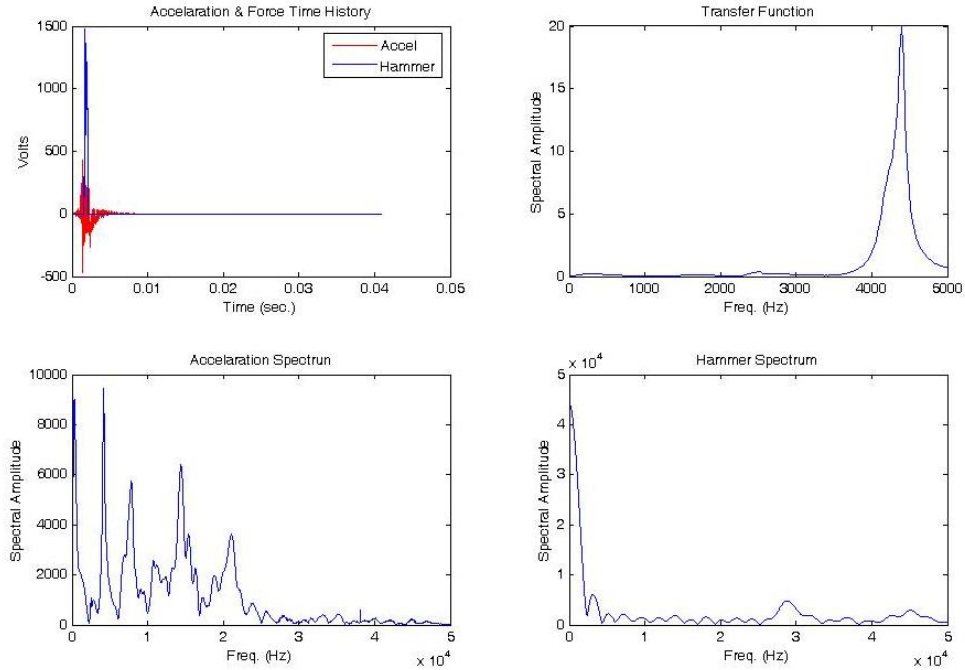

Figure E.20 Transfer Function for Specimen CFA-2 (Hit-8)

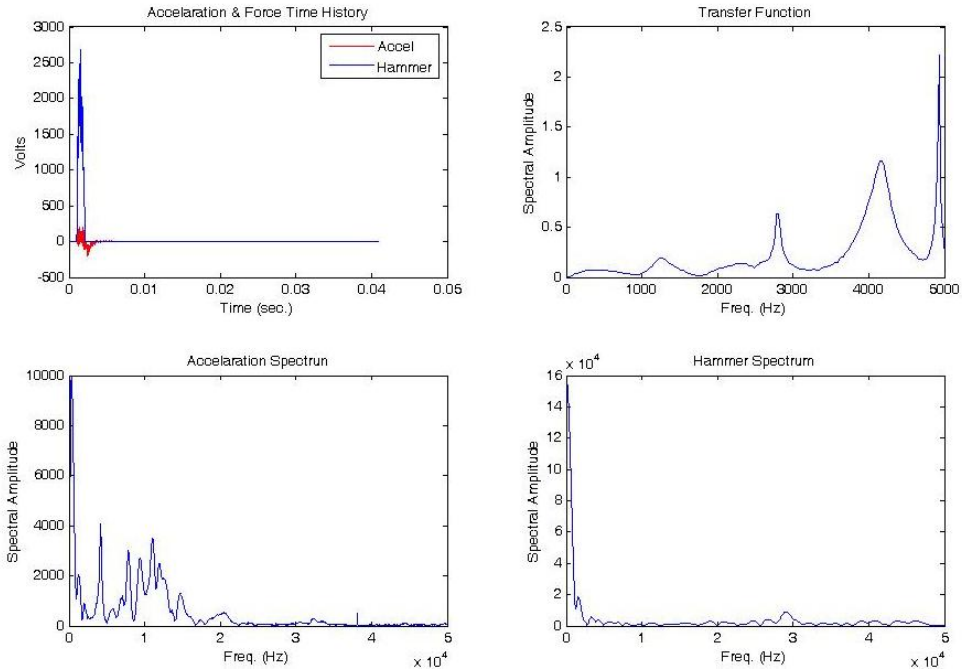

Figure E.21 Transfer Function for Specimen CFA-2 (Hit-9)

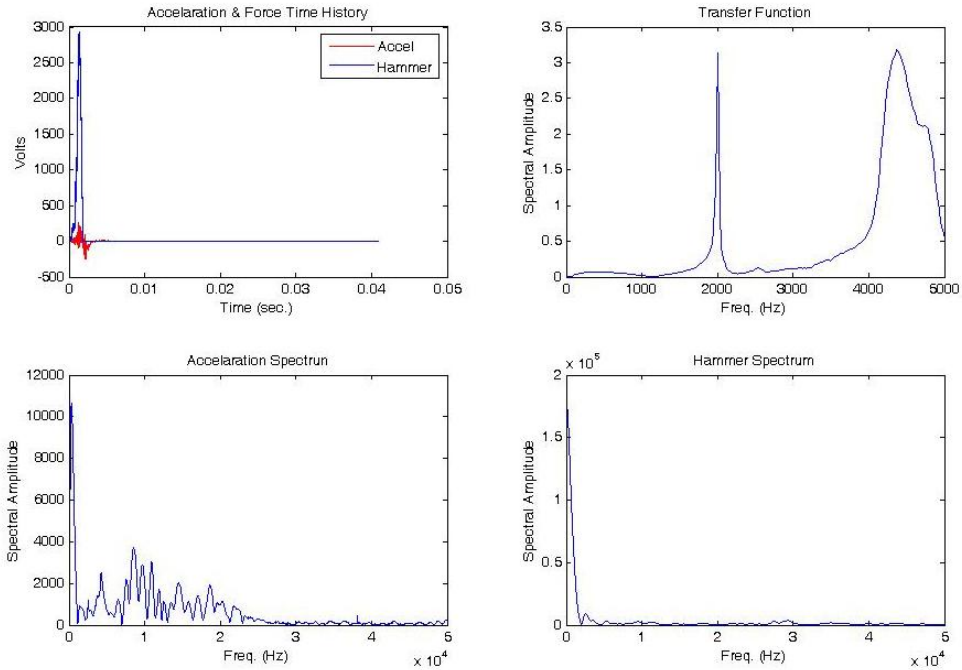

Figure E.22 Transfer Function for Specimen CFA-2 (Hit-10)

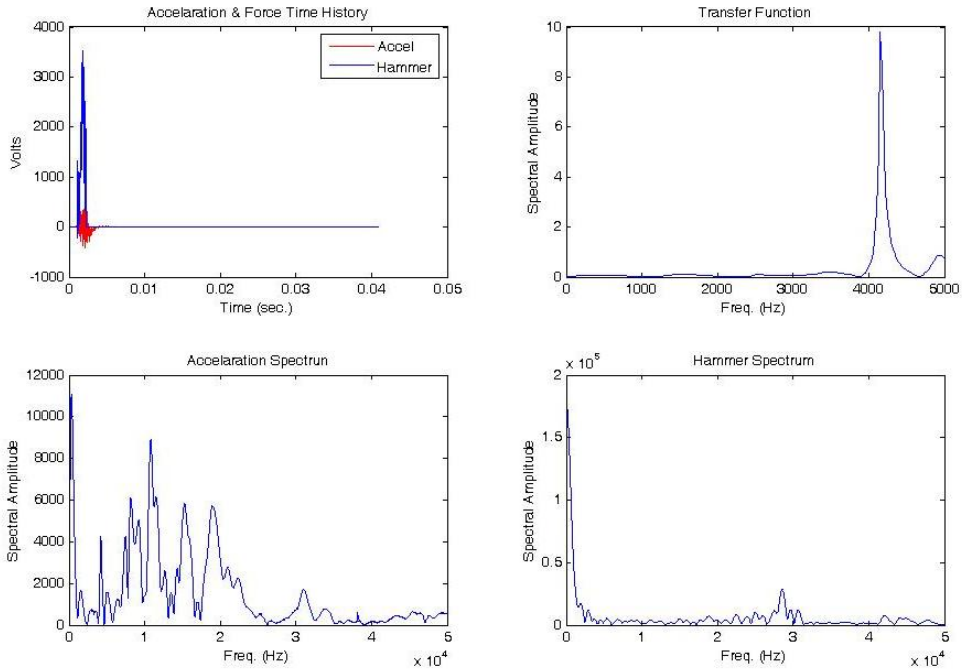

Figure E.23 Transfer Function for Specimen CFA-2 (Hit-11)

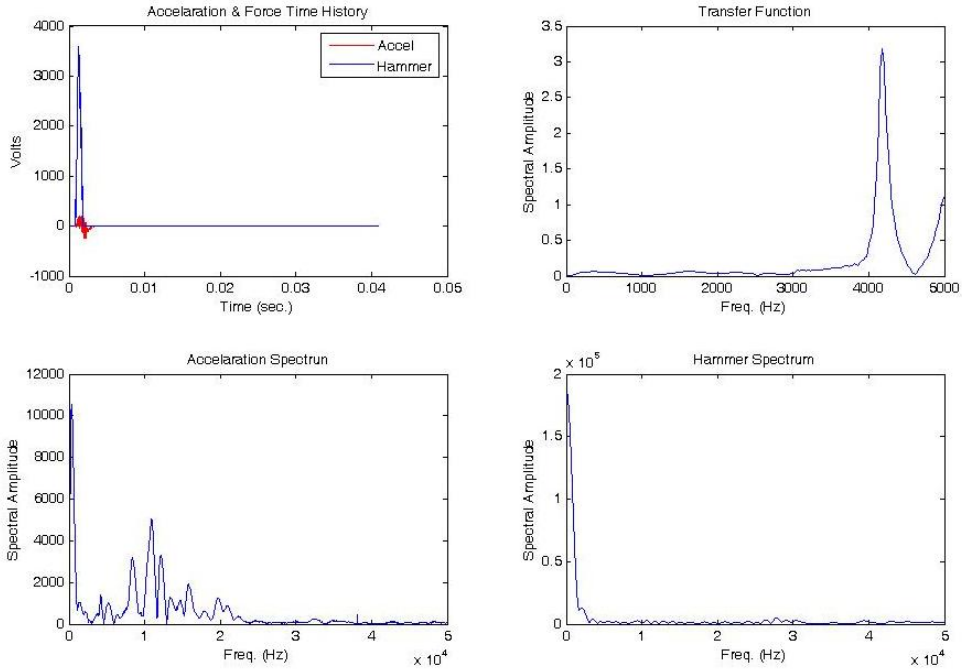

Figure E.24 Transfer Function for Specimen CFA-2 (Hit-12)

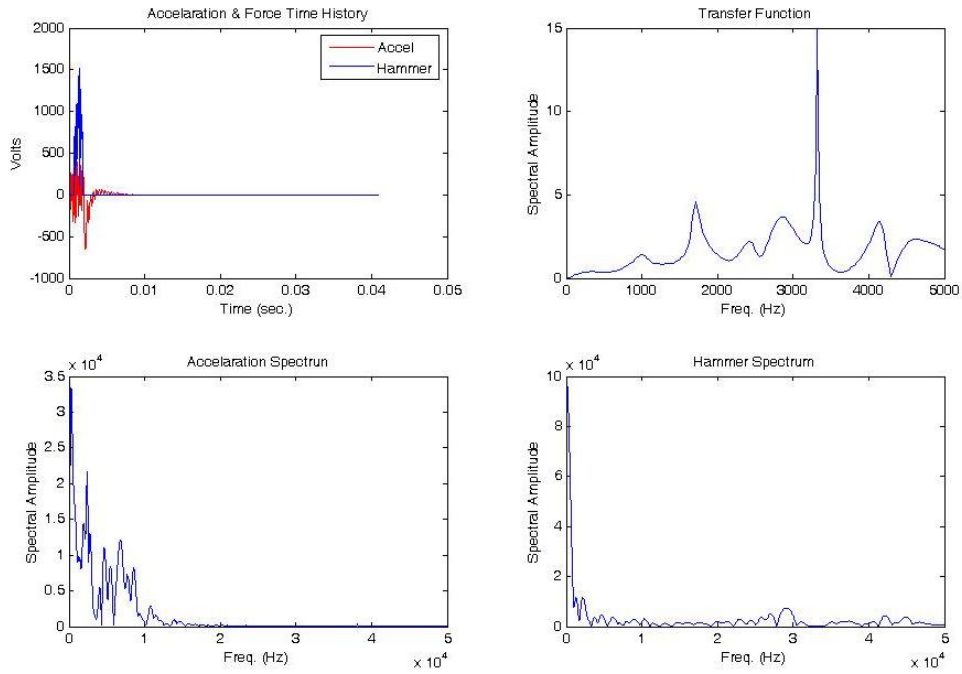

Figure E.25 Transfer Function for Specimen CKD-1 (Hit-1)

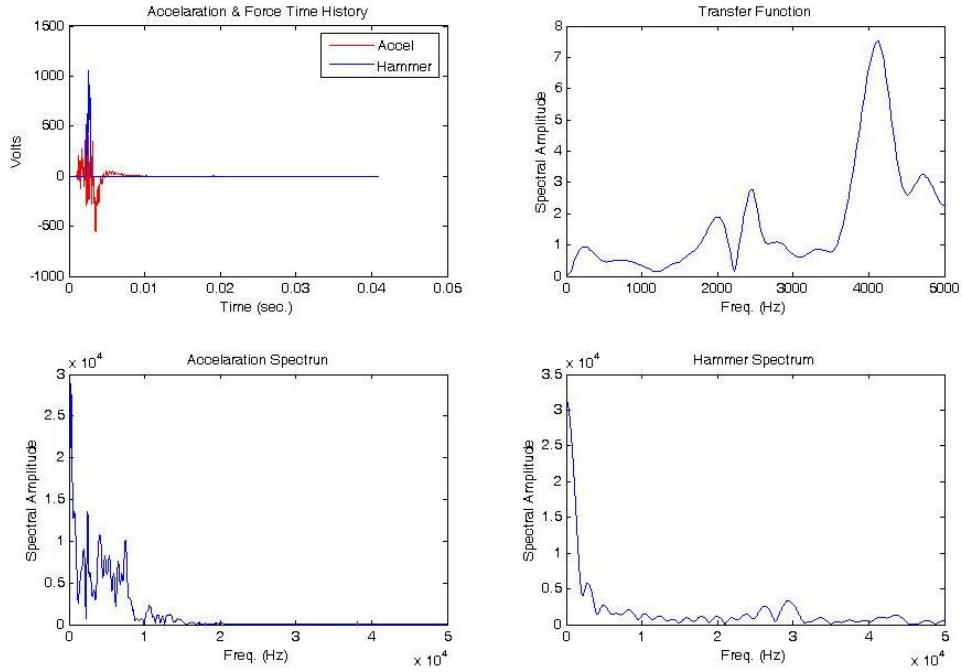

Figure E.26 Transfer Function for Specimen CKD-1 (Hit-2)

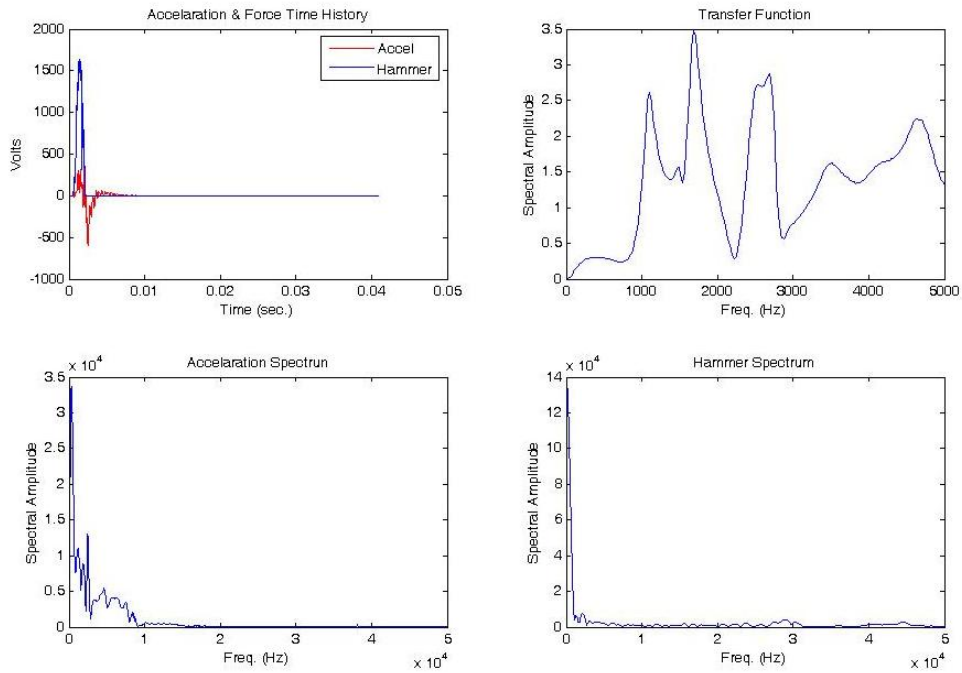

Figure E.27 Transfer Function for Specimen CKD-1 (Hit-3)

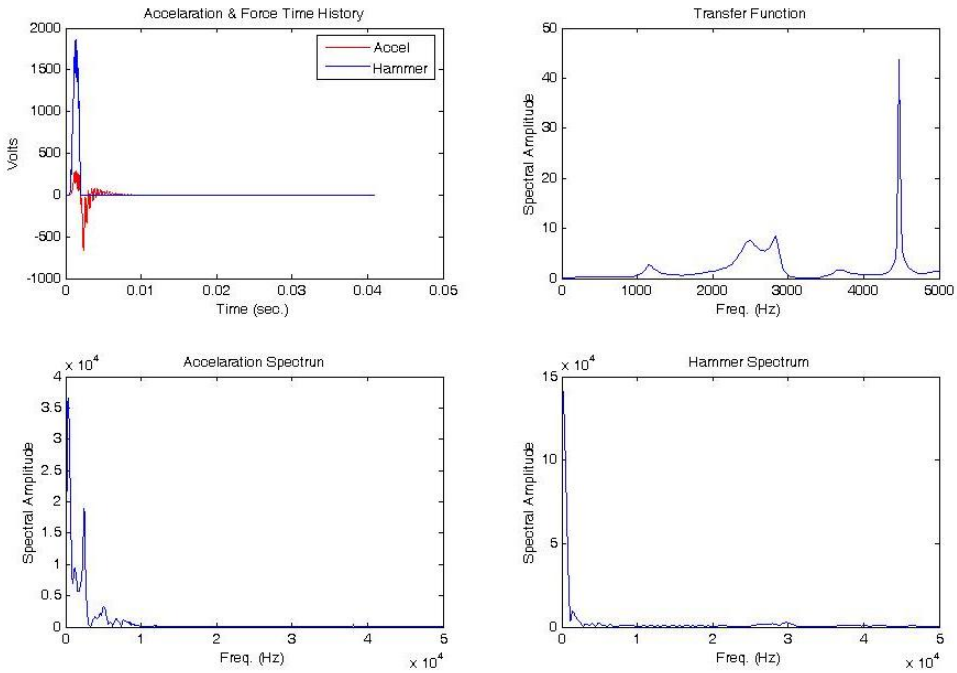

Figure E.28 Transfer Function for Specimen CKD-1 (Hit-4)

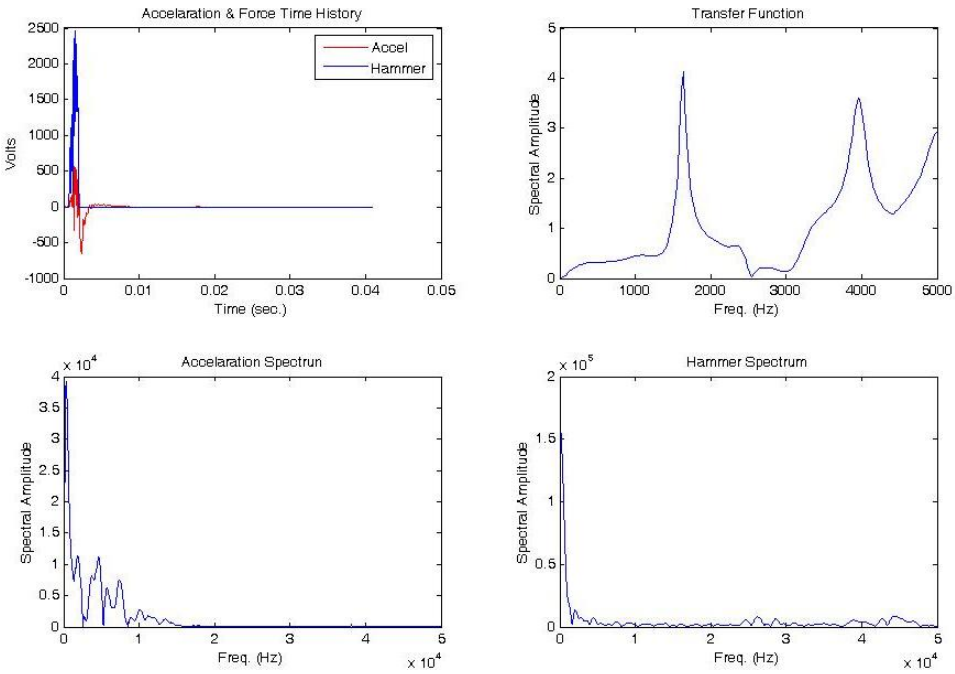

Figure E.29 Transfer Function for Specimen CKD-1 (Hit-5)

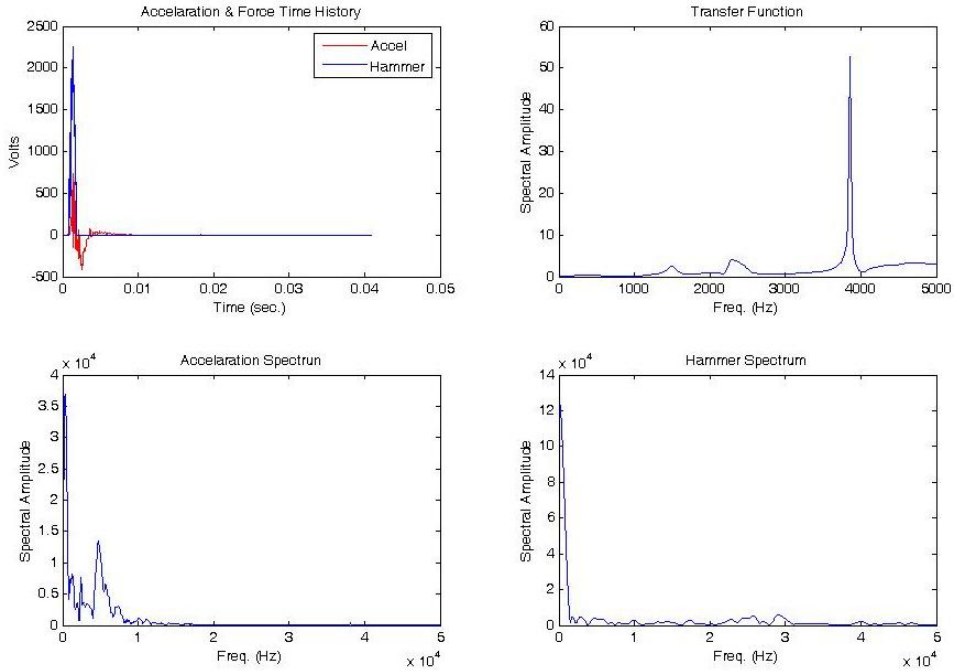

Figure E.30 Transfer Function for Specimen CKD-1 (Hit-6)

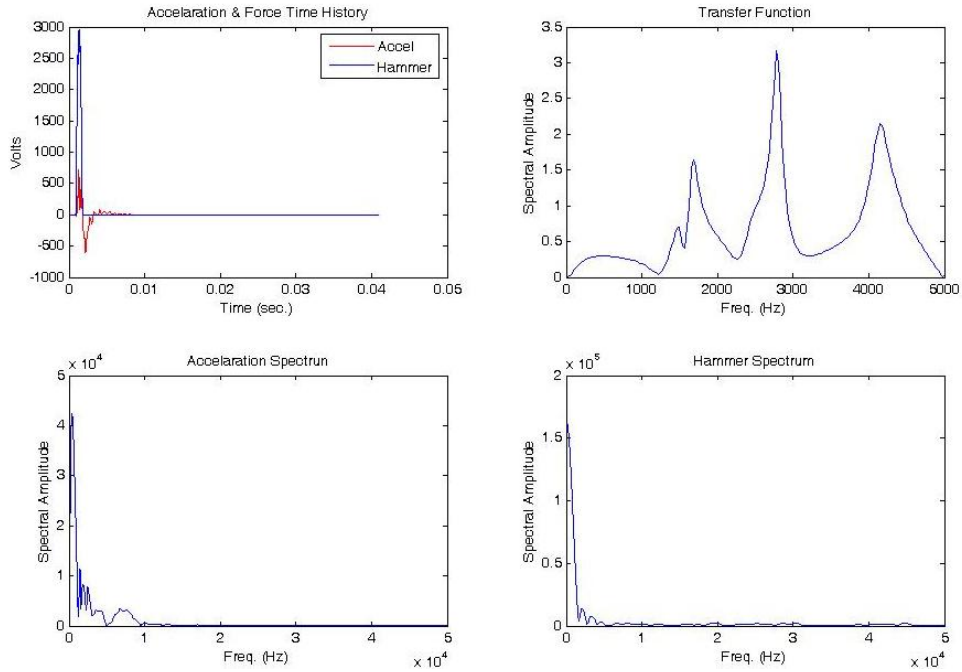

Figure E.31 Transfer Function for Specimen CKD-1 (Hit-7)

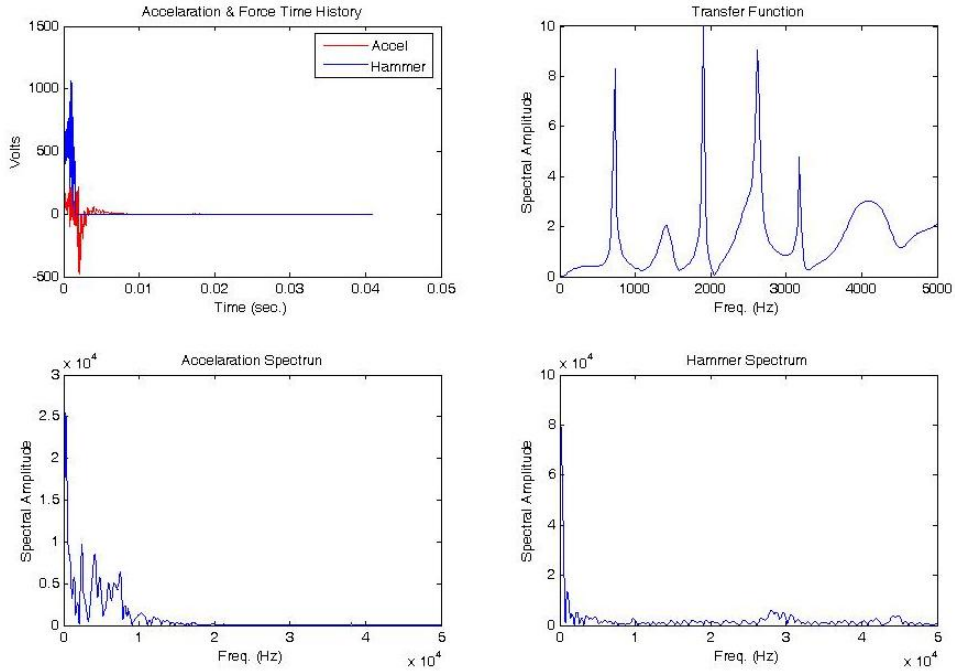

Figure E.32 Transfer Function for Specimen CKD-1 (Hit-8)

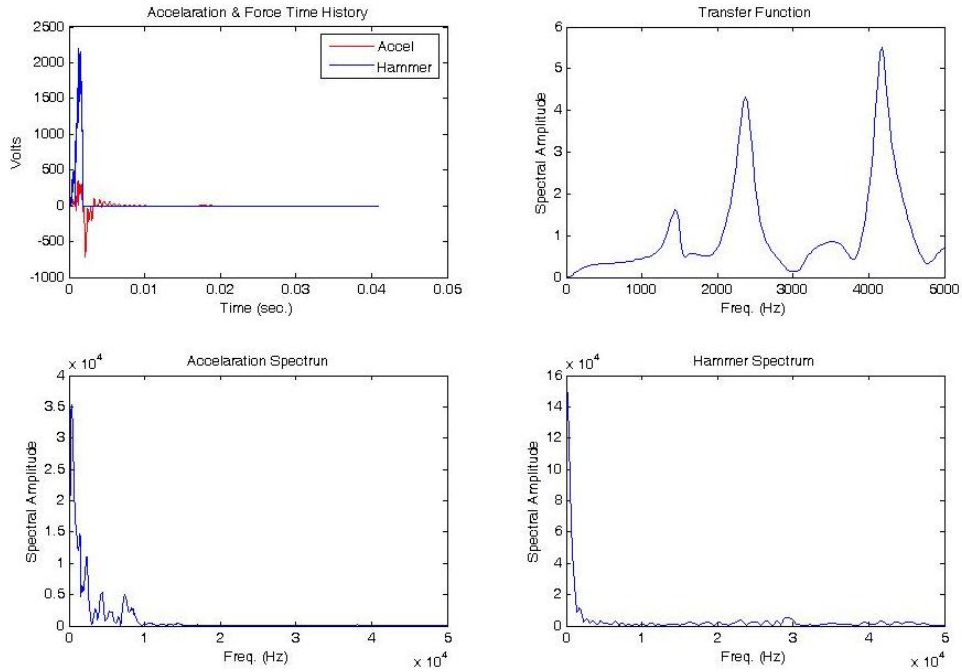

Figure E.33 Transfer Function for Specimen CKD-1 (Hit-9)

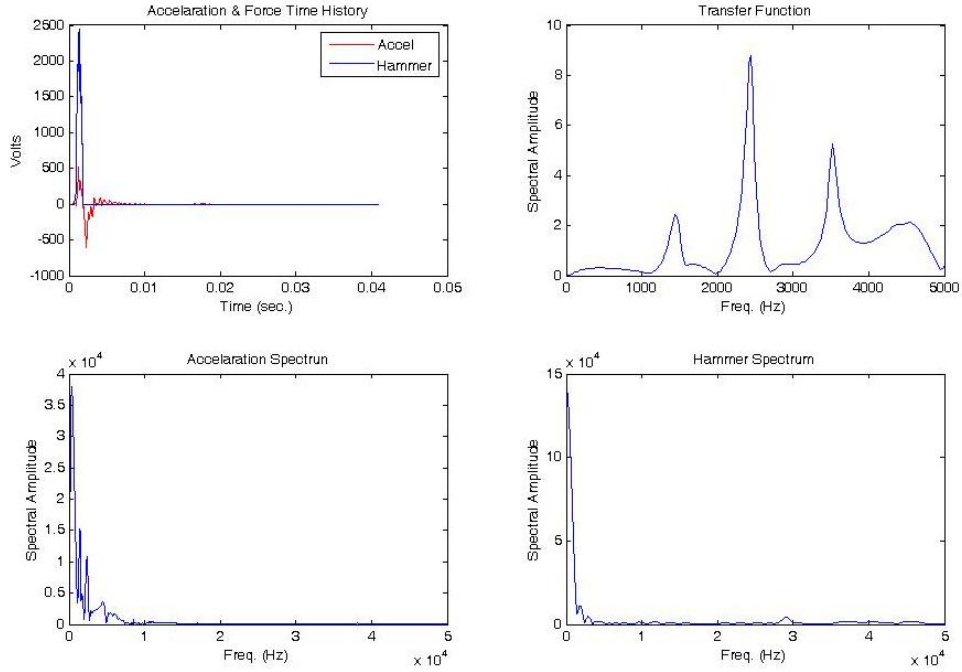

Figure E.34 Transfer Function for Specimen CKD-1 (Hit-10)

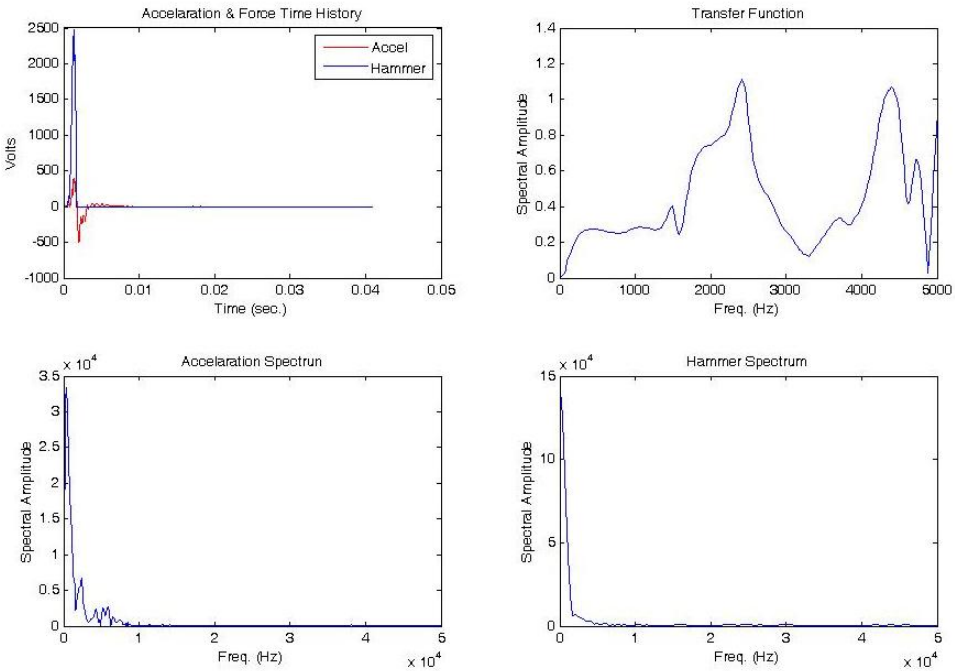

Figure E.35 Transfer Function for Specimen CKD-1 (Hit-11)

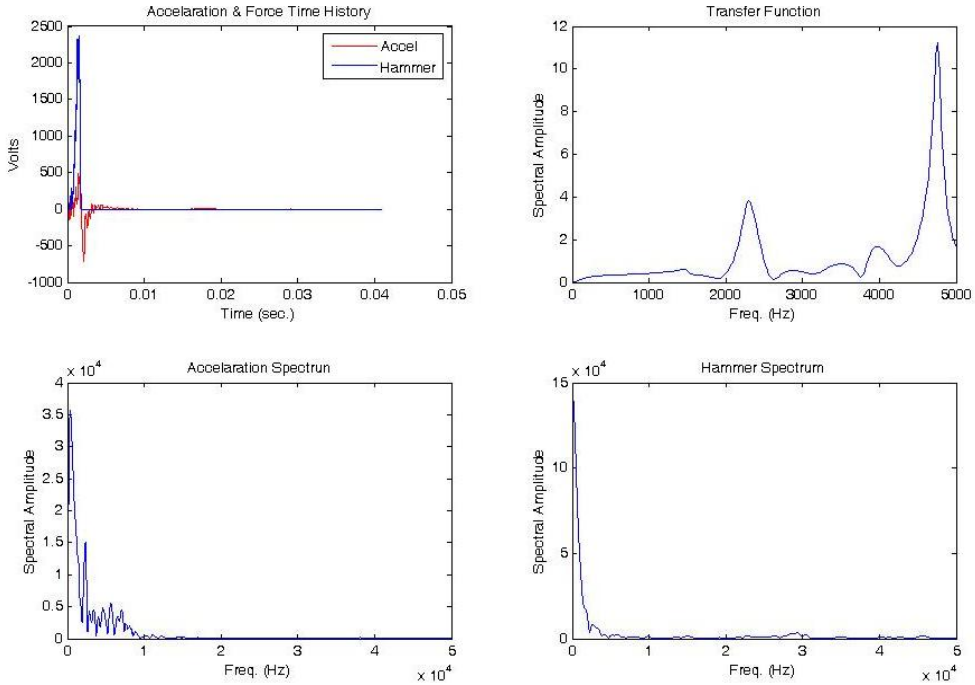

Figure E.36 Transfer Function for Specimen CKD-1 (Hit-12)

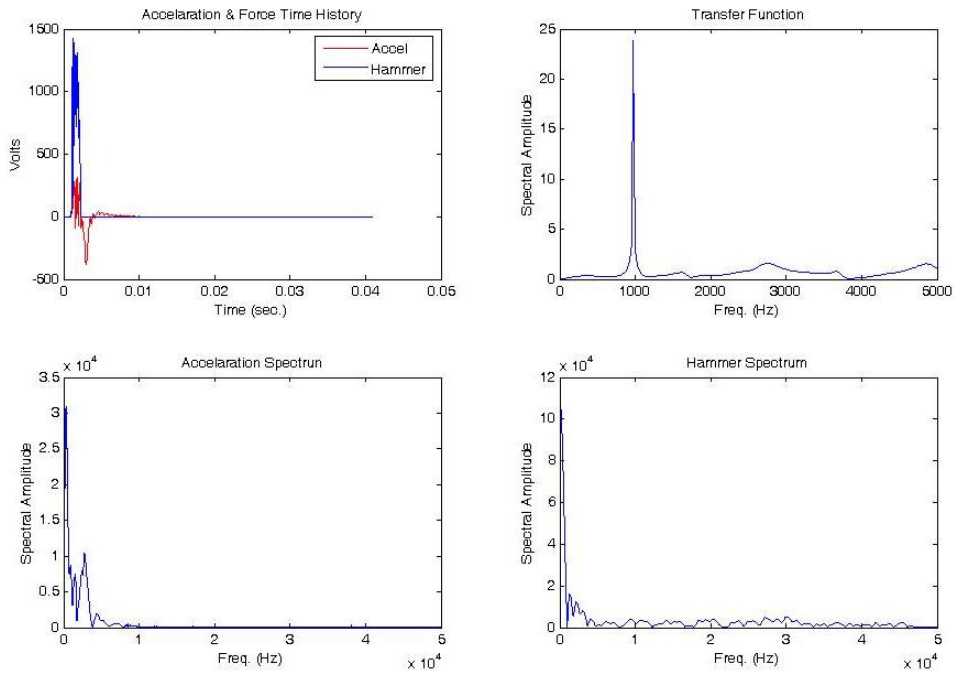

Figure E.37 Transfer Function for Specimen CKD-2 (Hit-1)

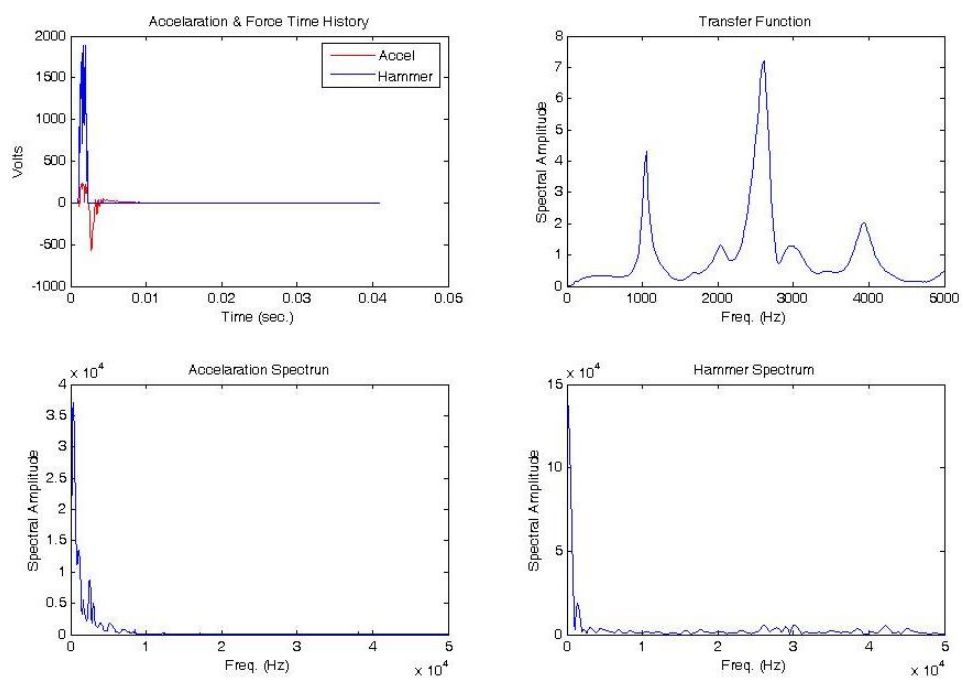

Figure E.38 Transfer Function for Specimen CKD-2 (Hit-2)

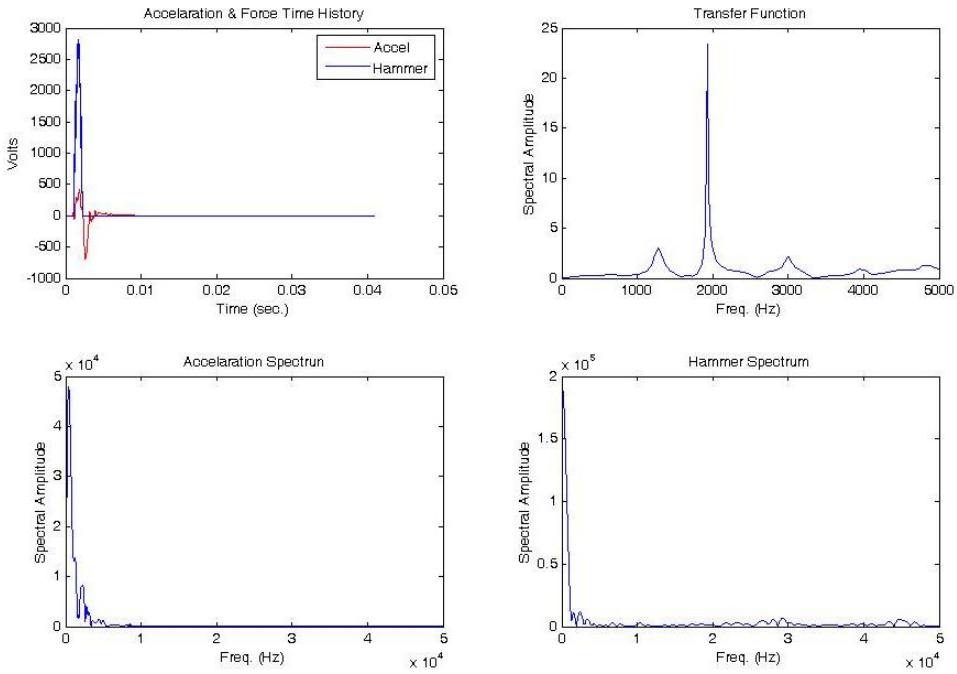

Figure E.39 Transfer Function for Specimen CKD-2 (Hit-3)

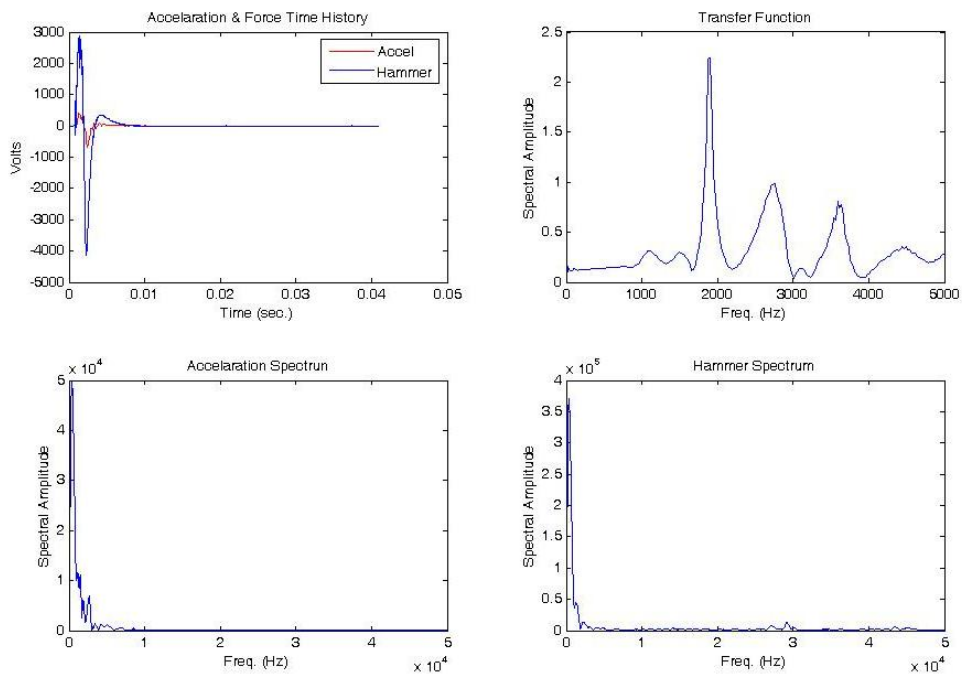

Figure E.40 Transfer Function for Specimen CKD-2 (Hit-4)

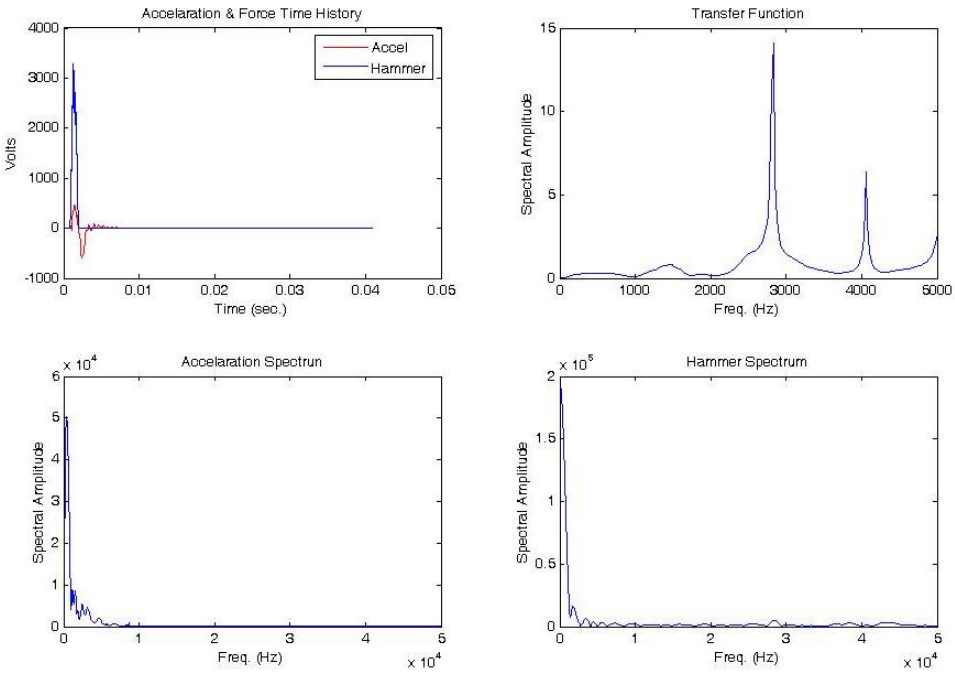

Figure E.41 Transfer Function for Specimen CKD-2 (Hit-5)

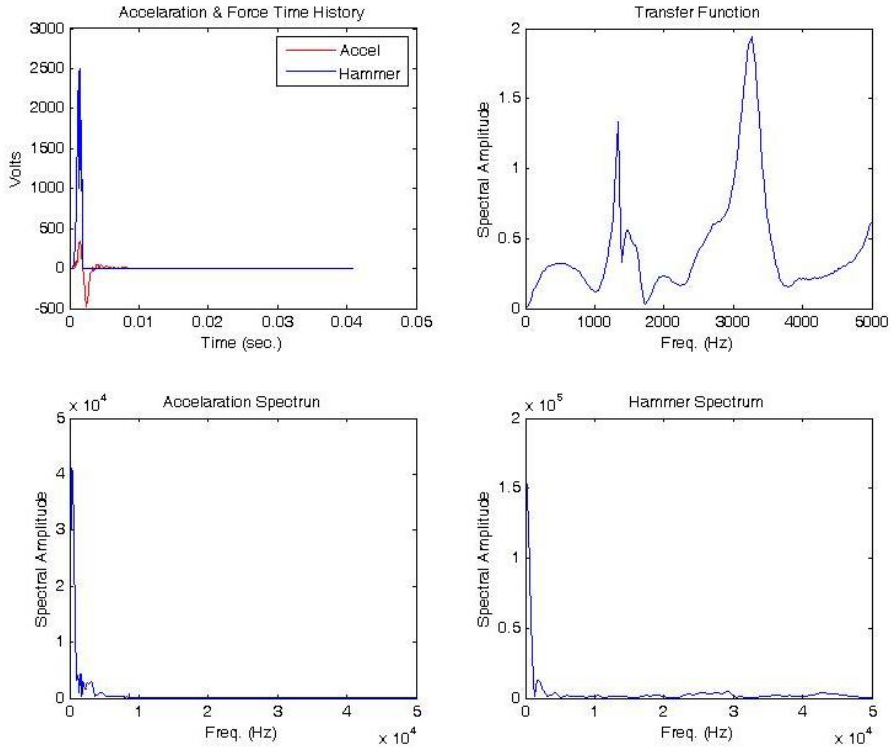

Figure E.42 Transfer Function for Specimen CKD-2 (Hit-6)

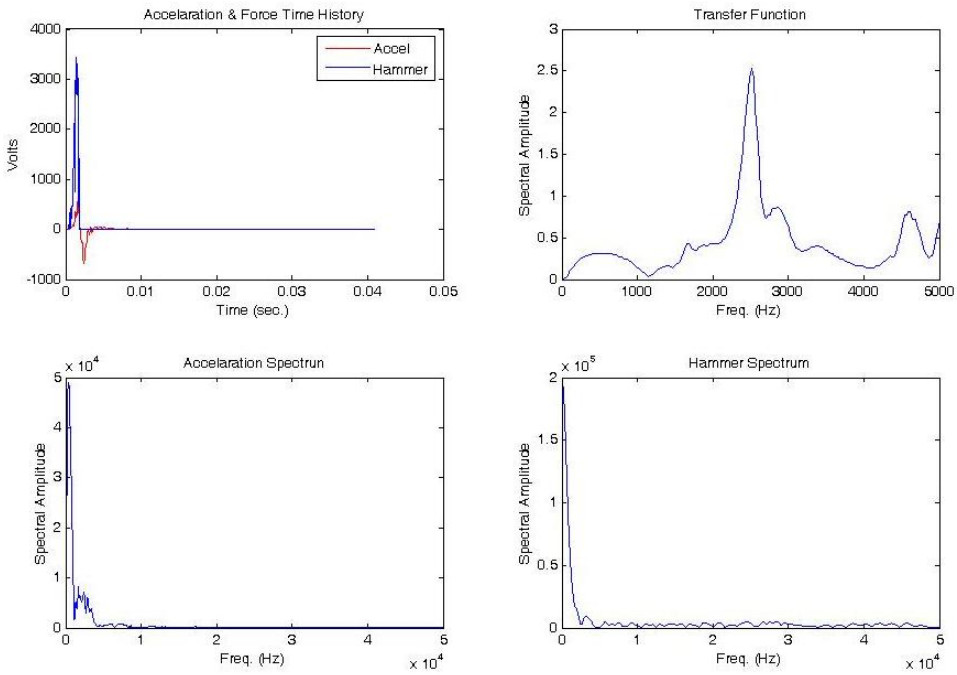

Figure E.43 Transfer Function for Specimen CKD-2 (Hit-7)

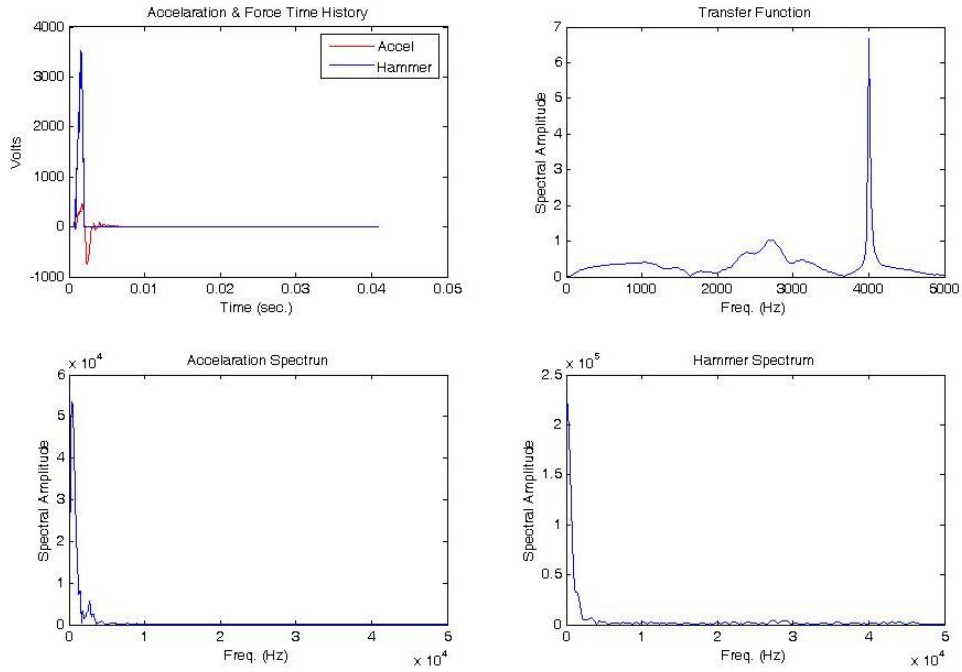

Figure E.44 Transfer Function for Specimen CKD-2 (Hit-8)

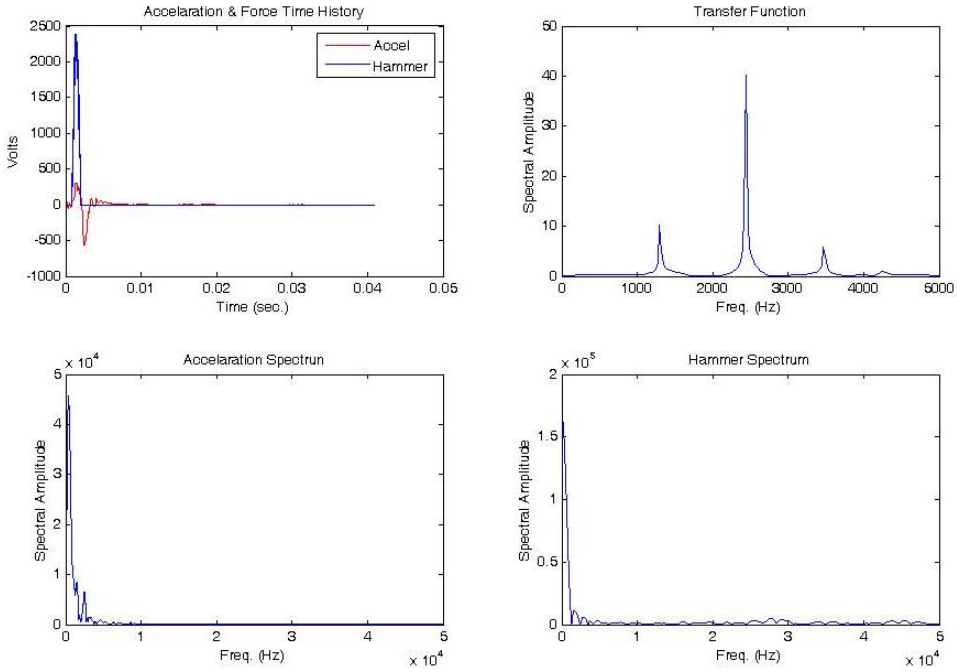

Figure E.45 Transfer Function for Specimen CKD-2 (Hit-9)

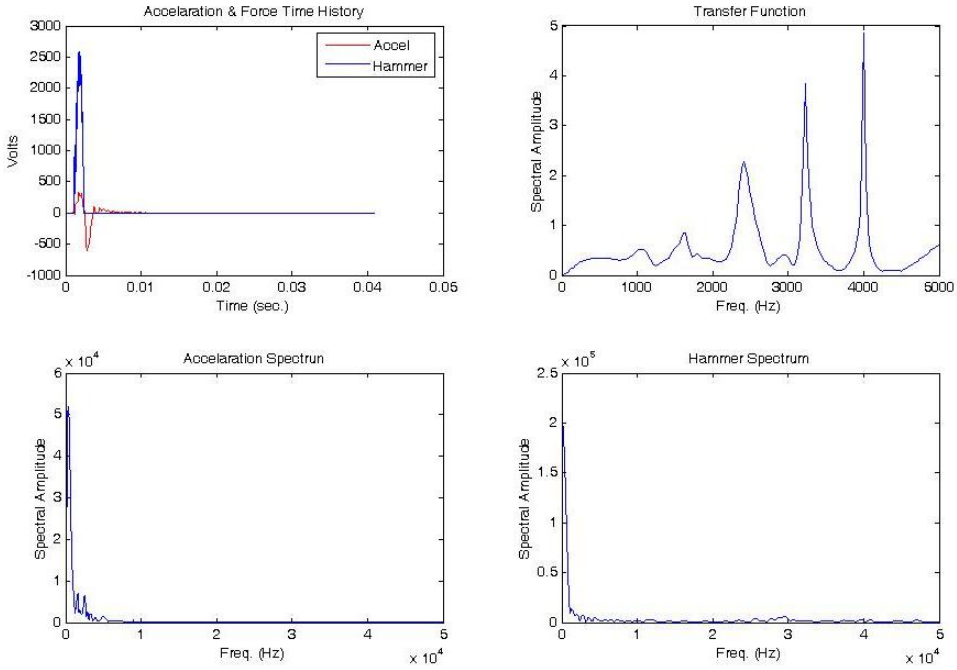

Figure E.46 Transfer Function for Specimen CKD-2 (Hit-10)

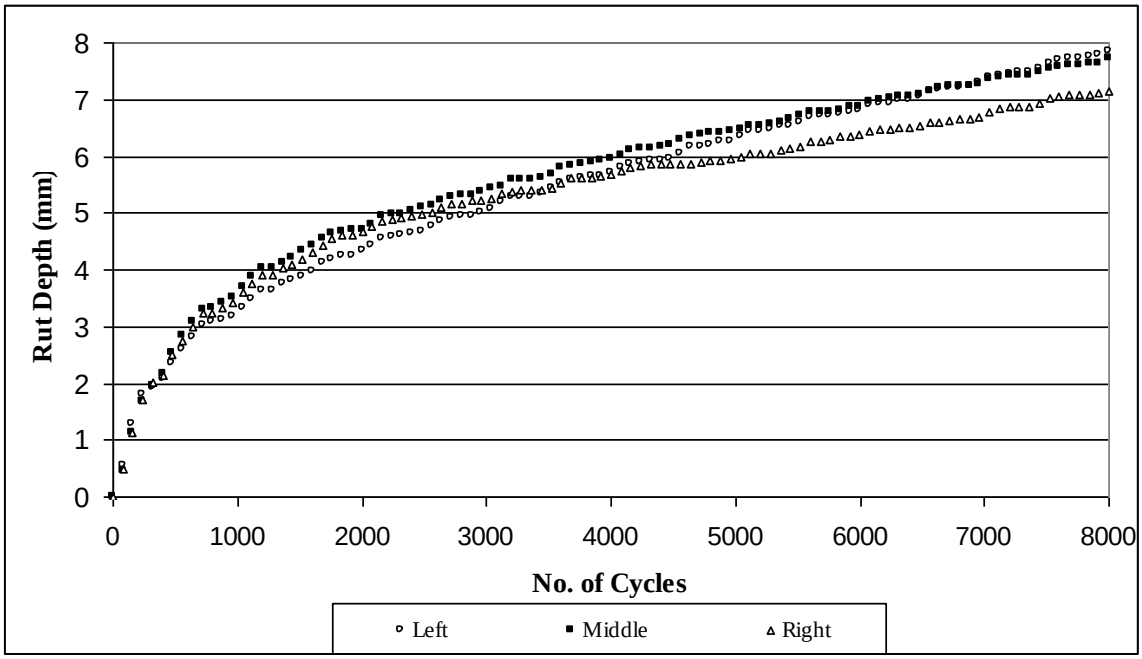

Figure F.1: APA Rut with Number of Cycles for Tar Creek Surface Mix

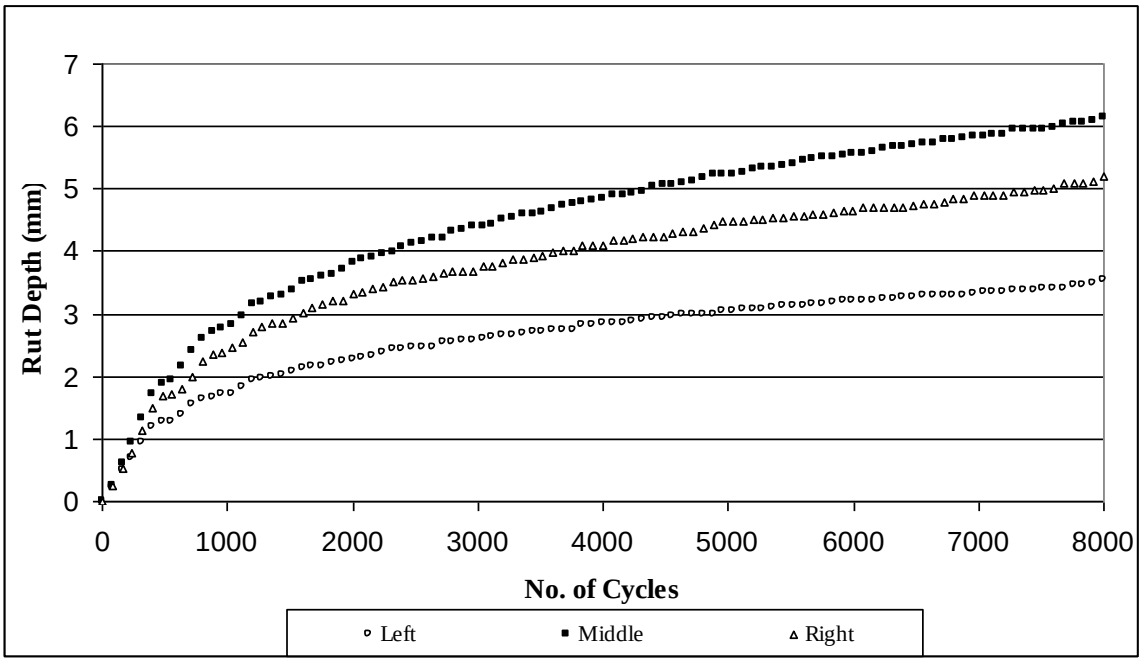

Figure F.2: APA Rut with Number of Cycles for Tar Creek Base Mix

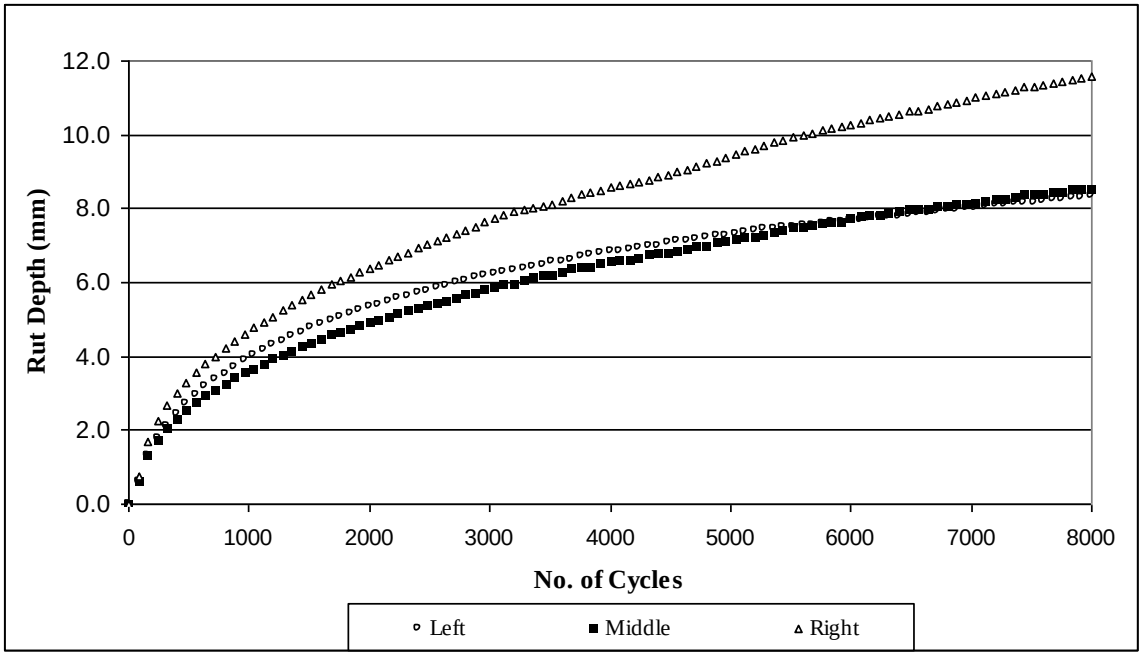

Figure F.3: APA Rut with Number of Cycles for Tar Creek Cores

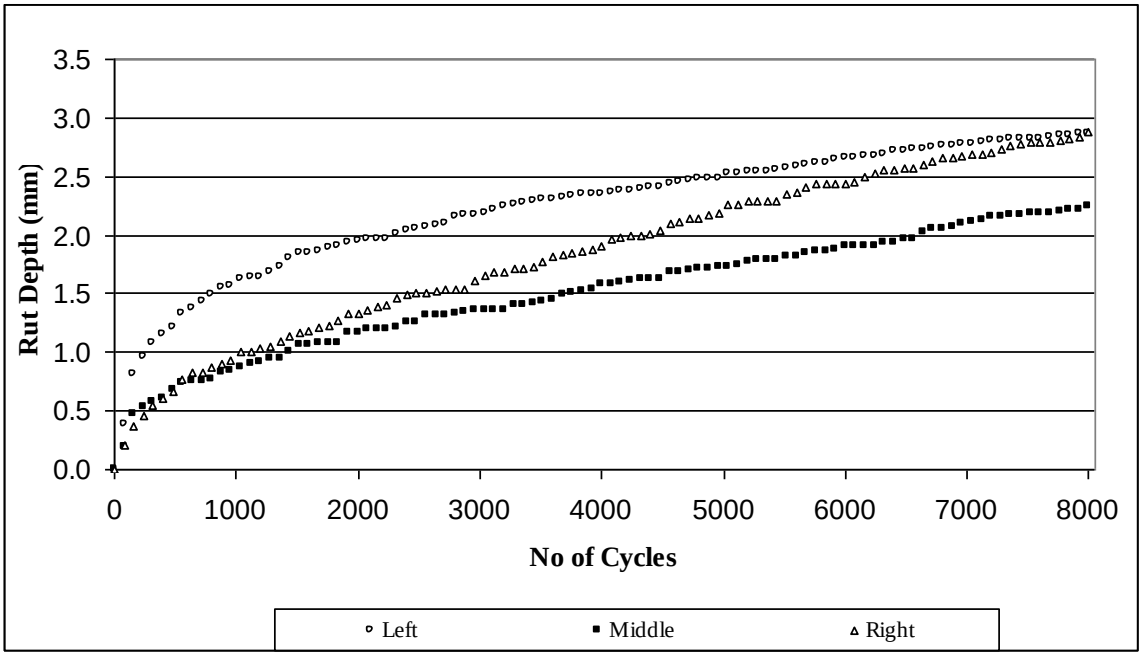

Figure F.4: APA Rut with Number of Cycles for Davis Base Mix

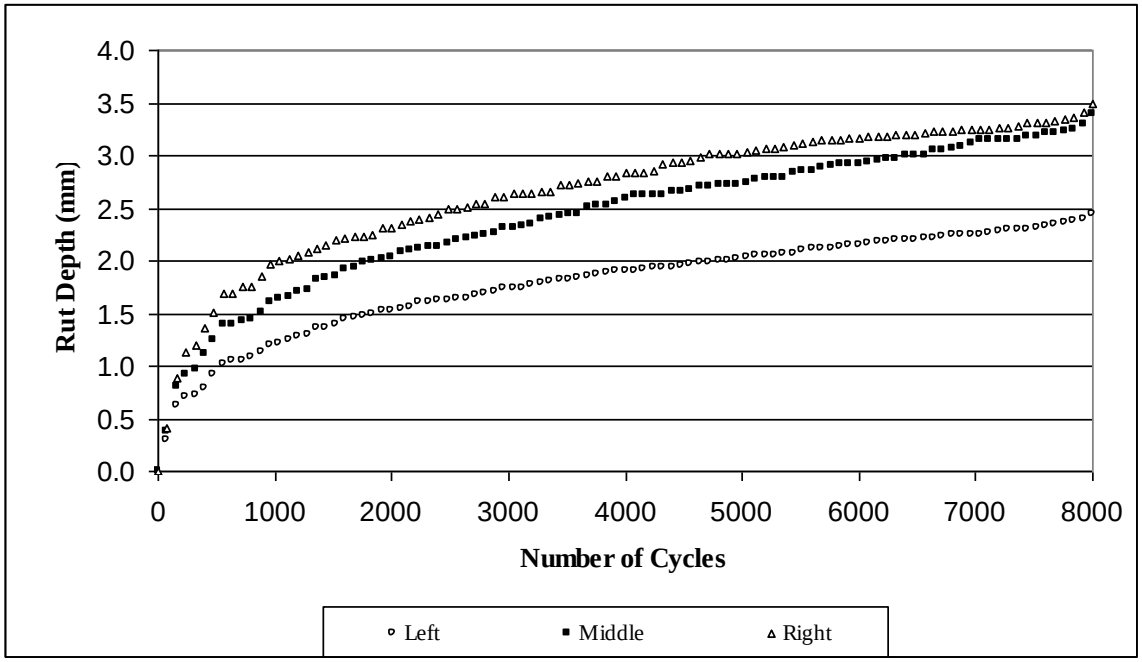

Figure F.5: APA Rut with Number of Cycles for Davis Cores

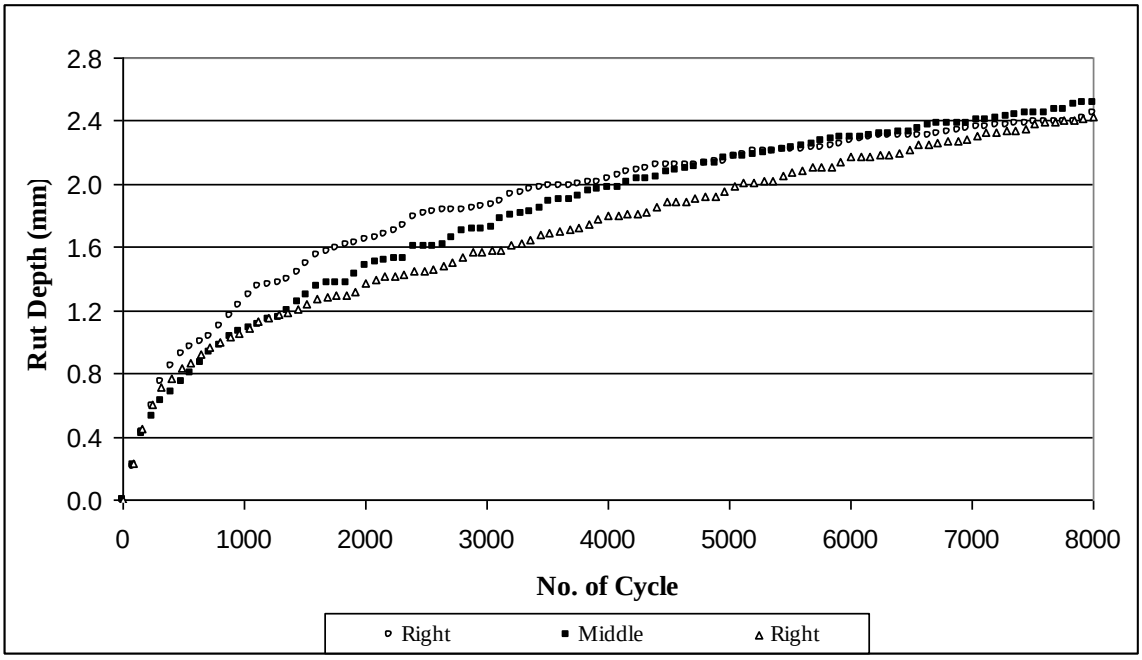

Figure F.6: APA Rut with Number of Cycles for OKC Base Mix

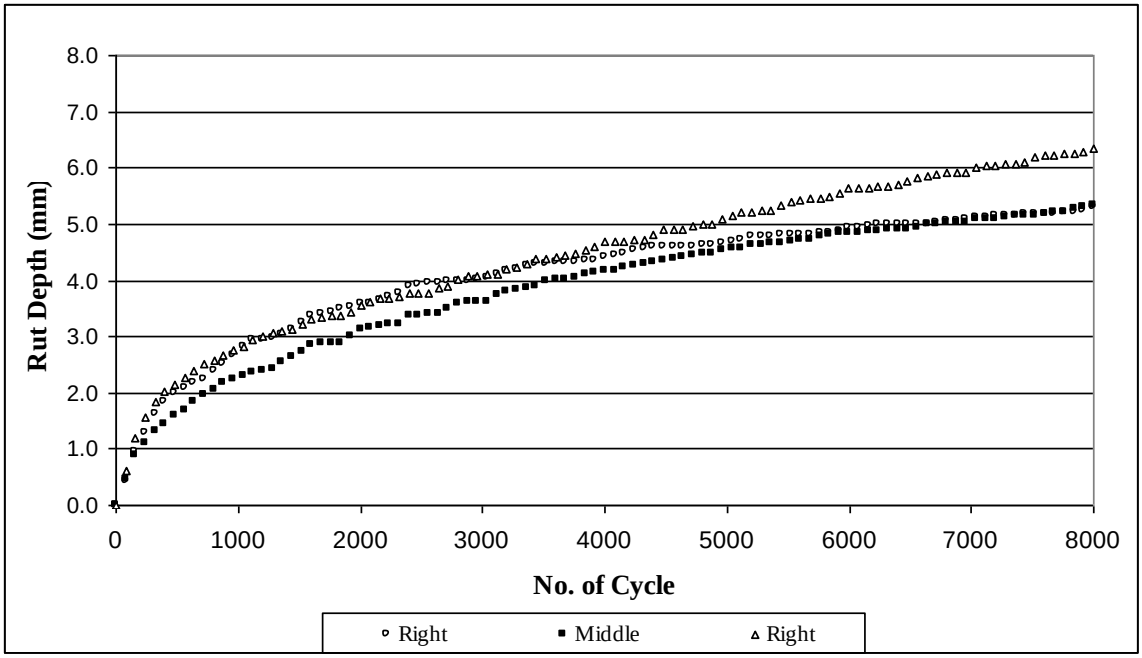

Figure F.7: APA Rut with Number of Cycles for OKC Cores

APPENDIX G

TEST ROAD RUT SURVEY

STATION	EASTBOUND RUT (inches)		WESTBOUND RUT (inches)	
	Outside WP	Inside WP	Inside WP	Outside WP
32 + 00	0.0	0.0	0.0	0.0
31 + 50	0.1	0.1	0.2	0.1
31 + 00	0.2	0.1	0.2	0.2
30 + 50	0.0	0.0	0.5	0.3
30 + 00	0.0	0.0	0.1	0.0
29 + 50	0.0	0.0	0.1	0.0
29 + 00	0.1	0.0	0.3	0.2
28 + 50	0.1	0.1	0.2	0.2
28 + 00	0.0	0.0	0.3	0.2
27 + 50	0.0	0.0	0.4	0.3
27 + 00	0.1	0.1	0.1	0.1
26 + 50	0.1	0.1	0.1	0.1
26 + 00	0.1	0.1	0.1	0.1
25 + 50	0.1	0.1	0.1	0.1
25 + 00	0.1	0.0	0.0	0.0
24 + 50	0.0	0.1	0.2	0.1
24 + 00	0.1	0.1	0.3	0.2
23 + 50	0.0	0.0	0.1	0.1
23 + 00	0.1	0.1	0.2	0.1
22 + 50	0.1	0.1	0.2	0.1
22 + 00	0.1	0.1	0.3	0.2
21 + 50	0.1	0.1	0.3	0.2
21 + 00	0.1	0.1	0.2	0.1
20 + 50	0.1	0.1	0.1	0.1
20 + 00	0.1	0.1	0.3	0.2
19 + 50	0.1	0.1	0.2	0.1
19 + 00	0.1	0.1	0.2	0.1
18 + 50	0.1	0.1	0.2	0.1
18 + 00	0.1	0.1	0.2	0.1
17 + 50	0.1	0.1	0.2	0.1
17 + 00	0.1	0.1	0.3	0.2
16 + 50	0.1	0.0	0.2	0.2
16 + 00	0.1	0.1	0.2	0.1
15 + 50	0.1	0.1	0.2	0.1
15 + 00	0.1	0.1	0.1	0.1
14 + 50	0.1	0.1	0.1	0.1
14 + 00	0.1	0.1	0.2	0.1
13 + 50	0.1	0.2	0.1	0.1
13 + 00	0.1	0.1	0.1	0.1
12 + 50	0.1	0.1	0.2	0.1
12 + 00	0.1	0.1	0.1	0.1
11 + 50	0.1	0.1	0.1	0.1
11 + 00	0.1	0.1	0.1	0.1
10 + 50	0.1	0.1	0.0	0.1

TEST ROAD RUT SURVEY (continued)

STATION	EASTBOUND RUT (inches)		WESTBOUND RUT (inches)	
	Outside WP	Inside WP	Inside WP	Outside WP
10 + 00	0.1	0.1	0.3	0.2
9 + 50	0.0	0.0	0.4	0.3
9 + 00	0.0	0.0	0.2	0.1
8 + 50	0.0	0.0	0.2	0.2
8 + 00	0.1	0.1	0.1	0.1
7 + 50	0.1	0.1	0.1	0.1
7 + 00	0.0	0.0	0.3	0.2
6 + 50	0.1	0.1	0.2	0.1
6 + 00	0.1	0.1	0.2	0.1
5 + 50	0.1	0.1	0.3	0.2
5 + 00	0.0	0.0	0.2	0.1
4 + 50	0.0	0.0	0.3	0.2
4 + 00	0.1	0.1	0.3	0.2
3 + 50	0.1	0.2	0.3	0.2
3 + 00	0.1	0.1	0.2	0.1
2 + 50	0.1	0.1	0.2	0.1
2 + 00	0.1	0.1	0.3	0.2
1 + 50	0.1	0.2	0.3	0.2
1 + 00	0.0	0.0	0.0	0.0
0 + 50	0.1	0.0	0.1	0.0
0 + 00	0.0	0.0	0.1	0.1
Average	***0.08***	***0.08***	***0.19***	***0.13***
Standard Deviation	***0.05***	***0.05***	***0.10***	***0.07***

Note: *Oklahoma DOT maximum allowable estimated rut for roadways with less than 0.3 million ESALs is 0.32 inches. Ninety-nine percent of the actual rut measurements met this criteria.*